



<https://theses.gla.ac.uk/>

Theses Digitisation:

<https://www.gla.ac.uk/myglasgow/research/enlighten/theses/digitisation/>

This is a digitised version of the original print thesis.

Copyright and moral rights for this work are retained by the author

A copy can be downloaded for personal non-commercial research or study,  
without prior permission or charge

This work cannot be reproduced or quoted extensively from without first  
obtaining permission in writing from the author

The content must not be changed in any way or sold commercially in any  
format or medium without the formal permission of the author

When referring to this work, full bibliographic details including the author,  
title, awarding institution and date of the thesis must be given

Enlighten: Theses

<https://theses.gla.ac.uk/>  
[research-enlighten@glasgow.ac.uk](mailto:research-enlighten@glasgow.ac.uk)

# **Photostimulated Luminescence as an Archaeological Dating Tool**

by

**Robert James Clark**

Submitted to

**University of Glasgow  
(Faculty of Science)**

for the degree of

**Doctor of Philosophy**

September, 1992

This research was conducted at the Scottish Universities Research and Reactor  
Centre, East Kilbride.

© R. J. Clark, 1992

ProQuest Number: 10992275

All rights reserved

INFORMATION TO ALL USERS

The quality of this reproduction is dependent upon the quality of the copy submitted.

In the unlikely event that the author did not send a complete manuscript and there are missing pages, these will be noted. Also, if material had to be removed, a note will indicate the deletion.



ProQuest 10992275

Published by ProQuest LLC (2018). Copyright of the Dissertation is held by the Author.

All rights reserved.

This work is protected against unauthorized copying under Title 17, United States Code  
Microform Edition © ProQuest LLC.

ProQuest LLC.  
789 East Eisenhower Parkway  
P.O. Box 1346  
Ann Arbor, MI 48106 – 1346

*Thesis  
9500  
Copy 1*

GLASGOW  
UNIVERSITY  
LIBRARY

# **Photostimulated Luminescence as an Archaeological Dating Tool**

## **Abstract**

Photostimulated Luminescence (PSL) is the process where charge carriers trapped at impurity and defect sites in a crystalline lattice are evicted by photon absorption and recombine with the emission of electromagnetic radiation. In this particular field of study, the charge carriers initially become trapped after the absorption of ionising radiation, and the PSL signal is dependent upon the total absorbed dose. PSL is a relatively recent development in thermoluminescence dating and has shown good potential for implementation as an archaeological dating tool, for both heated (i.e. pottery) and unheated (i.e. quaternary sediments) samples. However, prior to such implementation, it is suggested that it is necessary to explore the fundamental physical mechanisms governing the PSL phenomenon. The work presented in this thesis is centred on the exploration of these mechanisms in feldspars. Theoretical considerations are discussed together with the development of a simple mathematical model. This is followed by thorough exploration of the PSL in feldspar using many analytical techniques including spectroscopic studies, thermal stability studies, exploration of the dependency upon stimulation temperature and the response to pulsed stimulation. The results generated by this research are then used to propose modifications to an existing energy model. The dose response in a feldspar is explored and this (in combination with the earlier studies) is used to propose a dosimetric technique that may be used for dating purposes. This technique is demonstrated to be able to recover known laboratory doses after the development and implementation of formulae to account for loss mechanisms during the measurement process. The results are discussed and further areas of study leading towards a reliable, accurate and precise dating tool are suggested.

## **Acknowledgements**

I would like to take this opportunity to thank the following people:

Fellow members of the thermoluminescence research group at SURRC for providing support and humour, especially when things did not quite seem to be going according to plan.

My Supervisor, Dr D. C. W. Sanderson, for his continuing guidance throughout the course of my research at SURRC.

Finally my wife, Julie, for support and catching all (I hope) of the spelling and grammatical errors that were not caught by the spell checker on the word processor.

## Contents

<u>Chapter</u>	<u>Page</u>
<b>1 - Introduction</b> . . . . .	<b>1</b>
1.1 - Luminescence . . . . .	1
1.2 - Historical Background . . . . .	2
1.3 - Perceived Advantages of Photostimulated Luminescence . . . . .	6
1.4 - Early Work in Photostimulated Luminescence . . . . .	8
1.5 - Project Aims . . . . .	9
<b>2 - Theoretical Background</b> . . . . .	<b>11</b>
2.1 - The Band Theory of Solids . . . . .	11
2.2 - Thermal Stimulation . . . . .	16
2.2.1 - Phosphorescence . . . . .	16
2.2.2 - Thermoluminescence . . . . .	22
2.3 - Photostimulated Luminescence . . . . .	25
2.4 - One Trap / One Centre Model . . . . .	28
2.4.1 - Variation in Modelled Bleaching Curves with Photon Eviction Coefficient . . . . .	31
2.4.2 - Variation in Modelled Bleaching Curves with Electron Capture Coefficient . . . . .	33
2.4.3 - Variation in Modelled Bleaching Curve with Dose . . . . .	36
2.4.4 - Discussion of Model Results . . . . .	40
2.5 - Natural Samples . . . . .	42
2.6 - Ratio of Photo and Thermal Eviction Energies . . . . .	43
2.7 - Summary . . . . .	51
2.8 - Dating Requirements . . . . .	51
<b>3 - Photo Stimulation Techniques and Instrumentation</b> . . . . .	<b>53</b>
3.1 - Continuous Monochromatic Stimulation . . . . .	53
3.2 - Pulsed Monochromatic Stimulation . . . . .	54
3.3 - Excitation Spectroscopy . . . . .	56
3.4 - Emission Spectroscopy . . . . .	57
3.5 - Phototransferred Thermoluminescence . . . . .	58
3.6 - Published Work . . . . .	59
3.7 - Scanning Excitation Spectrometer . . . . .	60
3.7.1 - Components . . . . .	61
3.7.2 - Light Source Characterisation . . . . .	65
3.7.2.1 - Power Spectrum . . . . .	65
3.7.2.2 - Lamp Source Stability . . . . .	69
3.7.3 - Control Software . . . . .	72
3.7.3.1 - General . . . . .	72
3.7.3.2 - Implementation . . . . .	74
3.8 - Pulsed Infra-Red LED system . . . . .	76
3.8.1 - Components . . . . .	76

## Contents

<u>Chapter</u>	<u>Page</u>
3.8.2 - LED Response Time . . . . .	77
3.8.3 - Control Software . . . . .	79
3.9 - Pulsed Tunable Dye Laser System . . . . .	80
3.9.1 - Components . . . . .	81
3.9.2 - Control Software . . . . .	82
3.10 - Optical Filtering . . . . .	83
3.11 - Future Developments . . . . .	84
3.12 - Summary . . . . .	86
<b>4 - Photostimulated Luminescence of Feldspar - I . . . . .</b>	<b>88</b>
4.1 - Excitation Spectroscopy . . . . .	89
4.1.1 - Excitation Spectra . . . . .	89
4.1.1.1 - Microcline . . . . .	89
4.1.1.2 - IAEA Feldspar, F1 . . . . .	92
4.1.1.3 - Comparison With Published Spectra . . . . .	95
4.1.1.4 - Survey of Feldspathic Minerals . . . . .	97
4.1.1.5 - Summary . . . . .	103
4.1.2 - Monochromatic Bleaching . . . . .	104
4.1.3 - Temperature Dependence . . . . .	107
4.1.4 - Thermal Stability . . . . .	112
4.1.5 - High Dose Response . . . . .	119
4.2 - Emission Spectroscopy . . . . .	121
4.2.1 - Variation with Bleaching . . . . .	125
4.2.2 - Variation with Temperature . . . . .	127
4.2.3 - Summary . . . . .	133
4.3 - Low Dose Dependence and Sensitivity . . . . .	135
4.3.1 - Xenon Lamp . . . . .	135
4.3.2 - Laser . . . . .	137
4.3.3 - Infra-Red LED . . . . .	138
4.4 - Summary . . . . .	141
<b>5 - Photostimulated Luminescence of Feldspar - II . . . . .</b>	<b>144</b>
5.1 - Thermal Assistance . . . . .	144
5.1.1 - Infra-Red Stimulation . . . . .	144
5.1.2 - Visible / Red Stimulation . . . . .	147
5.1.3 - Visible / Green Stimulation . . . . .	148
5.1.4 - Summary . . . . .	149
5.2 - Thermal Stability . . . . .	151
5.3 - Thermal Sensitisation . . . . .	157
5.4 - Pulsed Stimulation . . . . .	161
5.4.1 - Infra Red LED Stimulation . . . . .	161
5.4.2 - Laser Stimulation . . . . .	163
5.4.3 - Time Domain Analysis . . . . .	165

## Contents

<u>Chapter</u>	<u>Page</u>
5.5 - Modifications to Proposed Models . . . . .	169
5.6 - Summary . . . . .	177
<b>6 - Dose Evaluation . . . . .</b>	<b>179</b>
6.1 - Differences Between Natural and Laboratory Irradiated Samples . . .	179
6.2 - Single Disc Additive Dose Methodology . . . . .	182
6.2.1 - Without Preheat . . . . .	183
6.2.2 - With Preheat. . . . .	186
6.3 - Corrections for Loss of Signal During PSL Measurement. . . . .	189
6.3.1 - Theory . . . . .	189
6.3.2 - Application . . . . .	193
6.4 - Methodologies for Checking the Efficiency of the Preheating Regime . . . . .	198
6.5 - Discussion . . . . .	200
6.6 - Summary . . . . .	204
<b>7 - Conclusion . . . . .</b>	<b>205</b>
7.1 - Summary of Results . . . . .	205
7.1.1 - Spectroscopy . . . . .	205
7.1.2 - Thermal Stability . . . . .	207
7.1.3 - Thermal Assistance . . . . .	207
7.1.4 - Pulsed Stimulation . . . . .	208
7.1.5 - PSL Model . . . . .	208
7.1.6 - Dose Response and Evaluation . . . . .	209
7.2 - The Future . . . . .	210
7.3 - Conclusion . . . . .	212
<b>8 - Bibliography . . . . .</b>	<b>214</b>

## List of Figures

<u>Figure</u>	<u>Page</u>
Figure 2.1 - Variation in probability density function of the symmetric and asymmetric electron wave functions. . . . .	13
Figure 2.2 - Energy bands and localised energy states within an insulator. . . . .	15
Figure 2.3 - One trap / one centre luminescence model . . . . .	17
Figure 2.4 - Computed first and second order TL glow curves . . . . .	23
Figure 2.5 - Modelled bleaching Curve . . . . .	30
Figure 2.6 - Variation in the Modelled Bleaching Curve with Photo Eviction Cross Section . . . . .	31
Figure 2.7 - Variation in modelled bleaching curve with electron capture coefficient of the centre . . . . .	34
Figure 2.8 - Modelled bleaching curves, variation with dose . . . . .	37
Figure 2.9 - Ratio of modelled bleaching curves to the 1 Gy curve . . . . .	37
Figure 2.10 - Modelled dose response curve, integrated over 0 to 1000 s . . . . .	39
Figure 2.11 - Modelled dose response curve, integrated over 0 to 4000 s . . . . .	39
Figure 2.12 - Dependency of dielectric constant upon frequency of applied electromagnetic field. . . . .	45
Figure 2.13 - Configurational coordinate diagram showing thermal and photo eviction. . . . .	47
Figure 3.1 - Schematic Diagram of the PSL excitation spectrometer. . . . .	62
Figure 3.2 - Block diagram of the excitation spectrometer control structure. . . . .	64
Figure 3.3 - Typical xenon lamp power spectrum . . . . .	66
Figure 3.4 - Xenon lamp power spectrum for monochromator slit widths = 1 mm . . . . .	67
Figure 3.5 - Xenon lamp power spectrum for monochromator slit widths = 4 mm . . . . .	68
Figure 3.6 - Variation in Xe Lamp Power Density with Monochromator Slit Widths . . . . .	68
Figure 3.7 - Xenon lamp warm up characteristics . . . . .	70
Figure 3.8 - Xenon lamp stability as shown by peak positions. . . . .	71
Figure 3.9 - Xenon lamp stability as shown by peak heights. . . . .	72
Figure 3.10 - Block diagram of the PSL software control structure. . . . .	73
Figure 3.11 - Block diagram of the LED system control interface. . . . .	77
Figure 3.12 - LED response to TTL pulses . . . . .	78
Figure 3.13 LED pulse shape . . . . .	79
Figure 3.14 - Block diagram of the Laser control interface . . . . .	82
Figure 4.1 - Microcline excitation spectrum (100 Gy) with 500 nm grating. . . . .	90
Figure 4.2 - Microcline Excitation Spectrum (1 kGy) with 1000 nm Grating . . . . .	91
Figure 4.3 - Power Normalised Microcline Excitation Spectrum . . . . .	92
Figure 4.4 - F1 Feldspar Excitation Spectrum . . . . .	93
Figure 4.5 - Normalised F1 Feldspar Excitation Spectrum . . . . .	94
Figure 4.6 - F1 Excitation Spectrum Recorded Using a Slide Projector . . . . .	95
Figure 4.7 - Albite Excitation Spectra . . . . .	99
Figure 4.8 - Muscovite Excitation Spectra . . . . .	99

## List of Figures

<u>Figure</u>	<u>Page</u>
Figure 4.9 - Potassium Feldspar Excitation Spectra . . . . .	100
Figure 4.10 - Microcline and Plagioclase Excitation Spectra . . . . .	100
Figure 4.11 - Feldspathic Mineral PSL Sensitivities at 540 nm . . . . .	102
Figure 4.12 - Ratio of 500 nm peak to 840 nm peak for survey minerals . . . . .	102
Figure 4.13 - Ratio of the 840 nm peak to the 900 nm peak in the survey minerals . . . . .	103
Figure 4.14 - Monochromatic bleaching of the microcline excitation spectrum . .	105
Figure 4.15 - Microcline monochromatic bleaching curves at 500 and 880 nm. . .	106
Figure 4.16 - Variation of the Microcline Excitation Spectrum with temperature. . . . .	109
Figure 4.17 - Microcline Excitation Spectrum at -140°C . . . . .	110
Figure 4.18 - Variation in Microcline Unnormalised Infra-Red Peaks Ratio with Temperature . . . . .	111
Figure 4.19 - Microcline Room Temperature Excitation Spectrum . . . . .	113
Figure 4.20 - Microcline Room Temperature Excitation Spectrum After 200°C for 1 minute . . . . .	114
Figure 4.21 - Microcline Room Temperature Excitation Spectrum after 250°C for 1 Minute . . . . .	114
Figure 4.22 - Microcline Room Temperature Excitation Spectrum after 350°C for 1 Minute . . . . .	115
Figure 4.23 - Microcline Room Temperature Excitation Spectrum After 400°C for 1 Minute . . . . .	115
Figure 4.24 - Pulse Annealing of 1 kGy Microcline from 150 - 350 °C . . . . .	116
Figure 4.25 - Microcline room temperature excitation spectrum after annealing at 400°C for 30 s . . . . .	117
Figure 4.26 Excitation Spectrum from F1 feldspar with geological signal only . .	118
Figure 4.27 - Microcline High Dose PSL Growth Curve . . . . .	120
Figure 4.28 - Typical F1 feldspar room temperature emission spectrum. . . . .	124
Figure 4.29 - F1 feldspar emission spectrum, variation with bleaching. . . . .	125
Figure 4.30 - Variation in Emission Peak Ratios with Bleaching . . . . .	126
Figure 4.31 - F1 Feldspar emission spectra, temperature dependence. . . . .	128
Figure 4.32 - F1 Emission Spectrum at 150 K . . . . .	129
Figure 4.33 - Variation of F1 Emission Peak Ratios with Temperature . . . . .	130
Figure 4.34 - Variation of F1 560:400 nm Peak Ratio with Temperature . . . . .	130
Figure 4.35 - F1 Emission Spectrum at 350 K . . . . .	131
Figure 4.36 - F1 Emission Spectrum at 320 K . . . . .	132
Figure 4.37 - F1 Xenon Lamp Growth Curve at 480 nm . . . . .	136
Figure 4.38 - F1 Laser Growth Curve . . . . .	137
Figure 4.39 - F1 LED Growth Curve . . . . .	139
Figure 4.40 - F1 LED Bleaching Curve for 2,000,000 Pulses per Bleaching Event . . . . .	140
Figure 5.1 - Arrhenius plot of microcline from 30°C to 150°C under infra red stimulation. . . . .	145

## List of Figures

<u>Figure</u>	<u>Page</u>
Figure 5.2 - Arrhenius plot of Microcline feldspar at 625 nm from 25°C to 120°C .....	147
Figure 5.3 - Arrhenius plot of microcline feldspar PSL at 500 nm from 25°C to 120°C .....	149
Figure 5.4 - F1 Arrhenius rise at 500 nm with cryogenic component subtracted. ....	150
Figure 5.5 - Pulsed Isothermal Decay of 480 nm PSL of the Feldspar F1 at 175°C - 225°C .....	152
Figure 5.6 - Arrhenius plot of the thermal lifetimes of the components of the 480 nm PSL .....	154
Figure 5.7 - Log-log plot of F1 Isothermal Decay; g is the gradient. ....	156
Figure 5.8 - Thermal sensitisation of 500 nm stimulation .....	158
Figure 5.9 - Evidence that the sensitised luminescence requires 500 nm stimulation .....	159
Figure 5.10 - Variation in sensitised 500 nm signal with sensitising temperature .....	160
Figure 5.11 - Microcline pulsed LED PSL .....	161
Figure 5.12 - Pulsed laser PSL response of 1 kGy F1 .....	163
Figure 5.13 - Luminescence time domain after laser pulse .....	164
Figure 5.14 - F1 Pulsed PSL response recorded on a fast MCS .....	166
Figure 5.15 - F1 PSL from 2 $\mu$ s pulses recorded with a dwell time of 5 ns .....	166
Figure 5.16 - The Hütt & Jaek PSL model .....	169
Figure 5.17 - A PSL model for the feldspar F1 .....	174
Figure 6.1 - Pulsed Isothermal Decay of of 480 nm PSL from Feldspar F1 at 200°C. (Corrected for Bleaching) .....	186
Figure 6.2 - Uncorrected LED additive dose growth curves. ....	188
Figure 6.3 - Corrected LED additive dose growth curve. ....	196

## List of Tables

<u>Table</u>	<u>Page</u>
Table 2.1 - Variation in Dielectric Constant of Silicate Minerals with Frequency .....	50
Table 3.1 - Variation in Power Density of the Xe Lamp with Monochromator Slit Widths. ....	69
Table 4.1 - Feldspathic Minerals used in Excitation Spectra Survey .....	98
Table 4.2 - PSL Stimulation Regions .....	103
Table 5.1 - Infra red thermal assistance energies .....	146
Table 5.2 - Thermal assistance activation energies for the components of the excitation spectrum. ....	150
Table 6.1 - LED dose evaluation, no preheat. ....	184
Table 6.2 - Xenon Lamp Dose Evaluation, no preheat. ....	185
Table 6.3 - Dose Evaluation with Preheat .....	187
Table 6.4 - Xenon Lamp and LED Growth Curve Correction Factors. ....	194
Table 6.5 - F191 PSL Growth Curves at 480 nm: $I_1$ - $I_4$ Curves corrected for multiple bleaching/annealing by methods 1 - 4. ....	195
Table 6.6 - Final corrected dose estimates for the single disc additive dose technique. ....	196

## 1 - Introduction

### 1.1 - Luminescence

Luminescence is the phenomenon where some of the energy of radiation incident upon a material is absorbed and re-emitted as electromagnetic radiation (after McKeever, 1988). The incident energy is absorbed by charge carriers which are excited from one energy state (e.g. the ground state) to a higher level and the luminescence may be emitted upon relaxation of the charge carriers to the original energy state. In this process the energy of the luminescence will be less than that of the incident radiation, behaviour described by Stokes' law. This is the process used in lasers and fluorescent lamps. However, if an intermediate energy state exists, then the charge carriers can relax to this state after excitation and be temporarily stored (or trapped). Thus the luminescence is generated following the eviction of the charge carriers from this 'trap' by absorption of some stimulating energy (e.g. heat or electromagnetic radiation), and relaxing to the original energy state again. In this case the energy of the emitted wavelength will be greater than the absorbed *stimulating* energy that frees the charge carriers from the traps, in optical terms, an *anti-stokes* transition. In both cases, the wavelength of the emitted light is characteristic of the material and not the incident energy.

At this stage it is important to distinguish between the two energy absorption steps. Firstly, there is the initial absorption of energy that gives rise to Stokes luminescence and populates the traps (referred to as the *initial* energy), and secondly there is that which depopulates the trap (the *stimulating* energy) and hence gives rise to stimulated luminescence. The luminescence takes place with a time constant ( $\tau_c$ ) characteristic of the material after the absorption of the initial energy and this parameter enables luminescence to be sub classified into two categories; *fluorescence*, where  $\tau_c < 10^{-8}$  s and *phosphorescence*, where  $\tau_c > 10^{-8}$  s (McKeever, 1988 from Garlick, 1949). Thus fluorescence can be considered to take place simultaneously with the excitation and

phosphorescence is characterised by a delay between the excitation and emission of luminescence. This delay can be from a few nano seconds up to greater than  $10^9$  years and thus requires the presence of some form of energy storage mechanism, such as a trap.

The long term phosphorescence results from the storage of the initial energy (e.g. radiation) by trapping of charge carriers. Luminescence generated by stimulated eviction of these trapped charge carriers by electromagnetic radiation and its application to dating techniques are the subjects of this thesis. Hence the name given to this phenomenon is *photostimulated luminescence (PSL)*. Although it is photo stimulation that is of interest, much of the background to this work has developed since the 1940's with research into phosphorescence (e.g. Jablonski, 1935; Randall and Wilkins, 1945a, b & c) and thermoluminescence (TL) (e.g. Halperin & Braner, 1960). Thus it is necessary to introduce these phenomena and their application to luminescence dating before introducing the potential of PSL to the dating problem.

## 1.2 - Historical Background

"I also brought it (a diamond) to some kind of Glimmering Light, by taking it to bed with me, and holding it a good while upon a warm part of my Naked Body" (Boyle, 1664).

This is one of the earliest scientific recordings of TL, presented by Robert Boyle in a paper read before the Royal Society on 28 October 1663 which expounded on his research into luminescence. This demonstrates that the phenomenon of TL is not a 20th century discovery, even though the vast majority of published work post dates the 1930's. Indeed there is some evidence (Becker, 1974) that medieval alchemists were aware that some minerals glowed faintly when heated in the dark.

Before the turn of the 20th century light detectors did not have enough sensitivity for phosphorescence and TL to be studied quantitatively. The main application of TL was

as a geological tool in mineral identification. The phenomenon itself was also of interest to physicists and chemists, as clearly demonstrated in a letter sent by Kelvin to Thompson in 1899, reproduced below. This may be one of the earliest discussions of the phenomenon of anti-stokes PSL.

Dear Thompson - I have looked in vain in Encyclopedias and text-books for something that every one doesn't know regarding the phosphorescence of luminous paint, Cantons phosphorus, etc...

(1) Can you tell me what is known regarding the effect of temperature? I find with little copper plates and a glass plate painted with Balmain's luminous paint that the warmth of my hand greatly increases the glow due to the previous illumination; and that, if of two similar plates, equally dosed with light, I keep one for an hour or two warmer by 10° or 20°C than the other, it glows more brightly than the other till it cools, and becomes darker than the other in a minute or two, when it is cold like the other. Hence it appears that the warmth causes the stored light to be given out faster. I suppose this is well known, but I haven't found it told anywhere that I can remember.

(2) Is there good information as to the excitement of ordinary phosphorescence by different parts of a homogenous spectrum? I have heard it said that the phosphorescent light may be of either shorter or longer period than the originating light. In Stokes' fluorescence he found the fluorescent light always of longer period than the originating.

(3) Do you know of Dewar's splendid phosphorescence of egg-shells and other ordinary solids at very low temperatures? Was it generated by incident light at the low temperature, and did it only appear brilliantly when the temperature was raised? I have been looking through the *Phil. Mag.* and can find nothing of it.

(4) Do you know what Edmond Becquerel did in respect of ultra-red radiation on phosphorescence? I remember him telling me of it or showing it to me a great many years ago, but I can't remember exactly what it was.

(5) Do you know anything of Stokes' experiments on the subject?

Yours very truly, Kelvin.

In his fourth point, Kelvin refers to Becquerel's work in luminescence. It was this work (trying to record luminescence from uranium using photographic emulsions) that led to the discovery of natural radiation in 1896. This discovery enabled Rutherford to use  $\alpha$  particles in his scattering experiment which led to the development of the Rutherford model of the atom in 1911, which in turn led to the Bohr model in 1913, the basis of

atomic physics, and it was with the theory of discrete energy levels for the electrons that luminescence phenomena could begin to be understood.

With the development of photomultipliers in the 1940's much greater sensitivity in light detection could be achieved. Thus the developments in both theory and instrumentation made quantitative analysis of the phenomenon possible, enabling application to the field of radiation dosimetry. According to Chen & Kirsh (1981), the first person to give an explanation of long time and temperature dependent phosphorescence was Jablonski (1935) . In 1945, Randall & Wilkins gave a series of papers to the Royal Society, presenting results from investigations into the origins and mechanisms of phosphorescence and laying the foundations of a theory of TL. This theory still forms the basis of the rate equations and dynamics of TL and phosphorescence used today (Chen & Kirsh, 1981; McKeever, 1988; Aitken, 1985). Refinements have been made continually since the presentation of these papers (e.g. Garlick and Gibson, 1948; Adirovitch, 1956; Halperin & Braner, 1960; and Visocekas, 1978), and are continuing as new aspects of the phenomena of luminescence (such as PSL) are explored.

In 1953 it was suggested (Daniels *et al*, 1953) that TL could be used as a dating tool in archaeology and geology on the premise that the natural TL from rocks is generated by radiation exposure from constituent radio-elements (i.e. uranium, thorium and potassium) within the materials. The resulting radiation dose (and hence TL signal) gradually built up over the lifetime of the material, and thus the age of the sample could in principle be established by measuring the acquired dose (as represented by TL intensity) and the annual dose rate. This insight established the concept of TL dating, however it was not until the discovery of natural TL from archaeological pottery (Kennedy & Knopff, 1960; Grögler *et al*, 1960) that real progress in establishing TL as an archaeological dating tool began. Subsequent to these discoveries, laboratories around the world began to develop the TL dating of ancient ceramics, including Oxford (Aitken *et al*, 1964; Aitken *et al*, 1968), Kyoto (Ichikawa, 1965), Wisconsin (Mazess & Zimmerman, 1966) and Denmark (Mejdahl, 1969).

It was not long after these beginnings in the development of TL dating before it was realised that for *any* heated material containing similar minerals to pottery, a date could be established which would give the time since the most recent heating of the sample. This extension was applied to burnt flint (Göksu *et al* , 1974) and thus other burnt stones (Mejdahl, 1983 and Sanderson *et al*, 1988), and also to volcanic lava (Wintle, 1973; Guérin & Valladas, 1980). As stated earlier, thermal energy is not the only means of stimulating luminescence from a sample, *light* can also be used to stimulate luminescence and thus (if a sample is exposed to light for long enough) parts of the luminescence signal can be removed (or *bleached*) from the sample. Hence sunlight is a means of resetting the TL 'clock' (formally the time since the last zeroing of the sample by heating) and thus it is possible to date wind blown and water lain sediments by TL (Wintle & Huntley, 1979; 1982). This extension to the dating of sediments opened up a whole new area for TL. However as more sediments were studied, problems associated with the zeroing mechanism (i.e. light rather than heat) became apparent. Laboratory simulations of bleaching of TL demonstrated the existence of a residual component which was not readily bleached, thus qualifying the assumption that the TL signal was totally zeroed upon deposition of the sediment (Wintle & Huntley, 1979; 1980). Consequently methods for circumventing this problem were explored, one of which lead to the *partial bleach method* (Wintle and Huntley, 1980). However, in 1985 a radically new approach to the dating of sediments was suggested in order to solve the problem of incomplete bleaching of the TL signal. This used a readout mechanism (photostimulation) that mimicked the zeroing mechanism (i.e. light), thus increasing the likelihood of total effective zeroing of the signal during sedimentary deposition. Thus, the first steps in the PSL dating of sediments were taken (Huntley *et al*, 1985).

Although the use of PSL was a new approach in dating of sediments, it would be a mistake to think that PSL work in the radiation dosimetry field was not instigated before 1985. Phototransferred TL (PTTL) had already been investigated for archaeological dating (Bailiff, 1976; Bowman, 1979), and the phenomenon of PSL was already established in solid state physics e.g. work on Beryllium Oxide in the 1950's (Albrecht & Mandeville, 1956) and was explored for dosimetric purposes in parallel to the

development of TL dating and dosimetry (Tochilin *et al*, 1969; Rhyner & Miller, 1970). Even before this infra red stimulated PSL dosimetry was used in the second world war in radium doped phosphors used as night sights, e.g. O'Brien (1948), Urbach (1948), Nail *et al* (1948), Shrader *et al* (1948).

### 1.3 - Perceived Advantages of Photostimulated Luminescence

As explained in the previous section, the rationale behind the use of optical stimulation in the work by Huntley *et al* (1985) was to use the same stimulating mechanism in the laboratory as the zeroing mechanism (i.e. light) for the sediments and wind blown sands during deposition. One problem with using TL for these samples is that part of the TL signal appears to be highly resistant to bleaching and as such provides a high background to the desired signal which can make interpretation of the TL signals problematic. However, optical stimulation has other advantages over TL which do not just apply to the field of sediment dating.

The recording of TL signals from mineral samples is a process which has many potential technical problems which can impose limitations on the measurement technique. There is interference due to black body radiation from the heater plate with high temperature signals; the problem of *spurious* TL from heat stimulated chemical changes and phase transformations (Aitken, 1985), the possible cracking of crystals on heating and subsequent release of trapped vapours, and the burning of contaminants of the sample disc; the problem of thermal contact between sample and temperature sensor, and the related problems of temperature gradients within the samples and also the problem of sample and heater plate oxidation. All of these are associated with the heating of the sample, and it may be reasonable to surmise that the substitution of a recording technique that does not involve heating (i.e. PSL) should eliminate these effects from measurements.

PSL also has advantages in its own right. TL is a destructive measurement. The glow curves are recorded at the expense of reducing the trapped charge population to zero

and thus removing the signal during the process of measurement. It is possible, in principle, to record a PSL signal without zeroing the signal. Potentially a measurable signal could be recorded whilst only reducing the trapped charge carrier populations by a fraction of a percent, given sufficient sample sensitivity. Repeated measurements of the signal *on the same sample* may then offer improved precision over that available on a single readout. Furthermore it may be possible for standard additive dose runs to be performed on single samples thus removing the need for normalisation and lowering the minimum sample size needed for dating. By varying stimulation wavelengths it may be possible to select particular sets of traps and even perhaps to record signals from traps that are deeper than those readily accessible by TL (as the TL resulting from these traps may be obscured by the black body radiation associated with the high temperatures that would be required to record the TL of these traps). Altogether, therefore, the precision, accuracy and age limits of PSL dating may offer improvements over TL.

However it must be realised that PSL may have a different suite of problems to counter these benefits. Some problems that can be immediately proposed are as follows. Sample orientation; interactions between inhomogeneities in the stimulating light beam and sample heterogeneities may lead to loss of precision. Similarly, instabilities in the illumination power may lead to random errors. Bleaching of the sample; it has been stated that the non destructive nature of PSL might lead to multiple readings of, and additive dose runs on, a single sample. However, in order to measure the luminescence signal, some of that signal must be removed (a direct corollary of the uncertainty principle). Whilst on a single measurement this may be negligible, the *cumulative* bleaching over a series of repeated measurements may be more significant and thus require systematic corrections. This and other potential systematic effects, for example long term stability under various stimulation schemes, remain to be evaluated. The range of applications may also be limited by the stimulation schemes used. For example, under synchronous detection it is necessary to isolate the detection and stimulation wavelengths. This may restrict the range of trap depths and materials that could be studied.

Thus, as with any analytical technique, PSL determination of absorbed radiation dose in dating materials and hence age holds many potential advantages and disadvantages. A thorough exploration of the mechanisms of the phenomenon and measurement techniques represents an important step in the development of dosimetric or dating methods. Possible areas for study include exploration of stimulation and emission characteristics, thermal stability of the measured signals, the dose response of the samples under study and sensitivity studies. Such studies are a prerequisite of reliable dating techniques.

#### 1.4 - Early Work in Photostimulated Luminescence

The exploratory work performed by Huntley *et al* in 1985 was performed using stimulation with the 514.5 nm line from an argon-ion laser, with emitted light being detected by a window centred on 400 nm defined by Corning 7-59 and 5-58 filters. The measurement technique used was to monitor the luminescence intensity resulting from continuous monochromatic exposure from the laser over a period of time, in effect observing the bleaching curve of the sample. The intensity of the luminescence signal was recorded for sediment samples of differing ages and the results showed that the signal indeed increased with age. Attempts were also made to measure the stored dose of a few samples by recording an integrated luminescence signal during fixed time intervals after the laser was switched on and constructing additive dose curves from separate subsamples. These results were compared to those calculated by the partial bleach TL method, showing some agreement with the results previously obtained.

This paper generated a lot of interest, leading to the start of PSL studies in other dating laboratories. Most of the work performed followed on from the techniques used by Huntley *et al*, namely continuous exposure from the 514.5 nm line from an argon-ion laser (Rhodes, 1988; Aitken & Smith, 1988; Godfrey-Smith *et al*, 1988; Smith, 1988 and Wheeler, 1988). The standard technique used for these early dating studies of quartz being to monitor the bleaching curve of the quartz during laser stimulation (Rhodes, 1988; Aitken & Smith, 1988 and Godfrey-Smith *et al*, 1988). As can be seen in these papers, the emphasis was on sediment dating applications without (at this stage)

exploring some of the other fundamental properties of the PSL phenomenon. An exception to this was the important work conducted by Hütt *et al* (1988). They began exploration of the excitation spectrum of potassium feldspar, using a xenon lamp and defining the excitation wavelengths with a monochromator (Hütt *et al*, 1988). They observed several excitation bands, including one in the infra-red region. This aroused a lot of interest which resulted in the adoption of broad band stimulation from infra-red LED's by other laboratories (e.g. Bailiff & Poolton, 1989, Duller & Wintle, 1991). An attempt to evaluate the trap depths was made, and the first model attempting to explain the observed excitation spectrum of potassium feldspar was proposed.

This project was defined and approved by the Science and Engineering Research Council (SERC) in 1987, and was started in the autumn of 1988 with the objectives of exploring spectroscopy and pulsed approaches. As shown above this project was started at the beginning of the work in PSL and represented an approach to the phenomenon that was not under detailed exploration. Some initial sediment samples had been dated in Canada and Oxford using the bleaching curve from quartz generated by continuous stimulation from the 514.5 nm line from an argon-ion laser. Other techniques and minerals were beginning to be explored (i.e. Zircon - Smith, 1988; Phosphorescence and Phototransfer - Wheeler, 1988) and there was also some exploration of the PSL excitation spectrum of feldspar and the mechanisms involved (Hütt *et al*, 1988).

### 1.5 - Project Aims

The aim of this project was to undertake an exploration into the origins and mechanisms governing the phenomenon of photostimulated luminescence in naturally occurring minerals (specifically feldspar) using spectroscopic and pulsed approaches. The principle objective is to place the phenomenon on a firm physical basis with a view towards its ultimate utilisation as a reliable archaeological dating tool.

The following sections present an introduction to the physical concepts behind luminescence in minerals including an extension of the TL rate equations, to include

photo stimulation and numerical solutions for continuous monochromatic stimulation. Practical stimulation techniques and their implementation are discussed together with a description of the instrumentation for excitation spectroscopy and pulsed measurements. Two sections discussing stimulation characteristics of alkali feldspars are followed by a treatment of the systematic effects that must be taken into account for dose evaluation using single aliquot methodologies. Finally, the status of dating methods based on these observations is discussed and areas requiring further attention are identified.

## 2 - Theoretical Background

Having introduced the concept of photostimulated luminescence and placed the development of this phenomenon as a dating tool into an historical context, it is now appropriate to expound on the theoretical considerations that apply to this particular project. In order to do this, an introduction to solid state physics and the band theory of solids will be laid down, to be followed by derivations of rate equations governing microscopic properties of the phenomena of phosphorescence and TL. Thereafter, an extension can be made to PSL by the addition of a term describing the photo stimulated release of trapped charge carriers, which will be derived from first principles. An example of a numerical technique to solve these rate equations will be demonstrated by the development of a simple computerised mathematical model, ending in a discussion of the applicability of solutions derived from this model to the more complex behaviour of real samples.

### 2.1 - The Band Theory of Solids

The aim of this section is to lay down the necessary introduction to the band theory of solids, define the terms used and to state relationships that will be required in the rest of this chapter. It is not intended to be a *complete* discussion of solid state physics, which can be found elsewhere (e.g. Kittel, 1986; Blakemore, 1985).

When considering the behaviour of electrons in a periodic atomic lattice, quantum mechanical considerations have to be taken into account. Each electron experiences a periodic potential, each potential well being centred on an ion core. Electrons are *fermions*, that is they obey the Pauli exclusion principle "*in a multi-electron atom there can never be more than one electron in the same quantum state*" (Eisberg & Resnick, 1985) and thus follow *Fermi-Dirac* statistics. The importance of this is that the solution of the Schrödinger wave equation for the electrons in a periodic lattice is a wave function whose boundary conditions are imposed by the periodicity of the lattice (for

an example of this the reader is directed to the *Kronig-Penney* model in which the periodic potential in an idealised system is approximated by a periodic square well potential). In a pure crystalline solid, the resulting wave functions of the electrons have discrete wavelengths and hence discrete energy states in order to propagate through the lattice. As electrons are fermions, there can only be one electron per energy state for each atom in the lattice and thus at absolute zero each available energy state will be filled by one electron from the ground state (the one with the lowest energy) to a maximum energy which is called the *fermi energy*. For temperatures above absolute zero there is a small probability that some of the electrons can have energies greater than the fermi energy, given by the Fermi-Dirac distribution.

At this stage it seems apparent that an electron can have any energy up to the fermi energy, however there is a second and very important implication of the effect of the periodic lattice upon the wave functions of the electrons, namely that the allowed energy states are grouped into sets, called *energy bands*, and separated by fixed energies referred to as *forbidden energy bands*. A practical demonstration of this effect is shown when Bragg reflection of the wave functions is considered. In a two dimensional array, each wave function has two solutions, one which propagates to the right, and one which propagates to the left. When half the wavelength becomes equal to an integer multiple of the interatomic spacing, the Bragg reflection condition is satisfied and thus the reflected wave interferes constructively with the original wave and a standing wave is formed (this is analogous to transverse vibrations in a light inextensible string). However, quantum mechanical waves differ from normal mechanical waves in that each time the Bragg condition is satisfied, two standing waves can be formed, one symmetric ( $\psi(+)$ ) and one asymmetric ( $\psi(-)$ ) resulting in a  $\pi/2$  phase difference between the two and can be represented by a cosine wave and a sine wave respectively. The probability density function ( $\rho$ ) of a particle gives the probability that the particle will reside in a certain location and is given by the square of the magnitude of the wave function as shown in equation <2.1> below.

$$\rho = |\psi|^2$$

$$\Rightarrow \rho(+)=|\psi(+)|^2 \propto \cos^2\left(\pi \frac{x}{a}\right) \quad <2.1>$$

$$\rho(-)=|\psi(-)|^2 \propto \sin^2\left(\pi \frac{x}{a}\right)$$

where  $a =$  interatomic spacing.

The result of this is that  $\rho(+)$  will tend to concentrate electrons on the positive ions centred at  $x = 0, a, 2a, \dots$  and  $\rho(-)$  will concentrate electrons away from the ion cores, as shown in Figure 2.1. At the positions of the ion cores the electrons experience minimum potential energy, whereas away from the ion cores the potential energy is

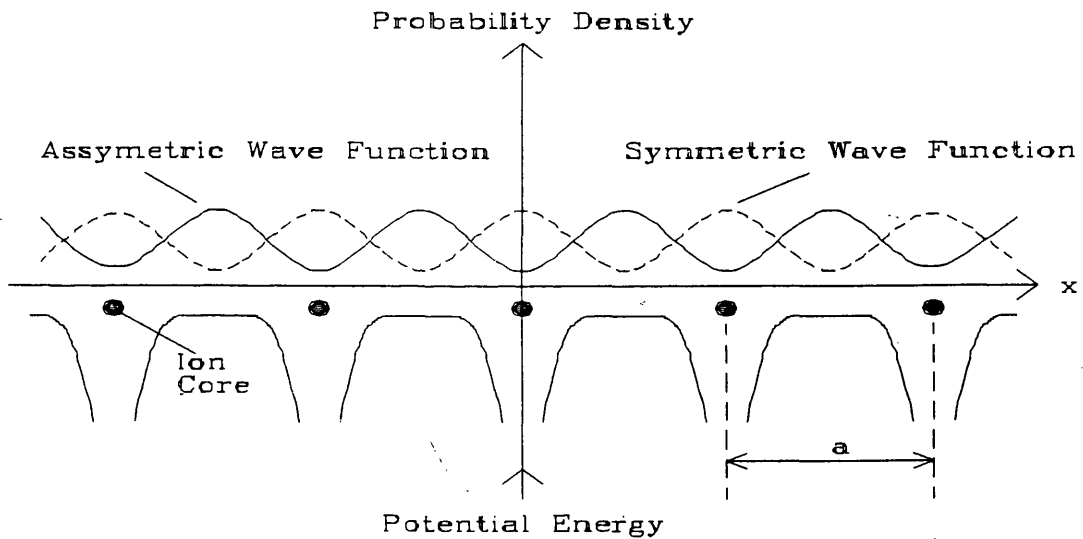


**Figure 2.1** - Variation in probability density function of the symmetric and asymmetric electron wave functions.

higher. Consequently the average potential energy for  $\rho(+)$  will be less than that for  $\rho(-)$  yielding an energy gap ( $E_g$ ) equal to the difference between the two. Thus the solutions to the wave equation for the electrons in a regular atomic array can have any discrete energy state up to that of  $\rho(+)$  and any energy state of  $\rho(-)$  and greater, but not in between.

The behaviour of the solid is dependent upon these energy bands. If the fermi energy is contained within a band so that there are allowed unoccupied energy states above the fermi energy, it is possible for electrons to acquire momentum by moving in to these energy states in an applied electric field and thus conduction occurs and the solid is a *conductor*. If the fermi energy resides between two energy bands, then all the energy states in the lower band will be filled, and none in the upper band and thus it will not be possible for the electrons to acquire momentum in an applied electric field and so conduction will not take place, the solid will be an *insulator*. If the energy gap between these two bands is very small, (i.e.  $\sim 0.1$  eV) then it is possible for thermal energy (even at room temperature) to promote the electrons into the upper, unoccupied, band thus permitting conduction resulting in a solid that is an insulator at absolute zero and a conductor at room temperature with the conductivity being dependent upon temperature. This is a *semiconductor*. In the case of insulators and semiconductors, the valence electrons (those in the outer shell of the atom and which give rise to the chemical properties of the atom) completely fill one band, the *valence band*, leaving the next band empty for conduction electrons and is thus referred to as the *conduction band*. The valence band and conduction band are separated by an energy known as the *band gap*.

The above discussion is based upon pure crystalline solids, however when naturally occurring crystalline structures are examined (especially for minerals), it is extremely unlikely (if not impossible) to find defect and impurity free solids, and indeed it is on these defects and impurities that the application of luminescence in this thesis depends. One assumption that will be made is that the density of impurity atoms and defects will be low when compared to the density of the atoms forming the crystalline matrix. This means that the energy bands will depend upon the crystalline matrix as before and maintain the same values as if the impurities / defects did not exist. The presence of impurities and defects will act as a local perturbation *at the site of the impurity or defect only*. Consequently, the allowed energy states of this perturbation are not restricted by the energy bands as the potential wells due to the lattice ions are different to that of the single impurity / defect site. Hence the wave function of the electron at such a site is governed not by a periodic potential, but by a single potential well. Consequently, the

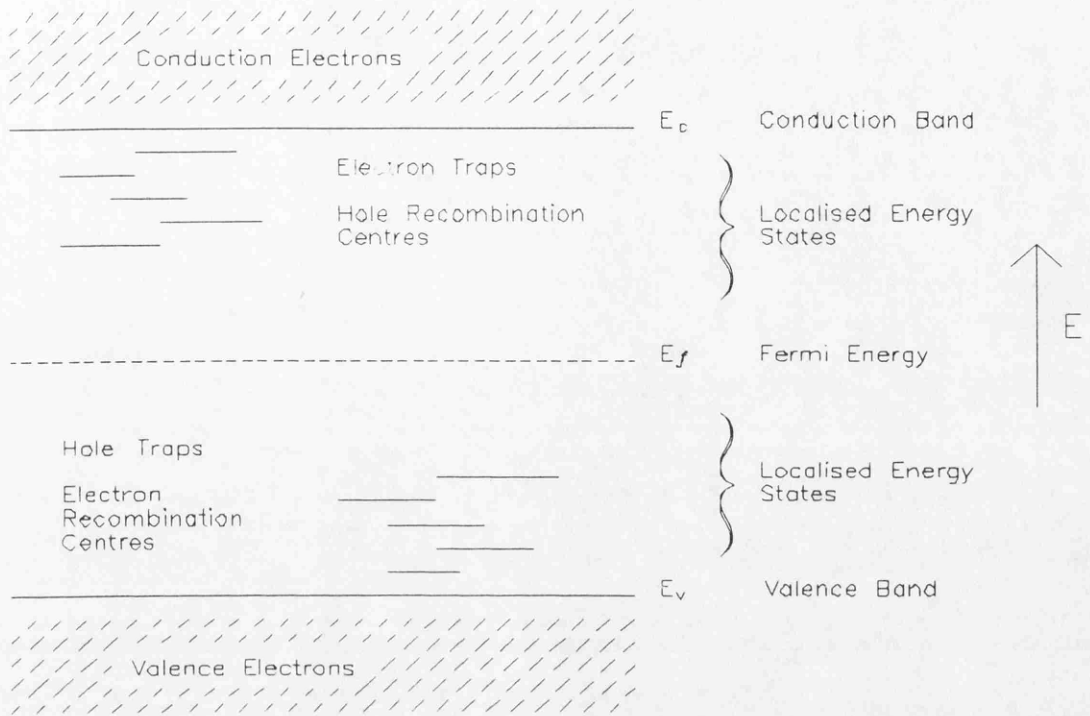


**Figure 2.2** - Energy bands and localised energy states within an insulator.

defect / impurity site can have allowed energy states within the band gap, above or below the fermi energy, and these are referred to as *localised energy states*. A term diagram showing the valence band, conduction band and localised energy states due to defects and impurities for an insulator can be seen in Figure 2.2.

The above discussion has been entirely in terms of electrons, however the absence of an electron (often referred to as a *hole*) can act as a positive charge carrier, and so two types of charge transport can be considered, electron and hole. Consequently the term 'electron' to represent a charge carrier will be avoided except to illustrate specific examples, and the term 'charge carriers' will be used instead. Having shown that the energy structure of insulators is controlled by bands separated by a band gap, and that defects and impurities can have localised energy states within this band gap, it is now possible to begin the exposition of the theory of stimulated luminescence.

## 2.2 - Thermal Stimulation

Although this project is primarily concerned with PSL and not TL, thermal stimulation can not be ignored since this contributes to luminescence at all temperatures greater than absolute zero. Consequently the theory of thermal stimulation must be comprehended before the concept of photo stimulation can be introduced. Thermal stimulation divides into two components, stimulation at constant temperature (known as phosphorescence) and stimulation with a temperature ramp (thermoluminescence).

### 2.2.1 - Phosphorescence

It is generally accepted that major progress in the development of the theory governing the processes of phosphorescence and TL was not made until 1945 with the work presented by Randall and Wilkins (Randall & Wilkins, 1945 a,b,c), although work in attempts to derive the theory had certainly started before then, for example see the work by Jablonski, 1935. The following exposition of the theories of phosphorescence and TL will be based on the same model as used by Randall and Wilkins and incorporates a single trapping site and a single recombination centre as shown in Figure 2.3. It must be remembered that even though *single* traps and centres are referred to, this is just a convenient way of referring to a single *type* of trap and centre. Each trap (centre) type will have a distribution of individual trapping *sites* (single defects or impurity ions) throughout the lattice and thus the following theory deals with *probabilities* of capture and eviction for a distribution of trapped charge carriers. As the trap is above the fermi energy, its initial electron population function must be zero. Likewise, as the centre is below the fermi energy, all available electron states must be occupied (McKeever, 1988). During irradiation, atoms in the valence band are ionized with electrons being promoted into the conduction band leaving holes behind. The charge carriers are then free to migrate around the relevant band until they encounter a free state at a lower energy level, be it the trap, the centre, the valence band (for the electron) or the conduction band (for the hole). Gradually the density of occupied states (the proportion of energy states occupied by an electron, hence the proportion of individual trapping sites occupied by an electron) in the trap will grow and that in the centre will decrease

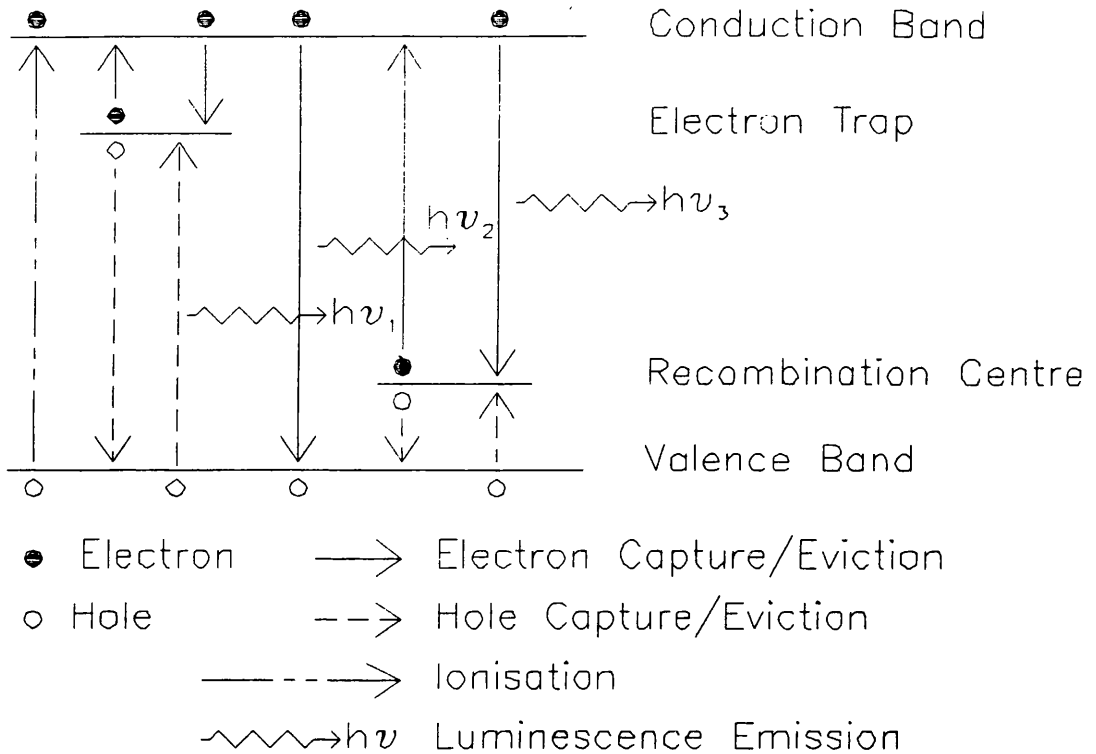


**Figure 2.3 - One trap / one centre luminescence model**

(i.e. the number of holes will grow). Once irradiation is removed, the trap and centre are no longer being filled with the relevant charge carriers and the system is left to recover back to its initial state, i.e. no electrons in the trap and no holes in the centre.

The lifetime of trapped charge carriers is dependent on the depth (the difference between the energy of a trapping state and the energy of edge of the relevant band) of the trap and the temperature. Charge carriers in a particular energy state and at a particular temperature have a distribution of energies governed by the Boltzmann distribution. This is a statistical distribution of energies and yields the probability that a particular charge carrier will have a particular energy. This probability is never zero and thus there is always a probability (albeit very small) that a charge carrier will have enough energy to be evicted from its trapping site even if the depth of the trap is much greater than the *average* energy of the trapped charge carriers. As the temperature is increased, so the average energy of the distribution of trapped charge carriers increases and the proportion of trapped charge carriers with enough energy to be evicted from the trap also increases. Once charge carriers are evicted thermally they are then free

to migrate around the relevant band until they again reach a lower free energy state and recombine, losing the excess energy by phonon (a quantum of the energy of lattice vibration) and photon (a quantum of electromagnetic energy) emission. It is this photon emission during relaxation of the charge carriers that is the luminescence signal.

Randall and Wilkins related the luminescence intensity simply to rate of change of electrons in the trap, assuming that all electrons evicted recombine in the centre, resulting in an analytical solution which is now termed first order kinetics. An analytical solution for the case where retrapping of the evicted electrons in the original energy states was solved by Garlick and Gibson (1948) and the solution for equal probability of retrapping and recombination in the centre is termed second order kinetics. Adirovitch (1956) introduced the use of a series of rate equations to account for charge carrier transport, and modern considerations of the theory tend to follow this path of the development of a family of rate equations, and it is in terms of the rate equations that the following theory will be discussed. These equations are simplified if one only considers the motion of the electrons, however it must be remembered throughout that whatever applies to electrons can also be applied to holes, albeit with differing probabilities and coefficients. Let us therefore consider the behaviour of trapped electrons;

The probability of eviction of electrons from a trap can be derived from thermodynamic considerations, using the *principle of detailed balance* with Shockley-Read statistics (Shockley & Read, 1952). For a detailed exposition of this approach, the reader is referred to Bräunlich, 1979.

Making the definitions;

- P = Probability of eviction of electrons from the trap per unit time ( $s^{-1}$ )
- E = Thermal trap depth (activation energy) (eV)
- v = Average thermal velocity of the electron in the conduction band ( $ms^{-1}$ )
- $\sigma$  = Capture cross section of electrons by the trap ( $m^2$ )
- N = Density of free states in the conduction band ( $m^{-3}$ )

T = Temperature of sample (K)

k = Boltzmann constant, =  $8.617 \times 10^{-5} \text{ eVK}^{-1}$

then it follows that the probability of thermal eviction of electrons from the trap to the conduction band is given by;

$$\begin{aligned} P &= \nu \sigma N e^{-\frac{E}{kT}} \\ &= s e^{-\frac{E}{kT}} \end{aligned} \quad <2.2>$$

where s is termed the frequency factor.

Likewise defining;

$A_T$  = Capture coefficient of electrons by the trap per unit time ( $\text{m}^3\text{s}^{-1}$ ) (In effect the probability of capture of electrons by the trap)

then the capture coefficient of the charge carriers by a trap is given by;

$$A_T = \nu \sigma \quad <2.3>$$

Hence the total rate of change of density of electrons,  $n$ , within a trap is given by;

$$\begin{aligned} \frac{dn_T}{dt} &= \text{capture} - \text{eviction} \\ &= A_T n_{cb} (N_T - n_T) - P_T n_T \end{aligned} \quad <2.4>$$

where

$N_T$  = Density of free states in the trapping sites ( $\text{m}^{-3}$ )

$n_T$  = Density of electrons in trap ( $\text{m}^{-3}$ )

$n_{cb}$  = Density of free states in the conduction band ( $\text{m}^{-3}$ )

Taking account of the motion of the holes and the rates of change of charge carriers in the centre, conduction band and valence band, we now get a system of four coupled differential equations thus;

$$\frac{dn_T}{dt} = A_T n_{cb} (N_T - n_T) + p'_T (N_T - n_T) - p_T n_T - A'_T n_v n_T \quad <2.5>$$

$$\frac{dn_c}{dt} = A'_c n_v (N_c - n_c) + p_c (N_c - n_c) - n_{cb} n_c A_c - p'_c n_c \quad <2.6>$$

$$\frac{dn_{cb}}{dt} = p_T n_T + p_c (N_c - n_c) - A_T n_{cb} (N_T - n_T) - n_{cb} n_c A_c - n_{cb} n_v A_v \quad <2.7>$$

$$\frac{dn_v}{dt} = p'_c n_c + p'_T (N_T - n_T) - A'_c n_v (N_c - n_c) - n_v n_T A'_T - n_{cb} n_v A_v \quad <2.8>$$

where the primed variables A and p refer to hole capture coefficients and eviction probabilities respectively.

Assuming that the lifetime of free charge in the conduction band is very much less than trapped charge, and that holes do not contribute to the signal, the luminescence intensity is proportional to the rate of capture of electrons by the centre which is equal to the rate of change of the centre hole population thus;

$$I \propto - \frac{dn_c}{dt} \quad <2.9>$$

If we now assume that the probability of retrapping (electrons relaxing to the trapping state from which they were evicted in the first place) is zero, all of the charge evicted from the trap must end up relaxing to the centre. Thus we get the following simplification;

$$A_T = A'_c = p_c = p'_T = A'_T = 0$$

$$\Rightarrow \frac{dn_c}{dn_t} = \frac{dn_T}{dn_t}$$
<2.10>

and thus equation <2.9> becomes

$$I = p_T n_T$$

$$= n_T s e^{-\frac{E}{kT}}$$
<2.11>

which is the same result for first order kinetics obtained from general considerations that Randall and Wilkins obtained without first deriving the coupled rate equations.

Introducing retrapping into the rate equations, whilst still ignoring contributions from hole transport, equations <2.5> - <2.8> can be solved to yield the result;

$$I = \frac{n_T^2 s e^{-\frac{E}{kT}}}{RN_T}$$
<2.12>

with  $R = \frac{A_T}{A_c}$

where R is the retrapping ratio. In the special case where R = 1, i.e. equal probability of retrapping as capture by the centre, equation <2.12> becomes

$$I = n_T^2 s' e^{-\frac{E}{kT}}$$
<2.13>

with  $s' = \frac{s}{N_T}$

which is the same result for second order kinetics that Garlick and Gibson (1948) derived, again without using a set of coupled rate equations. It must be remembered

equations <2.5> - <2.8> can only yield the analytical solutions shown in equations <2.11> and <2.13> if the assumptions about retrapping rates, relative charge concentrations and relative rates of change of charge carrier populations are made. If these assumptions are not made, then the equations have to be solved numerically, and this has been done by several people including McKeever & Chen (1980) and McKeever *et al* (1980). Also, it must be remembered that the kinetics described here only apply to the case of single traps and centres. As more traps and centres are introduced to the equations, if they interact in any way, then the equations become more complex as demonstrated by Levy (1983 & 1985). However, of course, numerical solutions to the rate equations are hampered by the number of variables that need to be known, consequently there will be occasions when the simplified analytical solutions are more applicable.

### 2.2.2 - Thermoluminescence

Having established the equations describing the various kinetic orders of phosphorescence, applying conditions of a linear heating ramp to these equations yields an equation describing the shape of a thermoluminescence glow peak. Looking at first order kinetics and applying a linear heating rate of  $\beta$  °Cs<sup>-1</sup> to equation <2.11> we get;

$$I = n_0 s e^{-\frac{E}{kT}} \quad \langle 2.14 \rangle$$

with  $\beta = \frac{dT}{dt}$

integrating this then yields

$$I(T) = n_0 s e^{-\frac{E}{kT}} \exp \left[ -\frac{s}{\beta} \int_{T_0}^T e^{-\frac{E}{kT}} dT \right] \quad \langle 2.15 \rangle$$

which is the expression as derived by Randall & Wilkins (1945a, b) for a first order TL glow peak. Similarly, a linear heating rate can be applied to equation <2.13> to derive the expression for a second order glow peak thus;

$$I(T) = \frac{n_0^2 s' e^{-\frac{E}{kT}}}{\left[ 1 + n_0 \frac{s'}{\beta} \int_{T_0}^T e^{-\frac{E}{kT}} dT \right]^2} \quad <2.16>$$

as laid out by Garlick and Gibson (1948). These integrals can be solved analytically, however numerical solutions (approximations) may be used to calculate peak shapes. Such computed solutions to these equations show that first order glow peaks are asymmetric in nature with the majority of the signal being emitted on the low temperature side of the peak maximum, whereas second order glow peaks are much more symmetrical, as the retrapping of the electrons effectively delays their

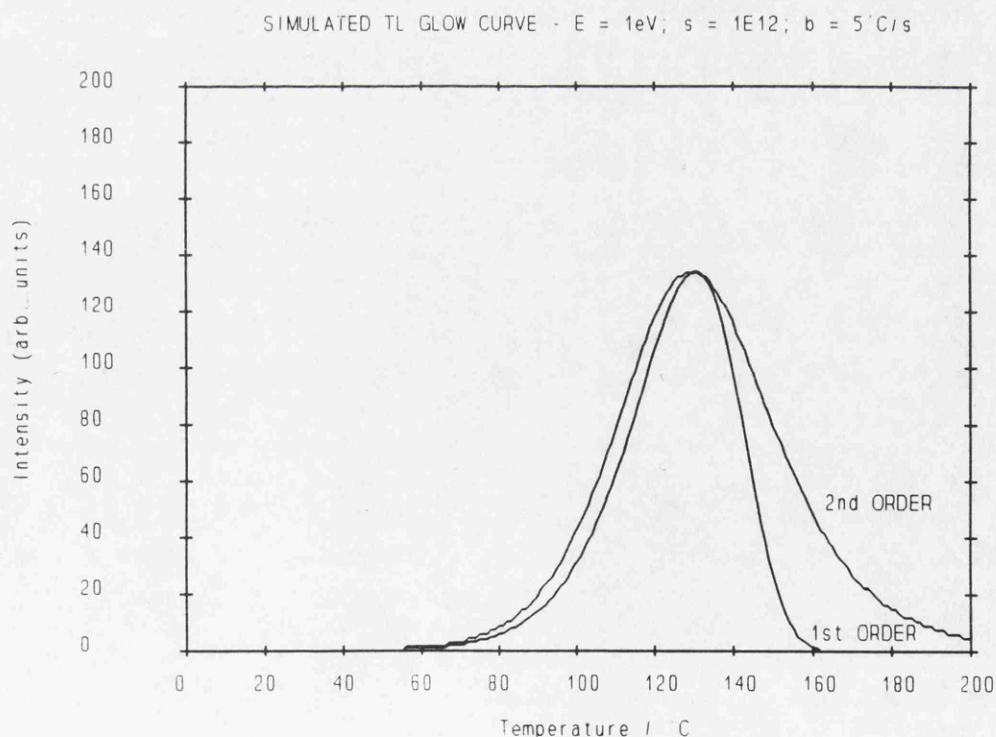


**Figure 2.4** - Computed first and second order TL glow curves

recombination and thus delays more of the signal to the high temperature side of the peak maximum. Computed first order and second order glow curves with coincident peak maxima can be seen in Figure 2.4.

If we consider the first order equation <2.15>, at temperatures close to the initial temperature ( $T_0$ ) the integral is close to zero, and thus the second exponential term of the equation tends to 1, leaving us with the equation

$$I \propto e^{-\frac{E}{kT}} \quad \text{for } T \approx T_0 \quad <2.17>$$

Thus for the *initial rise* of the glow peak (i.e. where T is very close to  $T_0$ ), we get that the natural log of the intensity is proportional to  $1/kT$  thus

$$\text{Ln}(I) \propto -\frac{E}{kT} \quad <2.18>$$

as shown by Garlick & Gibson (1948). Thus a plot of  $\text{Ln}(I)$  against  $1/T$  or  $1/kT$  (known as the 'Arrhenius plot') will yield a straight line with the gradient equal to  $-E/k$  or  $-E$  respectively. This is true for the initial rise portion of the glow peak irrespective of the order of kinetics (Chen & Kirsh, 1981) and this forms the basis of the *initial rise method* of evaluating the parameter E. This theory only applies to the initial rise to a single well defined peak, the initial rise to a multipeak glow curve does not necessarily imply that it is the initial eviction of charge carriers from a single trap that is being observed. In order to evaluate the activation energies of the various components of a multi trap and hence peak glow curve, the initial rise technique has to be modified in order to try and ensure that the initial rise being observed is in fact due to only a single trap. This modification is known as the *fractional glow* method. In this method the luminescence is recorded up to a temperature, T, well below that of the expected first peak maximum. The sample is then allowed to cool and is then heated to a slightly higher temperature. This cycle is repeated until eventually the maximum temperature reached is the same as that for a normal glow curve. This process thus removes charge carriers from successively deeper traps as the maximum temperature of each ramp is

increased and thus the luminescence signal on each ramp represents the initial eviction of charge from the corresponding traps. If the difference between the maximum temperatures on successive heatings is small then the luminescence signal on each rise should be due to only one trap, and thus the initial rise technique can be applied to each of the temperature ramps in order to derive the activation energies of the spectrum of traps under examination. An application of this technique can be found in Sanderson (1982 & 1987) and Strickertsson (1985).

### 2.3 - Photostimulated Luminescence

As stated in section 2.2, at temperatures above absolute zero there will always be thermal energy present to excite the trapped charge carriers, and so equations <2.5> - <2.8> will always apply. However, in the case of photostimulation, a photo eviction probability can be added into the system of equations. It is proposed that the photo eviction probability may be derived as follows:

Making the definitions;

- $P(\lambda)$  = Probability of charge carrier eviction when stimulated by light of a wavelength  $\lambda \pm \delta\lambda$  per unit time ( $s^{-1}$ ).
- $\Phi(\lambda)$  = Total incident photon flux at wavelength  $\lambda \pm \delta\lambda$  per unit area, per unit time ( $m^{-2}s^{-1}$ ).
- $\sigma(T,\lambda)$  = Photo eviction cross section at wavelength  $\lambda \pm \delta\lambda$  and temperature T ( $m^2$ ).

It follows that the probability of photo eviction of a charge carrier from a single trapping site is proportional to the total photon flux incident upon it, and also proportional to the photo eviction cross section, thus;

$$P(\lambda) = \Phi(\lambda) \sigma(T, \lambda) \quad <2.19>$$

Hence, as with thermal eviction, the total photo eviction rate is given by

$$\text{Eviction Rate} = n_T P(\lambda) \quad <2.20>$$

Once this term is added to equations <2.5> to <2.8> there are two eviction mechanisms for the trapped charge carriers, thermal and photo eviction. If the temperature is low with respect to the trap depth, then under photo excitation, photo eviction will dominate, however if the temperature is high with respect to the trap depth then thermal eviction will dominate. These rate equations only hold true (as with pure thermal stimulation) for a single trap and centre model and for no interaction between thermal and optical eviction. If there is any such interaction (e.g. a two stage eviction process involving thermal and photo eviction), or more than a single trap and centre, then these equations must be extended.

If one now pauses to consider photo eviction alone, then equation <2.19> can be developed further. Making the following definitions;

- $\mu(\lambda)$  = Photo absorption coefficient at wavelength  $\lambda \pm \delta\lambda$  ( $m^{-1}$ )
- A = Sample area ( $m^2$ )
- x = Trapped charge carrier depth beneath the illuminated surface (m)
- X = Sample thickness (m)
- $I_r$  = The interaction rate from the total volume being stimulated ( $s^{-1}$ )

Taking into account optical attenuation of the photon flux through the sample, the total interaction rate in a section of area A and thickness  $\delta x$  at a depth x is given by;

$$I_r(x) = \sigma(T, \lambda) A n_T \Phi(\lambda) e^{-\mu(\lambda)x} \delta x \quad <2.21>$$

Hence the total interaction rate from the entire sample is given by;

$$\begin{aligned}
I_r &= \lim_{\delta x \rightarrow 0} \sum_{x=0}^x A n_T \sigma(T, \lambda) \Phi(\lambda) e^{-\mu(\lambda)x} \delta x \\
&= A n_T \int_0^x \sigma(T, \lambda) \Phi(\lambda) e^{-\mu(\lambda)x} dx \quad <2.22> \\
\Rightarrow I_r &= \frac{A n_T \sigma(T, \lambda) \Phi(\lambda)}{\mu(\lambda)} [1 - e^{-\mu(\lambda)x}]
\end{aligned}$$

If one now assumes a fixed radiative recombination probability ( $p_r$ ), then the *detected* intensity,  $I$ , is given by;

$$I(\lambda) = \frac{Q(\lambda) A \Phi(\lambda)}{\mu(\lambda)} [1 - e^{-\mu(\lambda)x}] p_r n_T \sigma(T, \lambda) \quad <2.23>$$

where  $Q(\lambda)$  is the detector quantum efficiency at wavelength  $\lambda$ . The above equation can be rearranged thus;

$$p_r n_T \sigma(T, \lambda) = \frac{I(\lambda) \mu(\lambda)}{Q(\lambda) \Phi(\lambda) A [1 - e^{-\mu(\lambda)x}]} \quad <2.24>$$

Hence, if the optical absorption coefficients, quantum efficiencies and photon flux across the spectral excitation range are known, excitation spectra could be transformed to give an indication of the microscopic properties of the sample, namely the populated trap densities and the trap photo eviction cross sections.

If one now takes into consideration the emitted photons, then again these photons will be attenuated through the sample. Also these photons will be emitted over a  $4\pi$  solid angle, however the detector will only see  $2\pi$ . Consequently a term describing the attenuation of the *emitted* photons through the sample before travelling through the air to the detector would have to be introduced into equation <2.22>

## 2.4 - One Trap / One Centre Model

Having derived rate equations for both thermal and photo stimulation of the one trap / one centre model, it is possible to combine them in a set of four coupled differential equations, as shown below, as an example of how rate equations can be assembled for this model;

$$\frac{dn_{cb}}{dt} = G + p_T n_T + p_c (N_c - n_c) + p_{oT} n_T + p_{oc} (N_c - n_c) - n_{cb} (N_T - n_T) A_T - n_{cb} n_c A_c - n_{cb} n_v A_v \quad <2.25>$$

$$\frac{dn_T}{dt} = A_T n_{cb} (N_T - n_T) + p'_T (N_T - n_T) + p'_{oT} (N_T - n_T) - p_T n_T - p_{oT} n_T - A'_T n_v n_T \quad <2.26>$$

$$\frac{dn_c}{dt} = n_v (N_c - n_c) A'_c + p'_c (N_c - n_c) + p'_{oc} (N_c - n_c) - n_{cb} n_c A_c - p'_c n_c - p'_{oc} n_c \quad <2.27>$$

$$\frac{dn_v}{dt} = G + p'_c n_c + p'_{oc} n_c - n_v (N_c - n_c) A'_c - n_v n_T A'_T - n_{cb} n_v A_v + p'_T (N_T - n_T) + p'_{oT} (N_T - n_T) \quad <2.28>$$

where

$n_{cb}$  = density of electrons in the conduction band ( $m^{-3}$ )

$n_T$  = density of electrons in the trap ( $m^{-3}$ )

$n_c$  = density of holes in the centre ( $m^{-3}$ )

$n_v$  = density of holes in the valence band ( $m^{-3}$ )

$N_T$  = density of electron states in the trap ( $m^{-3}$ )

$N_c$  = density of hole states in the centre ( $m^{-3}$ )

$p_T$  = probability of thermal eviction of an electron from the trap ( $s^{-1}$ )

$p_{oT}$  = probability of photo eviction of an electron from the trap ( $s^{-1}$ )

$p_c$  = probability of thermal eviction of electron from the centre ( $s^{-1}$ )

$p_{oc}$  = probability of photo eviction of an electron from the centre ( $s^{-1}$ )

$A_T$  = capture coefficient of electrons by the trap ( $m^3 s^{-1}$ )

$A_c$  = capture coefficient of electrons by the centre ( $m^3 s^{-1}$ )

and the primed variables  $p$  refer to probabilities of hole eviction, and the primed variables  $A$  refer to the capture coefficients for holes.

and lastly,

$G$  = the electron - hole pair generation rate whilst under irradiation, and is given by;

$$G = \frac{Dm}{we} \quad <2.29>$$

where

$D$  = the radiation dose rate /  $\text{Gys}^{-1}$

$m$  = mass of the sample / kg

$w$  = the average ionisation potential / eV

$e$  = charge on the electron =  $1.6 \times 10^{-19}$  C

The resulting luminescence will be generated by the radiative relaxation of evicted charge to a lower energy level. Assuming that the energy given up in retrapping is by a phonon based process, this means the relaxation of electrons from the conduction band to the centre, the relaxation of electrons from the conduction band to the valence band and the relaxation of holes from the valence band to the trap, albeit with differing probabilities. Thus the intensity is given by;

$$I = n_{cb}n_cA_cP_r + n_{cb}n_vA_v + n_vn_T A_T'P_r' \quad <2.30>$$

where  $P_r$  = probability that the capture of an electron by the centre is radiative

$P_r'$  = probability that the capture of a hole by the trap is radiative

the energy lost in the capture of an electron from the conduction band by the valence band is great enough so that the energy lost must be by a radiative process.

In more realistic cases, the number of differential equations has to be increased in order to describe the variation in population density of each trap and recombination centre. Thus a case of three traps and three recombination centres would lead to a set of eight coupled first order differential equations. The model presented here can by no means

be described as realistic, however solutions to this model may be able to provide indications of the behaviour of a simple system which can be taken into consideration when examining more complex systems. A major problem with numerical solutions of the equations described above is the number of variables required. Many of the variables can not be determined by TL analysis alone, and many may well be inextricably linked so that individual values may not be measurable. Consequently it may be a straightforward step to extend the model to a more realistic scenario, however confidence in the applicability of the chosen variables to a real system and interpretation of the results must fall as the number of variables increases. Certainly developing such realistic models and producing and interpreting results of such a model could easily be many years' work in its own right, and thus is outside the scope of this project.

In order to solve the one trap / one centre model described above, a numerical solution is necessary, and thus a computer program was written using a fourth order Runge-Kutta predictor corrector method. All charge carrier transitions were considered, for

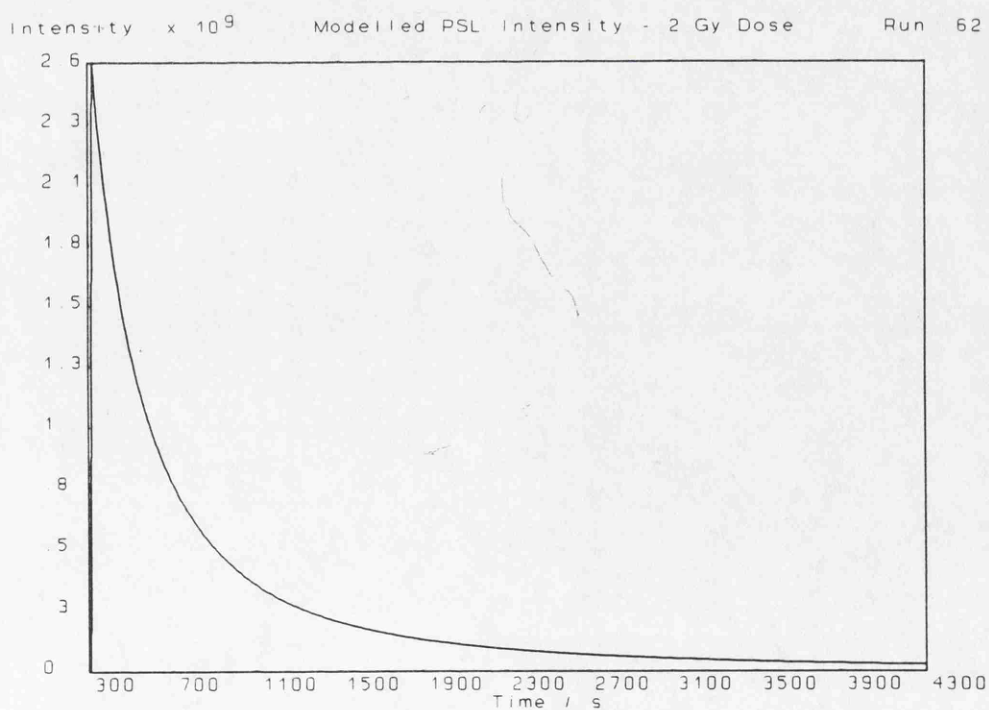


**Figure 2.5 - Modelled bleaching Curve**

completeness, even if the relevant probabilities were almost zero. One of the most important points about this was that it meant that the retrapping of charge was taken into full consideration. An example of the resulting simulated bleaching curves can be seen in Figure 2.5. Various simulations were performed including variations with photon eviction coefficient, electron capture coefficient and dose, the results of which can be seen in the following sections.

#### 2.4.1 - Variation in Modelled Bleaching Curves with Photon Eviction Coefficient

A series of bleaching curves were simulated by the model whilst varying the photon eviction cross section of the electron in the trap. This represents either variations in photo stimulating power or the ability of different wavelengths to evict the trapped electrons. All other variables including the centre and trap capture coefficients and the

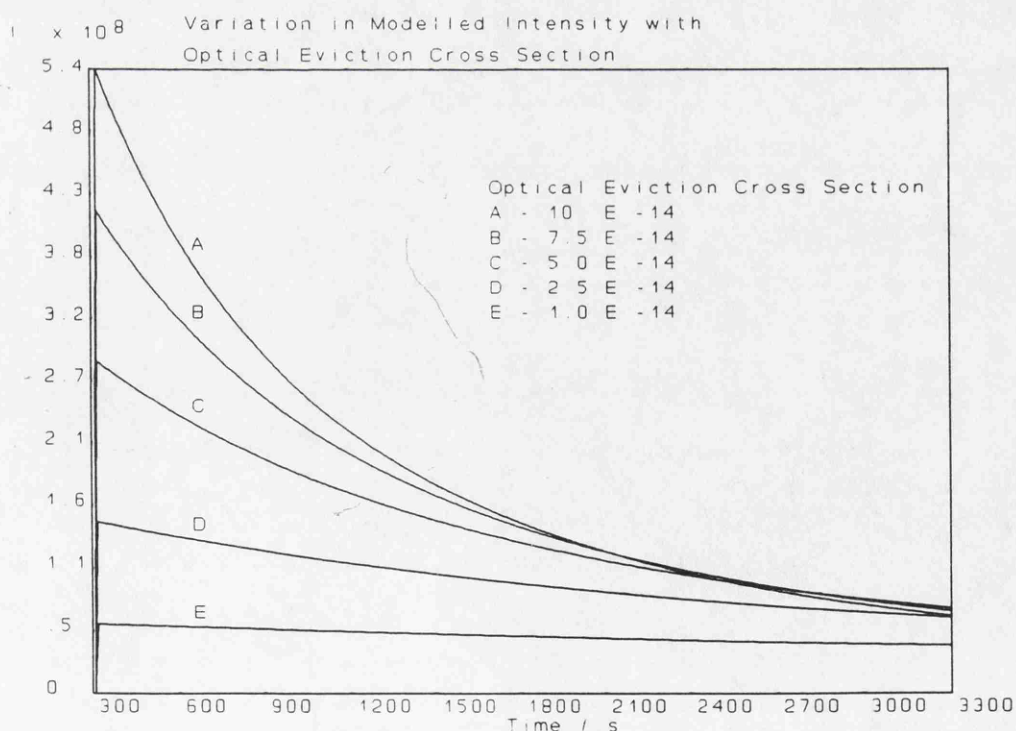


**Figure 2.6** - Variation in the Modelled Bleaching Curve with Photo Eviction Cross Section

sample temperature were held constant. The results can be seen in Figure 2.6 and the constant parameters used in the simulations can be seen in Box 1. As is obvious from the graph, as the photo eviction cross section is varied, so the dynamics of the bleaching curve vary. This behaviour is to be expected and can be explained as follows; the intensity is dependent upon the number of electrons recombining in the centre,

Frequency Factors :	Electron in Trap	$1 \times 10^{13} \text{ s}^{-1}$
	Electron in Centre	$1 \times 10^{13} \text{ s}^{-1}$
	Hole in Trap	$1 \times 10^{13} \text{ s}^{-1}$
	Hole in Centre	$1 \times 10^{13} \text{ s}^{-1}$
Capture Coefficients :	Electron by Trap	$1 \times 10^{-15} \text{ m}^3\text{s}^{-1}$
	Electron by Centre	$1 \times 10^{-14} \text{ m}^3\text{s}^{-1}$
	Electron by Valence Band	$1 \times 10^{-15} \text{ m}^3\text{s}^{-1}$
	Hole by Trap	$1 \times 10^{-15} \text{ m}^3\text{s}^{-1}$
	Hole by Centre	$1 \times 10^{-15} \text{ m}^3\text{s}^{-1}$
Densities of States :	Conduction Band	$6 \times 10^{22} \text{ m}^{-3}$
	Valence Band	$6 \times 10^{22} \text{ m}^{-3}$
	Trap	$1 \times 10^{15} \text{ m}^{-3}$
	Centre	$1 \times 10^{15} \text{ m}^{-3}$
Energies :	Trap Depth	1.2 eV
	Hole Depth	4.0 eV
	Band Gap	8.0 eV
	Work Function	10 eV
Probabilities :	Radiative Electron Recombination	= 1
	Radiative Hole Recombination	= 1
Miscellaneous :	Dose Rate	$7 \times 10^{-3} \text{ Gys}^{-1}$
	Dose Time	200 s
	Hence Dose	1.4 Gy
	Sample Mass	$1 \times 10^{-6} \text{ Kg}$
	Sample Thickness	$5 \times 10^{-4} \text{ m}$
	Sample Area	$1 \times 10^{-4} \text{ m}^2$
	Sample Temperature	284 K
	Absorption Coefficient	$1000 \text{ m}^{-1}$
	Photon Flux	$3 \times 10^{19} \text{ m}^{-2}\text{s}^{-1}$

**Box 1 - Constant Parameters for the simulations shown in Figure 2.6**

which in turn is dependent upon the capture coefficient and the number of electrons in the conduction band at that particular time. For a constant centre electron capture coefficient the intensity in this model becomes dependent solely upon the number of electrons in the conduction band. As the photo eviction cross section (and thus probability of photo eviction) increases for a given population of trapped electrons, the number evicted to the conduction band and thus recombining in the centre to yield luminescence will increase as the expected number of evicted electrons is simply the product of the eviction probability and the population of trapped electrons. Consequently the initial luminescence signal is greater with increased eviction cross section, however as more electrons are evicted from the trap to the conduction band, the population of electrons falls at a greater rate and hence the rate of reduction in evicted electrons and thus intensity is also increased, thus resulting in a steeper bleaching curve as can be seen in Figure 2.6.

#### 2.4.2 - Variation in Modelled Bleaching Curves with Electron Capture Coefficient

Following on from simulations of this model with varying photo eviction cross section, a set of simulations were compiled varying the capture coefficient of electrons by the recombination centre, with all other variables being held constant. The resulting simulations can be seen in Figure 2.7 and the constant parameters used in these simulations can be seen in Box 2. As can be seen, the variation in the modelled bleaching curves with the centre electron capture coefficient behaves in a similar fashion to the variation with photo eviction probability as shown in Figure 2.6. This is not unexpected and can be explained in the following manner; as the centre electron capture coefficient increases, the ability of the centre to capture electrons as compared to the trap increases, i.e. the order of kinetics falls. This means that the net rate of transfer of electrons from the trap to the centre increases with centre capture coefficient in a similar manner to the increase with trap eviction probability. The number of electrons recombining in the centre (and hence intensity) is dependent upon the number promoted to the conduction band at any particular time and this in turn is dependent upon the trap eviction probability and the number of trapped electrons. Hence the PSL

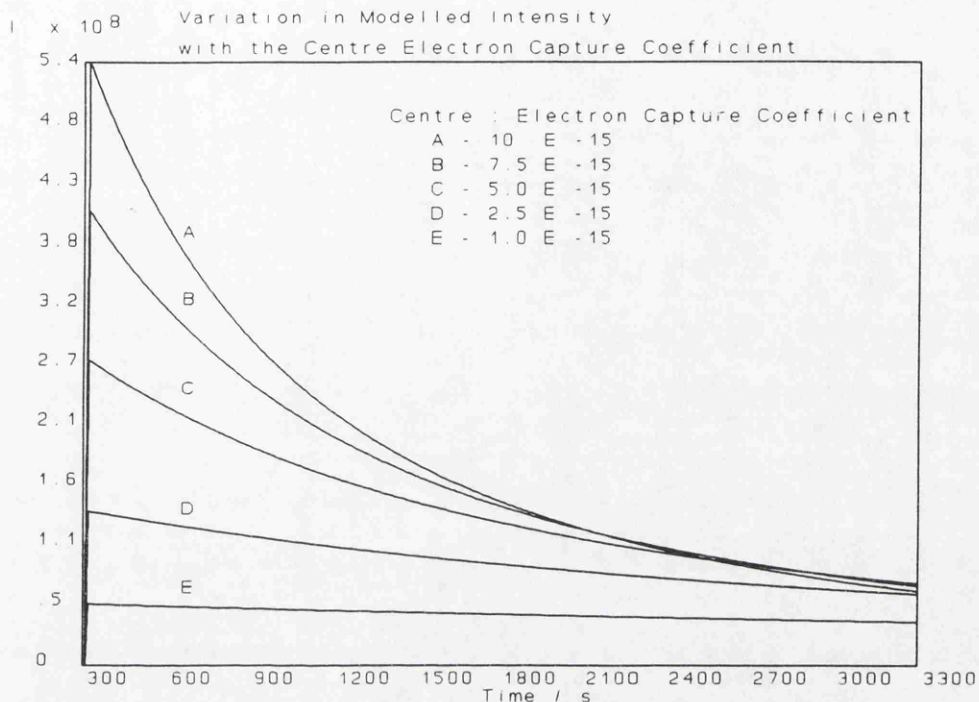


**Figure 2.7** - Variation in modelled bleaching curve with electron capture coefficient of the centre

intensity is directly dependent upon the trapped charge population for a fixed eviction probability.

It has already been stated that an increase in the centre electron capture coefficient results in an increase in the rate of transfer of electrons from the trap to the centre, hence the rate of decrease of the trapped electron population will also increase. Consequently (as with the case for the variation with eviction cross section) the initial intensity will be greater as more electrons recombine in the centre for a given number evicted to the conduction band, however the rate of decrease of the trapped electron population and thus rate of decrease in the number recombining in the centre (and hence intensity) is also greater. Thus with increased centre electron capture coefficient the bleaching curve should show a greater initial intensity with a faster fall of in intensity with time. This is clearly shown in Figure 2.7.

Frequency Factors :	Electron in Trap	$1 \times 10^{13} \text{ s}^{-1}$
	Electron in Centre	$1 \times 10^{13} \text{ s}^{-1}$
	Hole in Trap	$1 \times 10^{13} \text{ s}^{-1}$
	Hole in Centre	$1 \times 10^{13} \text{ s}^{-1}$
Photo Eviction Cross Section :	Electron in Trap	$1 \times 10^{-13} \text{ m}^2$
Capture Coefficients :	Electron by Trap	$1 \times 10^{-15} \text{ m}^3 \text{ s}^{-1}$
	Electron by Valence Band	$1 \times 10^{-15} \text{ m}^3 \text{ s}^{-1}$
	Hole by Trap	$1 \times 10^{-15} \text{ m}^3 \text{ s}^{-1}$
	Hole by Centre	$1 \times 10^{-15} \text{ m}^3 \text{ s}^{-1}$
Densities of States :	Conduction Band	$6 \times 10^{22} \text{ m}^{-3}$
	Valence Band	$6 \times 10^{22} \text{ m}^{-3}$
	Trap	$1 \times 10^{15} \text{ m}^{-3}$
	Centre	$1 \times 10^{15} \text{ m}^{-3}$
Energies :	Trap Depth	1.2 eV
	Hole Depth	4.0 eV
	Band Gap	8.0 eV
	Work Function	10 eV
Probabilities :	Radiative Electron Recombination	= 1
	Radiative Hole Recombination	= 1
Miscellaneous :	Dose Rate	$7 \times 10^{-3} \text{ Gys}^{-1}$
	Dose Time	200 s
	Hence Dose	1.4 Gy
	Sample Mass	$1 \times 10^{-6} \text{ Kg}$
	Sample Thickness	$5 \times 10^{-4} \text{ m}$
	Sample Area	$1 \times 10^{-4} \text{ m}^2$
	Sample Temperature	284 K
	Absorption Coefficient	$1000 \text{ m}^{-1}$
	Photon Flux	$3 \times 10^{19} \text{ m}^{-2} \text{ s}^{-1}$

**Box 2 - Constant parameters used in the simulations shown in Figure 2.7**

### 2.4.3 - Variation in Modelled Bleaching Curve with Dose

A series of bleaching curves were simulated as resulting from doses of 0.2 to 1.4 Gy and the resulting curves can be seen in Figure 2.8 with the constant parameters used being shown in Box 3. As can be seen from this graph, at no point in time along these bleaching curves is the dose response linear as the curves are non parallel in nature. This can be seen more easily if the ratios of the bleaching curves are taken with one curve, as shown in Figure 2.9.

These results would tend to suggest that a dose response (or growth curve) measured at any single point along the bleaching curve would not only yield a non linear response, but in an unpredictable way depending not only upon dose, but also upon all of the parameters involved. Perhaps the only part of the bleaching curve that is predictable is the initial intensity, a simple thought experiment can indicate this: the intensity is proportional to the number of (for example) electrons in the conduction band and the number of holes in the centre, with the number of electrons in the conduction band at any one time being dependent upon the number of electrons in the trap. Both electron and hole centre populations are proportional to dose, leading to a paradoxical quadratic dose dependence in their product. The only reliable way of achieving a linear dose response curve would be to interrogate the entire trapped charge population (as is the case in TL) by evicting the entire population which in practice would mean reducing the bleaching curve to zero and integrating the response over the entirety of the curve. This is demonstrated in Figure 2.10 and Figure 2.11 which show the response integrated over increasing times, note the supralinearity at low doses in Figure 2.10 which has almost entirely disappeared in Figure 2.11.

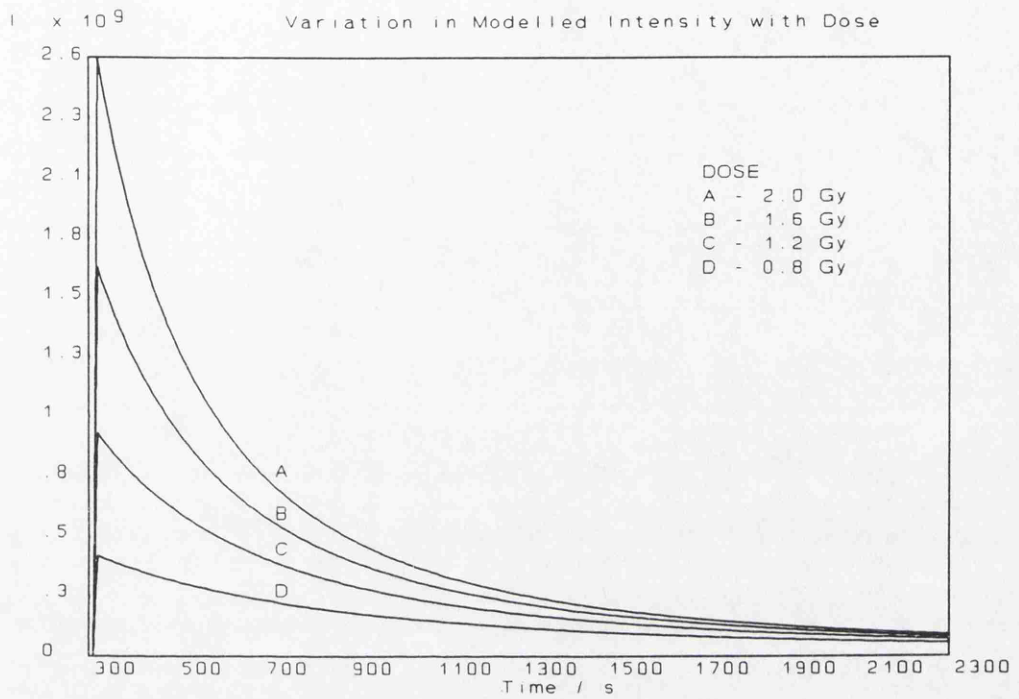


Figure 2.8 - Modelled bleaching curves, variation with dose

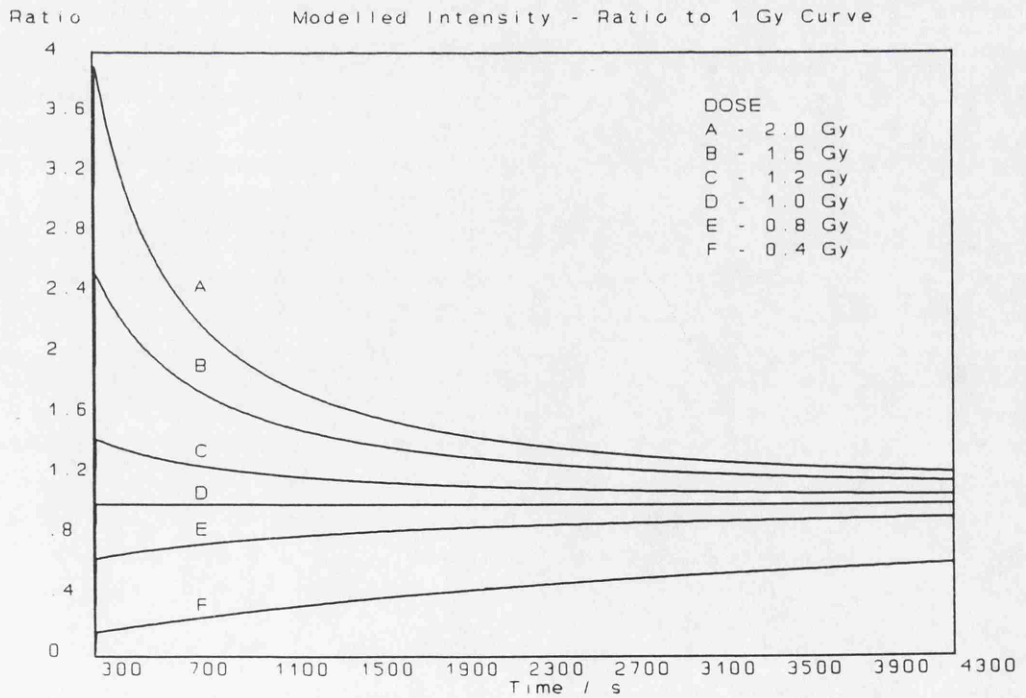
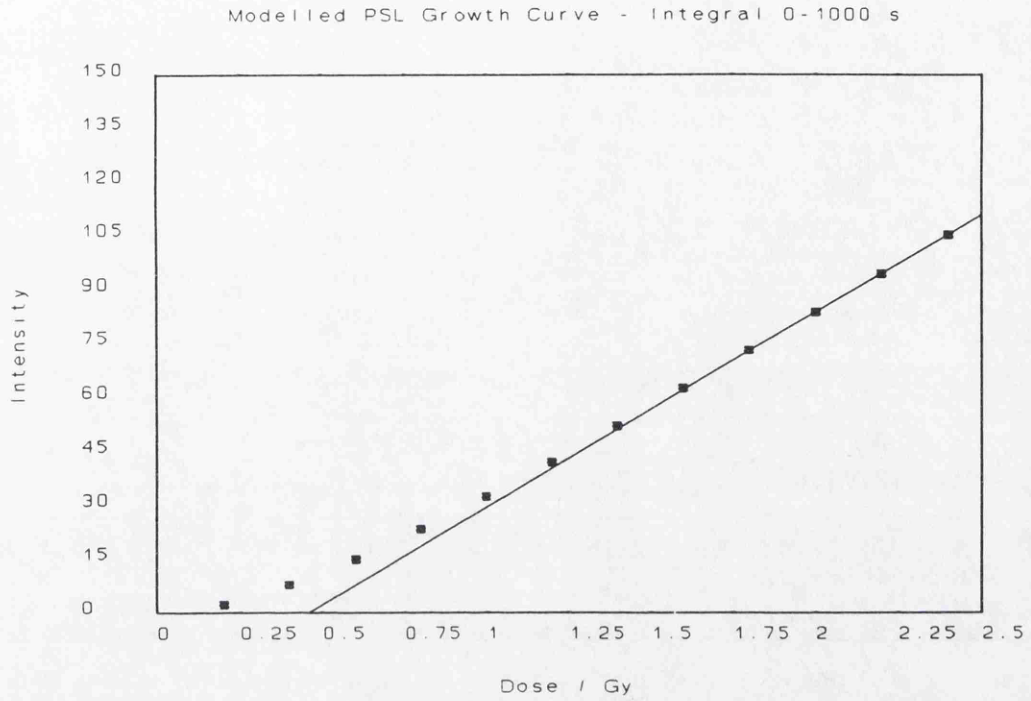


Figure 2.9 - Ratio of modelled bleaching curves to the 1 Gy curve

Frequency Factors :	Electron in Trap	$1 \times 10^{13} \text{ s}^{-1}$
	Electron in Centre	$1 \times 10^{13} \text{ s}^{-1}$
	Hole in Trap	$1 \times 10^{13} \text{ s}^{-1}$
	Hole in Centre	$1 \times 10^{13} \text{ s}^{-1}$
Photo Eviction Cross Section :		
	Electron in Trap	$1 \times 10^{-13}$
Capture Coefficients :	Electron by Trap	$1.0 \times 10^{-15} \text{ m}^3\text{s}^{-1}$
	Electron by Centre	$2.5 \times 10^{-14} \text{ m}^3\text{s}^{-1}$
	Electron by Valence Band	$1.0 \times 10^{-15} \text{ m}^3\text{s}^{-1}$
	Hole by Trap	$1.0 \times 10^{-15} \text{ m}^3\text{s}^{-1}$
	Hole by Centre	$1.0 \times 10^{-15} \text{ m}^3\text{s}^{-1}$
Densities of States :	Conduction Band	$6 \times 10^{22} \text{ m}^{-3}$
	Valence Band	$6 \times 10^{22} \text{ m}^{-3}$
	Trap	$1 \times 10^{15} \text{ m}^{-3}$
	Centre	$1 \times 10^{15} \text{ m}^{-3}$
Energies :	Trap Depth	1.2 eV
	Hole Depth	4.0 eV
	Band Gap	8.0 eV
	Work Function	10 eV
Probabilities :	Radiative Electron Recombination	= 1
	Radiative Hole Recombination	= 1
Miscellaneous :	Sample Mass	$1 \times 10^{-6} \text{ Kg}$
	Sample Thickness	$5 \times 10^{-4} \text{ m}$
	Sample Area	$1 \times 10^{-4} \text{ m}^2$
	Sample Temperature	284 K
	Absorption Coefficient	$1000 \text{ m}^{-1}$
	Photon Flux	$3 \times 10^{19} \text{ m}^{-2}\text{s}^{-1}$

**Box 3 - Constant parameters used in the simulations shown in Figure 2.8**



**Figure 2.10** - Modelled dose response curve, integrated over 0 to 1000 s

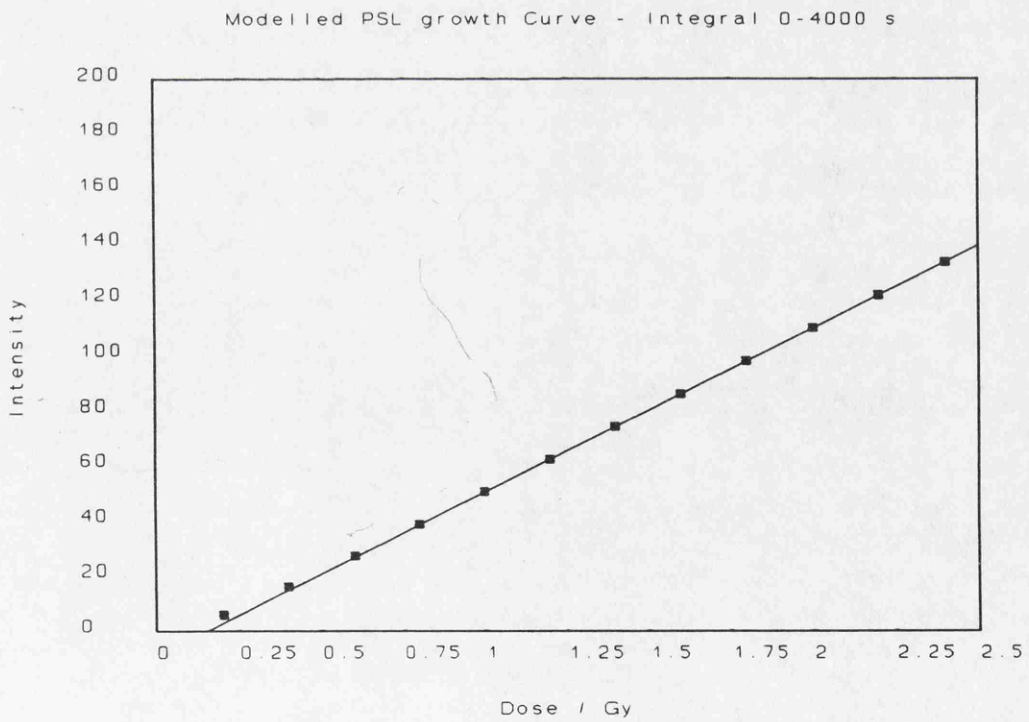


**Figure 2.11** - Modelled dose response curve, integrated over 0 to 4000 s

#### 2.4.4 - Discussion of Model Results

It is clear from all of the simulated bleaching curves that the decay is non exponential in nature, and moreover that the shape of the bleaching curve is dependent upon parameters such as photo eviction coefficient, electron capture coefficient and dose. The reason for such a departure from first order kinetics in a one trap / one centre model is *retrapping*. If the eviction probability is high, the lifetime of the charge carrier will be very short and it will appear as if the charge carriers are not retrapped, but proceed directly to the recombination centre. However, for lower eviction probabilities, the lifetime of the charge carrier in its energy state will be much longer thus introducing a delay between the initial eviction of the charge carrier and its recombination in a centre, hence producing non first order kinetics. In thermal stimulation, as the temperature passes the peak maximum, the lifetime of the trapped charge becomes very short and thus is perhaps likely to exhibit first order kinetics, however this does not happen with photo stimulation as the stimulating power is not increased during stimulation. Consequently unless high power lasers are used to measure the PSL giving rise to high eviction probabilities and thus low trapped lifetimes, it seems likely that the effect of retrapping may be significant, thus this was considered in all of the above simulations.

This non exponential nature of the curve is observed in real examples as is stated by Huntley *et al* (1985) and also by Bailiff & Foolton (1991). From this result, it would seem that the simplest requirement for the non-exponential behaviour of the bleaching curve is retrapping of charge carriers and a model with more complexity than just one trap and centre is not essential. An explanation of this departure from exponential behaviour was put forward by Huntley *et al* (1985), in which they proposed that the shape was due to progressively accessing trapped charge carriers that are less 'light sensitive', in other words that have a lower photo eviction probability which could only be due to a lower photo eviction cross section (see equation <2.19>) as the photon flux is constant. If this is solely the case (i.e. retrapping is negligible and so the kinetics are first order) then the bleaching curve would be expected to be the sum of multiple exponential curves, one for each trap being considered. Thus it should be possible to

deconvolute the bleaching curve into a series of exponential curves by subtracting the longest lived component and then successively shorter lived components from the bleaching curve. It must be remembered that a basic quantum mechanical principle at work here is the indistinguishability of identical particles (i.e. electrons) in that *'measurable results obtained from accurate quantum mechanical calculations should not depend on the assignment of labels to identical particles'* (Eisberg & Resnick, 1985) the corollary of this being that all charge carriers trapped in identical trapping states (i.e. due to one particular defect or impurity ion) *must* have equal photo absorption coefficients and thus differences in photo eviction sensitivities can only exist between different traps and not between charge carriers within the same traps (unless there are charge carriers which are trapped in different energy states within the same trap). It may be possible to transform the non exponential nature of the bleaching curve into an exponential curve (assuming first order kinetics) by preheating the sample so that all charge carriers trapped in sites shallower than the deepest trap from which the stimulating source can evict charge carriers, are removed, thus leaving in effect a single trapping site and hence a single photo eviction sensitivity.

However, the picture is complicated yet again when considering the recombination centres. A single trap exhibiting first order kinetics may still not yield an exponential bleaching curve if there is more than one recombination centre. As a recombination centre captures charge carriers, so its propensity to capture charge carriers is reduced as the number of available capture states within the centre falls. If there is more than one centre the reduction in capture probability as the available states are filled for each centre will differ, thus the relative proportions of charge carriers recombining in each centre will change. If the emission bands from all of these centres lie within the detection window then this will have no impact, however, if some of the emission bands lie outside the detection window then as the capture probabilities change, so the proportion of charge captured by centres emitting in the detection window as compared to that captured by centres not doing so will change, thus yielding a non exponential nature to the curve. This effect will have little importance if the bleaching time is short (i.e. so that a very small percentage of the trapped charge carriers are evicted) as the proportion of filled states in the centre will be small when compared to the initial

population of available states, however for long bleaching times (i.e. such that the majority of the trapped charge carrier population is evicted) this could have a significant effect upon the dynamics of the bleaching curve.

Thus, together with retrapping effects, it would seem unlikely that the bleaching curve should be exponential in nature. In other words it is straightforward to postulate that continuous monochromatic stimulation should generate a complex response which is likely to result in non exponential behaviour of the bleaching curve. It has also been postulated that there are many reasons why a bleaching curve may be non exponential, and thus determining the reasons why a particular curve has particular dynamics from the curve itself could be very difficult. Consequently it may be that an alternative stimulation technique would be required such as pulsing. In pulsed stimulation (using short pulses) it could be arranged so that the delay between successive pulses is long enough to allow the evicted charge carriers time to relax from the conduction (valence) band to lower energy states and also for charge carriers trapped in thermally unstable traps to be evicted and captured in thermally stable traps. This would allow the system to return to some form of equilibrium before the next perturbation from another pulse.

## 2.5 - Natural Samples

Having developed the above theory and drawn conclusions from the model, it must now be emphasized that these results *only* apply for the one trap / one centre model. In real mineral samples it is extremely unlikely that this will be the case. There will be many types of traps and recombination centres, all or some of which will interact, yielding competition in the eviction and capture process. Thus one can expect that the resulting photo eviction response and dynamics will be more complicated than those demonstrated by the model discussed above. However, this does not mean that the model has no bearing upon real samples as the only simplification was in the number of traps and centres and not in the dynamics of the PSL phenomenon. Indeed it can be argued that the results from the model, especially the implications of a non exponential bleaching curve, act as a demonstration of the complexities of the response of the simplest system

and as such may represent an indication of some of the problems that may be encountered when the PSL response from natural samples is examined.

## 2.6 - Ratio of Photo and Thermal Eviction Energies

In the analysis of luminescence results, it will be necessary to compare the activation energies associated with thermal and photo stimulation in order to be able to compare experimental results from both approaches and to use complementary thermal and photo techniques to yield more information about the sample being studied. It is known that the activation energy depends upon the stimulating mechanism used and Mott & Gurney (1953) proposed that the ratio of photo to thermal eviction energies should be equal to the ratio of the static to high frequency dielectric constant of the sample. In order to understand why the dielectric constant should vary with temperature and also why the eviction energy should depend upon the dielectric constant, it is necessary to consider the electronic properties of dielectric materials.

Let us consider an electron trapped in a site which possesses a single electron vacancy (the F centre). The trapping site is thus a positive ion and so has a net positive charge and, of course, the electron has a net negative charge, and both can be considered point charges. In free space, the potential energy between two point charges is well known as the Coulomb energy and shown in equation <2.31> below.

$$E_{coulomb} = - \frac{q_1 q_2}{4 \pi \epsilon_0 r} \quad \langle 2.31 \rangle$$

However, this is for free space, i.e. a vacuum, and as soon as these charges are placed in a dielectric medium, the potential energy becomes,

$$E_{coulomb} = - \frac{q_1 q_2}{4 \pi \kappa \epsilon_0 r} \quad \langle 2.32 \rangle$$

where  $\kappa$  is the dielectric constant of the medium. Now this potential energy has to be overcome before the charge can be successfully evicted to a state within the conduction band, and so the eviction energy (E) is proportional to the potential energy. Thus, if the same two charge carriers and hence the same electron and trap are placed into media with differing dielectric constants, then the ratio of the eviction energies is simply going to be given by the inverse ratio of the dielectric constants, as shown below

$$\frac{E_1}{E_2} = \frac{\kappa_2}{\kappa_1} \quad <2.33>$$

Thus it has been demonstrated that the eviction energy depends upon the dielectric constant of the medium, it now remains to demonstrate that the dielectric constant will vary with frequency of an applied electromagnetic radiation field, and for this the polarisation of a dielectric material must be examined.

Within a dielectric medium, there are three mechanisms for the formation of polarisation from electronic dipoles (Blakemore, 1985);

(1) - Partial or complete alignment of the dipole moments of polar molecules with the local electric field. Any asymmetric molecule composed of atoms with a difference of electronegativity has a permanent dipole moment. An electric field encourages the rotation of these groups for participation in the electric displacement, referred to as *dipole orientation* or *paraelectric response*.

(2) - The inducement of dipoles by relative movement of positive and negative ions in a partially ionic solid under the influence of an electric field. This mechanism is usually known as *ionic polarisation*.

(3) - *Electronic polarisation*. This is the only form of polarisation that occurs in every dielectric solid. This is due to the displacement of electrons in an atom relative to the nucleus under the influence of an electric field. Thus the electric field can be thought

of as deforming the electron cloud around every nucleus, regardless of whether there are any superimposed changes in internuclear spacings.

If the solid contains permanent dipoles, then all three of the above mechanisms will contribute to the static polarisability, however once an oscillating electromagnetic field is applied, only those mechanisms that can remain in phase with the field will contribute. Hence, the resulting function describing the polarisability must contain information about the polarisation (the real part) and also about the energy loss associated with phase lag (an imaginary part) and will be complex. The relationships connecting these two components are known as the *Kramers-Kronig dispersion relations*. As the frequency of the applied electromagnetic field increases from the static case, so one by one each of the three mechanisms becomes unable to remain in phase and so can not contribute to the polarisability thus reducing the dielectric constant as the material exhibits dielectric energy loss. For example at frequencies of the order of  $10^{10}$  Hz, the

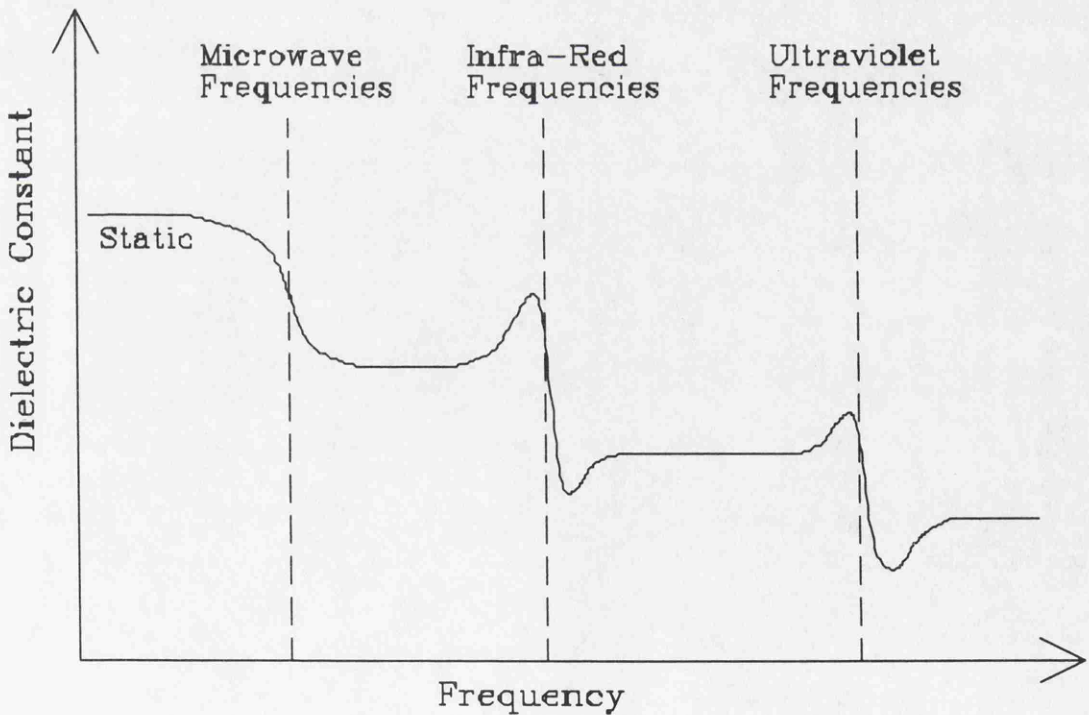


**Figure 2.12** - Dependency of dielectric constant upon frequency of applied electromagnetic field.

polarisation resulting from dipole orientation lags behind, thus the dielectric constant falls (the real component) accompanied by dielectric loss (the imaginary component). At around  $10^{13}$  Hz, ionic polarisation lags behind (the *reststrahlen* frequency) leaving only the contribution from electronic polarisation and even this lags behind once the frequency is larger than the order of  $10^{15}$  Hz, when the dielectric constant approaches unity. A graphical representation of this dependency of dielectric constant upon frequency of applied electromagnetic field is shown in Figure 2.12 (taken from Blakemore, 1985).

It has now been demonstrated that the eviction energy of a trapped charge carrier depends upon the dielectric constant, and that the dielectric constant depends upon the frequency of the applied electromagnetic field. It must be remembered that thermal eviction will take place usually in a static field (the earth's electromagnetic field) and so it is the static dielectric constant that will apply ( $\kappa_0$ ) and that photo eviction takes place within a high frequency oscillating electromagnetic field (the photons themselves) and thus the dielectric constant that will apply is that at the same frequency as the photons themselves ( $\kappa_\nu$ ), and thus the ratio of photo to thermal eviction energies will be (from equation <2.33>)

$$\frac{E_P}{E_T} = \frac{\kappa_0}{\kappa_\nu} > 1 \quad \text{<2.34>}$$

$$\text{as } \kappa_0 > \kappa_\nu \quad \forall \nu \geq \nu_0 \quad \text{where } \nu_0 \sim 10^{10} \text{ Hz}$$

A physical description of the actual process relates to the *Franck-Condon* principle which states that as the lattice vibrates slowly when compared to the time required for photon absorption, the lattice can be considered stationary during the photon absorption (Levy, 1968). Thus for thermal stimulation, during the eviction of the charge carrier, the crystal lattice has time to change the separations of the atoms in order to remain in equilibrium. However, during photo eviction of the charge carriers the crystal lattice

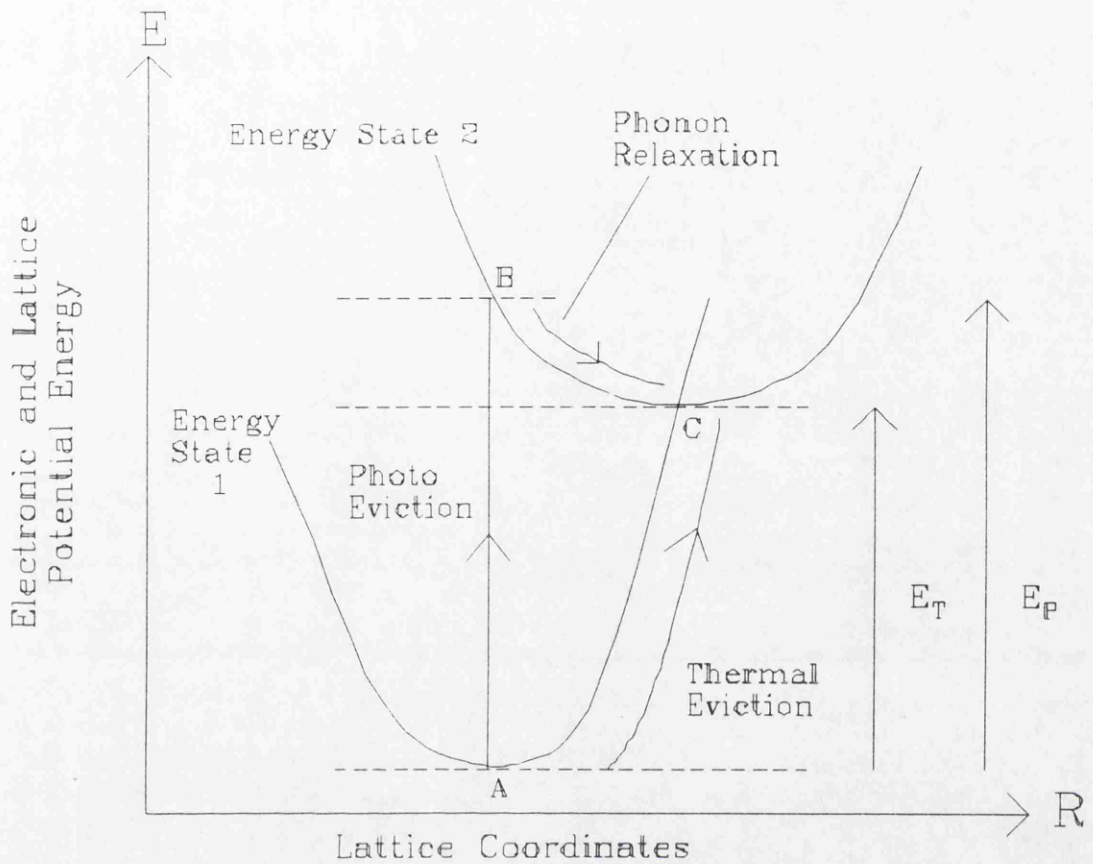


**Figure 2.13** - Configurational coordinate diagram showing thermal and photo eviction.

does not have time to reconfigure itself to reach the new equilibrium positions of the atoms, this has to wait until after the photo absorption when the lattice can then give up energy upon relaxation to the new equilibrium positions. Thus relative to thermal eviction, photo eviction requires extra energy which is dissipated by the lattice after the absorption process. The difference between thermal and photo eviction can be demonstrated with a configurational coordinate diagram as shown in Figure 2.13. Here the photo eviction is represented by the vertical line and the thermal eviction by the line following the curve.

The difference between the static and high frequency dielectric constant takes account of the Franck-Condon principle in the following manner. The static (or low frequency) dielectric constant results from all three types of polarisation of the lattice being able to keep step with the applied electromagnetic field, including dipole orientation and ionic polarisation. Hence the static dielectric constant is associated with movements of

the crystal lattice as accompanies thermal evicition. At high frequencies only electronic polarisation can keep in phase with the applied electromagnetic field and represents changes in electron-nucleus spacings as opposed to internuclear spacing. Thus for high frequencies, the dielectric constant is associated with static internuclear spacing as is the case for photo evicition. Consequently the difference between thermal and photo activation energies is shown in the difference between the static and high frequency dielectric constant.

Some studies of the dielectric properties of the silicate group of minerals has been studied, primarily for geologists, and the values obtained for the dielectric constant can be found summarised by G. V. Keller in Clark (1966) and a list of the values of the dielectric constant at various frequencies is reproduced in table 2.1 at the end of this section. This table shows that the ratio of optical frequency to radio frequency dielectric constant has an average value of  $0.41 \pm 0.05$  (sd), however this is still not the correct value as it is the static value of the dielectric constant that is needed, and the example of microcline shows that when this value is used the ratio drops from 0.41 to 0.26, thus implying that the photo activation energy will be four times that of the thermal activation energy. This table of values shows that for the feldspars listed, the photo activation energy will be at least 2.4 times the thermal and possibly much nearer to 3.8 following on from the microcline result.

However, the answer to this problem is not as clear cut as it seems from the above as the dielectric constant of the mineral will vary with temperature, as is clearly demonstrated by Ioffe & Yanchevskaia (1958). They show the variation in the dielectric constant with temperature and frequency for five feldspars - an Albite, two plagioclase, a labradorite and a microcline. In all cases the dielectric constant over all frequency ranges increases with temperature. Taking the example of microcline, the dielectric constant at 500 Hz rises from approximately 9 at room temperature to around 11 at 400 K; the dielectric constant at  $5 \times 10^5$  Hz rises from approximately 4.5 at room temperature to 5.5 at 400 K resulting in a ratio of high to low frequency of 0.5 at room temperature and around 0.5 at 400 K. This behaviour of the ratio between the two dielectric constants remaining constant seems to hold true for each of the minerals

examined, thus perhaps it is valid to use the room temperature ratio for measurements made at elevated temperatures, however these measurements do not extend to optical frequencies and will also only apply if both the thermal and photo activation energy measurements are to be compared at the same temperature. In the case of a thermal activation energy being calculated at elevated temperature (for example 400 K) then the dielectric constant will be that measured in a static electromagnetic field at 400 K. If the photo activation energy that is of interest is that measured at room temperature then the dielectric constant required for the photo stimulation will be that measured at high frequency at room temperature. Consequently the ratio of thermal to photo activation energies will be that of the high frequency dielectric constant at room temperature to the static dielectric constant at 400 K. Using the values from table 2.1 for microcline, and the temperature dependency of the static dielectric constant from Ioffe & Yanchevskaia (1958), the ratio will fall from 0.26 at room temperature to 0.21 at 400 K, thus implying that the photo activation energy at room temperature becomes equal to 4.8 times the thermal activation energy obtained at around 400 K (or 127°C).

This variation in dielectric constant with temperature also poses another problem, this time in the determination of thermal activation energies at elevated temperatures. Using the microcline example from Ioffe & Yanchevskaia (1958), between 300 and 400 K, the dielectric constant rises from 9 to 11 (approximately) which is an increase of 22 %. Now this in turn would seem to imply that from 300 to 400 K, the thermal activation energy will be reduced by 22 % (as the same argument for the difference in activation energy with frequency must surely apply for the difference with temperature). The implication of this is that the activation energy measured will fall as the temperature increases, hence a trap will have greater activation energy at room temperature than that measured at elevated temperature and thus the thermal stability of the trapped charge carriers will be greater than calculated as a too low activation energy would have been used. This then raises the following question: "is the limit on thermal stability actually greater than is currently thought ?" The answer to this question lies outside the scope of this thesis, however it would seem to be a very important point to try and solve.

**Table 2.1 - Variation in Dielectric Constant of Silicate Minerals with Frequency**

Mineral	Dielectric Constant - $\kappa$			$\kappa_r$ -- $\kappa_0$
	100 Hz ( $\kappa_0$ )	Radio Frequencies	( $\kappa_r$ ) Optical Frequencies	
Adularia, <i>a</i> axis	----	5.55	2.30	0.41
<i>b</i> axis	----	5.80	2.33	0.40
<i>c</i> axis	----	4.50	2.34	0.52
Microcline	8.82	5.62	2.31	0.26
Albite - Ab <sub>97</sub> An <sub>3</sub>	----	5.58	2.33	0.42
Ab <sub>99</sub> An <sub>1</sub>	----	5.45	2.34	0.43
Ab <sub>95</sub> An <sub>5</sub>	----	5.57	2.36	0.42
Ab <sub>96</sub> An <sub>4</sub>	----	5.52	2.36	0.43
Ab <sub>98</sub> An <sub>2</sub>	----	5.55	2.34	0.42
Ab <sub>94</sub> An <sub>6</sub>	----	5.63	2.36	0.42
Ab <sub>99</sub> An <sub>1</sub>	----	5.55	2.33	0.42
Ab <sub>98</sub> An <sub>2</sub>	----	5.39	2.34	0.43
Oligoclase - Ab <sub>76</sub> An <sub>24</sub>	----	6.03	2.39	0.40
Ab <sub>77</sub> An <sub>23</sub>	----	6.06	2.39	0.39
Andesine - Ab <sub>65</sub> An <sub>35</sub>	----	6.20	2.41	0.39
Ab <sub>61</sub> An <sub>39</sub>	----	6.47	2.41	0.37
Ab <sub>52</sub> An <sub>48</sub>	----	6.30	2.43	0.39
Labradorite - Ab <sub>43</sub> An <sub>57</sub>	----	6.61	2.45	0.37
Ab <sub>45</sub> An <sub>55</sub>	----	6.51	2.45	0.38
Anorthite - Ab <sub>4</sub> An <sub>96</sub>	----	7.24	2.51	0.35
Ab <sub>2</sub> An <sub>92</sub>	----	7.14	2.51	0.35
Ab <sub>7</sub> An <sub>93</sub>	----	7.05	2.49	0.35
Ab <sub>4</sub> An <sub>96</sub>	----	7.15	2.49	0.35
Quartz - along optic axis	----	5.05	2.36	0.47
across optic axis	----	4.69	2.41	0.51

## 2.7 - Summary

The theory laid out in this chapter has introduced the principles of luminescence. An introduction to solid state physics and the band theory of solids was followed by derivations of the rate equations describing phosphorescence and thermoluminescence. A term forming a mathematical description of the contribution of photo stimulation has been proposed and derived from first principles, and this has been added to the phosphorescence rate equations to generate a set of rate equations describing combined photo and thermal stimulations for a one trap and one centre model, with indications of extensions required for a multi trap / centre system.

These rate equations have been solved numerically for the case of combined photo and thermal stimulation in the one trap / one centre model. Bleaching curves have been simulated with variations in photo eviction coefficient, electron capture coefficient and dose. These results have shown that the bleaching curves are non exponential in nature and that the shape of the curves is dependent upon the chosen parameter sets. This non exponential behaviour was attributed to the contribution of retrapping in such a stimulation scheme.

Finally, the relationship of thermal and photo activation energies has been explored and a possible mechanism for the difference between the two stimulation techniques has been proposed.

## 2.8 - Dating Requirements

In order for accurate dating, the material used must have a good dosimetric nature. This means that it must have sufficient stability to retain trapped charge carriers beyond the time scales of interest; a dose response that is as simple as possible (i.e. non linearity and sensitisation are undesirable), well understood and characterised; sufficient sensitivity to be able to yield measurable luminescence signals in the dose range under examination and for the response to be reproducible from run to run (Chen & Kirsh,

1981; McKeever, 1988). There are other considerations, however the above four are dominant and thus the development of any system must explore these areas thoroughly before a reliable and accurate dating technique can be established.

The following chapter discusses various possible photo stimulation techniques and then describes the instrumentation used in this project.

### **3 - Photo Stimulation Techniques and Instrumentation**

Following on from the theoretical considerations in the previous chapter, the differing photo-stimulation techniques available are examined together with an assessment of their advantages and disadvantages as applied to the problems of kinetic analysis and dating. Once the differing techniques have been expounded, the instrumentation used in the course of this project will be described.

#### **3.1 - Continuous Monochromatic Stimulation**

The original technique used by Huntley *et al* (1985) which initially stimulated the recent increase in research interest in PSL dating was based upon continuous monochromatic stimulation. This technique involves recording the luminescence signal stimulated by a single wavelength band (the bandwidth being dependent upon the stimulation source, i.e. 1 or 2 nm for a laser, 5 nm or more, perhaps, for a non laser system). A lot of the work carried out using this technique has been performed with an argon ion laser, the 514.5 nm line was selected for stimulation from the many lines available, with luminescence being monitored at shorter wavelengths in the blue / UV region of the spectrum (e.g. also see Godfrey-Smith *et al* , 1988; Aitken & Smith, 1988; Rhodes, 1988 and Questiaux, 1991). With the discovery of an infra red stimulated luminescence band in feldspars by Hütt *et al* (1988) this stimulation technique was extended to stimulating at around 880-900 nm mainly using infra red diodes (e.g. Questiaux, 1991; Bailiff & Poolton, 1991 and Spooner & Franks, 1990).

The usefulness of this technique to the problem of kinetic analysis is limited, as it merely results in the observation of the bleaching curve at that particular wavelength and power density. This technique alone can not yield information about the most efficient stimulating regions, the most efficient detection regions, or any interaction between different stimulation regions unless it is repeated many times at differing wavelengths. This is not possible with infra-red diodes, and highly restricted with non-tunable lasers (such as the argon-ion) due to the lack of lines and their spacing. Thus

as a prime research tool it would appear to be of little benefit, particularly if the kinetic considerations shown by the one trap / one centre model in the previous chapter are also taken into account.

However, as a dating tool this technique need not be so readily dismissed. Once the optimum stimulation and detection bands have been established and characterised with respect to such matters as fading and thermal stability, then this technique does hold some potential advantages. With a narrow stimulation band from a laser, or with broader bands in infra red stimulation it is fairly straightforward to separate the stimulation and detection bands and certainly it should be possible to obtain good signal to background ratios with the high power densities that can be obtained with lasers. However, the question of suitability on kinetic grounds still remains. The questions raised by the one trap / one centre model still apply and raise objections to the suitability of continuous stimulation for the evaluation of the stored dose, which is the heart of the dating problem. Consequently it would seem that continuous monochromatic stimulation may be of little ultimate value in both kinetic analysis and dating problems, despite its widespread use.

### 3.2 - Pulsed Monochromatic Stimulation

The solution to the problem of continuous stimulation proposed in the previous chapter was pulsed stimulation, where the pulse widths are on a time scale pertinent to that of charge carrier dynamics, i.e. on the order of microseconds, with the delay between pulses long enough to allow the system to return to equilibrium before the next perturbation i.e. milliseconds and greater. This technique was developed at the SURRC as a part of the PSL research program, the major part of which is represented herein. With this technique, within-pulse and post-pulse luminescence is recorded on a short timescale (e.g.  $\mu\text{s}$ ) from many repeated pulses and summed. In this manner the resulting luminescence directly reflects the charge carrier recombination dynamics and provides the opportunity for *time domain analysis*.

Observations of luminescence on these time scales should give a curve characteristic of the time taken for charge carrier transport between the trap and recombination centre. This time will depend on a number of factors including charge carrier mobility (for example electrons have a greater mobility than holes and thus will have a shorter recombination time, similarly ions or free radicals); trap / centre proximity (if the centres are associated with the traps and formed in close proximity to the traps then the recombination time should be shorter than if the centres and traps are not correlated); charge carrier retrapping (after eviction from traps, charge carriers can be temporarily non-radiatively captured by vacant traps before thermal release. This will delay their eventual capture by recombination centres, thus increasing the recombination time. As the dose increases close to saturation limits, so the number of traps available for retrapping decreases and the number of vacant recombination centres increases. This should lead to a decreased recombination time scale as the dose increases). Also the recombination time for tunnelling effects or localised transitions should be different for charge carrier recombination via the conduction band, which has implications in the study of materials said to exhibit 'anomalous fading' since tunnelling has been put forward as one means of fading (Visocekas, 1979; Visocekas *et al*, 1983)

As with any monochromatic stimulation technique, exploratory work to establish the optimum stimulating and detection regions is also required. This complementary work would also be needed to provide information on trap and centre interactions and relative sensitivities and stabilities. Thus this technique is not sufficient on its own to yield information on all aspects of the PSL process, however it does represent a powerful tool for the exploration of charge carrier recombination dynamics and lifetimes, and thus holds the potential to provide valuable information on the mechanisms of PSL and related processes in the samples under examination.

### 3.3 - Excitation Spectroscopy

Excitation spectroscopy is the process of recording the variation in luminescence with changes in excitation wavelength. At the beginning of this project very little work had been performed in this field, the only example being by Hütt *et al* (1988) who used a Xenon lamp coupled to a monochromator yielding a discrete potassium feldspar excitation spectrum. Since then, this has been followed up by Hütt & Jaek (1989) using an excimer dye laser, Bailiff & Poolton (1991) studied photo generation and bleaching from 250 nm to 1  $\mu\text{m}$  of the luminescence signal stimulated by infra red diodes, a related characteristic which is not excitation spectroscopy, but rather the effect of differing photo-excitation on the luminescence stimulated at one particular wavelength. Thus the amount of work performed in this area seems to be very restricted, especially considering the importance of this work for kinetic analysis. The knowledge established by excitation spectroscopy has implications for other forms of stimulation (see sections 3.1 and 3.2) in order to establish the relative stabilities and sensitivities of differing excitation wavelengths, and thus help to optimise the excitation band.

For a given detection window, excitation spectroscopy can provide information on the relative efficiencies of differing wavelength regions in stimulating luminescence and thus provide invaluable knowledge on the wavelength regions to be used when attempting to stimulate luminescence and thus to maximise efficiency. However, the advantages and uses of excitation spectroscopy do not end here, rather observations of the excitation spectrum can provide a lot of information, especially if recorded with variations in other parameters such as sample temperature, bleaching, annealing and dose. Excitation spectroscopy is probably one of the only techniques that can observe the interactions (if any) between differing excitation bands, which is very important for understanding the structure of the luminescence model. Also, as demonstrated in section 2.3, it may be possible to derive the spectral dependencies of the photo eviction coefficients. To achieve greater understanding, emission spectroscopy is necessary to provide similar information to that yielded by excitation spectroscopy, but with respect to the emission bands. Due to the importance attached to excitation spectroscopy, this stimulation technique forms a large part of the work carried out in this project.

### 3.4 - Emission Spectroscopy

Emission spectroscopy is the process of recording the luminescence emission spectrum for a given stimulation band. Just as it is necessary to stimulate the sample in a wavelength region that yields a luminescence response, so it is just as necessary to observe this emission by defining an appropriate detection window, a process which is greatly facilitated by emission spectroscopy. Just as with excitation spectroscopy, however, knowledge of the best detection window to use is not the only information that emission spectroscopy can yield. Each emission peak can correspond to a different recombination centre and thus knowledge of the emission spectrum can add in more understanding of the luminescence model in the samples under investigation. Also, as with excitation spectroscopy, observations in variations of the whole emission spectrum with other parameters (e.g. temperature, bleaching, annealing and dose) could yield information on the properties of these centres such as relative capture efficiencies, centre densities, filling rates, energy depth below the conduction band and also can help to identify the nature of the centre.

It has long since been recognised in TL studies that emission spectroscopy is important, and has been investigated in alkali halides (e.g. Halperin *et al*, 1959) and mineral samples for geological and dating considerations (e.g. Levy *et al*, 1971; Bailiff *et al*, 1977; Akbar & Prescott, 1985; Kirsh & Townsend, 1988 and Andersson *et al*, 1990.). Emission spectroscopy has even been labelled as an *essential* requirement (Townsend & Kirsh, 1989) and although this view may be extreme, emission spectroscopy holds the potential to yield valuable data on the luminescence mechanisms. Recently some work has been performed on the emission spectra during photo stimulation (Huntley *et al*, 1991, Jungner & Huntley, 1991 and Bailiff & Poolton, 1991) being performed at a single temperature and representing only a beginning in the study of the PSL emission spectra. As with TL, variations in the emission spectra with dose, bleaching, temperature, preheating and thermal treatments will all need to be covered in some detail in order to help with the understanding of the PSL phenomenon. It is of debate as to how much of this knowledge is necessary before reliable dating can be pursued,

however it does seem apparent that some understanding of the emission bands and their interactions would be useful. As a start to this, the emission spectra of a potassium feldspar together with its variation with temperature and time has been observed under infra-red stimulation as part of this project, however the interactions between excitation and emission bands remain to be studied.

### 3.5 - Phototransferred Thermoluminescence

Phototransferred Thermoluminescence (PTTL) is the process of transfer of charge carriers from traps to different trapping states by photo eviction. In dating studies, the phototransfer has been from deep traps to shallower ones. The mechanism is as follows; charge carriers trapped in deep (peak temperature  $\gg$  stimulation temperature) states can be photo evicted and are left free to migrate around the relevant band until they find vacant trapping or recombination states. Trapping states whose TL peak temperatures are greater than the temperature at which the photo stimulation takes place can trap these free charge carriers with relatively high thermal stability (and hence trapped lifetimes) thus acquiring an additional future TL signal that is dependent upon the trapped charge population of the deep trap. If these shallower traps had already been emptied of charge carriers (for example by preheating) then the total charge population (and hence signal) acquired will be dependent upon the population of the initial deep trap. Thus a signal representative of the total absorbed radiation dose since zeroing has been transferred from a deep trap (with corresponding high thermal stability) to a shallower one. The advantage of this is that a signal from a trap that has high thermal stability but which is not directly measurable (i.e. the required eviction temperature is too great for the heater, or that any signal would be lost in the black body background) can be recorded as a portion of it has been transferred to a much more accessible trap.

The effect of photo stimulation upon the TL glow curves has been studied for quite a long while, with PTTL in sodium chloride being identified by Stoddard in 1960 which was followed up by Braner & Israeli in 1963. The major importance of this work at the time was in the rejection of a single trap / multi centre model being proposed by

Bonfiglioli *et al* (1959) and in the development of the model originally proposed by Randall & Wilkins (1945 a, b & c). PTTL was proposed as a solution to the anomalous fading of the TL signal in zircon and fluorapatite by Bailiff (1976), which was followed up by Zimmerman (1979). A study into the potential of PTTL in the dating of quartz was carried out by Bowman in 1979 and also by Sasidharan *et al* (1979) who all performed PTTL studies at or above room temperature. Low temperature PTTL was explored as a technique to avoid sensitisation changes upon heating by Mobbs (1979) in deep sea sediment cores. Cryogenic PTTL studies also have big advantages in that they reduce the black body background and thus could increase detection sensitivity and also allow broader detection bands. The trapping sites below storage temperature will already be empty of charge and hence no heating would be required to empty them, which could otherwise interfere with the trapped charge population that were to interrogate. Also heating above room temperature may not be required, thus reducing or eliminating many of the other problems associated with TL measurements, such as spurious signals and oxidisation.

### 3.6 - Published Work

Prior to the start of this project, the vast majority of work performed in PSL was using continuous excitation with the 514.5 nm line from an argon-ion laser. The first example was Huntley *et al* (1985) who used this laser line in conjunction with a photon counting system. This was followed up in later work by the same lab (Godfrey-Smith *et al*, 1988), with some expansion to other wavelengths by using a dye laser (from 684 to 615 nm) and also by using various lines from a krypton ion laser. Similar work using the argon-ion laser was also being performed in the Oxford laboratory (Rhodes, 1988; Aitken & Smith, 1988; Smith, 1988 and Wheeler, 1988) concentrating upon observations of the bleaching curve of various materials under continuous stimulation. The only alternative approach was undertaken by Hütt *et al* (1988) in Tallin, Estonia. They began exploration of the excitation spectrum of potassium feldspar using a xenon lamp coupled to a monochromator.

This was the limit of PSL research at the instigation of the project described in this thesis. During the course of this project (which was intended as a thorough exploration of the PSL phenomenon in order to attempt to put it on a firm physical basis) the exploration of PSL by other groups began to be extended beyond the initial research. In Estonia, the initial excitation spectroscopy was followed by repeated excitation scans, only this time using an excimer dye laser, as reported in Hütt & Jaek (1989). The discovery of infra red stimulation bands from feldspars (Hütt *et al*, 1988) led to stimulation by infra-red LEDs, which have many advantages, perhaps the most important being low cost, relative high power and size (they being small enough to include in a standard TL chamber with very little modification). This enabled many other laboratories to begin work in PSL. The characteristics of such LED's have been explored by the Durham laboratory (Poolton & Bailiff, 1989) and also in Oxford (Spooner & Franks, 1990) and this has been followed up by a lot of work using such diodes. For example see Bailiff & Poolton, 1989; Bailiff & Poolton, 1991; Huntley *et al*, 1991, Questiaux, 1991 and Duller, 1991. Although infra red stimulation has caused a lot of interest, this does not mean that other stimulating sources have been ignored, for example Bailiff & Poolton (1989) also used a xenon lamp and a He-Ne laser has been used to provide high power red stimulation (Jungner & Huntley, 1991), and the 514.5 nm line from an argon-ion laser is still often used (e.g. Questiaux, 1991; Huntley *et al*, 1991 and Stoneham & Stokes, 1991).

### 3.7 - Scanning Excitation Spectrometer

The original design concept of the excitation spectrometer was as a highly flexible two dimensional research tool, ultimately being capable of generating both excitation and emission spectra, synchronously if so required (using both continuous and pulsed stimulation via a Pockels cell), with full temperature control being incorporated (from cryogenic to high temperatures). The flexibility of the spectrometer was to be derived from its modularity, thus allowing for easy reconfiguration depending upon the research requirements. At the start of this project all of the components for the spectrometer

were present, and the spectrometer had been configured and run as a manually operated continuous excitation spectrometer.

The primary contribution of this project to the excitation spectrometer involved software development, spectrometer characterisation and implementation of the system as a scanning excitation spectrometer. The software development included automation of the spectrometer with automatic data acquisition together with the development of full data presentation and analysis. Characterisation of the spectrometer included power spectra analysis and stability. The following sections describe the components in detail, power characteristics, and then proceed to describe the computer software written for this project.

### 3.7.1 - Components

A schematic diagram of the excitation spectrometer can be seen in Figure 3.1. This spectrometer is based on a 300 W Cermax™ xenon lamp. This lamp differs from conventional ribbon xenon lamps in that it has a built in parabolic reflector, and has both of the electrodes situated along the optic axis giving rise to a unidirectional parallel beam from the lamp, yielding power densities in the beam equivalent to those from much more powerful conventional xenon lamps (e.g. 1 kW lamps). The lamp has a specially coated window to enable ozone free operation which yields a short wave spectral cut off of about 320 nm. The output of the lamp is coupled to an F/3.4 monochromator by a spacer tube (which collects stray light from the lamp and maintains the optimum spacing between the lamp and monochromator to minimise the effects of the on-axis cathode) and focused on to the entrance slit by a 70 mm focal length lens.

The monochromator has a symmetrical Czerny-Turner optical configuration with easily changed diffraction gratings so that any desired part of the spectral region can be covered from the vacuum UV to the far IR. Throughout the course of this project, two gratings have been used in the monochromator; a 500 nm blazed grating which has 1200 lines/mm with a useful working range of 350-900 nm and a 1000 nm blazed

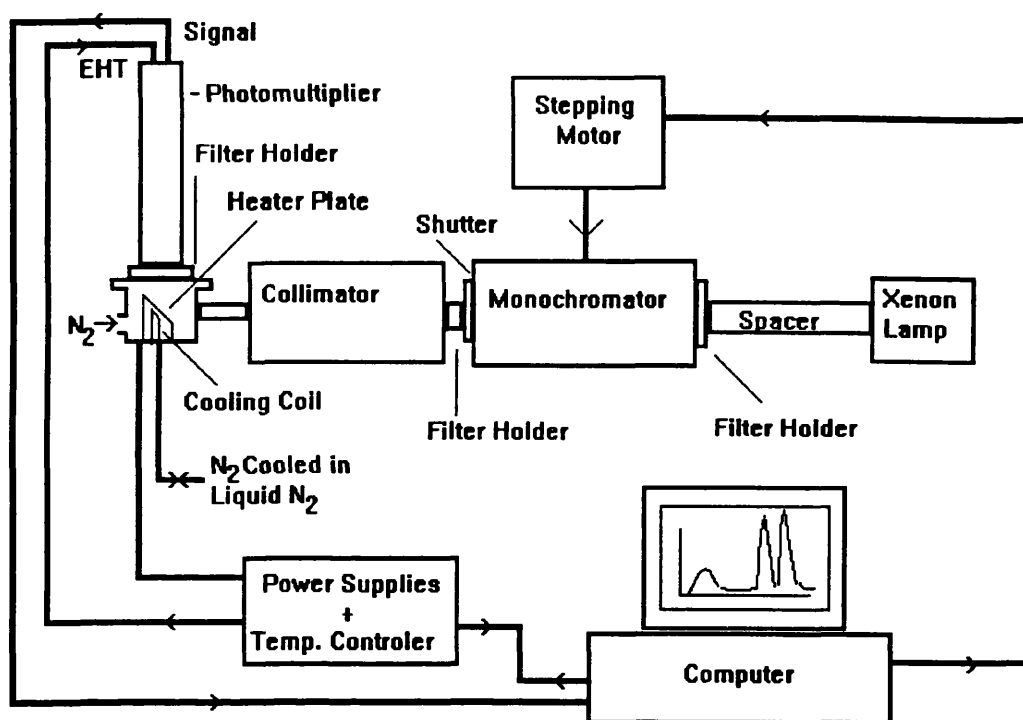


**Figure 3.1** - Schematic Diagram of the PSL excitation spectrometer.

grating which has 600 lines/mm with a useful working range of 660-1500 nm. The useful working ranges are those quoted in the instruction manual, however the gratings can be used beyond these ranges although a decrease in efficiency will be observed beyond these limits. The monochromator has adjustable entrance and exit slits, and the width of these governs the spectral bandpass from as low as 0.5 nm (0.1 mm slit width and 500 nm grating) to as high as 75 nm (8 mm slit width and 1000 nm grating). Filter holders are positioned outside both slits, with the filtering on the exit side being of great importance in order to control second order emission from the grating (half the principal wavelength). Wavelength selection can be performed manually or by the use of a stepping motor which enables uniform wavelength scanning.

The stepping motor has a high torque motor connected through a slipping clutch to the grating mount of the monochromator and each step corresponds to a wavelength shift of 0.1 nm with the 500 nm grating (0.2 nm for the 1000 nm grating). The stepping motor can be operated manually with the availability of 18 scan speeds from 0.3 to 960 nm/min (500 nm grating) and the choice of operating in single increments adjustable from 0.1 to 20 nm (500 nm grating). Alternatively, the stepping motor can be driven

externally from a computer by either using the front panel settings with external start and stop pulses (the wavelength range scanned can be monitored by counting sync pulses which are emitted for every step of the motor) or by directly inputting stepping clock pulses generated by the computer. The advantage of this second method of computer control is that it allows for any scan speed, not just those set internally by the stepping motor, and this is the form of computer control that was implemented in the PSL control program.

The output beam from the monochromator passes directly in to a collimator which collects and focuses the light onto a 3 mm aperture to help define the output beam. This does inevitably reduce the beam power, however beam homogeneity is of great importance and so the improvement in quality of the beam at the expense of power is deemed acceptable. The light from the aperture is collected and collimated into a beam approximately 20 mm in diameter and is then ready to be taken into the sample chamber.

Sample discs are mounted on a 45° plate made from Inconel 600 (a nickel, chrome and iron alloy) such that the incident light is horizontal and the emitted light is detected vertically. The sample plate can be heated resistively from room temperature to around 500°C controlled by a phase angle trigger unit. Cooling of the sample is achieved by passing nitrogen through a coil suspended in liquid nitrogen to cool it to near LNT, this gas is then passed through a cooling coil made out of capillary tubing which is silver soldered to the back of the sample plate, and then vented to the lab. The temperature upon cooling is controlled by the flow rate of the cooled gas through the cooling coil and under conditions of maximum cooling it is possible to cool the sample plate to approximately -140°C in just a couple of minutes. The temperature of the sample plate is monitored by a Chromel-Alumel thermocouple spot welded to the back of the sample plate prior to the attachment of the cooling coil. The output of the thermocouple is amplified by an AD595 thermocouple amplifier chip which is a linear device, so care has to be taken at extremes of high and low temperature to adjust the reading displayed for the non-linearity of the thermocouple itself.

The sample chamber can be purged with oxygen free dry nitrogen to help remove spurious signals upon heating and prevent any oxidation of the sample plate. The chamber is vacuum sealed and is connected to a turbo pump to enable evacuation of the chamber. This could have benefits for the cooling of the sample and also would ensure total replacement of the oxygen atmosphere by dry nitrogen by evacuating the chamber and then filling and purging with the nitrogen.

Detection of the resulting luminescence is performed with a Thorn EMI 9893QB fast photon counting photomultiplier with a quartz window and alkali photocathode. This photomultiplier gives rise to a possible unfiltered detection window from less than 200 nm to approximately 600 nm, with peak sensitivity at around 350 nm yielding a quantum efficiency of about 24%. These tubes exhibit high gain with a low dark count (typically approximately 20 cps with a nominal gain of  $8.3 \times 10^7$  at 2250 kV). Pulses from the photomultiplier are passed through a Thorn EMI amplifier and discriminator (C604-A) which emits ECL logic pulses which are then converted to TTL logic pulses

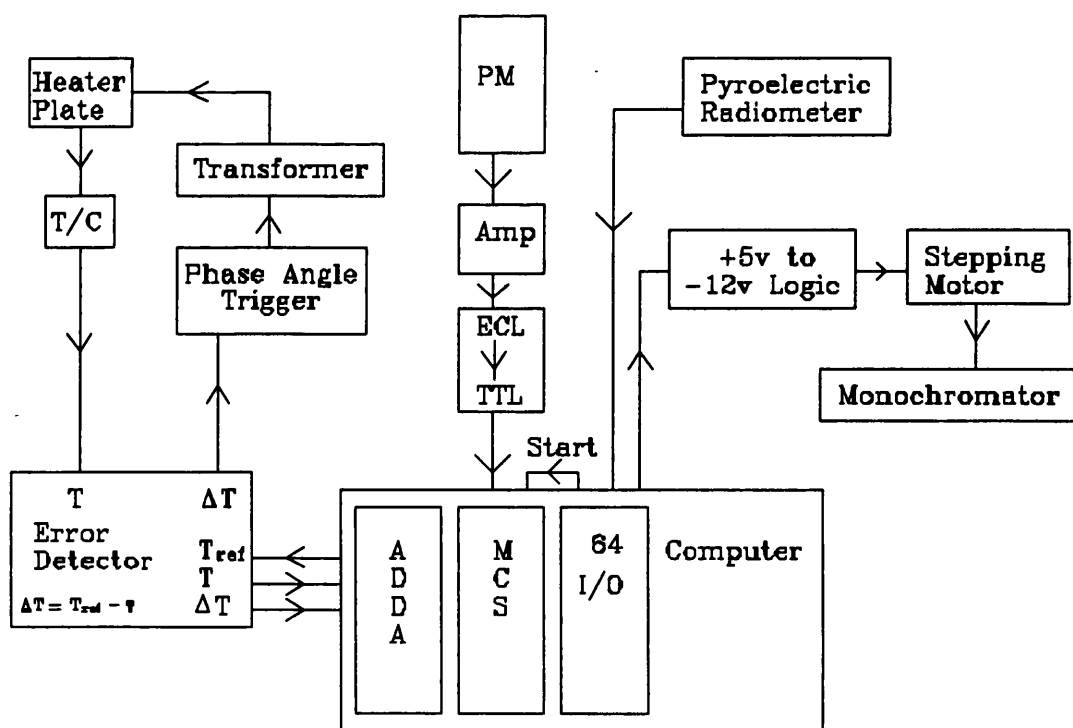


Figure 3.2 - Block diagram of the excitation spectrometer control structure.

and recorded using an EG&G Ortec ACE™ MCS card. Control electronics, including high voltage supply, thermocouple amplifier, heater phase angle trigger and error detector, temperature reference and power supplies are contained in a rack unit with computer control of heating rates and PSL scan speeds being provided by a Personal Computer through a control program developed for the purpose (this is described more fully in section 3.7.3). A block diagram of the control structure and computer interface can be seen in Figure 3.2.

### 3.7.2 - Light Source Characterisation

Understanding of the characteristics of the stimulation source is a prerequisite to accurate experimentation and for valid interpretation of the data generated by that experimentation. With the excitation spectrometer there are several characteristics that need to be established, there is the light source power spectrum and its variation with changing slit widths on the monochromator, and there is the light source stability both in terms of power fluctuations and spectral stability during the course of continuous use and also with respect to the long term stability of the light source during its lifetime.

#### 3.7.2.1 - Power Spectrum

In order to record the power spectrum of the xenon lamp in this spectrometer, a pyroelectric radiometer (Molelectron model PR200) was used. This radiometer has a spectral range and uniformity of 0.2 to 20  $\mu\text{m}$  at  $\pm 3\%$ , extending out to 40  $\mu\text{m}$  at  $\pm 5\%$  and is then uncalibrated out to 500  $\mu\text{m}$ . It has a built in optical chopper in the detector head and is capable of resolving radiant power in the nanowatt range with a maximum of 200 mW (limited by a 50  $\text{Wcm}^{-2}$  damage threshold). The radiometer has a calibration accuracy of 5% with a linearity of under 2% up to 50  $\text{mWcm}^{-2}$  and then 5% up to 200  $\text{mWcm}^{-2}$ , with a resolution of  $3 \times 10^{-8} \text{ Wcm}^{-2}$ . Output from the radiometer is via a 3½ digit digital display and is also available through an analogue BNC socket and a digital BCD interface. Use of the radiometer allows detailed exploration of the light source

power variations with changes in the monochromator and also allows periodic checking and characterisation of the light source.

The radiometer was interfaced to the computer via the BCD digital output to enable automatic data acquisition, with the monochromator being driven by the computer via the stepping motor as in excitation spectroscopy. However, due to the fact that there is a minimum response time of at least 1 second (being the fastest response time consistent with readout precision) for the radiometer to adjust to a change in power (for powers less than 2mW this response time increases, however the range needed for the

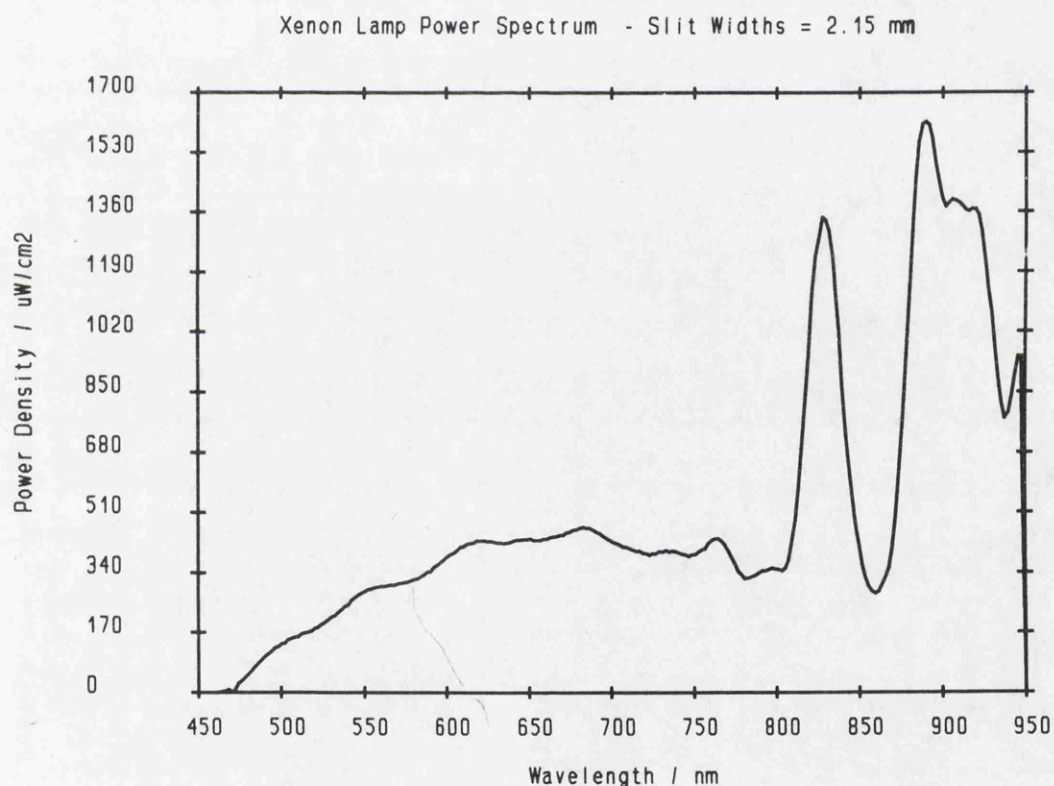


**Figure 3.3** - Typical xenon lamp power spectrum

xenon lamp fortunately only had a 1 s response time), the scan speed used to acquire the power spectrum may well be less than that used in excitation spectroscopy. The radiometer was allowed to warm up for at least two hours before measurements were taken to allow the pyroelectric crystal to come into thermal equilibrium with its

surroundings. After careful and detailed zeroing of the instrument, power spectra could be recorded. The resulting typical power spectrum can be seen in Figure 3.3.

As can be clearly seen from Figure 3.3, the power spectrum of the lamp is smooth up to 750 nm (the rise from zero at 450 nm being due to the action of a long wave pass filter to block the second order spectrum from the monochromator reducing the transmitted power of the lamp below the sensitivity of the range setting of the radiometer) after which two sharp peaks are seen with evidence for other peaks on their edges. The resolution of these peaks can be increased by reducing the monochromator slit widths (Figure 3.4) or reduced by increasing the slit widths (Figure 3.5). This demonstrates clearly the need for power normalisation of excitation spectra, which is essential for regions above 750 nm as if the spectral lines coincide with a PSL peak, then the sharp spectral lines will result in sharp lines in the excitation spectrum. Power spectra were also recorded in response to variations in the monochromator slit widths from 1 to 8 mm. The resulting power density variation can be seen in Table 3.1 and is shown graphically in Figure 3.6.

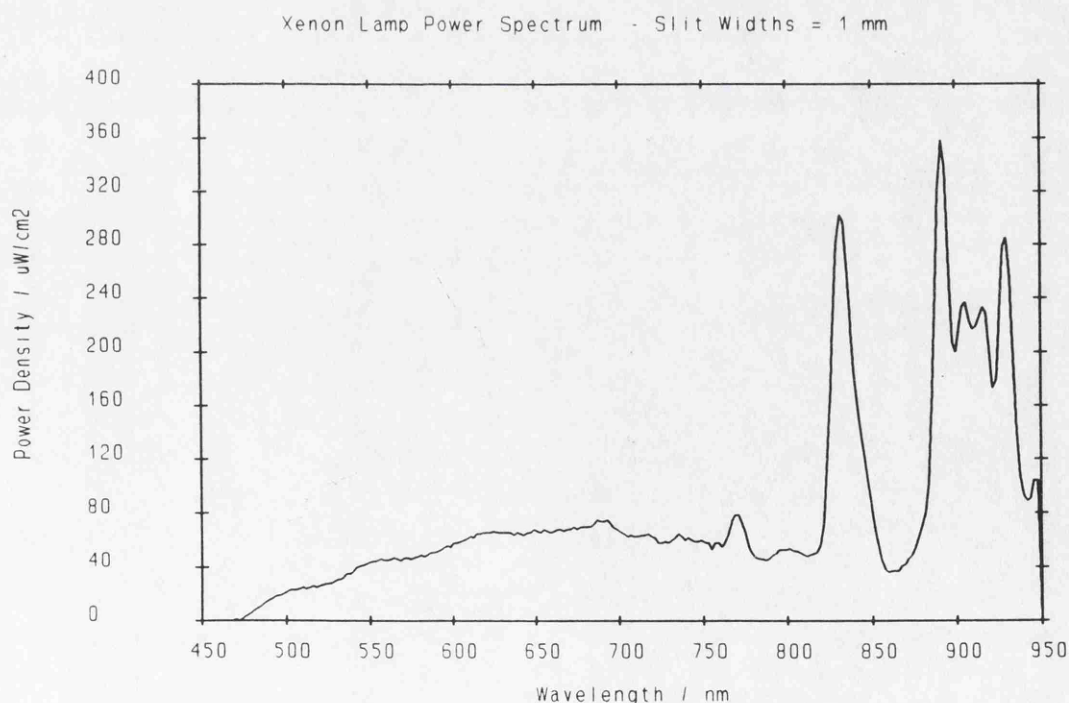


**Figure 3.4** - Xenon lamp power spectrum for monochromator slit widths = 1 mm

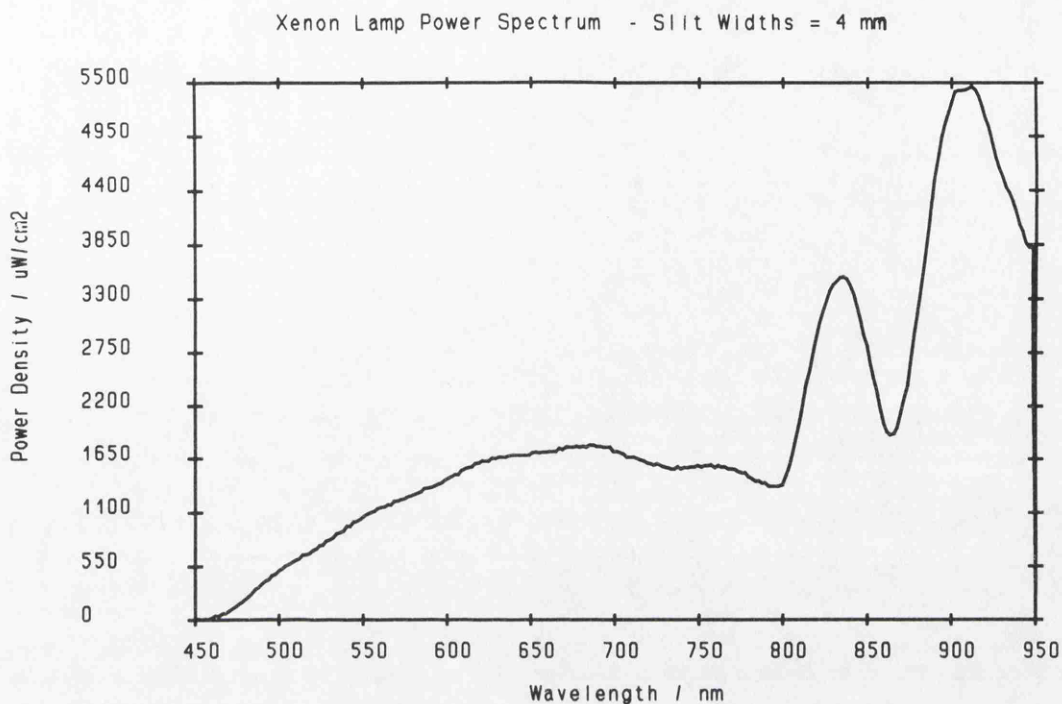


**Figure 3.5** - Xenon lamp power spectrum for monochromator slit widths = 4 mm

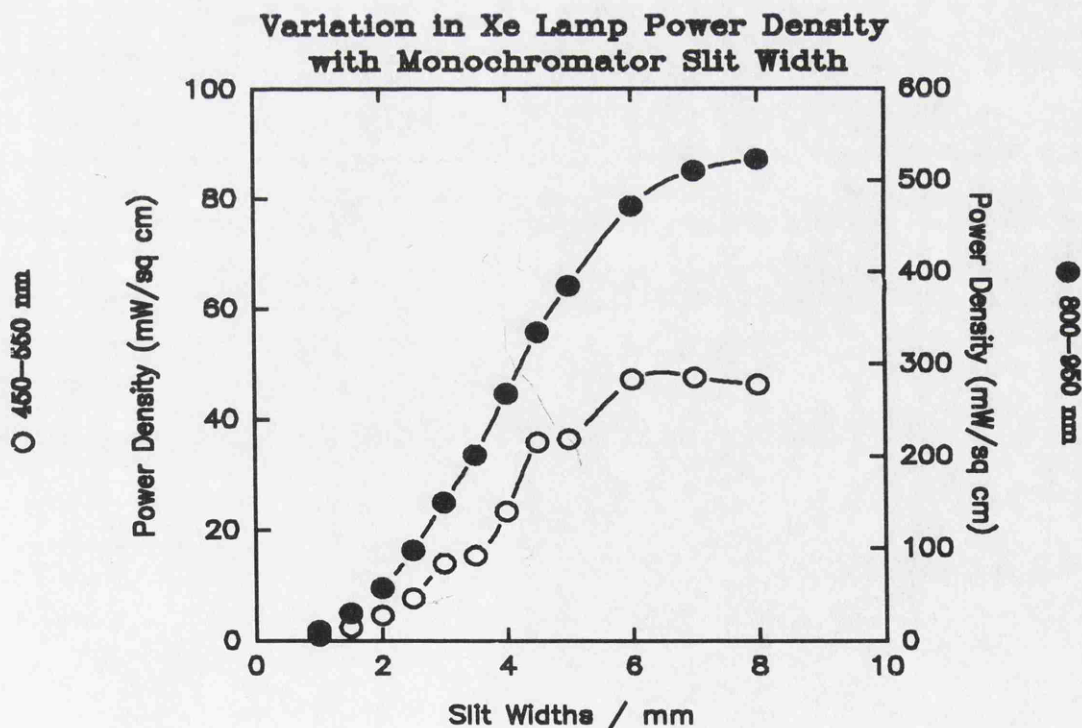


**Figure 3.6** - Variation in Xe Lamp Power Density with Monochromator Slit Widths

**Table 3.1 - Variation in Power Density of the Xe Lamp with Monochromator Slit Widths.**

Monochromator Slit Width (mm)	Integrated Power Density (mWcm <sup>-2</sup> )	
	450-550 nm	800-950 nm
1.0	0.850	10.859
1.5	2.428	30.156
2.0	4.582	57.067
2.5	7.680	97.515
3.0	13.115	149.455
3.5	15.310	201.170
4.0	23.300	267.345
4.5	35.810	334.145
5.0	36.360	384.590
6.0	47.100	471.685
7.0	47.475	510.010
8.0	46.160	522.840

### 3.7.2.2 - Lamp Source Stability

The warm up characteristics of the lamp were measured by a photodiode through an analogue-digital / digital-analogue converter (ADDA) card in the computer. Ten readings were taken and averaged every ten seconds for an hour. In order to reduce scatter further, consecutive sets of 5 average readings were then averaged to produce the graph shown in Figure 3.7. As can be seen, the power of the lamp increases over approximately the first 6 minutes after which it tails off over the rest of the hour. The most rapid change in the power occurs within approximately the first 20 minutes, and so on this basis it was decided that the lamp should be allowed to warm up for at least half an hour before any quantitative analysis was to be performed. It is not necessary

to allow the lamp to warm up if all that is required is to see if a signal exists, however to ensure that the lamp was given sufficient time to warm up before quantitative analysis, it was the practice to always let it warm up before any experimentation.

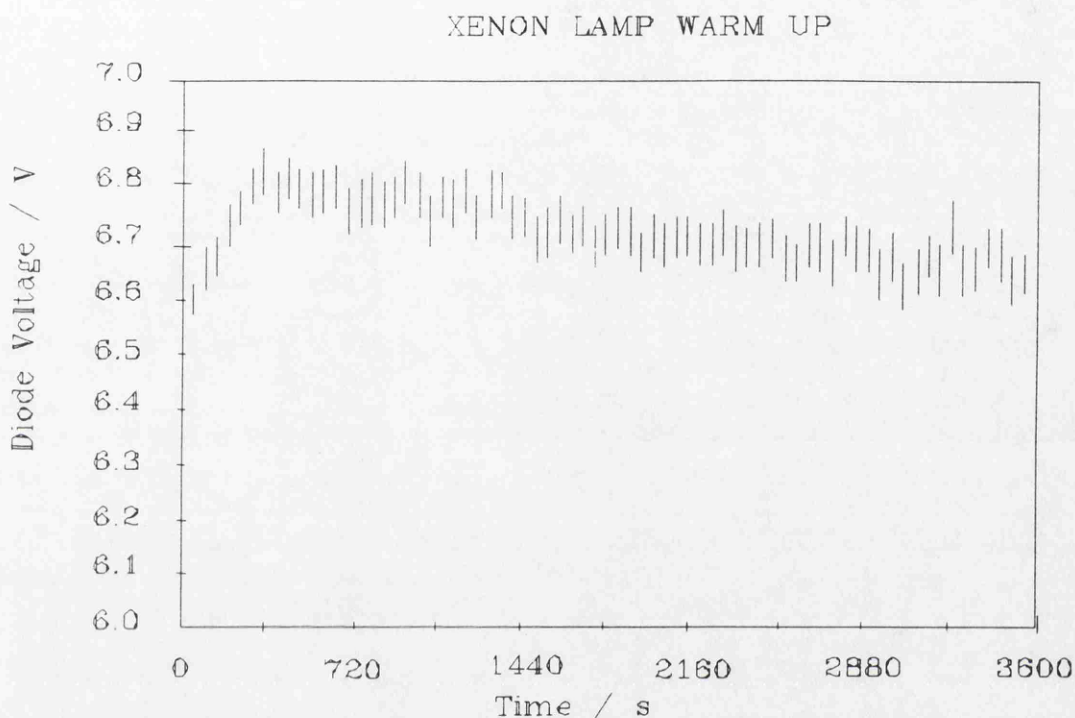


**Figure 3.7** - Xenon lamp warm up characteristics

Power stability of the lamp over the course of a day was measured using the pyroelectric radiometer. Power spectra were recorded approximately every 10 minutes for  $\frac{3}{4}$  hour, after which power spectra were recorded every 30 minutes for the rest of the day (a total observed time of about  $7\frac{1}{2}$  hours). Two indicators of stability were looked at, peak position and peak height.

The peaks utilised for this were the principal infra red ones at approximately 840 and 900 nm, as they are well defined and are relevant to the important Infra Red PSL of alkali feldspars. These results, therefore, can not be relied on directly as an indicator of stability in the blue / green part of the spectrum, however they may serve as a guide to the degree of fluctuation in power that could be expected. The results can be seen

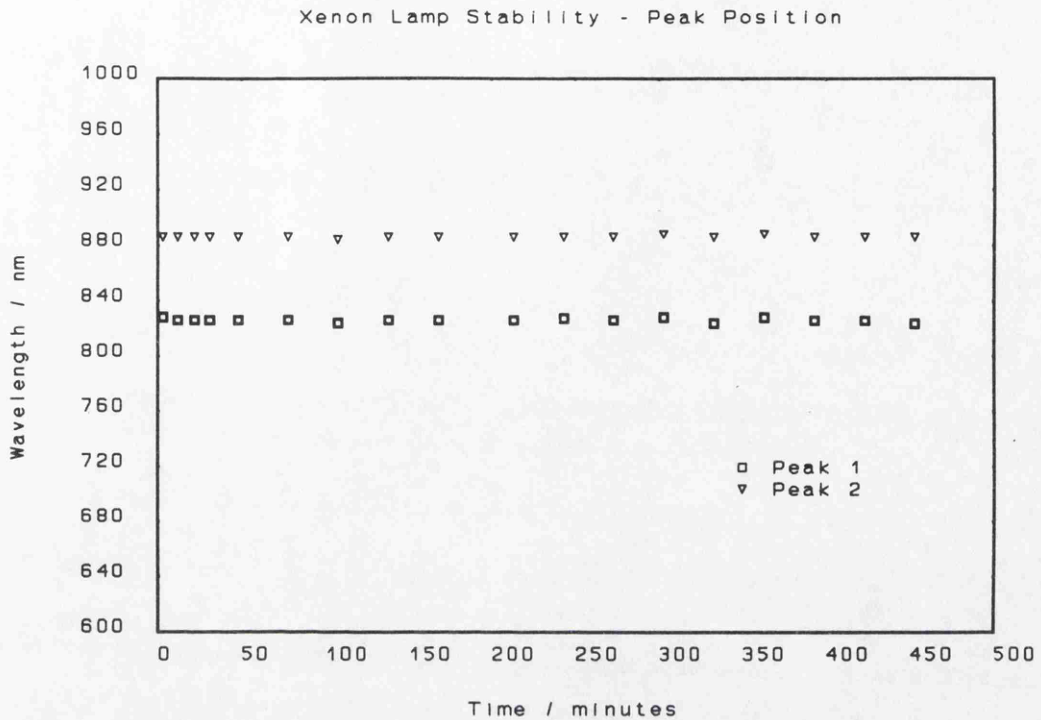


**Figure 3.8** - Xenon lamp stability as shown by peak positions.

in Figure 3.8 and Figure 3.9. It can be seen that the power drops off from the initial value (which is in agreement with the warm up characteristics recorded much earlier as depicted in Figure 3.7) for both of the peaks shown and that the position of the peaks remains invariant within run to run scatter. Again, these results show that the fluctuations in power are much reduced after the initial ½ hour after switching the lamp on, thus supporting the decision to allow for a ½ hour warm up period. However it is clear that even after allowing for this warm up period, there is still significant fluctuation in power level which would give rise to problems in accurate quantitative work (such as dose evaluation), and thus it does show the need for light source power monitoring during quantitative measurements if a high degree of precision is required. The possibilities for such source monitoring are discussed further in section 3.11.

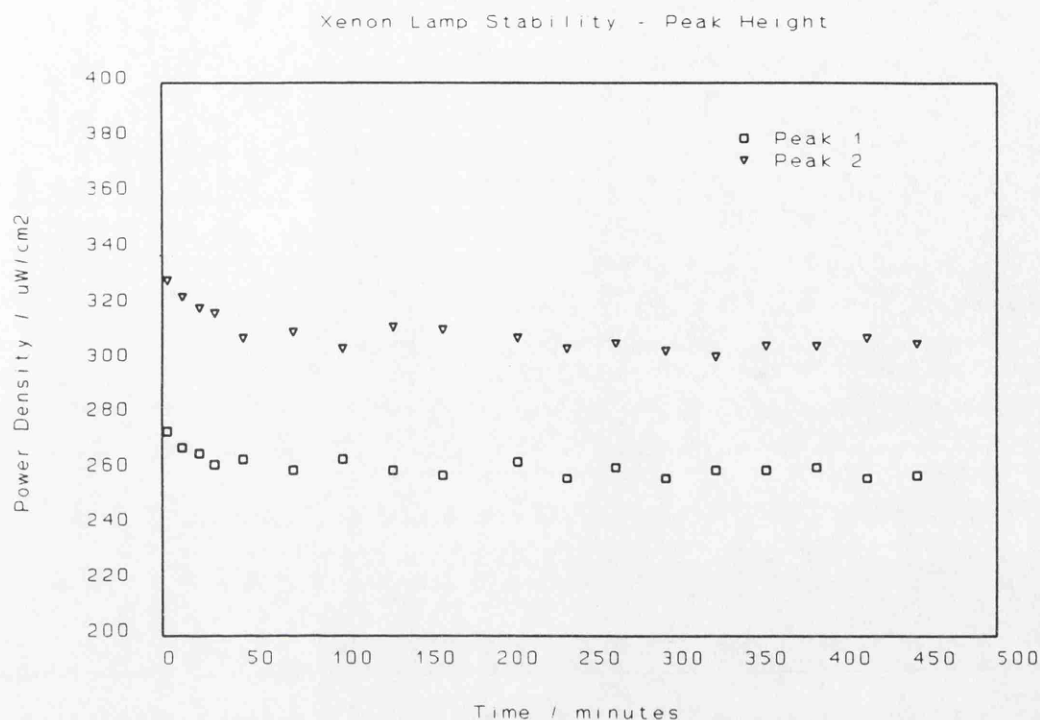


**Figure 3.9** - Xenon lamp stability as shown by peak heights.

### 3.7.3 - Control Software

#### 3.7.3.1 - General

The control software (developed as part of this project) was written in Borland Turbo Basic and was designed as an integrated package with the aim of combining data acquisition and manipulation / analysis without having to leave the program environment. The software is designed as a flexible research tool implementing full instrumental control and data acquisition coupled to data manipulation and analysis. The software is structured to allow for later dedication to specific tasks, e.g. for the sole recording of TL glow curves, and also leaves the capability for expansion to new instrumentation and analytical tasks as they are required. Mass disc storage of the data is in ASCII file format with a header detailing sufficient information concerning the particular data set to identify it without reference to primary laboratory records. Although ASCII files use disc space less efficiently than binary or random access files,

it was decided that the ability to be able to view or print ASCII files directly from the computer's operating system was an advantage which far outweighed the disadvantage of file size. Also ASCII files are easily transportable between different systems and this permits data transport via electronic mail or over a networked system. Although such data transport was not envisaged at the start of the construction of his software, nor has it yet been needed, it is characteristic of this software that the possibility of such transport was considered.

The software performs the following options; Data input/output to disk, arithmetic combination of spectra, arithmetic manipulation of individual spectra, graphical representation of the data with HPGL output, isothermal decay analysis (both continuous as in the case of TL and pulsed annealing in the case of PSL), arrhenius transformation, linear regression analysis, statistical analysis, conversion and

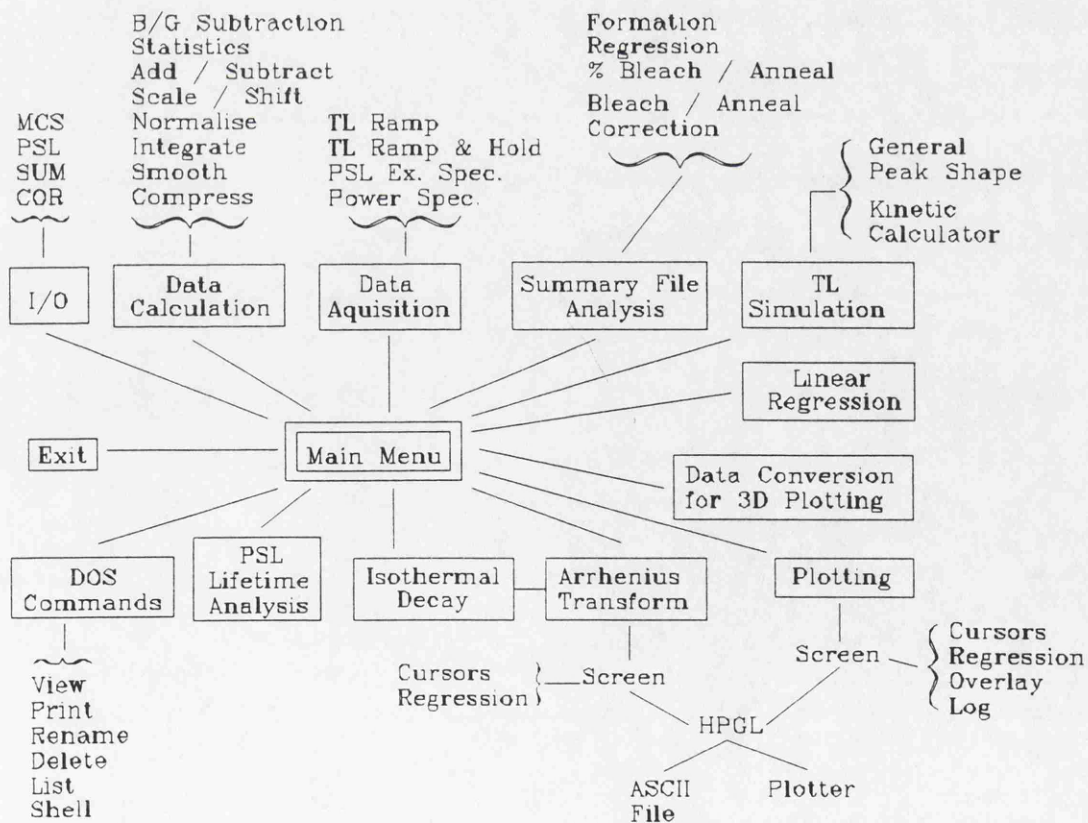


Figure 3.10 - Block diagram of the PSL software control structure.

concatenation of data for 3D plotting by UNIRAS, TL measurements, PSL excitation spectroscopy, pyroelectric radiometer measurements of the spectral output of the xenon lamp and simulation of TL glow curves including a kinetic calculator to calculate the effect upon lifetimes of changes in the trapping and storage parameters. Also, to facilitate the user's need not to exit from the program until full data analysis/manipulation has been finished, various DOS commands have been incorporated into the program including access to a complete DOS shell if so desired. A block diagram of the software control structure can be seen in Figure 3.10.

### 3.7.3.2 - Implementation

Data acquisition is performed through an EG&G Ortec ACE Multi-Channel Scalar (MCS) card which can store up to 4096 channels with a minimum dwell time of 2  $\mu$ s. It can be operated in a single pass mode, or in a multi pass mode with successive passes either overwritten or summed. In conjunction with the control program, the MCS card is operated in a multi-pass mode with successive passes overwriting the previous pass. The MCS card is set up with a high pass count, the dwell time required for the data acquisition and an external start of pass trigger. The emulator is then activated and lies dormant until receiving the start of pass trigger (a rising TTL edge supplied by the I/O card). The program is then run from within the MCS emulator and the data acquired is read directly from the memory location in the PC written to by the MCS card. Unfortunately, it is not possible to directly change any of the MCS parameters externally to the emulator, thus if differing dwell times are required (i.e. for different scan speeds or heating rates) the PSL program has to be terminated and re started with the new dwell time set up.

PSL excitation spectroscopy is controlled by a computer driven stepping motor connected to the monochromator. The stepping motor is controlled by negative 12 volt logic which is converted from positive logic TTL pulses from the I/O card via a set of transistors. The timing of the scan rate is controlled by a software loop which has the disadvantage of changing characteristics from one computer to another. The stepping

motor has no knowledge of the absolute wavelength of the monochromator, and so this necessitates the manual setting of start wavelength on the monochromator, however after this the software can keep track of the wavelength by counting the number of pulses sent to the stepping motor. Similarly, TL ramps are timed by a software loop, and reference temperatures are transmitted to the temperature controller via a 14 bit ADDA card. The actual temperature of the heater plate can also be monitored through the same ADDA card. Data from the pyroelectric radiometer is read through the I/O card, however although the range can be monitored by the computer, it has to be set manually as does the speed of response and the power / power density option. Unfortunately the range setting does not switch automatically when it goes over range, instead the output goes to zero and sets a flag. Thus either the range has to be altered manually within a scan (thus giving rise to some channels with no data) or the low power sensitivity has to be sacrificed in order to prevent high power regions from sending the radiometer over range.

Turbo Basic was chosen for its advantages over GWBasic in speed as a compiled language, the full screen editor, greater memory handling abilities and the high level programming facilities such as global and local variables within procedures as well as the more traditional BASIC subroutine and the end of reliance upon line numbers that is endemic of interpreted BASIC's. In point of fact, the development of the software has reached a stage which precludes the use of interpreted BASIC's where the total program size is limited to 64 kbytes and total array / string space is also limited to under 64 kbytes, as the program code is currently 72 kbytes long with a variable space of 77 kbytes and compiles to a 148 kbyte EXE file. The size of the program has necessitated the splitting of the code into two 64 kbyte segments and the dividing of the text into various sub programs, all of which are incorporated upon compilation into the one EXE file.

## 3.8 - Pulsed Infra-Red LED system

### 3.8.1 - Components

This system uses high power GaAlAs infra-red LED's supplied by RS Components Ltd for the work presented here, although it will drive many different LED's. Peak emission is at around 880 nm with a rated spectral bandwidth (FWHM) of 80 nm at a power of 20 mW driven at 100 mA, with a rise/fall time of  $\sim 0.5 \mu\text{s}$ . The driver for these LED's was built in house by Mr K. J. Cairns, from a design by Dr D. C. W. Sanderson. It is capable of generating pulses from 1  $\mu\text{s}$  to 5 s in width, with delays between pulses from 10  $\mu\text{s}$  to 0.5 s giving rise to repetition rates from continuous mode to  $\sim 90 \text{ kHz}$ . The LED's are driven by a constant potential source with resistive current limitation to facilitate control of pulsing. Several arrays of LED's can be driven; a cluster of 3 LED's directed such that they can be used in any of the chambers that possess an angled heater plate and arrays of 8, 16 or more LED's in a circular arrangement can be used in conjunction with flat heater plates found in more conventional TL ovens.

Data acquisition is via a similar photomultiplier and associated electronics to the scanning excitation spectrometer (see section 3.7) with the MCS card being used solely with its own emulation software as control for this has not yet been built into the control software. Each pass of the MCS is synchronised to the LED pulse and can be triggered externally by either the rising or falling edge of the LED pulse. Data is normally acquired with the MCS in multi-pass mode with the results of each successive pass being summed to give the combined signal from a total number of pulses. A block diagram of the control structure for this system can be seen in Figure 3.11. The temperature of the sample can be controlled in a similar manner to the excitation spectrometer, except that the temperature reference is generated internally via a potentiometer rather than externally via an ADDA card in the computer. The LED system also lacks the cooling coil in the excitation spectrometer, however if cooling of the sample is required then the arrangement of three LED's can replace the xenon lamp light source in the excitation spectrometer and thus samples can be measured and hence

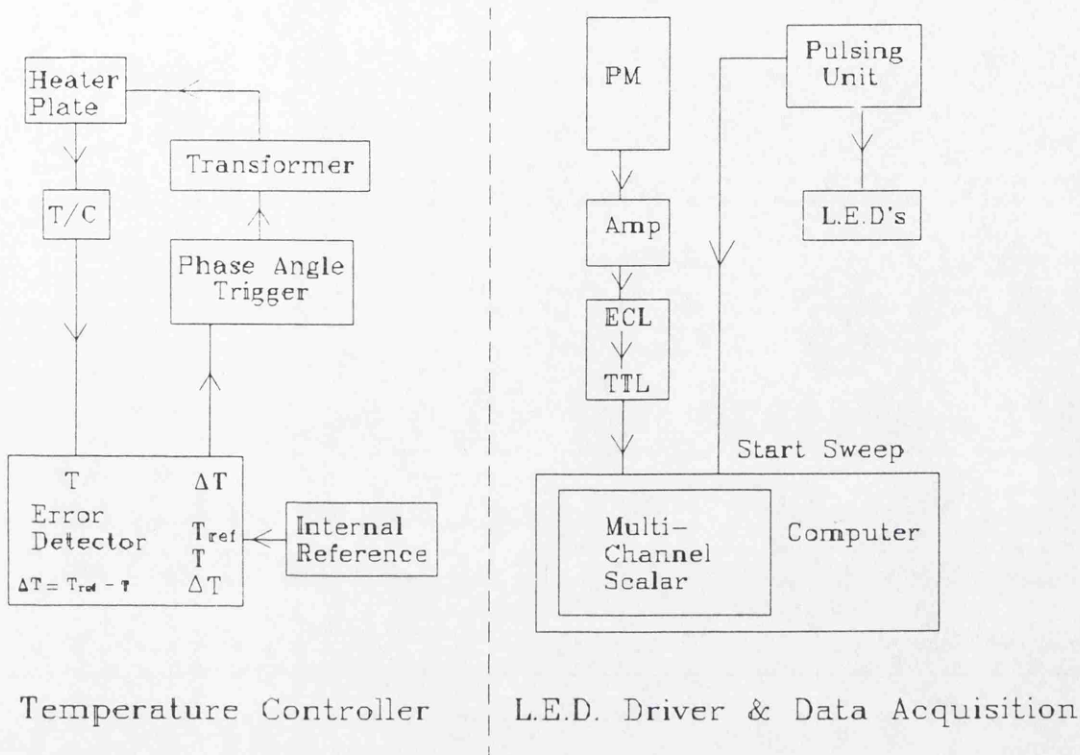


**Figure 3.11** - Block diagram of the LED system control interface.

cooled in the excitation spectrometer system.

### 3.8.2 - LED Response Time

In order to measure the rise and fall time of the LED's in response to the TTL driving pulse, the light output from the LED's was monitored by a photodiode driven in photo conductive mode (in which the photodiode is reverse biased which should result in a linear response to the incident light irradiance), the output of which was recorded on a 40 MHz digital storage oscilloscope (Tektronix model 2211, 40 MHz analogue, 20 MHz digital). The photodiode was a PIN type which has an intrinsic semiconductor layered between the normal p-n junction of a photodiode in order to give a good long wavelength response. The peak response of the photodiode (type BPX65 obtained from RS Ltd) was at 850 nm with a quoted average rise time of 0.5 ns and maximum rise time of 1 ns. The resulting trace recorded on a time base of  $20 \mu\text{scm}^{-1}$  in response to  $20 \mu\text{s}$  pulses separated by a delay of  $20 \mu\text{s}$  can be seen in Figure 3.12.

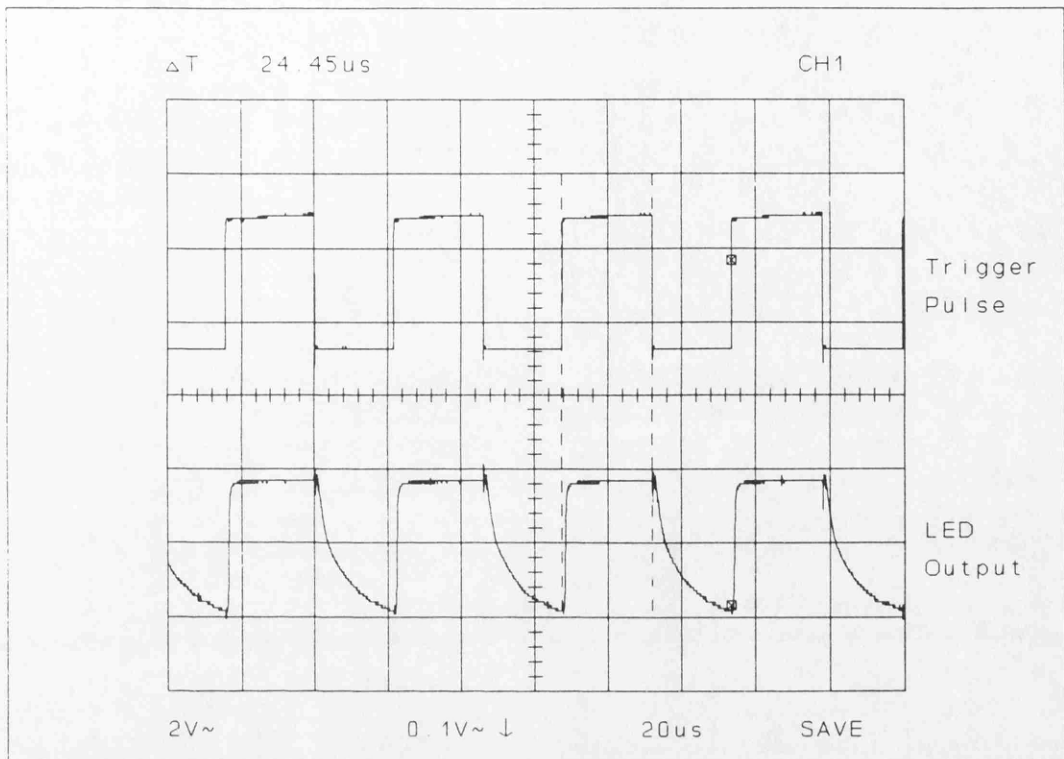


**Figure 3.12** - LED response to TTL pulses

The pulse shape can be seen more clearly in an enlarged section of the trace defined by the two cursors as shown in Figure 3.13. This clearly shows a delay in the LED output after the rise of the TTL pulse, followed by a fast rise. After the TTL pulse falls there again is a delay before the LED responds, followed by an exponential decay. Observations of this pulse shape using a shorter time base of  $0.2 \mu\text{scm}^{-1}$  enabled easy measurement of these parts of the pulse. The delay before the LED rise was recorded to be approximately  $0.6 \mu\text{s}$ , followed by a rise time (10%-90%) of  $0.7 \mu\text{s}$ . After the fall of the TTL pulse, there again was a delay of  $0.8 \mu\text{s}$  before the LED responded and then a fall time (90%-10%) of  $13 \mu\text{s}$ . The rated rise and fall time for the LED was of the order of  $0.5 \mu\text{s}$  and it can be seen that the start of the LED pulse matches this well. However the long decay after the end of the triggering TTL pulse was not expected. The shape of this decay looks like an exponential decay as if an element in the LED / photodiode circuitry were undergoing capacitive discharge. The driving TTL pulse shown above drives two transistors which switch the high current to the LED's, however a pulse indicating LED is also driven by the final transistor and the rise and

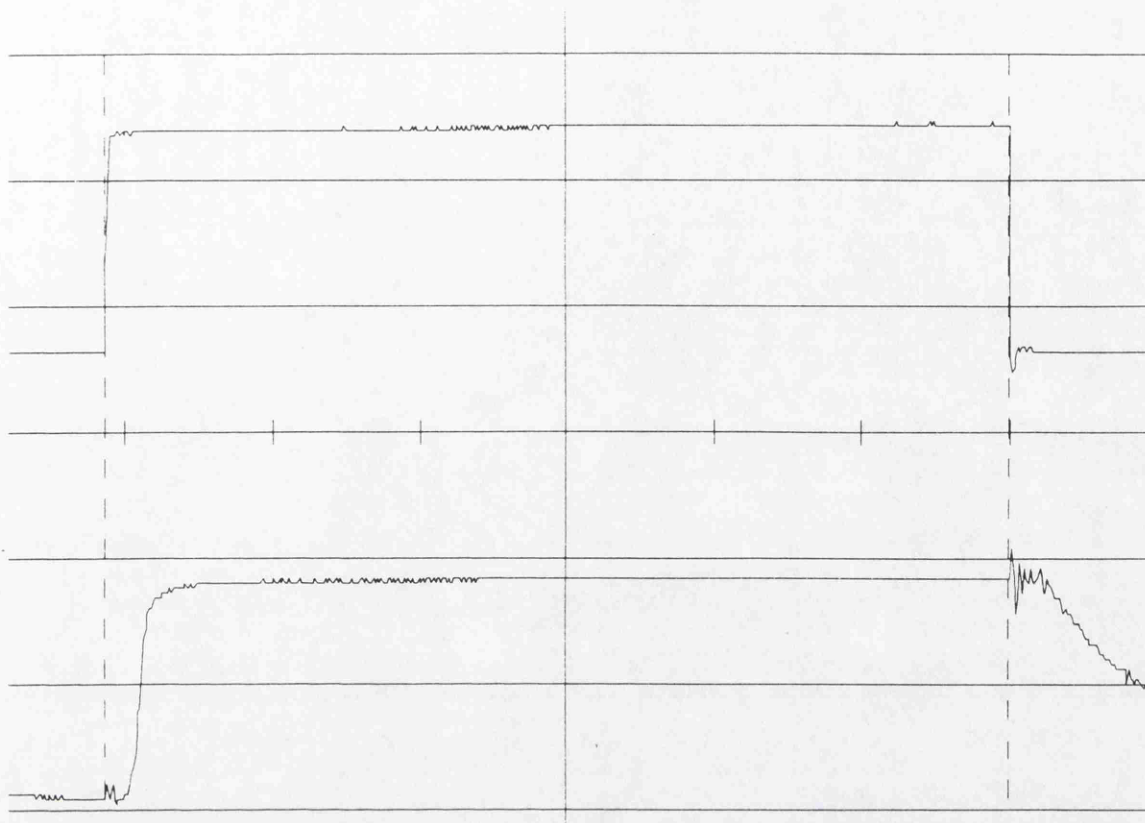


**Figure 3.13** LED pulse shape

fall of the current to the LED's will be limited by the rise and fall of the current through the indicating LED, which is only a general purpose LED which has a much longer decay than the high power GaAlAs LED's being driven.

### 3.8.3 - Control Software

At the present stage of development of this pulsed system, control of the data acquisition is performed manually within the confines of the MCS emulator and thus saved as .MCS files from the emulator. Operating in this manner has several advantages over incorporating control into the PSL software package, the most important being flexibility of control. As the dwell time, pass length and pass count can not be changed externally to the emulator, if flexibility in these settings is required (as is the case for stimulation and detection optimisation) then control has to remain within the emulator. Once a fixed stimulation regime has been decided upon then it will be comparatively simple to pass control to the PSL software package.

Files saved from the MCS emulator (.MCS) can be read by the PSL software and analyzed in exactly the same manner as those acquired via the PSL software. For total compatibility it is possible to save .MCS files in the PSL format once they have been read into the PSL software. The MCS emulator does have an external channel advance trigger which could bypass the internal dwell time and thus allow flexibility in the dwell setting, however the pass length and pass count still can not be changed outside the emulator, thus the operator would have freedom to change the dwell, but not the pass count and pass length if this method of control were to be incorporated into the PSL software. Another disadvantage of this method of controlling the MCS is that external timing would be required and achieving this (especially in the  $\mu\text{s}$  time scale) would add further complications to the implementation of the software, which at this stage seems to be over complicating the issue and would reap little benefit, however this does not preclude the possibility of incorporating such control into the PSL software in the future.

### 3.9 - Pulsed Tunable Dye Laser System

From the outset of this project it was conceived that pulsed stimulation could be a very important technique in PSL research. The response to pulsed stimulation should yield high signal to background ratios, and this coupled to the greater power input of a laser over the xenon lamp should yield much greater sensitivity. It has also been proposed that observations of the charge carrier dynamics on a short timescale (i.e. microseconds) could yield valuable information on the dynamic processes in PSL. In order to record data of this sort, a pulsed source is required that can generate well defined, high power pulses, with the greatest flexibility being obtained from a device that is tunable throughout the spectral region of concern. It was decided that the optimum stimulating source within reasonable cost constraints was a high power pulsed nitrogen dye laser.

### 3.9.1 - Components

The pump laser is a 2.3 MW pulsed nitrogen laser (model PL2300 from Photon Technology International Inc.), yielding 1.4 mJ per pulse with a width of 600 ps at  $337.1 \pm 0.05$  nm. The energy stability of the laser is quoted at 5% and the repetition rate is adjustable from single shot to a maximum rate of 20 Hz. Nitrogen input to the system is from standard laboratory grade (99.999%) nitrogen direct from the cylinder and the gas is used in continuous flow through the laser, as opposed to some nitrogen lasers which use sealed nitrogen chambers. The laser is spark gap triggered, using a combination of two spark gaps in a nitrogen atmosphere to switch the required high voltage to the laser channel. The output from this laser is fed directly into a high power dye laser module (model PL201 from Photon Technology International Inc.) yielding a final rated output of 480 kW, being 240  $\mu$ J per pulse over 500 ps at  $500 \pm 1$  nm with a 500 nm peak emission dye. The laser is capable of pumping a wide range of dyes resulting in a possible continuously tunable range of 360-900 nm, although the power drops off considerably with dyes above 650 nm. The dye is contained in a standard 1 cm cuvette and requires no stirring or circulation. The dye laser is configured as a Littrow cavity with wavelength selection being governed by a diffraction grating yielding a 1 mm output beam.

The ensuing beam is coupled to the sample chamber via an in house built x10 beam expander assembled from a plano concave lens of focal length -10 mm and a plano convex lens of focal length 100 mm arranged with coincident foci. The concave lens is used rather than a convex lens to avoid focusing of the laser beam with its associated high power density. The sample chamber is similar to that in the scanning excitation spectrometer in that the sample is held on a 45° plate which can be heated in the same manner as the LED system. Signal detection is also performed in a similar manner to the excitation spectrometer, with the exception that control of the data acquisition is not provided by the control program, rather the MCS emulator is used with an external trigger provided from the laser itself, 1  $\mu$ s before the laser pulse. A block diagram of the control structure can be seen in Figure 3.14.

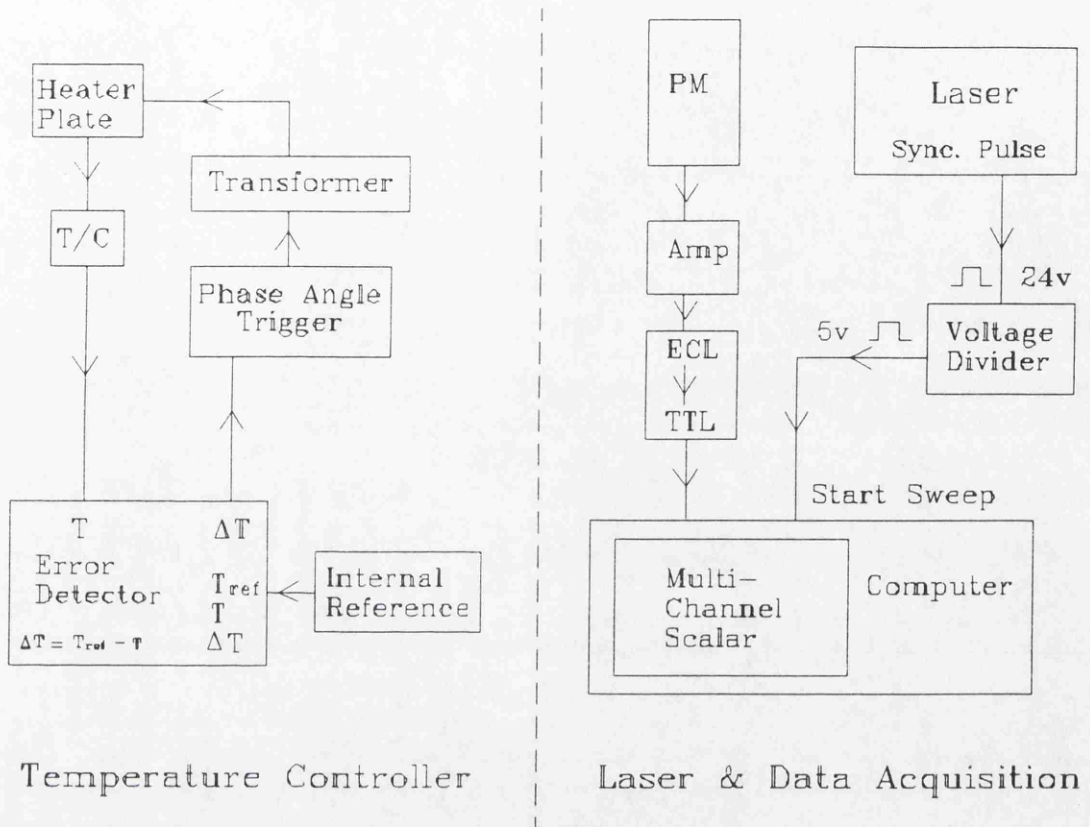


**Figure 3.14** - Block diagram of the Laser control interface

### 3.9.2 - Control Software

As with the LED system, control of the data acquisition in this system is performed by the MCS emulator with the start of the sweep being synchronised to each laser pulse via a synchronisation pulse generated by the laser  $1 \mu s$  before the laser pulse. As with the LED system, data acquisition is normally collected with the MCS in multi-pass mode with the output from successive passes (and hence laser pulses) being summed, although the much higher power output of the laser does mean that measurable signals can be obtained from a single pulse. Again, as with the LED system, data are saved directly from the emulator in .MCS format with data analysis and presentation being performed within the PSL software.

### 3.10 - Optical Filtering

One main difficulty with optical stimulation techniques is the separation of the stimulation and detection windows. With synchronous stimulation and detection, the separation has to be provided by optical filtering of both the stimulating light and the photomultiplier. Long wave pass filters between the stimulating source and the sample provide a sharp lower edge to the possible stimulating wavelengths, which is essential to block white light leakages through monochromator systems and super fluorescence of dye laser systems. These filters also play an important role in blocking the short wavelength tail of LED's which can extend out to 2 or 3 times the FWHM wavelength and thus just penetrate the high wavelength edge of the detection window. Achieving optimum filtering of the photomultiplier is quite an involved process as one is trying to achieve maximum width of detection window with minimum cross over into the stimulation window. For high wavelength stimulation, this can be achieved quite easily with the use of short wave pass interference filters. However, these tend to have very limited transmission below 400 nm and so to be able to detect on the short wavelength side of short wavelength stimulation, it is probably better to use colour glass filters, although for extreme detection in to the UV, quartz filters would be required.

The filter combinations used in the above systems are as follows;

#### Excitation Spectroscopy

Stimulation: Schott GG420 Long pass filter (scan 400-800 nm) (3 mm)  
Schott GG475 Long pass filter (scan 450-900 nm) (3 mm)  
Schott RG780 Long pass filter (scan 750-1500 nm) (3 mm)

*Note: the upper wavelength limit of the scans is due to interference from the second order transition through the monochromator which is at half the principal wavelength.*

Detection: Schott UG11 } Band pass filters (detection band 300-400 nm)  
Schott BG39 }

#### 480 nm Excitation - Laser and Lamp

Stimulation: Schott GG420 Long pass filter (3 mm)

Detection: Schott UG11 Band pass filter (6 mm)

#### Infra-Red LED

Stimulation: Schott RG780 Long pass filter (3 mm)

Detection: 600 nm Short pass filter, manufactured by Envin Scientific Products Ltd. (3 mm)

### 3.11 - Future Developments

Although the excitation spectrometer is a useful and flexible tool, there is plenty of scope for further development in the future. Perhaps the principal way in which it could be adapted is to reconfigure it to couple the detection side to an emission spectrometer. One way of doing this would be to divert the output through a set of rotating band pass interference filters (similar to the spectrometer used in Bailiff & Poolton, 1991 and described in Bailiff *et al*, 1977) which would give broad band emission spectroscopy for an excitation wavelength well defined by the monochromator. Alternatively the monochromator could be coupled to the emission side of the spectrometer, thus giving well defined, high resolution (if desired and sensitivity permits) emission spectroscopy

(similar to the spectrometer used by Dalal *et al*, 1988) to broad band excitation wavelengths defined by optical filters. The current photomultiplier would limit wavelength detection to the bluer end of the visible spectrum and to extend the detection limit into the red end, a red sensitive photomultiplier with its associated cooling mechanisms (to reduce the inherently high dark count of such tubes) would be required. If well defined emission (high resolution) spectroscopy is to be acquired from well defined (high resolution) excitation wavelengths, then monochromators would be required on both the excitation and emission sides of the spectrometer. The original design of the spectrometer included provision for emission spectroscopy, and thus reconfiguring the spectrometer should be relatively straightforward.

At present all of the systems rely upon the stimulation and detection regions being well separated, however it does seem likely that stimulation and detection would need to be investigated within the same wavelength region (especially if combined excitation and emission spectroscopy were to be performed). Consequently to allow for this, it will be necessary to arrange for asynchronous detection using a pulsed means of stimulation. This would necessitate either rapid switching of the photomultiplier or some external shutter between the photomultiplier and the sample in order to protect it from seeing the stimulating pulses. A problem arises in that for high efficiency, the switching time would have to be very short (i.e. microseconds) which could create problems in the switching of high voltage to the photomultiplier and thus perhaps the better approach would be to use a Pockels cell between the photomultiplier and sample which can have switching times as short as 10ns (Hecht & Zajac, 1974), providing that the extinction ratio is high enough. The possibility (if not probability) of the requirement for pulsing was foreseen, and thus a Pockels cell was acquired with the original spectrometer components. Hence the move to asynchronous detection from pulsed stimulation should be straightforward.

Direct *in situ* monitoring of the excitation beam power would also help to remove uncertainties from the final results by making automatic corrections for fluctuations in the output power of the excitation source, be it a lamp, LED's, or a laser, as the PSL measurement is made. Even a well characterised source is not free from the

uncertainties of run to run reproducibility and fluctuations of at least 5% of beam power can be expected in most sources. Such *in situ* monitoring could be achieved by placing a photodiode directly in the beam path if the beam is wide enough, or by splitting of a reference beam from the main beam by partial reflection and monitoring that with some photoelectric device. Needless to say, in such monitoring there will always be some uncertainty in beam power as there will be uncertainties in the monitoring technique, although it would be expected that these should be less than those inherent in the source.

Finally, another development of the system that could prove invaluable to any PSL dosimetric system is sample automation. The question of excitation beam homogeneity leads to the importance of maintaining run to run sample orientation, and the necessity of removing samples for irradiation automatically generates uncertainties in this respect. An automatic sample changer with a built in irradiator would ensure that the same alignment and geometry is maintained after each irradiation. This problem of orientation is important if an additive dose run is performed on a single sample or on a set of samples as even the set of samples will need to be dosed and read three times to give the  $N+\beta$ ,  $\beta$  and normalisation doses.

### 3.12 - Summary

As outlined above, there are three major research tools available for use in this project, the excitation spectrometer, the pulsed infra red diodes and the pulsed dye laser. The spectrometer at the start of this project was built, and during the course of this project it was characterised and implemented as a research tool with the development of a comprehensive software suite to provide automated control of the spectrometer and wide ranging and varied data analysis. The major advantage of the spectrometer is flexibility of use in that it can yield information on the relative behaviour of different components of the excitation spectrum under many different stimulating conditions. The pulsed systems are important in terms of sensitivity, signal to background ratios, and also in the ability to be able to observe charge carrier recombination dynamics directly.

These three research tools have many potential roles beyond this project, especially the pulsed laser, and thus are undergoing continuous review and development. The work presented in the following chapters represents a comprehensive introduction to the PSL phenomenon in feldspar, always with a view to its potential in dating. It is hoped that the research tools described above will be able to eventually yield a complete description of the phenomenon, however this is necessarily a lengthy and complex task that lies beyond the scope of a single PhD project and thus the following work forms an important part of a continuing research topic.

#### **4 - Photostimulated Luminescence of Feldspar - I**

Having introduced theoretical considerations, measurement techniques and instrumentation, a series of spectroscopic experiments was undertaken with the aim of placing the phenomenon on a firm physical basis, bearing in mind the dating application. The work begins with detailed exploration of the excitation spectrum (of samples with high doses to provide high measurement sensitivities) in order to identify useful stimulation bands, incorporating studies of the effect of monochromatic bleaching at differing wavelengths (in order to check for interactions between various stimulation bands and provide information upon the luminescence kinetics). This is followed by investigations of the temperature dependence of the stimulation bands (in order to observe whether there are thermal interactions with the photon eviction process that could affect kinetic analysis and thermal stability), exploration of the thermal stability of the stimulation bands (as the dating task requires thermally stable signals over the timescales being measured) and the high dose response (in order to obtain some information on the likely upper dating limit).

Just as it is important to identify and understand the nature of the stimulation bands, so knowledge of the emission bands can provide very useful information, especially for detection optimisation. Thus the work presented moves into emission spectroscopy to identify the emission bands and their response to bleaching and variations in temperature. The information resulting from the excitation spectroscopy and the emission spectroscopy can then be combined to optimise the stimulation and detection efficiencies of each stimulation region used. This optimisation, coupled to changes in stimulation techniques, will be shown to increase sensitivity such that doses in the Gray region can be measured (as will be required for dating) and low dose growth curves constructed as the first major step towards the development of a technique that may be implemented as a dating tool.

In all the following experiments, the samples are mounted on 1 cm stainless steel discs with silicon grease spray, with a mass of between 5 and 10 mg.

## 4.1 - Excitation Spectroscopy

The excitation spectroscopy referred to here is the variation in luminescence output of the minerals examined with excitation wavelength, with all excitation spectra recorded being acquired using the scanning excitation spectrometer described in section 3.7 above. Many excitation spectra have been obtained for the potassium feldspar microcline and the IAEA standard feldspar, F1, yielding a consistent and highly reproducible data set. Variations in excitation spectra have been observed with variations in power of the lamp, monochromator slit width, scan speeds, temperature and dose. Excitation spectroscopy has formed the main bulk of the work carried out in this project as it is such a valuable tool for helping to come to some understanding of the underlying mechanisms behind the PSL phenomenon, providing pointers to trap depths, thermal assistance and correlations between different stimulation bands that may result from similar trapping sites. Consequently, the results presented in this section form only a summary of a very much larger data set.

### 4.1.1 - Excitation Spectra

#### 4.1.1.1 - Microcline

The first excitation spectroscopy performed in this laboratory was on the mineral microcline, and much of this work was performed as part of the MAFF project N384, 'The Development of Luminescence Tests to Identify Irradiated Foods' as the development of the spectrometer and related optical techniques was required by both projects. Initially, the spectra were recorded with a 500 nm blaze grating installed in the monochromator as the response of this grating was expected to coincide with the most likely stimulation region. A typical spectrum can be seen in Figure 4.1 from a sample of microcline which had been annealed at 500°C for 5 minutes prior to receiving a dose of 100 Gy in the <sup>90</sup>Sr β source and was stored in the dark prior to scanning. The sample was preheated at 180°C for 1 minute to remove phosphorescence

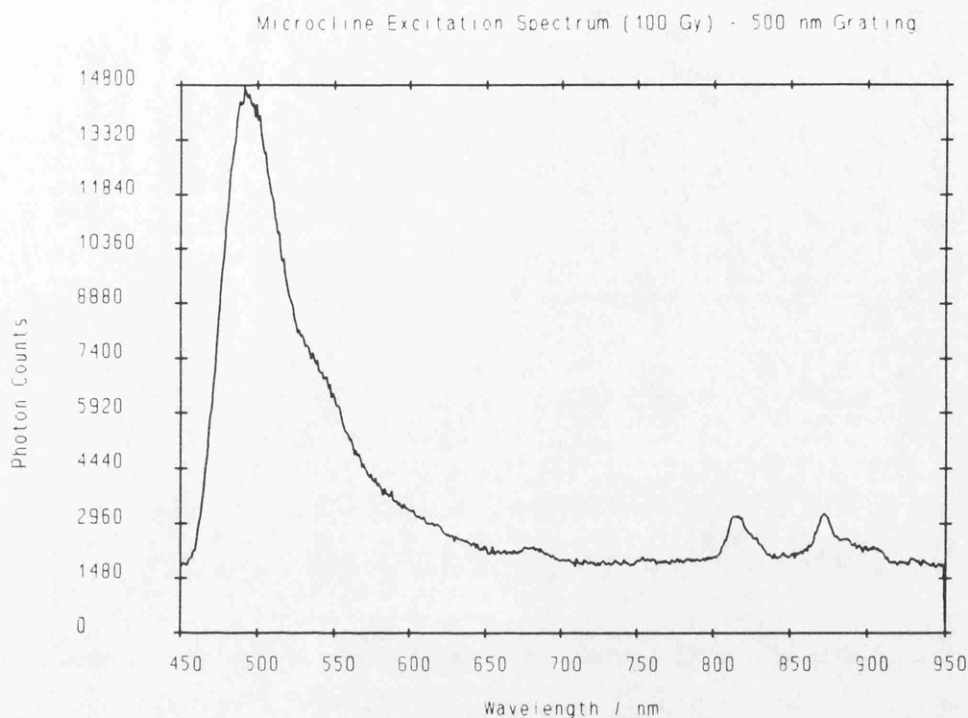


**Figure 4.1** - Microcline excitation spectrum (100 Gy) with 500 nm grating.

and low temperature TL components. The excitation spectrum was recorded with a scan speed of 240 nm/minute with slit widths of 2.5 mm (11.5 nm bandpass) on the monochromator with a 3 mm GG475 Schott colour glass filter between the monochromator and the sample for order sorting purposes. Detection was in the blue / u.v. region, being defined by the presence of a KG1, UG11 and BG39 filters in the photomultiplier casing, before the tube. From this graph, there appear to be three peaks, at 490, 816 and 871 nm, however the lamp power spectrum (section 3.7.2 and Figure 3.3) must be taken into account. In particular it can be shown that the two infra-red peaks arise from a superimposition of the lamp spectral lines upon a single broad smooth, continuous excitation peak. These results were not power normalised, however this important spectral correction became possible at a later stage in the project.

The existence of a stimulation peak in the infra-red region provided great interest as the a trap at a depth equivalent to 850 nm (1.46 eV optical depth) raises many interesting questions concerning the stability and stimulation mechanisms responsible. A mechanism was proposed (Hütt *et al*, 1988) during the early stages of this project. This

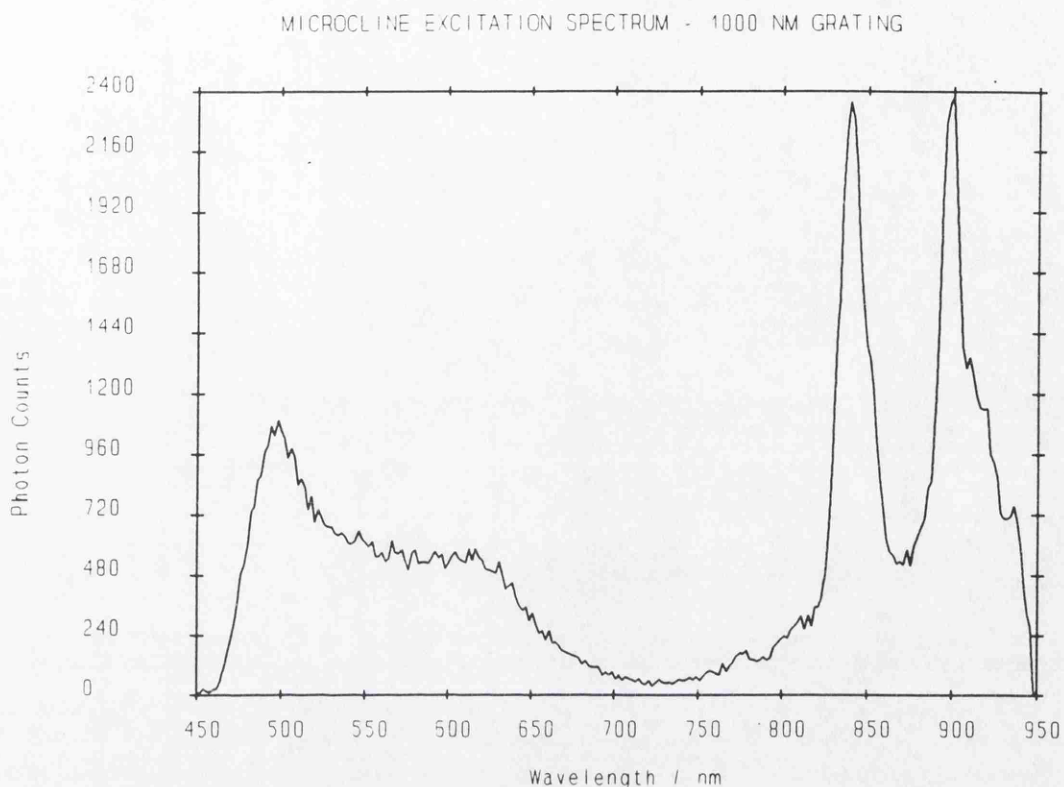


**Figure 4.2 - Microcline Excitation Spectrum (1 kGy) with 1000 nm Grating**

was that the optical stimulation merely promoted charge from a ground state to a metastable excited state, from which the thermal energy present at room temperature was great enough to evict the charge into the conduction band before it had a chance to relax back to the ground state, thus giving rise to luminescence. In order to examine this region in more detail, a second monochromator grating with a 1000 nm grating was obtained which was particularly suitable for the range from 660 - 1500 nm. A typical microcline excitation spectrum recorded with this grating is shown in Figure 4.2, acquired using the same filters, speeds and preheating regime as the previous spectrum. Power normalisation of this spectrum was possible using averaged power spectra recorded using a pyroelectric radiometer. This is depicted in Figure 4.3, indicating what appears to be a single broad stimulation peak centred on approximately 860 nm. However, in a spectral region where the normalisation procedure accounts for numerous sharp spectral lines, the resulting spectra are of course subject to residual fluctuations arising from the difficulties of precise spectral alignments. This can be mitigated by substitution of a spectrally smooth stimulating source (see below). Other factors to note

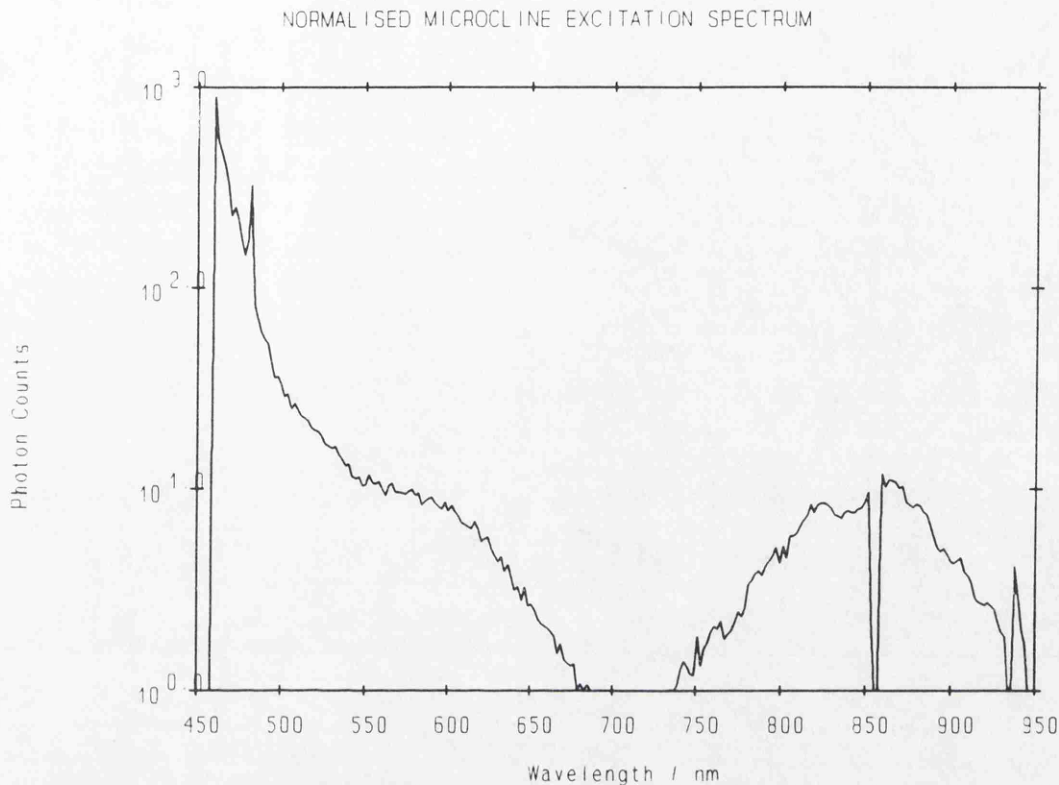


**Figure 4.3** - Power Normalised Microcline Excitation Spectrum

concerning the normalised excitation spectrum (Figure 4.3) are that it is plotted with a log intensity scale as the power normalised green/visible excitation band is much greater in intensity than the infra-red band (as opposed to Hütt & Jaek, 1989, who state the opposite of this), and that the sharp rise and edge at around 450 nm is an artifact generated by the presence of the GG475 order sorting filter between the monochromator and the sample.

#### 4.1.1.2 - IAEA Feldspar, F1

After exploring some of the excitation properties of the microcline samples, a decision was taken to base more detailed investigations on an international reference feldspar. This would be readily available to other laboratories for use in complementary studies. An IAEA secondary potassium feldspar standard (IAEA F1) was selected on grounds of ready availability, good homogeneity and moderate cost. Since this decision was made, several other luminescence laboratories are known to have obtained supplies of

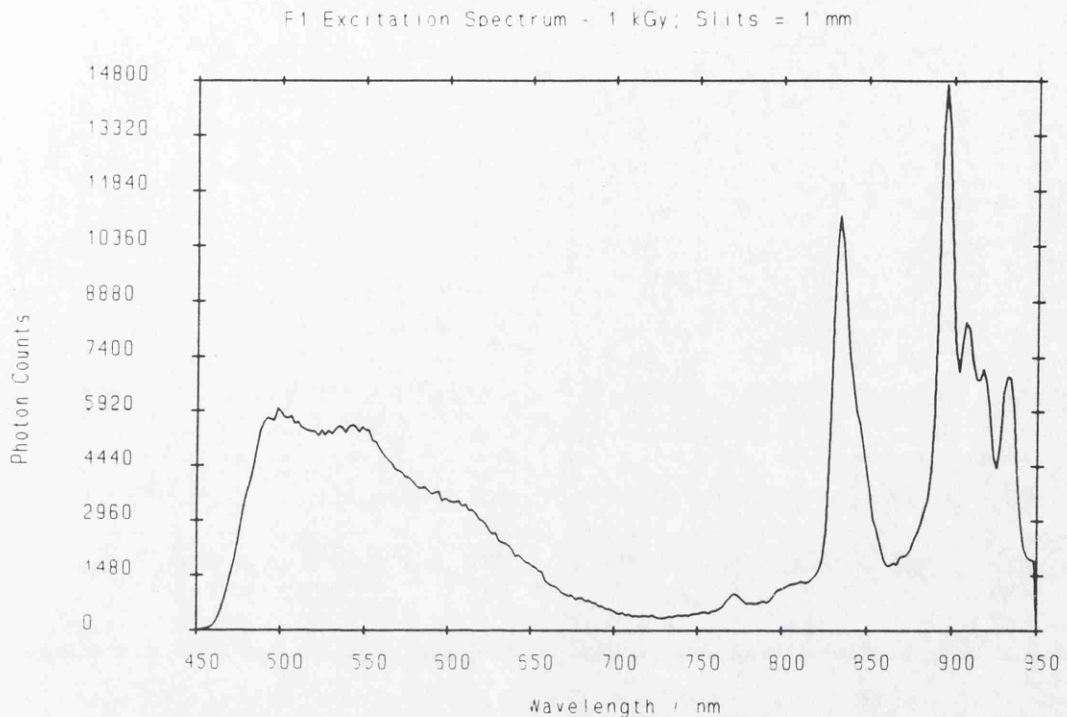


**Figure 4.4** - F1 Feldspar Excitation Spectrum

the same material. Excitation spectroscopy was performed on this material (irradiated in bulk by a 200 TBq  $^{60}\text{Co}$  source to 1 kGy), however unlike the microcline, all spectra were recorded using the 1000 nm blaze grating in the monochromator. A typical excitation spectrum for this material is shown in Figure 4.4 and power normalised in Figure 4.5. The resulting stimulation spectrum was recorded using a scan speed of 240 nm/minute with monochromator slit widths set to 1 mm, resulting in a spectral excitation band pass of approximately 9 nm. Again the order sorting filter was a GG475 and the detection window was again defined by the same UG11, BG39 and KG1 filters and there was no preheat. In comparison to the microcline spectra, it can be seen that there is a strong similarity between the spectra of the two minerals. Both of the minerals appear to have excitation bands centered on about 500, 600 and 860 nm. However, in the case of the IAEA F1 feldspar, an additional stimulation band has appeared at approximately 550 nm.

In order to verify the apparent single broad peak nature of the infra-red stimulation band, an excitation spectrum in this region was recorded using a stimulating source with

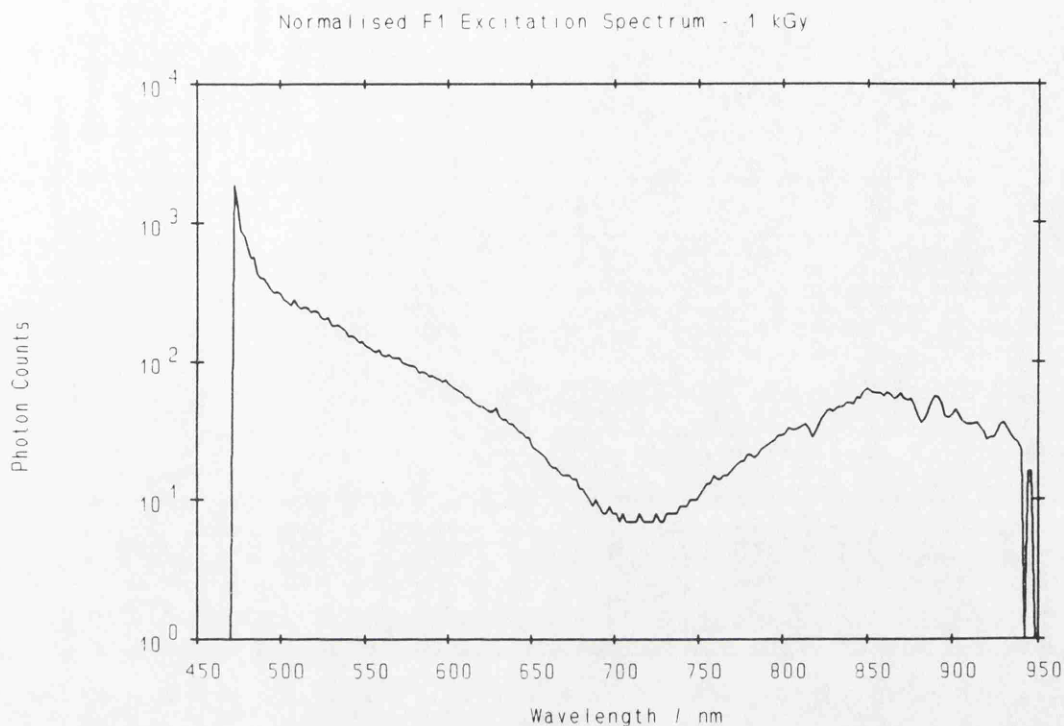


**Figure 4.5** - Normalised F1 Feldspar Excitation Spectrum

a smooth spectrum. Such a source was found in a Kindermann projector which housed a 250 W tungsten lamp. The heat absorbing filter was removed (which is situated between the bulb and the slide) and the projector was coupled to the scanning excitation spectrometer in place of the xenon lamp. As the power output of the projector was significantly less than that of the xenon lamp, it was necessary to use greater slit widths on the monochromator, and thus lower resolution of the excitation wavelengths. Again the spectrum was recorded using the same settings and filters as before with the exception that the monochromator slit widths were set to 6mm and the order sorting filter was changed to an RG645. The resulting spectrum can be seen in Figure 4.6. As can be seen, this sample is confirmed in having a single broad excitation band, centered on approximately 890 nm. However, it must be remembered that this spectrum was recorded using an excitation spectral bandpass of approximately 56 nm and so the possibility that there is unresolved structure within this band can not be ruled out.

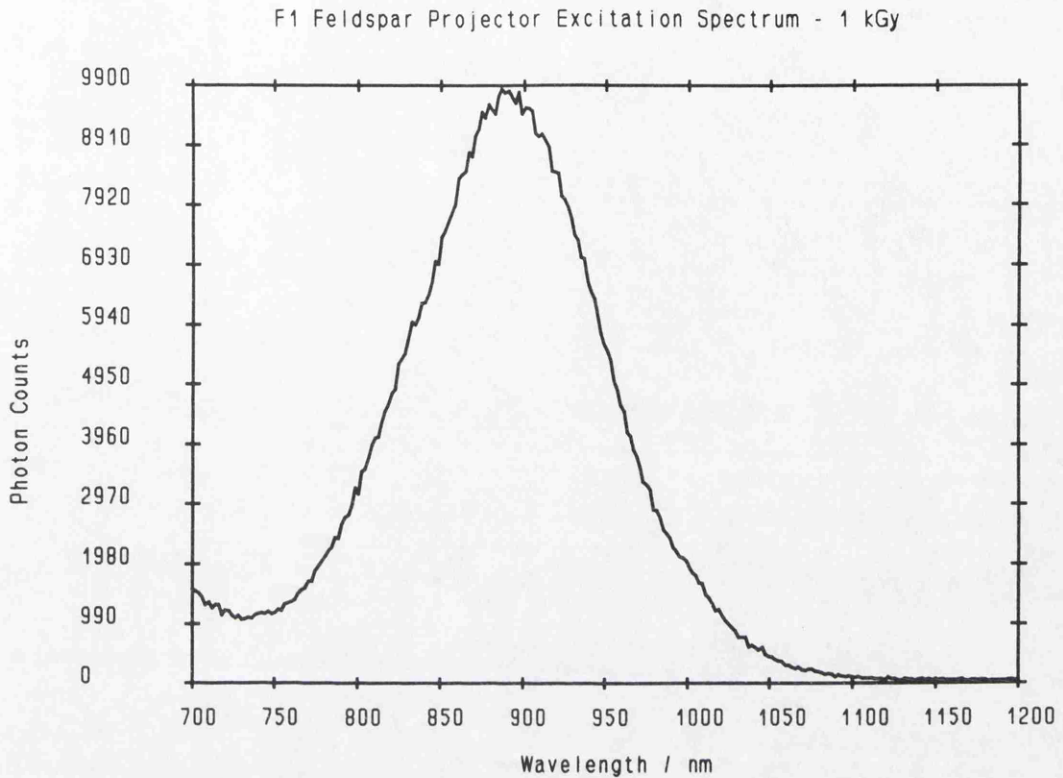


**Figure 4.6** - F1 Excitation Spectrum Recorded Using a Slide Projector

#### 4.1.1.3 - Comparison With Published Spectra

PSL excitation spectra of feldspars have been studied in Estonia (Hütt *et al*, 1988 and Hütt & Jaek, 1989) and thus comparisons will be made of the above results to the work published by this laboratory. In Hütt *et al* (1988) the excitation spectra of potassium feldspars after various irradiation and preheating treatments were recorded using a xenon lamp and have stated to have been corrected for the energy distribution of the lamp. Regrettably, few experimental details are given. In particular it is unclear from the text whether response corrections were based on measured spectral distributions of the instrument or using nominal values. Also details of order sorting filters are not described even though this could have important implications in generating harmonic effects. The results identify stimulation peaks at 2.25, 1.43 and 1.33 eV which corresponds to wavelengths of 552, 869 and 934 nm respectively. A point to note is that the excitation lower limit for these excitation spectra was 550 nm and thus the low wavelength (high energy) cut off is likely to be due to the filters (shown in a diagram,

but not in the text) separating the excitation and emission wavelengths. The major difference between these excitation spectra and those presented above is the presence of two peaks in the infra-red region. It has been shown above that for the two potassium feldspars studied in this thesis, the infra-red band (after power normalisation) is composed of a single broad peak, a fact which was reinforced by the observation of a single broad peak due to stimulation by a smooth infra red source.

This discrepancy is demonstrated again in Hütt & Jaek (1989) where this time the excitation spectrum was recorded using a pulsed excimer dye laser, showing peaks at the same energies as before, however it appears that no measurements were made below 540 nm and thus it is not clear whether the edge at 540 nm is due to a true edge of a stimulation peak or just due to the effect of edge cut filters separating the excitation and detection bands. From the results presented in sections 4.1.1.1 and 4.1.1.2 it has been shown that if the stimulation band can be extended towards 400 nm whilst avoiding overlap into the detection band then the excitation band at around 550 nm will extend down to below 500 nm with evidence that the peak (even at wavelengths as short as 480 nm) is due only to the presence of the edge cut filters separating the excitation and detection windows. Unfortunately, no mention is made in Hütt & Jaek (1989) as to whether or not the excitation spectrum is corrected for the relative power output of the laser, this is especially important in the case of dye lasers as the power output will vary greatly from dye to dye and also across the tuning range within each dye. This lack of experimental detail, especially the absence of details about the dyes used and power corrections to the excitation spectra, is highly regrettable.

Another difference between these published spectra and those presented above are the claims as to the relative sensitivities between the green and infra red excitation bands. In the results above it has been clearly shown that on power normalisation of the spectra, the PSL per unit power from green stimulation is an order of magnitude or more greater than that yielded by infra red stimulation (Figure 4.5). This difference between the two bands will be even greater if the response per photon is considered. However, in both Hütt *et al* (1988) and Hütt & Jaek (1989), it has been stated that the converse is true, and that the signal is relatively weak when using green stimulation as

opposed to infra-red. It must be remembered that different samples were used for these studies, and that one cannot be certain whether this difference is due to the samples used, or whether it is due to differences in analysis. Nevertheless it is notable, however, that all of the excitation spectra published by the Estonian group are very similar to the *unnormalised* excitation spectra presented above (i.e. Figure 4.4), albeit with lower resolution. Given the lack of clear detail in these papers, doubts remain as to the nature or adequacy of any normalisation procedures adopted. The only way for this question to be resolved would be for the analysis of the same sample by different groups, and it is suggested that the IAEA F1 feldspar should be used for this purpose. It will be shown later that there are also difficulties in reconciling the stimulation model proposed by Hütt & Jaek (1989) with the totality of spectral and thermal evidence.

#### 4.1.1.4 - Survey of Feldspathic Minerals

In order to observe any variations between the excitation spectra of different feldspathic minerals, and also any variations within a single mineral family, a variety of such minerals were obtained from the SURRC geology department. These minerals had been separated for geological dating and a total of 30 samples were obtained including Albite, Muscovite, Microcline, Plagioclase and Potassium Feldspar. The samples are summarised in Table 4.1. Each sample was given a dose of 1 kGy on top of any residual geological signal and stored for a day before scanning to reduce room temperature phosphorescence. Duplicate aliquots from each sample were scanned at a rate of 240 nm/minute from 450 to 950 nm with slit widths of 2 mm, which is equivalent to a spectral bandpass of just under 20 nm. The order sorting filter used to reduce / eliminate second order effects from the monochromator was a 3 mm GG475.

Examples of the excitation spectra obtained from each feldspathic family can be seen in Figure 4.7 to Figure 4.10. These results show that there is a wide range of sensitivities within and between sample types. This can be seen more clearly (as measured at 540 nm), in Figure 4.11, spanning some 3.5 orders of magnitude. The structure of all of the excitation spectra was similar to those already observed from the microcline and F1 feldspars shown above, however marked differences were observed

**Table 4.1 - Feldspathic Minerals used in Excitation Spectra Survey**

Sample N°	Mineral	Reference N°	Location	Reference
PL003	Albite	RC14	S.Harris	Unpublished
PL004	Albite	RC168	S.Harris	Unpublished
PL005	Albite	RC169	S.Harris	Unpublished
PL006	Albite	RC164	S.Harris	Unpublished
PL007	Muscovite	RC14	S.Harris	Unpublished
PL008	Muscovite	RC64	Norway	Pidgeon & Råheim, 1972
PL009	Muscovite	RC64 (Flakes)	Norway	Pidgeon & Råheim, 1972
PL010	Muscovite	RC72	Norway	Pidgeon & Råheim, 1972
PL011	Muscovite	RC80	Norway	Pidgeon & Råheim, 1972
PL012	Muscovite	RC61 (Flakes)	Norway	Pidgeon & Råheim, 1972
PL013	Muscovite	RC301	S.Harris	Lyon <i>et al</i> , 1975
PL014	Muscovite	RC164	S.Harris	Unpublished
PL015	Muscovite	RC167	S.Harris	Unpublished
PL016	K-Feldspar	RC167	S.Harris	Unpublished
PL017	K-Feldspar	RC174	Greenland	van Breemen <i>et al</i> , 1974
PL018	K-Feldspar	RC72	Norway	Pidgeon & Råheim, 1972
PL019	K-Feldspar	RC64	Norway	Pidgeon & Råheim, 1972
PL020	K-Feldspar	RC81	Norway	Pidgeon & Råheim, 1972
PL021	K-Feldspar	RC485	Greenland	Pidgeon & Hopgood, 1975
PL022	K-Feldspar	RC484	Greenland	Pidgeon & Hopgood, 1975
PL023	K-Feldspar	RC491	Greenland	Pidgeon & Hopgood, 1975
PL024	K-Feldspar	RC503	Greenland	Pidgeon & Hopgood, 1975
PL025	K-Feldspar	RC1396C	Assynt	van Breemen <i>et al</i> , 1979
PL026	K-Feldspar	RC389	Nigeria	van Breemen & Bowden, 1973
PL027	K-Feldspar	RC456	Nigeria	van Breemen & Bowden, 1973
PL028	K-Feldspar	RC683B	Aberdeen	Unpublished
PL029	Microcline	RC630	S.Harris	Unpublished
PL030	Microcline	RC165	S.Harris	Unpublished
PL031	Plagioclase	RC246	Greenland	Unpublished
PL032	Plagioclase	RC659	N.Harris	Unpublished

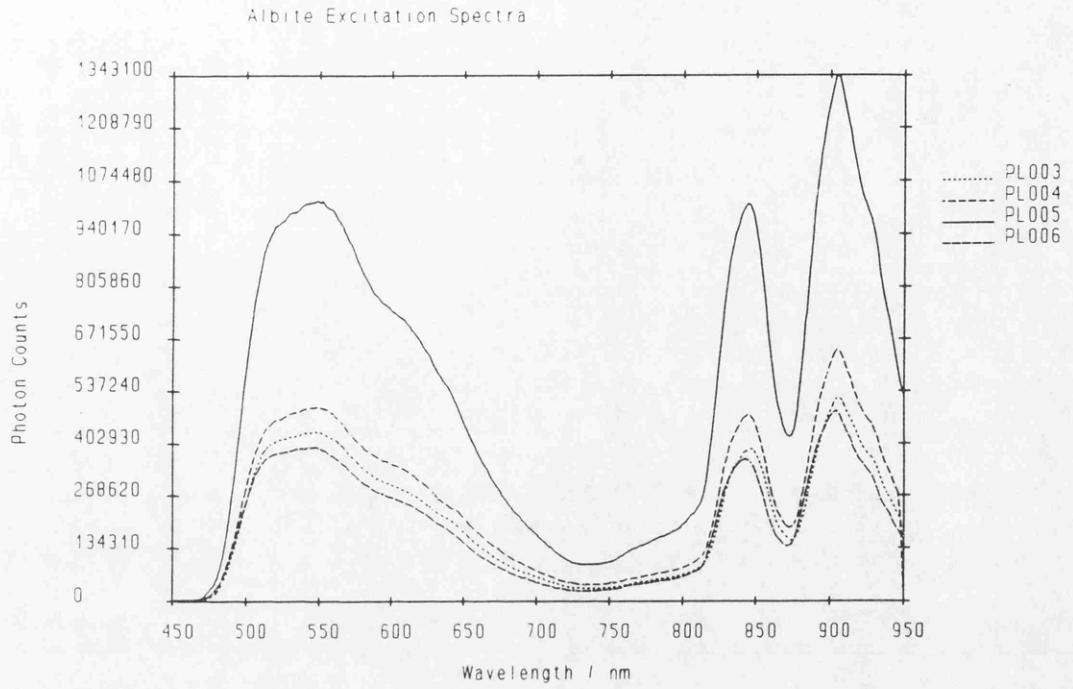


**Figure 4.7 - Albite Excitation Spectra**

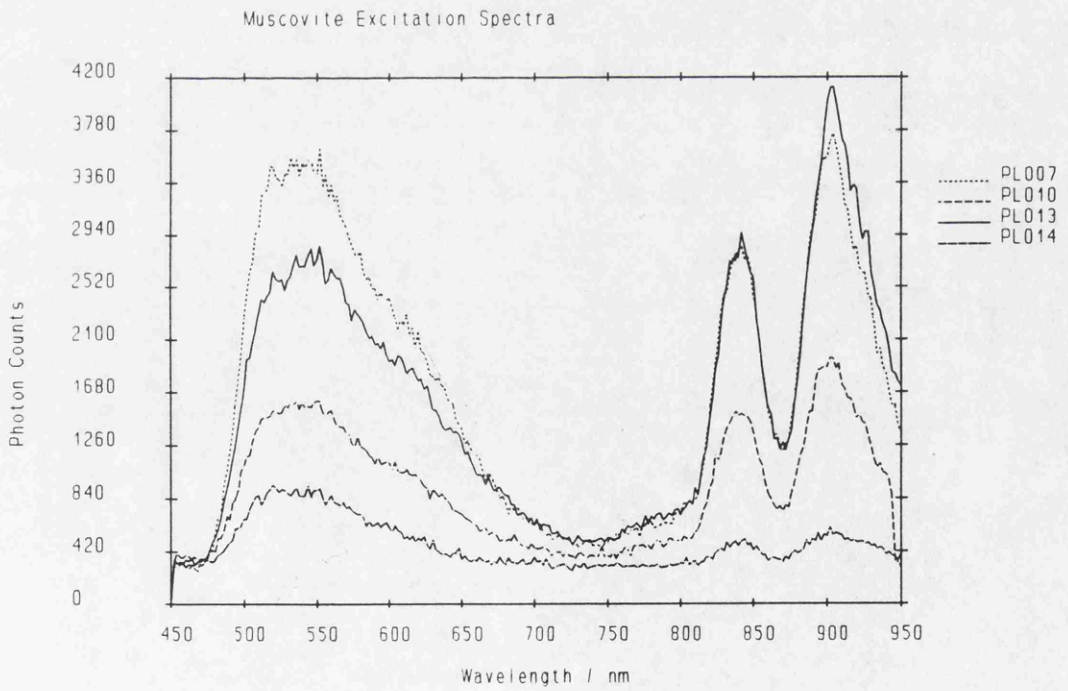


**Figure 4.8 - Muscovite Excitation Spectra**

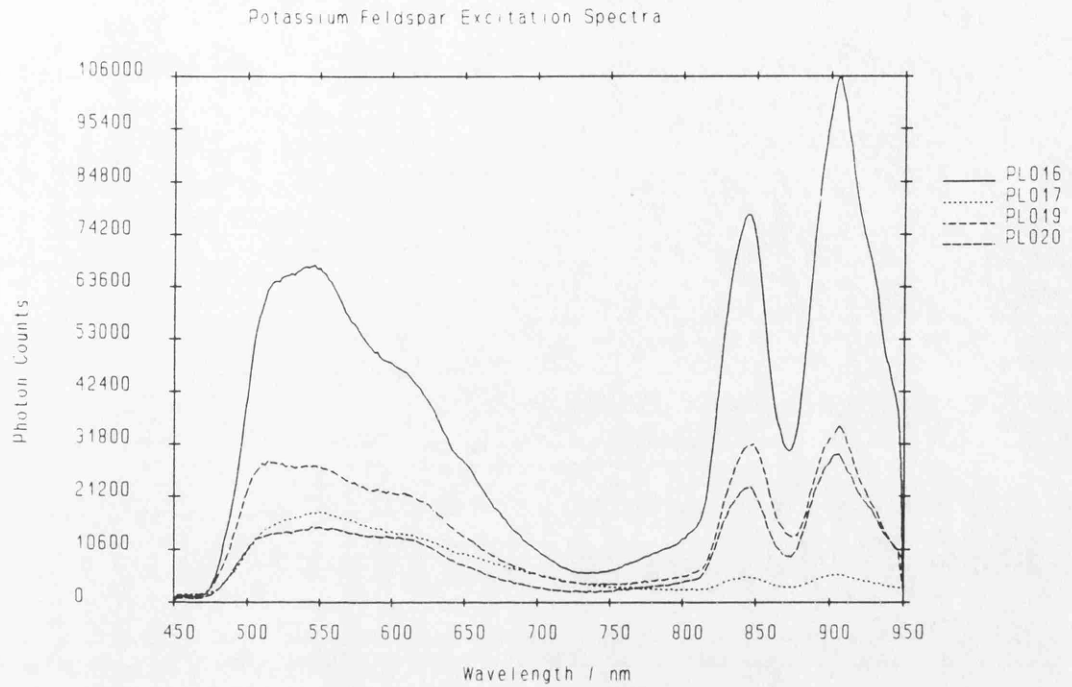


**Figure 4.9 - Potassium Feldspar Excitation Spectra**

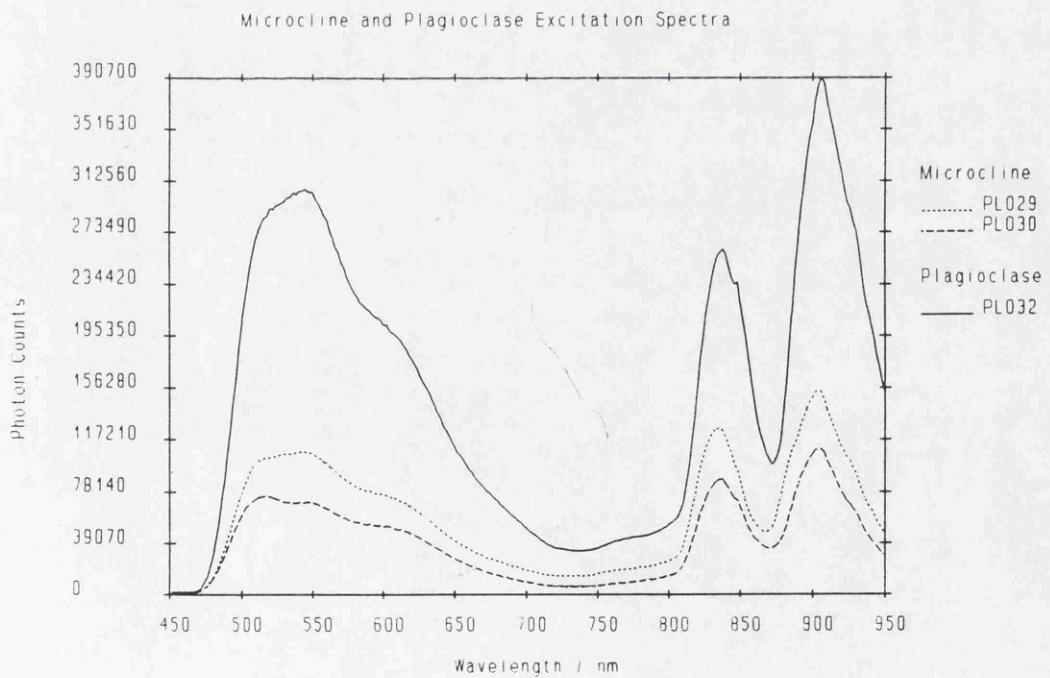


**Figure 4.10 - Microcline and Plagioclase Excitation Spectra**

in the relative intensities between the green and infra red stimulation bands. This can clearly be seen in Figure 4.12. There were also variations in the ratio of the 840 nm peak to the 900 nm peak, as shown in Figure 4.13. It has been shown that in the previous excitation spectra, the twin peaks observed in the infra-red region are the result of the superposition of twin peaks in the lamp power spectrum on a single broad excitation peak. All of the peaks observed in this survey in the infra-red region fall in exactly the same places as those observed previously. Thus, although these spectra are not power normalised, there is no evidence to show that the twin infra-red peaks are any more than a single broad band stimulation peak. Thus any change in the ratio of these two peaks results from a shift in the stimulation peak maximum.

Another variation in the relative intensities between stimulation regions can be seen in Figure 4.9 for the potassium feldspars. From this graph it can be seen that the green stimulation peak is a lot flatter in PL020 than PL016, perhaps demonstrating small variations in the energy levels of the traps being stimulated in this wavelength region.

This survey of feldspathic minerals has shown that all the minerals studied possess stimulation regions in the green, red and infra-red wavelength regions. However, the relative strengths of these stimulation bands varies markedly between mineral families, and also within mineral families. The spectra also show minor variations in the structure of the stimulation bands which may well point to small variations in the underlying trap structure.

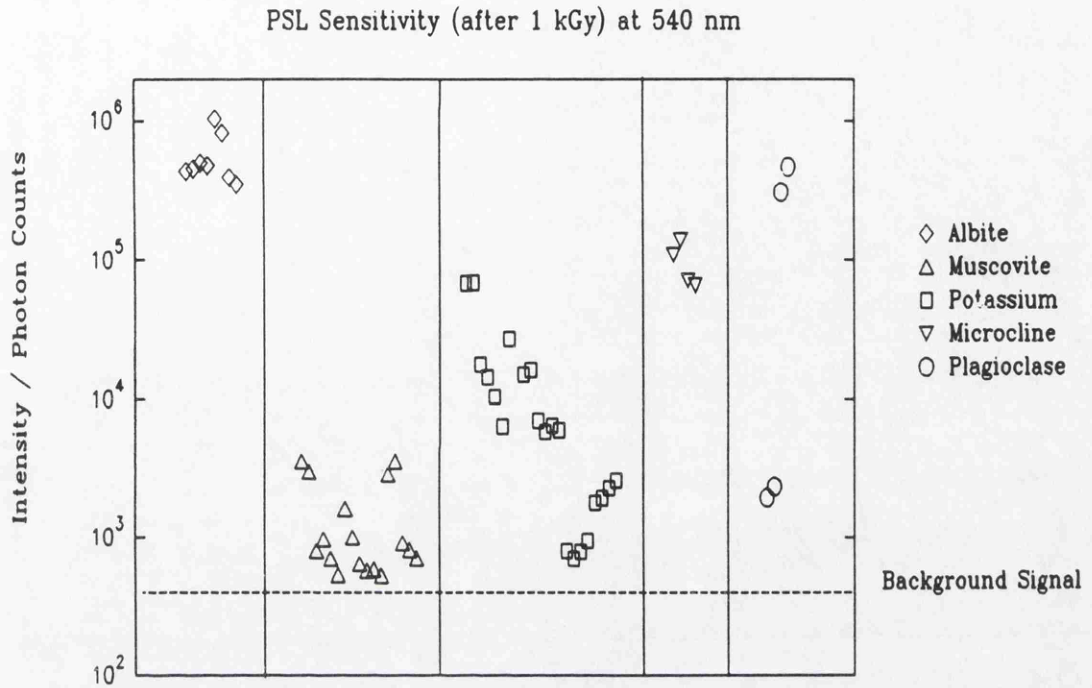


**Figure 4.11** - Feldspathic Mineral PSL Sensitivities at 540 nm

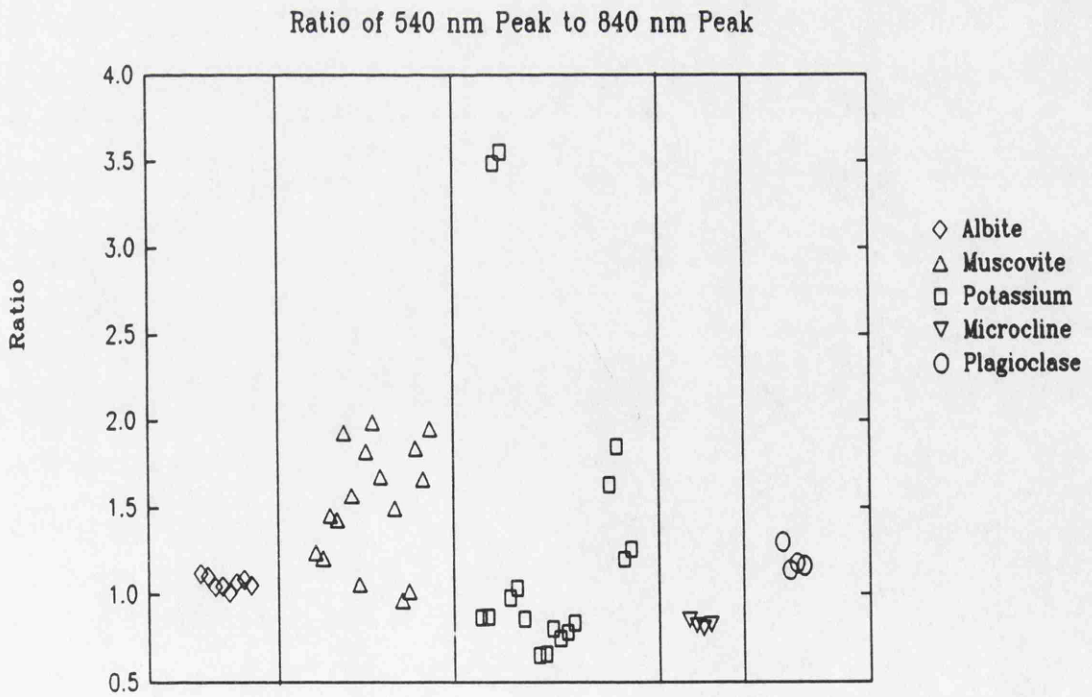


**Figure 4.12** - Ratio of 500 nm peak to 840 nm peak for survey minerals

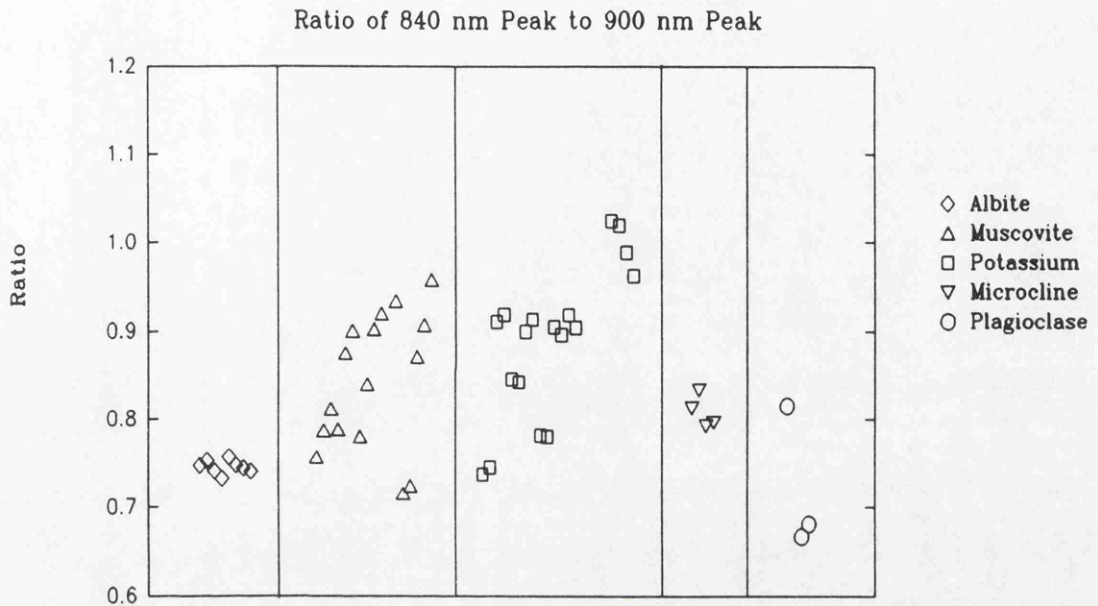


**Figure 4.13** - Ratio of the 840 nm peak to the 900 nm peak in the survey minerals

#### 4.1.1.5 - Summary

In summary, the results presented above show that the excitation spectra of both the

**Table 4.2** - PSL Stimulation Regions

Sample	Stimulation Peak Wavelengths / nm			
	Green	Orange	Red	Infra-Red
Microcline	500	-----	600	860
F1	500	550	600	860

microcline and F1 feldspars are composed of several stimulation regions, as shown in Table 4.2, with the apparent collection of sharp lines in the infra-red region being due to lines in the xenon lamp emission spectrum which happen to coincide with a broad smooth stimulation peak. It must be noted that the presence of a stimulation peak at 500 nm appears to be only an artifact of the presence of filters separating the stimulation

and detection regions. The stimulation region in the green part of the spectrum shows every sign of being continued down towards and beyond the blue end of the visible spectrum, and may even be a continuum starting at 700 nm with several peaks being superimposed upon it (i.e. at 600 and 550 nm and perhaps many more at wavelengths lower than 500 nm).

The survey of the 30 feldspathic minerals has shown that the underlying structure of the detailed excitation spectroscopy extends across a wide range of feldspars, with stimulation bands in the green, red and infra-red stimulation regions. Variations in peak maxima between and within mineral families has been observed, and this may well result from differences in the underlying trap structure. In all cases it seems likely that the infra-red stimulation band comprises a single, broad stimulation peak. It is also apparent that when power normalised, the green stimulation regions will be greater in intensity than the infra-red for all of the samples.

#### 4.1.2 - Monochromatic Bleaching

With the observation of the excitation regions shown above, this information can now be used to select wavelengths to use in monochromatic and broad beam bleaching studies. These studies should be able to provide information on the effect on the whole excitation spectrum of bleaching at a single wavelength.

The monochromatic bleaching experiment presented here was performed as part of the MAFF project N384 "The development of luminescence tests for the detection of irradiated food" and is included as the results will be used later in the discussion and interpretation of the results of the project presented in this thesis. This bleaching study was performed upon microcline feldspar, three equal aliquots of which were dispensed onto stainless steel discs and irradiated in a  $^{90}\text{Sr}$   $\beta$  source to 100 Gy at a rate of approximately 2.5 Gy per minute. The first aliquot was scanned to acquire the 100 Gy unbleached excitation spectrum over 450-950 nm, the second was exposed to illumination of  $500 \pm 6$  nm for a period of 30 seconds before recording the excitation

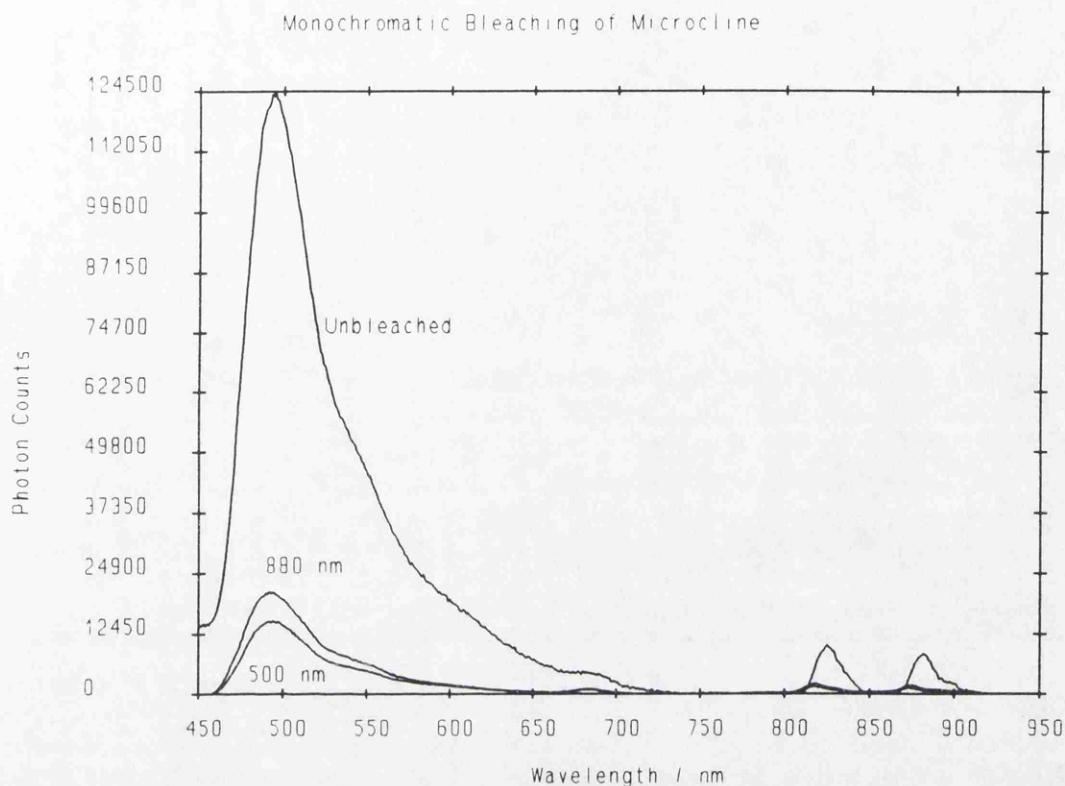


**Figure 4.14** - Monochromatic bleaching of the microcline excitation spectrum

spectrum and the third was illuminated at  $880 \pm 6$  nm for 30 seconds before recording the excitation spectrum. Background phosphorescence was subtracted based on the region from 720-780 nm, this being a region of the excitation spectrum that does not exhibit PSL. The resulting excitation spectra can be seen in Figure 4.14.

As can be seen, bleaching at a wavelength of 500 nm reduces both the green and the infra red stimulation regions, which is in good agreement with the results presented by Hütt *et al* (1988) and Bailiff & Poolton (1991). Also it can be seen that exposure to 880 nm photons also bleaches both the green and infra red stimulation regions. The bleaching curves obtained during the course of this experiment can be seen in Figure 4.15. These curves have been normalised to the initial intensity so that the differences between the shapes of the two curves may be clearly illustrated.

It is interesting to observe in Figure 4.14 the bleaching of the 500 nm signal by photons of longer wavelength (880 nm) and thus lower energy. It is extremely improbable for

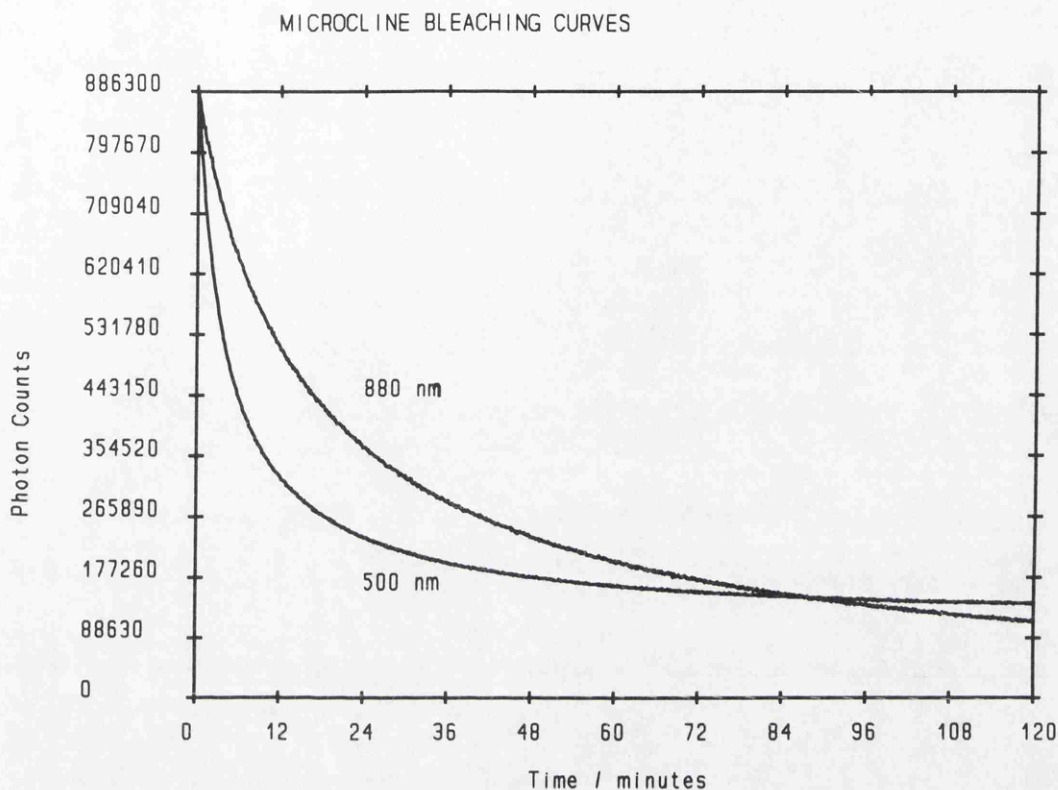


**Figure 4.15** - Microcline monochromatic bleaching curves at 500 and 880 nm.

a photon of less energy than the depth of the ground state of the trap to directly evict charge carriers from that trap to the conduction band. However, 880 nm (1.4 eV, optical) photons are managing to evict 500 nm (2.5 eV, optical) depth charge carriers. One way that this can happen is for the 880 nm photons to be promoting the charge carriers into an excited state where absorption of thermal energy or a second photon then promotes the charge carriers into the conduction band. Consequently this means that when recording the excitation spectrum, some of the PSL signal seen at 500 nm can also be stimulated by 880 nm. The possible implications of this will be discussed in section 5.5.

The bleaching curves shown in Figure 4.15 are non exponential in nature. A single trap exhibiting first order kinetics (no retrapping of the evicted charge carriers) should yield an exponential bleaching curve. It seems apparent that the bleaching kinetics are not from such a trap for either of the two wavelengths used. It has already been argued (section 2.4) that it is unlikely that the bleaching kinetics would be first order, and this

is supported by the shapes of these bleaching curves. It was stated that there are a number of reasons for non first order kinetics, including retrapping and many traps being bleached at the same time, however all of these reasons have similar implications in that the shape of the bleaching curve can not be expected to remain constant with changes in the parameters affecting it.

The most important parameter for dating and dosimetric applications is the variation with dose, and if the shape of the bleaching curve can not be expected to remain constant with dose then the only part of the bleaching curve that will be affected solely by the change in dose will be the initial signal (as this is dependent upon the initial trapped charge carrier population which in turn is dependent upon the absorbed dose). This raises the question as to what defines the initial part of the bleaching curve, it could be several seconds, or it could be as short as a few milliseconds or even less. Hence it would seem likely a better route towards a dating technique would be to use only short exposures of light and perhaps even to use very short pulses (i.e. of the order of microseconds) which could have the advantage of allowing the charge carriers to return to some equilibrium after the one perturbation and before the next. Hence all dosimetric work described in this thesis will either use very short exposures (i.e. 1-2 seconds) for the continuous sources (the xenon lamp) or pulsed stimulation in the microsecond time domain for the non-continuous sources (the LED's and the nitrogen dye laser).

#### 4.1.3 - Temperature Dependence

Following the discovery that 880 nm photons could bleach the 500 nm region of the excitation spectrum, and the proposal that the luminescence mechanism in the infra-red region involves a thermally assisted optical transition (Hütt *et al*, 1988 and Hütt & Jaek, 1989) an examination of the dependence of excitation spectra on sample temperature was undertaken. Such studies should, for the first time, provide a clear indication of the relative influence of thermal assistance upon the various excitation regions already identified above. It is to be expected that the intensity of excitation bands exhibiting thermal assistance should depend upon the stimulating temperature such that it is

reduced as the sample is cooled and enhanced as the temperature increases. For a single trapping state solely participating in a thermally assisted transition, the temperature response should follow an Arrhenius form, as described in section 2.2.2. The model proposed in Hütt & Jaek (1989) describes photo eviction from a ground to an excited state residing only 0.2 eV below the conduction band, from which charge carriers are thermally evicted to the conduction band. In such a model, the temperature dependency of the luminescence generated by photo excitation should be related to the 0.2 eV thermal transition.

In order to test these hypotheses, the excitation spectrum of the microcline feldspars was examined on several samples at various temperatures from -140°C up to 150°C. The samples were cooled and heated by the mechanisms described in section 3.7.1 with the temperature being monitored by a thermocouple spot welded to the back of the heater plate. All of the samples were scanned at a rate of 240 nm/minute with 2 mm slit widths (18 nm bandpass). The order sorting filter used was a 3 mm Schott GG475. The samples were all derived from a bulk microcline sample irradiated to a dose of 1 kGy in the 200 TBq <sup>60</sup>Co source some 6 months previous to these experiments and stored in the dark in the meantime. Prior to recording the excitation spectra, all of the samples were preheated to 180°C for 1 minute. After the preheat, the sample was scanned at room temperature before being cooled for the sequence of excitation spectra at successively higher temperatures. These spectra were not power normalised as a small shift in the infra-red peak is more easily seen as a change in the ratio of the twin infra-red peaks, generated by the lamp power spectrum.

An example of the general response of the microcline samples to changes in temperature can be seen in the 3D plot in Figure 4.16. This plot was created from 5 excitation spectra recorded at 50°C intervals from -100°C to 100°C. The data was transferred into UNIRAS (a 3D plotting program) and interpolated in order to see the graph shown. As can be seen, all regions of the excitation spectrum increase in intensity as the temperature increases which would suggest at least some degree of thermal assistance for all of the trapping sites observed in these spectra. However, this effect is most pronounced in the infra-red stimulation region with the peaks growing from almost zero

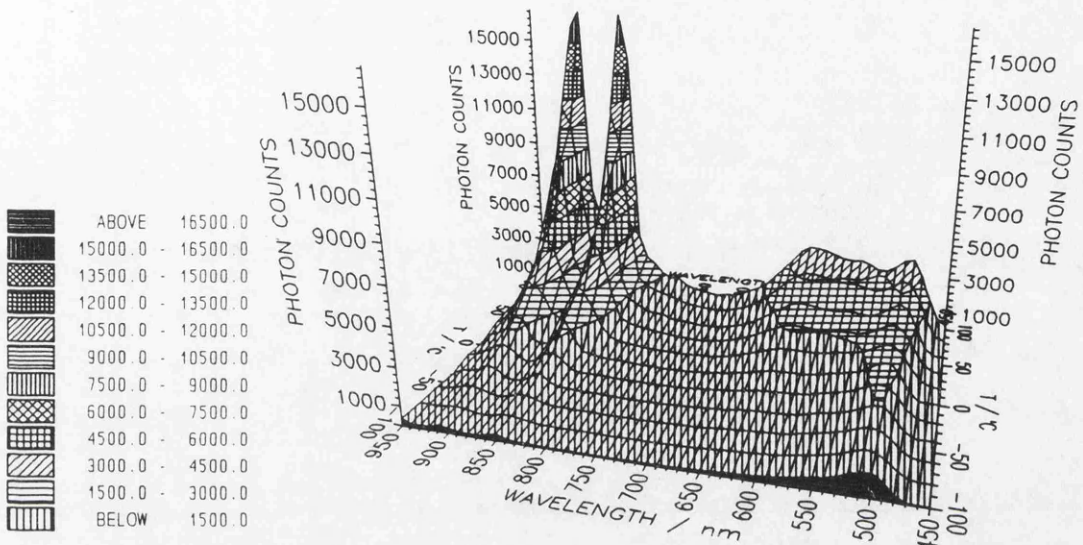


**Figure 4.16** - Variation of the Microcline Excitation Spectrum with temperature.

at  $-100^{\circ}\text{C}$  to well over 15000 counts at  $100^{\circ}\text{C}$ . Similarly, although to a much lesser extent, the feature at 600 nm also grows in from almost zero at  $-100^{\circ}\text{C}$ . The stimulation region around 500 nm shows some degree of thermal assistance, however, a clear remnant of that signal is left behind even at  $-100^{\circ}\text{C}$ . Thus from these results, it would seem likely that the infra-red region and that associated with the 600 nm peak behave in a similar fashion, as does *one* component of the 500 nm region, however there does appear to be another component in this region that is not affected by the stimulation temperature in the temperature region under examination.

Although there is a high degree of temperature dependency in the infra-red stimulation region, a very small fraction of the infra red peaks can still be seen even at  $-140^{\circ}\text{C}$ , as shown in Figure 4.17. Comparing this to the excitation spectrum recorded at room temperature (Figure 4.2) it can be seen that the room temperature infra-red peaks are approximately 50 times that at  $-140^{\circ}\text{C}$ . Using equation <2.2> the ratio of the thermal evicition probabilities of a trap 0.2 eV below the conduction band (as stated earlier, 0.2 eV being the energy for the thermal assistance level as reported by Hütt *et al*, 1989) should theoretically be 15717 between temperatures of  $25^{\circ}\text{C}$  and  $-140^{\circ}\text{C}$ . If this

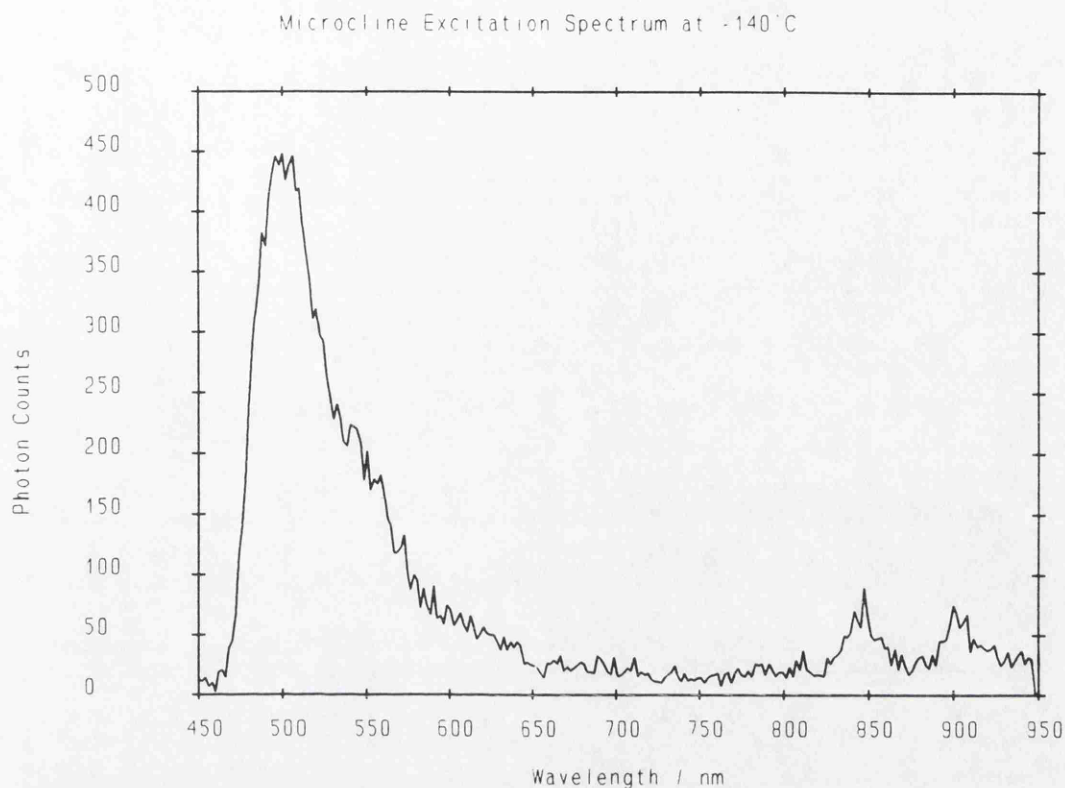


**Figure 4.17** - Microcline Excitation Spectrum at  $-140^{\circ}\text{C}$

discrepancy is due to a difference between the temperature recorded and the actual sample temperature, then (again using equation <2.2>) in order to achieve a ratio of 50 the sample temperature would have to have been as high as  $-75^{\circ}\text{C}$ , a difference of  $65^{\circ}\text{C}$  to that actually recorded. This seems too high to be explained entirely in terms of a discrepancy between sample temperature and recorded temperature, thus it may be that another mechanism is responsible for this.

One feature that does become apparent with the variation in stimulating temperature is that the infra-red stimulation peak shifts with temperature. This is made most apparent in unnormalised plots as a difference in the ratio of the two apparent infra-red peaks. As the stimulating temperature falls, so the ratio of the higher wavelength peak to lower wavelength peak decreases, thus indicating a shift in the true single peak to a lower wavelength. This can be seen in Figure 4.2 and Figure 4.17, however it is shown more clearly in Figure 4.18, where the actual variation of the ratio of the higher wavelength peak to the lower wavelength peak is shown.

INFRA-RED PEAK SHIFT WITH TEMPERATURE AS SHOWN BY A  
CHANGE IN THE RATIO OF THE UNNORMALISED PEAKS

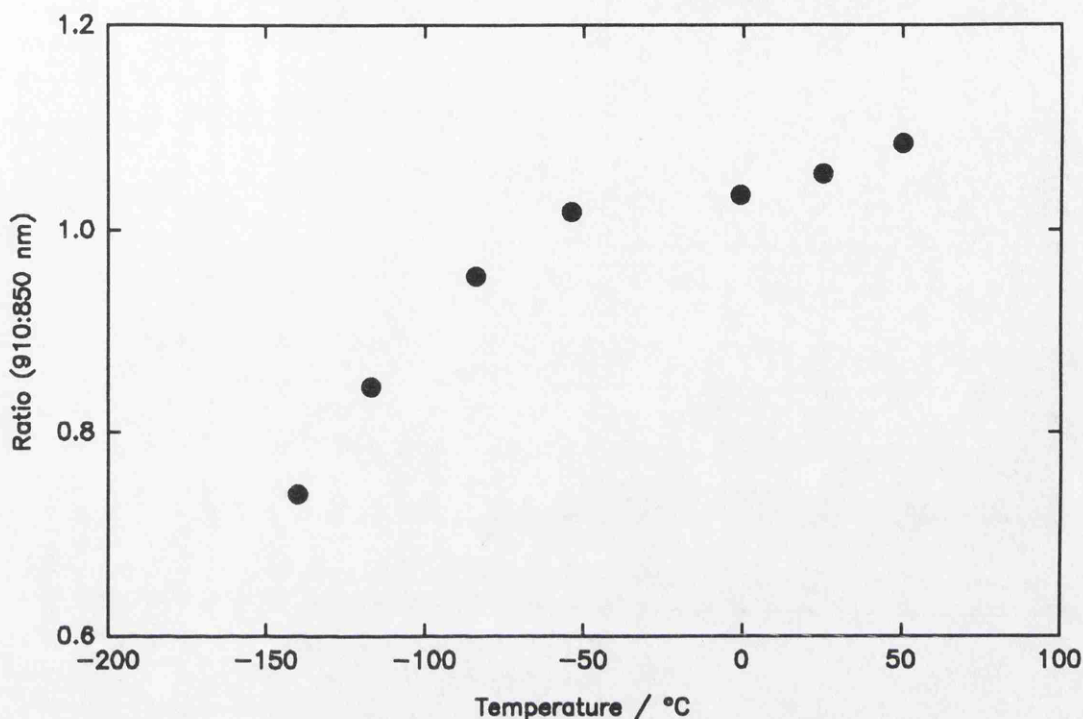


**Figure 4.18** - Variation in Microcline Unnormalised Infra-Red Peaks Ratio with Temperature

This shift in stimulation peak wavelength with temperature is to be expected due to thermal broadening of the ground state energy. As the temperature falls, so the average thermal energy of the charge carriers occupying the lower state falls, thus the charge carriers will require greater average energy input in order to be evicted from the trapping sites. This means that photons of greater energy (and hence lower wavelength) will be needed in order to evict the charge carriers successfully hence this would be observed as a shift in the stimulation peak wavelength to higher energy and hence lower wavelength, as indeed is shown in Figure 4.18.

Thus in summary, these studies of the variation in excitation spectrum with stimulating temperature have shown thermal assistance across the entire spectrum. The green region of the spectrum appears to be composed of at least two components, one of which is thermally assisted and one which does not appear to be within the temperature region studied. The red and infra-red regions appear to be almost totally thermally assisted, although there is a residual infra-red stimulated signal at  $-140^{\circ}\text{C}$  which should not be

present from a thermally assisted process which has a thermal activation energy of 0.2 eV. The infra-red region shows a shift to higher wavelength as the temperature is increased which is indicative of thermal broadening of the ground and excited states. The thermal assistance in the infra-red region has been identified by many people (e.g. Hütt *et al*, 1988; Duller & Wintle, 1991; Bailiff & Poolton, 1991), however the thermal assistance in the rest of the excitation spectrum has not been previously reported.

The complex behaviour shown here indicates that more detailed work is required across the entire excitation spectrum. A critical test of the thermal assistance model would be observations of an arrhenius rise in each of the stimulation regions, which (if due to a single trap) should yield linear plots and thus indicate the activation energy of the thermal step. Such experiments were performed, the results of which are presented and discussed in section 5.1.

#### 4.1.4 - Thermal Stability

As stated in section 2.8, thermal stability is a prerequisite for reliable dating. Having shown that the excitation spectrum contains distinct stimulation bands with varying degrees of thermal assistance, a series of experiments was planned to examine the thermal stability of these features. Initial spectroscopic studies of thermal stability are presented here. More detailed analysis of thermal stability for particular stimulation bands is presented in chapter 5. All of these results were acquired using a 500 nm blaze monochromator grating and therefore the unnormalised response in the 500 nm stimulation region is greater in intensity than the infra-red response. A single disk of the microcline feldspar was dispensed and irradiated to a dose of 100 Gy in a  $^{90}\text{Sr}$  source and stored overnight to allow the room temperature phosphorescence to decay. The sample was scanned from 450 to 950 nm at a scan speed of 960 nm / minute with a 10 nm bandpass. The room temperature excitation spectrum was recorded, and then the sample was heated to 50°C for 1 minute in a nitrogen atmosphere, allowed to cool and then the room temperature spectrum was recorded again. This cycle of preheat and readout at room temperature was repeated at intervals of 50°C up to a maximum

temperature of 500°C. The resulting excitation spectra are shown in Figure 4.19 to Figure 4.23.

It can be seen that the spectral shape appears to be unchanged up to a temperature of 200°C (as shown by Figure 4.19 and Figure 4.20). However, there is clear evidence that the infra-red stimulated luminescence is annealed more easily thereafter than that at 500 nm. By 250°C approximately one third of the 500 nm signal remains, whereas for the infra-red signal only one sixth remains (Figure 4.21). By 350°C (Figure 4.22) the infra-red peak has disappeared totally leaving the 500 nm peak still with approximately one third of its initial signal. This remained until the sample was preheated at 400°C (Figure 4.23) where this peak is now totally annealed (the remaining signal being just the background).

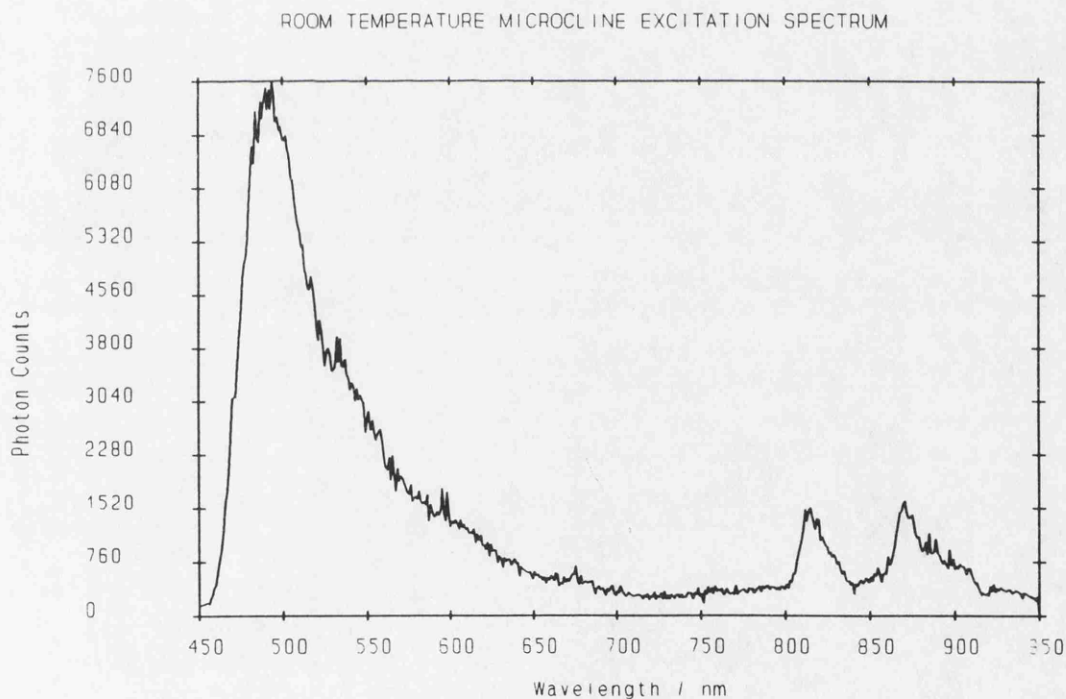


**Figure 4.19** - Microcline Room Temperature Excitation Spectrum

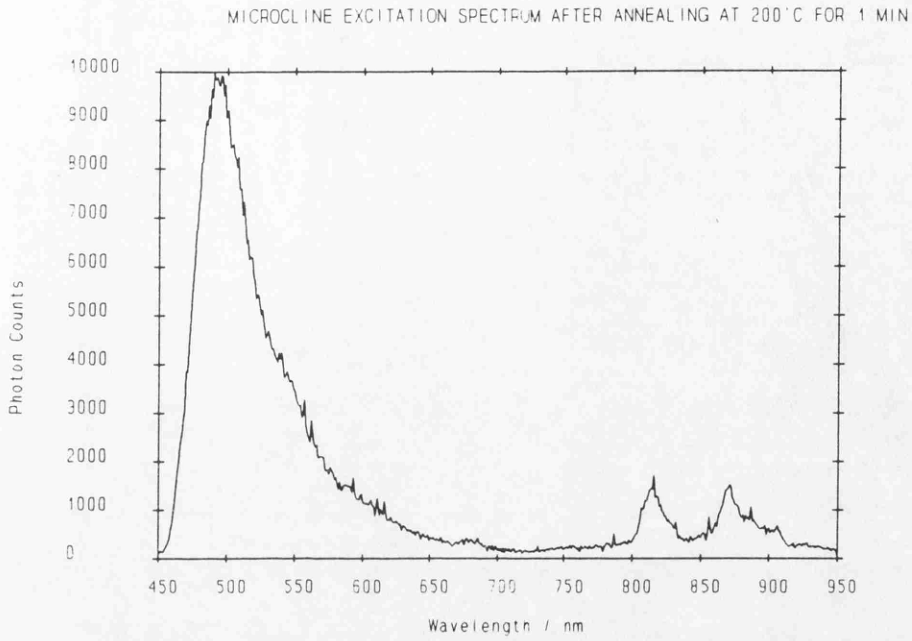


**Figure 4.20** - Microcline Room Temperature Excitation Spectrum After 200°C for 1 minute

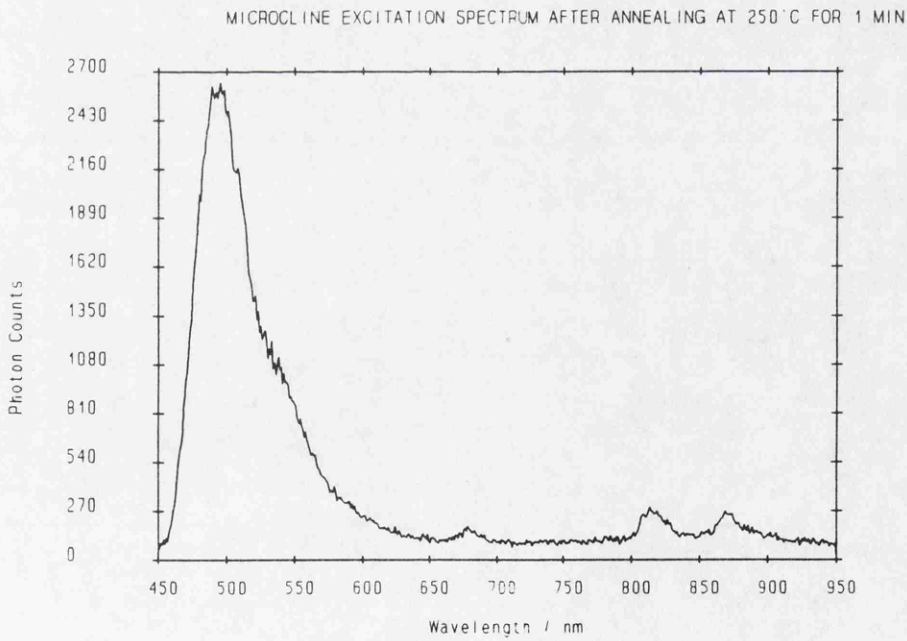


**Figure 4.21** - Microcline Room Temperature Excitation Spectrum after 250°C for 1 Minute

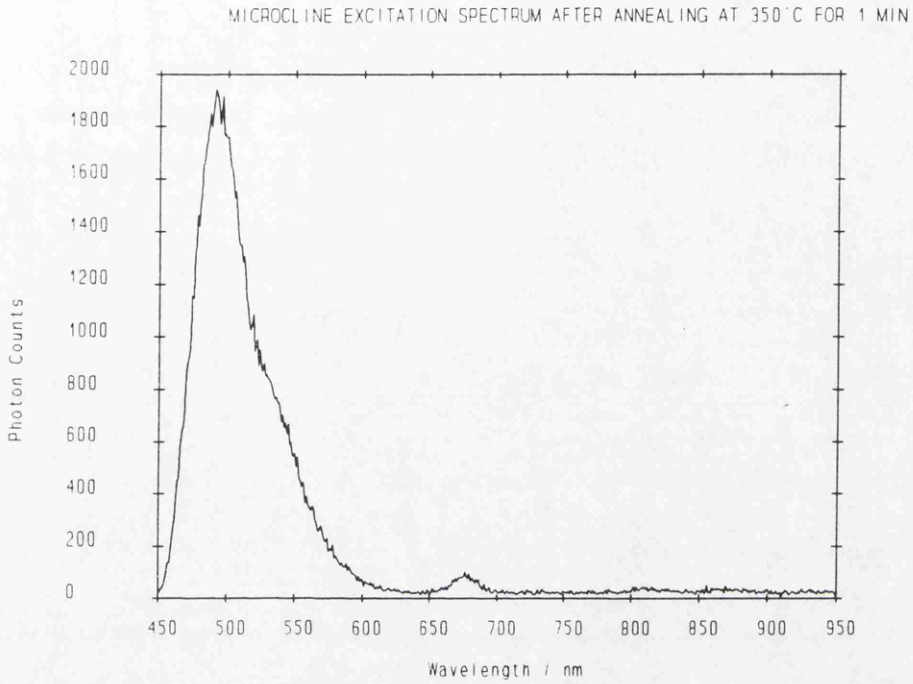


**Figure 4.22** - Microcline Room Temperature Excitation Spectrum after 350°C for 1 Minute

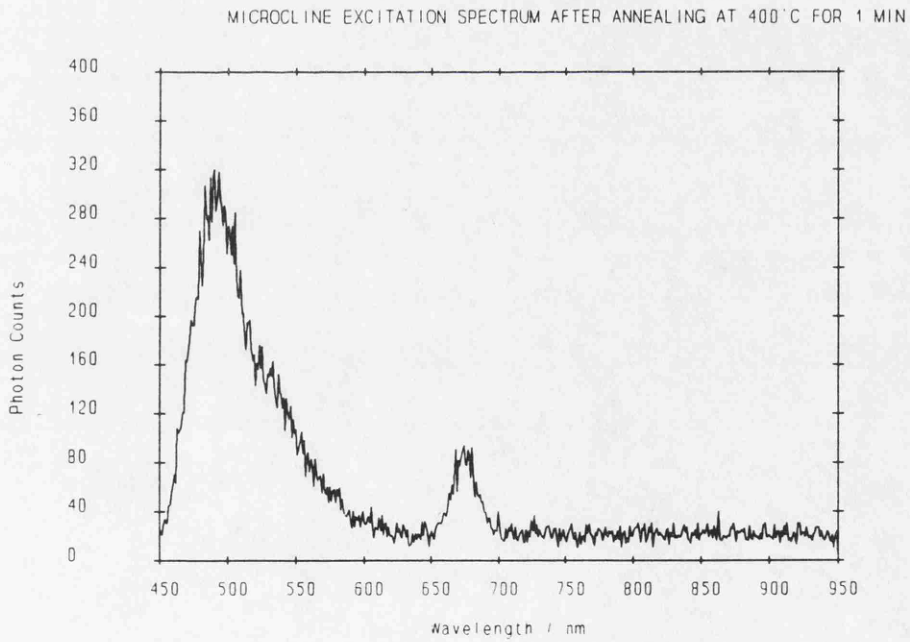


**Figure 4.23** - Microcline Room Temperature Excitation Spectrum After 400°C for 1 Minute

In order to verify the above results, a similar experiment was performed on the microcline feldspar, successively annealing from 150°C to 450°C in 50° steps for 30 s and recording the excitation spectrum between each heating. The samples had a 1 kGy dose and were measured using the 1000 nm blaze grating which yields more power in the infra red region and hence makes observation of the annealing of this region easier. The samples were heated to the annealing temperature at a rate of 2°Cs<sup>-1</sup> and the excitation spectra were recorded from 450 to 950 nm at a scan rate of 240 nm per minute with a bandwidth of 20 nm. A summary of the results is shown in Figure 4.24.

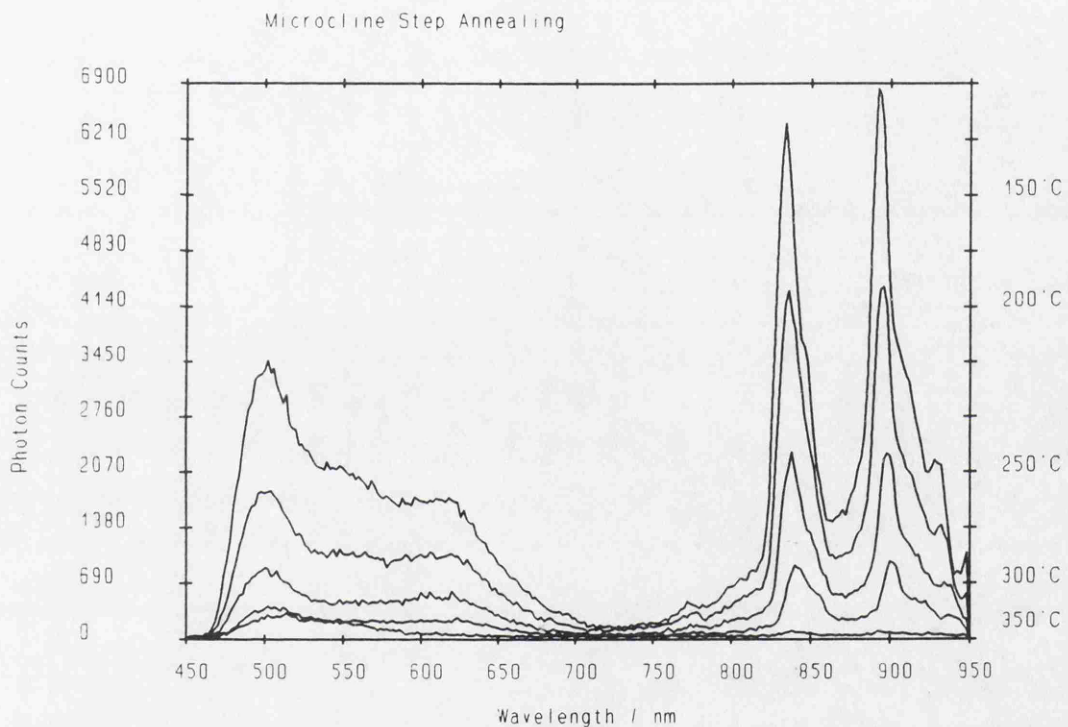


**Figure 4.24** - Pulse Annealing of 1 kGy Microcline from 150 - 350 °C

As can be seen, up to 300°C although the entire spectrum is reduced in intensity, all parts of the excitation spectrum can still be observed, including the features at around 500, 600 and 900 nm. However by 350°C, the infra red peaks and the peak at 600 nm are annealed out leaving behind only the 500 nm peak which is of the same order of magnitude as the 500 nm peak after annealing at 300°C. This remnant of the excitation spectrum can be seen more clearly in Figure 4.25 which shows that there is clearly a more stable component of the green stimulation band surviving after annealing at 400°C for 30 seconds, after which all traces of the infra-red stimulated PSL have been

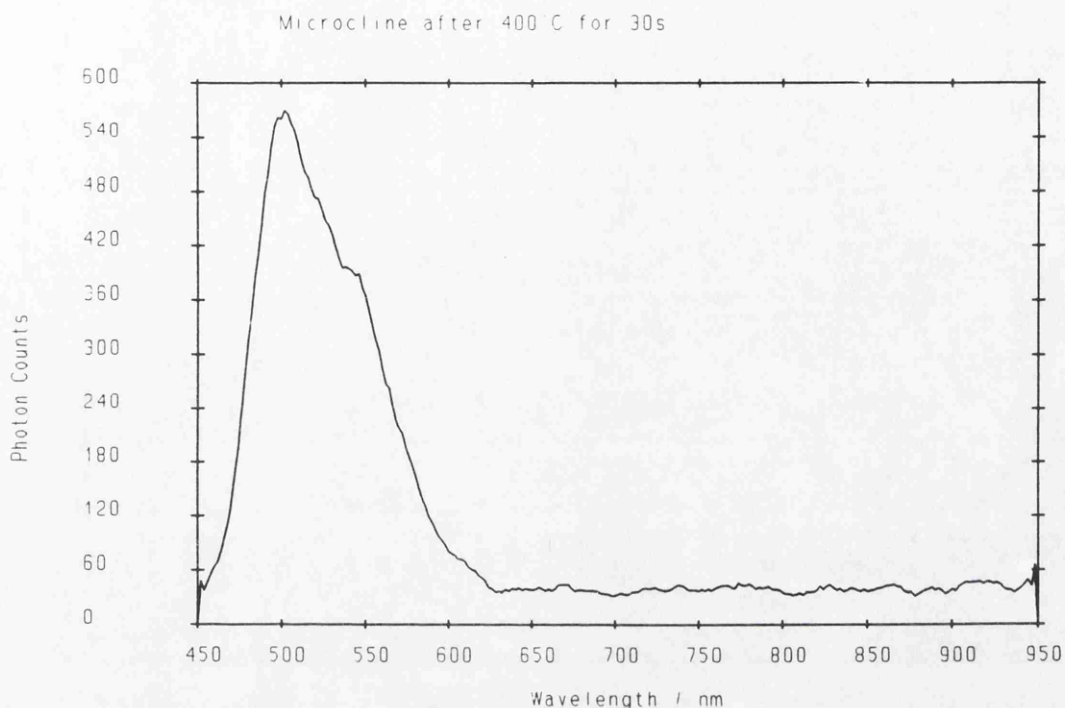


**Figure 4.25** - Microcline room temperature excitation spectrum after annealing at 400°C for 30 s

removed. Hence these results provide clear evidence that the infra red component of the excitation spectrum is thermally less stable than that stimulated in the green region. This also shows that the behaviour of the 600 nm region is similar to the infra red and thus perhaps suggests some link between the two.

It is known (Sanderson *et al*, 1988 and private communication) that the plateau test used in TL dating to determine the temperature ranges for age calculation typically show that glow curve regions below approximately 300°C are of questionable stability. Those areas around the start of the plateau (circa 300°C in this case) may be considered to be meta stable over such time scales. As the infra-red stimulation region and parts of the rest of the excitation spectrum can be annealed by temperatures at around 300°C it might be supposed that this PSL signal may be meta stable over archaeological timescales. Meta stability could pose problems in dating applications as part of the signal would survive over the timescale concerned, but part would fade in an unquantifiable manner.

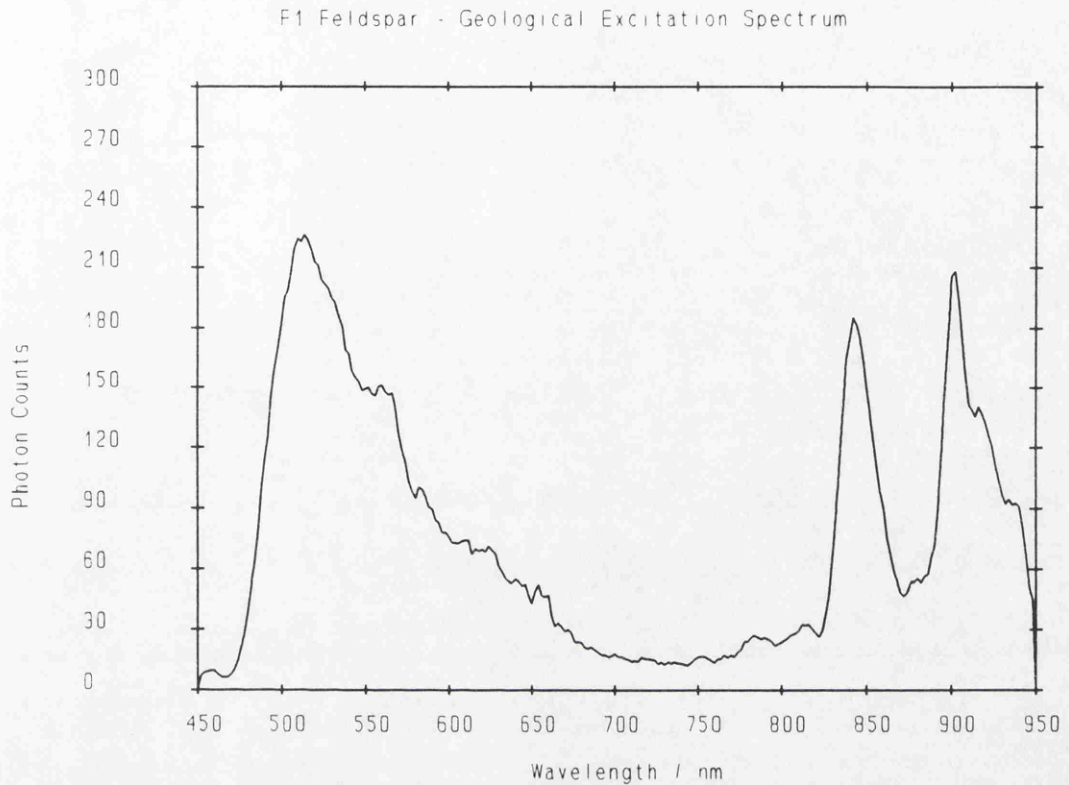


**Figure 4.26** Excitation Spectrum from F1 feldspar with geological signal only

Evidence of this meta stability in the infra-red stimulation region can be seen from Figure 4.26 which shows the excitation spectrum from the F1 feldspar which contained only its natural geological signal. The excitation spectrum was recorded at a scan speed of 240 nm in the same manner as the excitation spectra due to recent laboratory irradiation shown earlier. It is immediately apparent from comparison of Figure 4.26 and Figure 4.4 excitation spectra that the relative intensity of the green stimulation region has increased substantially, implying loss of part of the infra-red stimulated signal. Also the geological excitation spectrum shows that features at approximately 550 nm and 600 nm previously identified in the F1 excitation spectrum are missing, also consistent with the pulsed annealing results which showed that these regions were affected in a similar manner to the infra-red region in response to annealing temperature.

This evidence further supports the idea that the infra-red stimulation region is not only thermally less stable than the green, but that it is potentially meta stable over

archaeological or geological timescales. Similarly concerns arise for the 550 and 600 nm regions which were shown in section 4.1.3 to also share thermal assistance mechanisms with the infra-red region.

Whether infra-red stimulation is useful for dating purposes depends upon the degree of instability in the sample being used and the age of the event being measured. For short timescales the infra-red region could be sufficiently stable and be a useful tool, however its usefulness over long timescales may be called into question. For these longer time scales it would appear that stimulation in the green region might be more appropriate, given the new evidence presented here demonstrating that green stimulation contains a component which is not infra-red associated and which has greater thermal stability.

#### 4.1.5 - High Dose Response

In order to form some conclusions as to likely upper dating limits, observations of the thermal stabilities of the various stimulation regions must be combined with exploration of the saturation limits of the PSL signal. During the course of the MAFF project to develop tests for the detection of irradiated herbs and spices, some work was performed on the PSL dose response of microcline from 10 Gy up to 10 kGy. This work is presented in Sanderson (1991) and is presented here as it has important implications for the upper dating limit.

A sample of microcline was dispensed on to a 1 cm stainless steel disc, annealed at 500°C for 5 minutes to remove any residual PSL signals and then its excitation spectrum was recorded at a rate of 960 nm / minute and monochromator slit widths of 2.5 mm. The sample disc was then given a dose of 10 Gy and then scanned again at room temperature to record the excitation spectrum. The fraction of the PSL signal removed by a scan at a rate of 960 nm / minute is less than 1 %, so the same disc could be used to record excitation spectra from successive cumulative doses, thus the disc received another 10 Gy in order to be able to record an excitation spectrum due to a total dose of 20 Gy. This process was continued so that eventually excitation

Microcline High Dose PSL Growth Curve

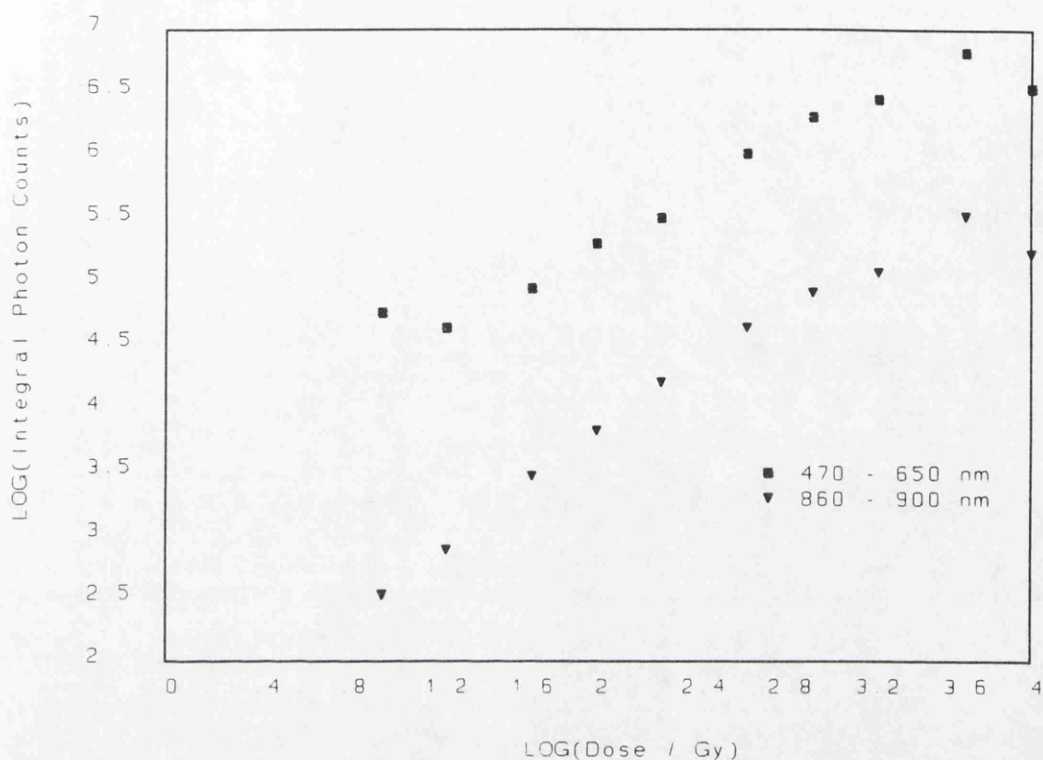


**Figure 4.27** - Microcline High Dose PSL Growth Curve

spectra could be recorded for doses on a logarithmic scale up to a total of 10 kGy. Once this had been accomplished, the PSL signal resulting from each dose was expressed as an integral from 470 to 650 nm and also from 860 to 900 nm with the room temperature phosphorescence due to the irradiation being subtracted based on the average count rate from 720 to 780 nm, a region where there is no PSL signal, and thus any signal must be due to thermal stimulation, ie. room temperature phosphorescence. All of the doses up to a total combined dose of 200 Gy were given by a  $^{90}\text{Sr}$   $\beta$  source at a rate of 1.88 Gy / minute, and the rest of the doses were given by a 200 TBq  $^{60}\text{Co}$   $\gamma$  source at a rate of 2 kGy / hour. The resulting growth curve (plotted on a log-log graph in order to show each order of magnitude equally well) can be seen in Figure 4.27.

As can be seen from this graph, there is continuous growth up to 10 kGy for both wavelength regions, although the curve does seem to become increasingly sublinear at

the high doses ( $\sim 1$  kGy), which is to be expected once saturation effects begin to take place. A dose of 10 kGy can be equivalent (assuming an annual dose rate of  $3 \text{ mGy.a}^{-1}$ ) to 3.3 million years and thus it would seem that, providing the stability of trapped charge carriers is sufficient, it could be possible to have an upper age limit of over a million years. In comparison, high dose TL glow curves have also been observed (Sanderson *et al*, 1989) up to a limit of 48 kGy, showing a saturating response with the saturation effects beginning in the 1 - 5 kGy region (a more complete description of the regression analysis performed in Sanderson *et al* (1989) can be found in Clark, 1989). A comparison between the two sets of data would seem to suggest that the saturation limit shown by the microcline under photo stimulation is higher than for TL, however it must be remembered that the TL studies were performed upon real dating samples and it is to be expected that the saturation limits will vary from sample to sample. However, the possibility remains that the saturation limits for PSL dating are the same or perhaps greater than for TL dating.

#### 4.2 - Emission Spectroscopy

Stimulation spectroscopy and other associated and varied stimulation techniques can provide a lot of information about the trapping centres being stimulated. However, they provide little or no information on the second half of the luminescence mechanism, namely the recombination centres. One powerful technique for examining the recombination centres is *emission spectroscopy*. Whilst in photo stimulation it is a necessary requirement that the stimulating wavelength used has enough energy to be able to evict charge from its trapping site, it is also necessary to have a detection window that allows for transmission of the resulting stimulated signal. For this reason alone, it can be argued that emission spectroscopy is an important requirement for the development and optimisation of any luminescence technique, and indeed it has even been labelled as an *essential* requirement (Townsend and Kirsh, 1989; Dalal *et al*, 1988). As well as identifying possible detection windows, emission spectroscopy can also be used to assist in the interpretation of observed phenomena, such as variation

with temperature (both cryogenic and above room temperature) and variation with fading / bleaching.

Emission spectroscopy can be observed resulting from stimulation at a single wavelength. However, observations of the emission spectra combined with excitation spectroscopy have the potential to yield much more information concerning the stimulation mechanisms. If this is then coupled to time domain analysis then a very flexible and powerful spectroscopic PSL research tool could be developed. The SURRC excitation spectrometer was conceived with such spectroscopy in mind and could be reconfigured as an emission spectrometer with further modifications. However, after discussion of these developments, it was decided that the pressures of time meant that a study of the emission spectrum would have to be in collaboration with another laboratory that already had a working TL emission spectrometer that could be adapted for use with optical stimulation. Thus Professor P.D. Townsend of the University of Sussex kindly agreed to give time on his emission spectrometer and to assist with its reconfiguration for optical stimulation. This spectrometer is based upon a monochromator and the samples can be cooled to near LNT if required. Data acquisition is performed via a cooled extended red sensitive photomultiplier and collected by a Superbrain microcomputer. Fuller details of the emission spectrometer can be found in Kirsh *et al*, 1987.

The stimulating source used in obtaining the PSL emission spectra was the ring of 8 infra-red LED's driven in continuous mode by the pulsing unit described in section 3.8. Infra-red stimulation was used to enable easy discrimination between the stimulation and emission wavelengths. Although it would be highly desirable to observe emission spectra across the excitation spectrum, the problem of separating the stimulation and emission bands at wavelengths less than those used was looked upon as being potentially insurmountable during the time available. The ring of LED's was mounted vertically against an observation window in the side of the sample chamber at an angle of 90° to the detection port, with the entire port being shrouded to reduce to a minimum any light leaks into the chamber. The sample was aligned such that it was at an angle of 45° to both the LED's and the detection port to try to maximise stimulation and detection

efficiency. Initially, scattered light through the monochromator from the LED's saturated the photomultiplier, however this was readily overcome by placing a 1mm Schott BG39 band pass filter between the sample chamber and the monochromator which effectively blocked the high wavelength emission of the LED's whilst still maintaining a detection window of 300 to 750 nm.

The samples used were all the IAEA F1 feldspar and had either the natural geological dose, a recent 1 kGy dose, or a 1 kGy dose which had been given approximately 8 months previously and stored at room temperature. The samples were of mixed grain size ( $< 160 \mu\text{m}$ ), and mounted on 1 cm diameter stainless steel disks with a silicon grease spray. The disks were mounted vertically in the sample chamber, and were fixed to the cryostat / heater plate by vacuum grease with all experiments below room temperature being performed under conditions of high vacuum. The samples were exposed to continuous stimulation from the LED's and emission spectra were observed in response to bleaching of the sample and changes in sample temperature. All emission spectra shown have been corrected for photomultiplier and monochromator efficiency.

A typical room temperature emission spectrum can be seen in Figure 4.28, yielding well resolved peaks at 340, 400 and 560 nm, with less well resolved peaks at approximately 420 and 640 nm (although it must be noted that the actual light level at 640 nm before correction for photomultiplier and monochromator efficiency is very low and thus this inflection in the curve could be due to noise).

The two emission bands at 340 and 400 nm have been observed in potassium feldspars by Huntley *et al* (1991), under stimulation from infra-red diodes (775-980 nm diode emission with a peak at 880 nm) and also under stimulation with 514 nm stimulation from an argon-ion laser using a micro channel plate detector. Jungner & Huntley (1991) also observed these emission peaks under stimulation at 633 nm from a He-Ne laser although with poorer resolution as optical filters were used to define the detection windows. In neither case was the 560 nm peak reported for pure (14% K) potassium feldspars, however Huntley *et al* (1991) do show the presence of such a peak for sodium rich plagioclase feldspars stimulated with the infra-red diodes. The feldspar F1

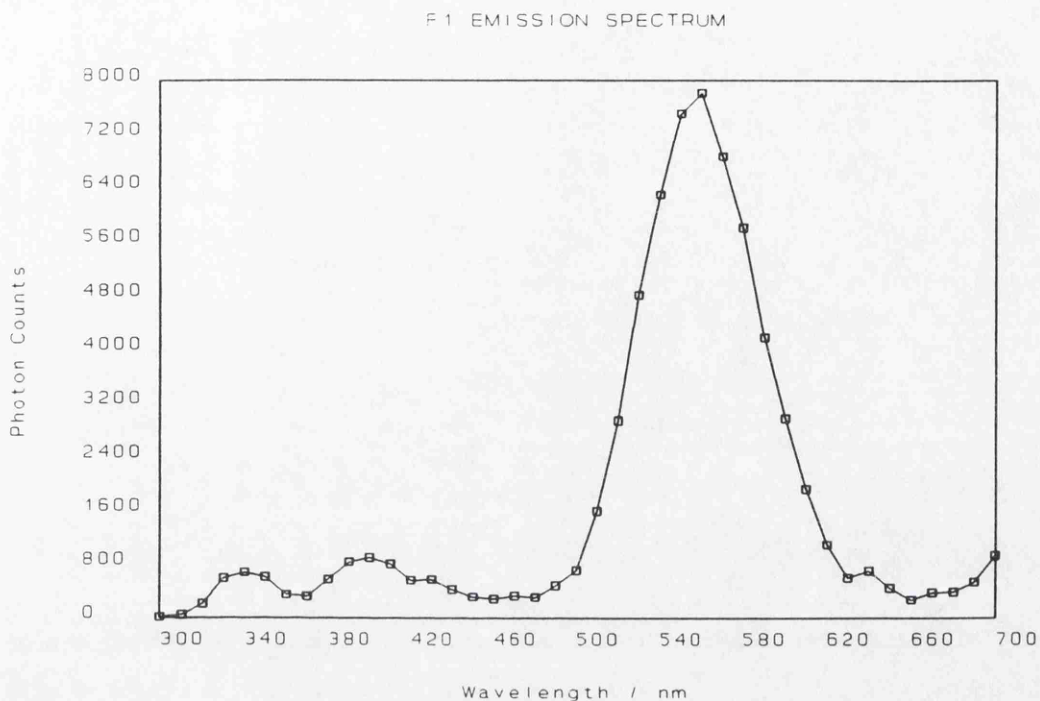


**Figure 4.28** - Typical F1 feldspar room temperature emission spectrum.

is dominated by potassium (8.3% K or 12%  $K_2O$ ), however it does contain some sodium (2.8%  $Na_2O$ ) and thus in comparison with the reported spectra it would seem possible that the existence of the 560 nm peak is due to the sodium content. This is backed up by Bailiff & Poolton (1991) who show (under stimulation by infra-red diodes emitting at 950 nm, 205 nm FWHM) that for microcline and orthoclase (pure potassium feldspars) the emission spectrum is dominated by emissions at 440 nm and a band at or less than 340 nm whereas for albite (a pure sodium feldspar) the emission band is dominated by a peak at 560 nm, with lesser peaks at 400 and (or less than) 340 nm. Thus it would seem (combining these four studies of emission spectra) that the same recombination centres are used across the entire excitation spectrum as they were all observed under stimulation at 514, 633 880 and 950 nm.

#### 4.2.1 - Variation with Bleaching

In order to observe any changes in the emission spectrum with bleaching of the trapped charge population, 32 successive scans were made using continuous stimulation from the LED's. Each scan immediately followed the previous one and took approximately 30 s,

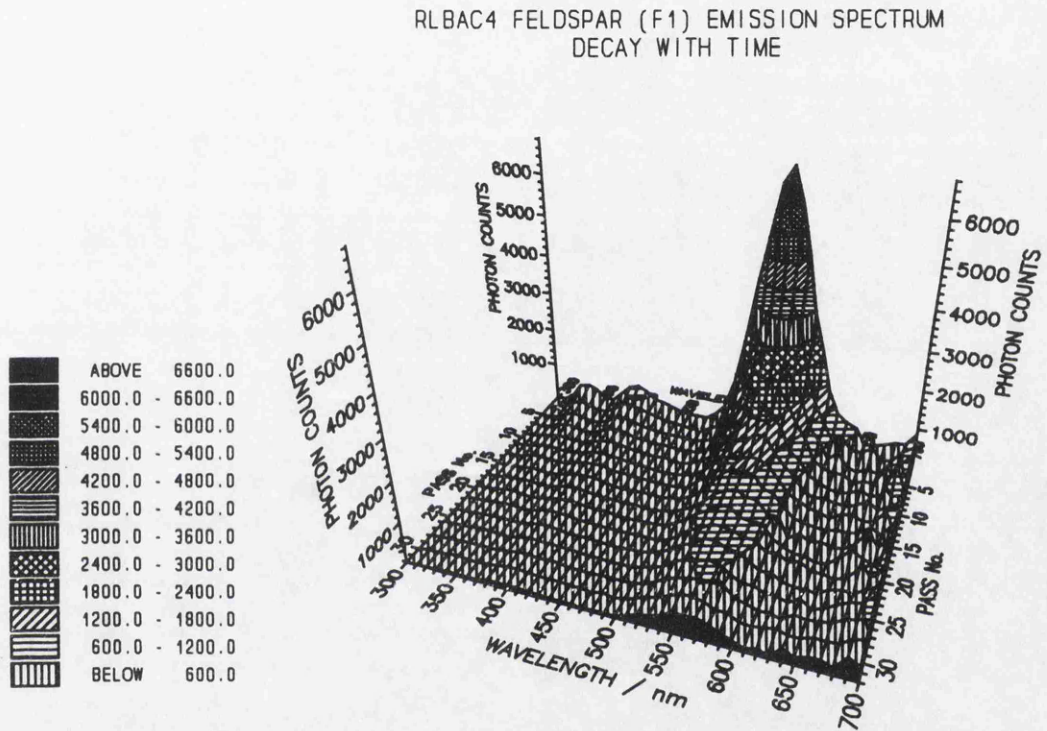


**Figure 4.29** - F1 feldspar emission spectrum, variation with bleaching.

resulting in a total bleaching time of 16 minutes. The resulting 3D plot of the variation of emission spectrum with bleaching can be seen in Figure 4.29. As can be seen, all three of the emission peaks decay with bleaching, however upon closer examination of the emission spectra, it becomes clear that the ratios between the three peaks vary with bleaching, as is shown in Figure 4.30.

The lines fitted to these ratios result from linear regression analysis, and the gradients are as follows;

(1) - 560:340 Ratio;  $g = 0.022 \pm 0.055$

(2) - 560:400 Ratio;  $g = -0.12 \pm 0.02$

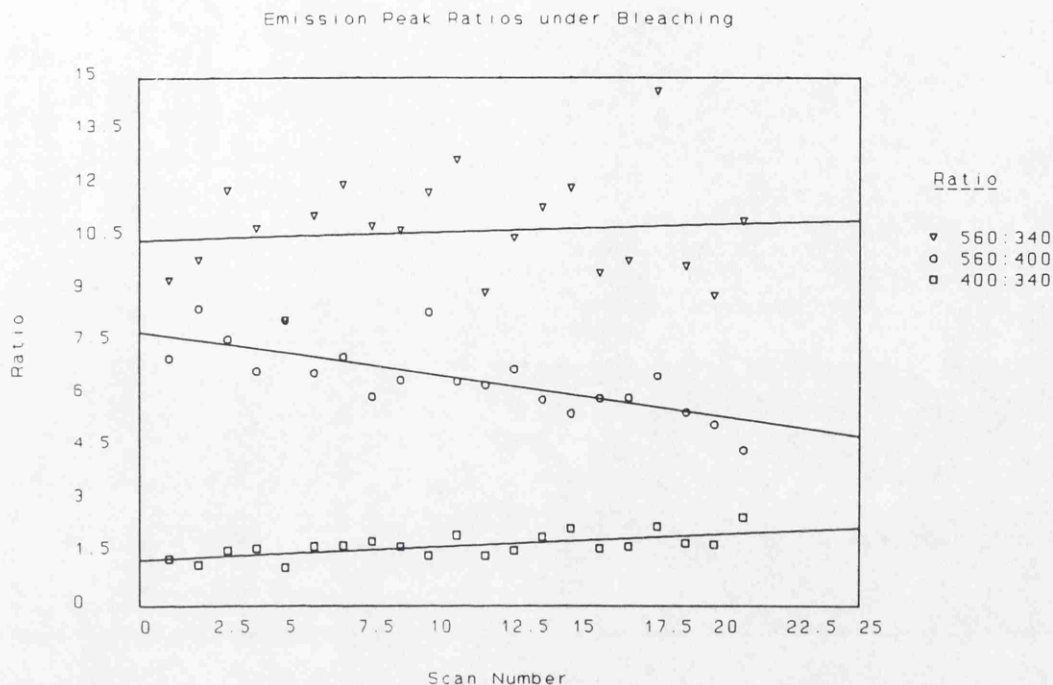


**Figure 4.30** - Variation in Emission Peak Ratios with Bleaching

(3) - 400:340 Ratio;  $g = 0.036 \pm 0.010$

hence we see that ratio 2 decreases (within error) during bleaching, ratio 3 (within error) increases with bleaching and ratio 1 (within error) remains constant. Hence this implies that during bleaching the 400 nm peak decreases at a slower rate than the other two which (within error) remain constant relative to one another.

The question that must now be asked is what are the implications of a constant ratio between two emission peaks during the bleaching (and hence centre filling) process? A constant ratio would tend to imply that the relative capture probabilities between the two centres remains invariant, but capture probabilities depend upon the capture coefficients of the centre and the density of free states within the centre. Assuming that the capture coefficients remain constant with bleaching, constant relative capture probabilities would thus imply constant relative densities of free states between the two centres. This in turn implies that the percentage rate of change of the densities of free states must be equal for both centres. Thus the only way for this to happen is for the capture coefficients of each of the two recombination centres to be equal, and the

probability of this being the case for two different centres must surely be very small, if not negligible.

Hence it would seem that a constant ratio between two emission peaks during bleaching (assuming that the centres are independent of the traps) would imply that both emission peaks result from the same centre. One possible mechanism for this could be for a fixed proportion of the available states in the centre to be in an excited state to which the charge carriers relax by photon emission, and then subsequently relax to the ground state by phonon emission, however this would require that the capture coefficient of the excited state is the same as that for the ground state which seems unlikely.

This argument depends upon whether or not the ratio of two emission peaks under conditions of bleaching remains constant. It must be noted that the results presented above contain a lot of scatter and have only been observed over a small part of the bleaching curve. In order to be able to analyze these ratios in more detail, it would probably be necessary to record the variation in emission spectrum throughout the whole of the bleaching cycle and this could well be problematical as the 340 nm peak has a much lower intensity than the 560 nm peak and so would reach the lower limits of detection much sooner. The circumstances required for a constant ratio are quite restrictive and thus at this stage it is much easier to believe that in fact the ratio does change, only it has not been observed within the limitations of this particular experiment. However, this does mean that much further work in this area is required in order to resolve this point.

#### 4.2.2 - Variation with Temperature

A sample of the freshly irradiated (1 kGy) F1 feldspar was used for this experiment, and was cooled to an initial temperature of 150 K. The sample was not preheated. A steady heating rate of 10°C per minute was applied to the sample, with the emission spectra being recorded continuously. As each emission spectrum took 30 s to acquire, the spectra were separated by 5°C intervals, with the temperature varying by 5°C

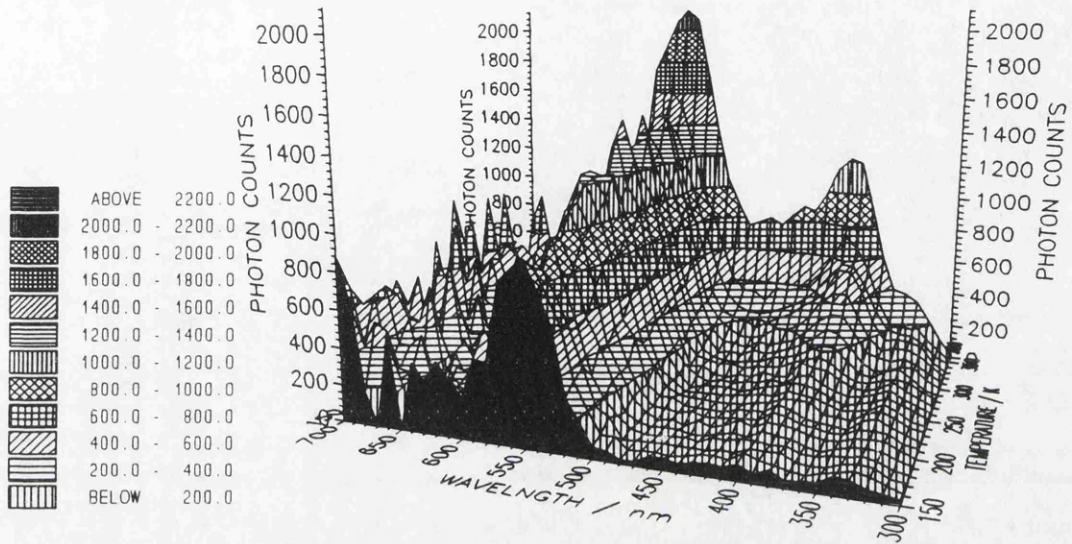


**Figure 4.31** - F1 Feldspar emission spectra, temperature dependence.

during the course of each emission spectrum. A 3D plot of the results can be seen in Figure 4.31.

From these results it can clearly be seen that there is still a strong emission peak at 560 nm even at 150 K (-123°C), which is shown more clearly in Figure 4.32, with a hint of the 340 and 400 nm peaks, although these would be at the lower limit of detection of the system (the data above 600 nm is most likely just noise due to the corrections for photomultiplier and monochromator response as sensitivity at this end of the spectrum is very low thus requiring large correction factors and so small fluctuations in small signals will be greatly exaggerated upon correction). It can be seen that the 560 emission peak is reduced by less than an order of magnitude, and thus if one were monitoring the PSL stimulated by infra-red diodes and detecting in as wide a band as possible (i.e. one which included the 560 nm peak), you would clearly see PSL at -120°C. Hence it would seem likely that there is an element of the infra-red stimulation band that is not phonon assisted.

F1 Emission Spectrum at 150 K

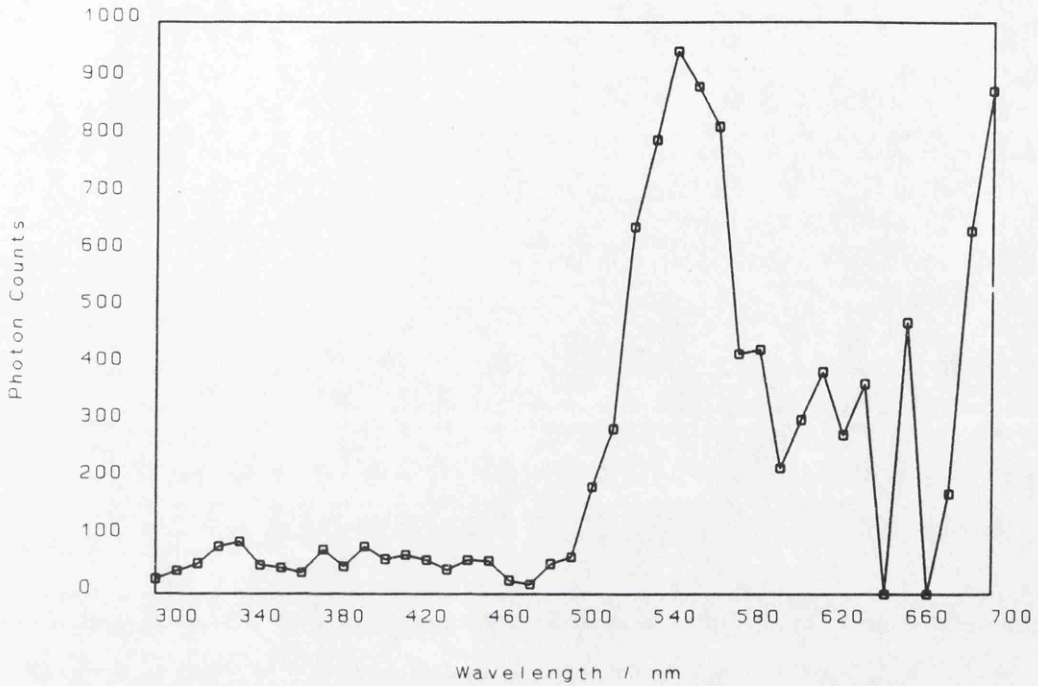


**Figure 4.32** - F1 Emission Spectrum at 150 K

Due to the short fading time and lack of preheat there may still be charge trapped in shallow sites which possibly could be evicted directly by the infra-red stimulation and thus yield a signal even at 150 K . The ratio of the 560 nm peak to the two minor peaks is approximately the same (given sensitivity problems) for this 150 K emission spectrum as in the one at room temperature. Hence it would seem that if this signal is due to shallower trapped charge carriers that do not have thermal assistance upon photo eviction, the evicted charge carriers are free to recombine in any of the centres and hence there appears to be no link between a particular centre and shallow traps.

Looking at the ratios of the three peaks, as can be seen in figures 4.33 and 4.34, it can be seen that the ratios change very little from 150 K to about 230 K, however at about 230 K (-43°C), it can be seen that the 340 nm peak grows relative to the 560 nm peak and that the 400 nm peak grows relative to the 340 nm peak, and in fact the 340 nm peak starts to merge with the 400 nm peak as thermal broadening of the emission peaks sets in above room temperature, as can be seen in figure 4.35. This rapid increase in the ability of the 400 nm peak to capture evicted charge carriers compared to the

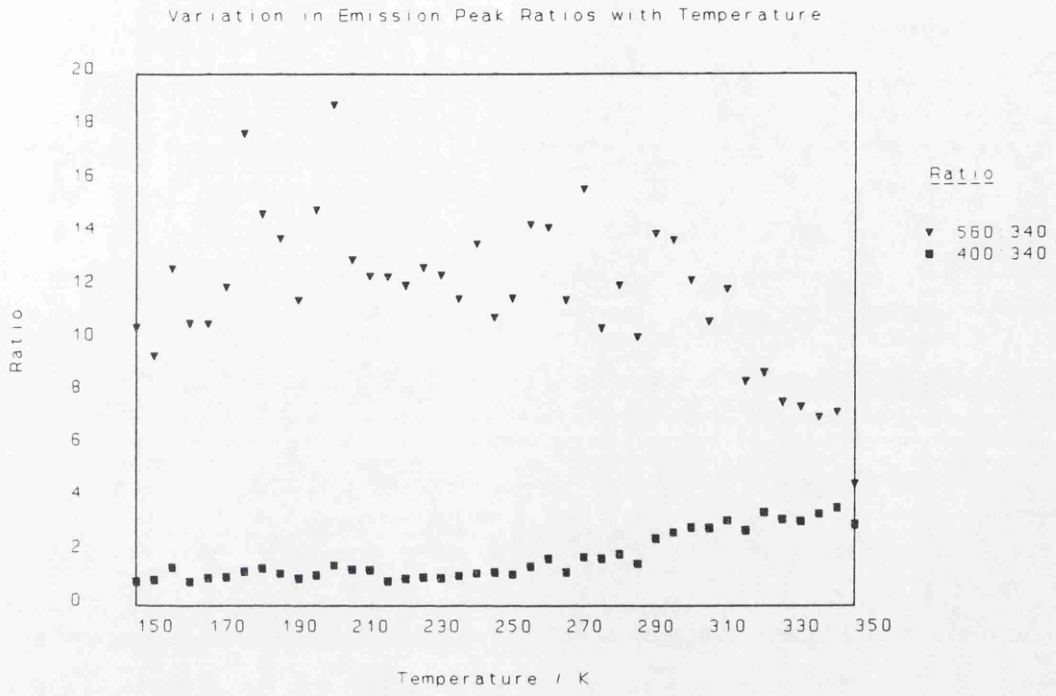


**Figure 4.33** - Variation of F1 Emission Peak Ratios with Temperature

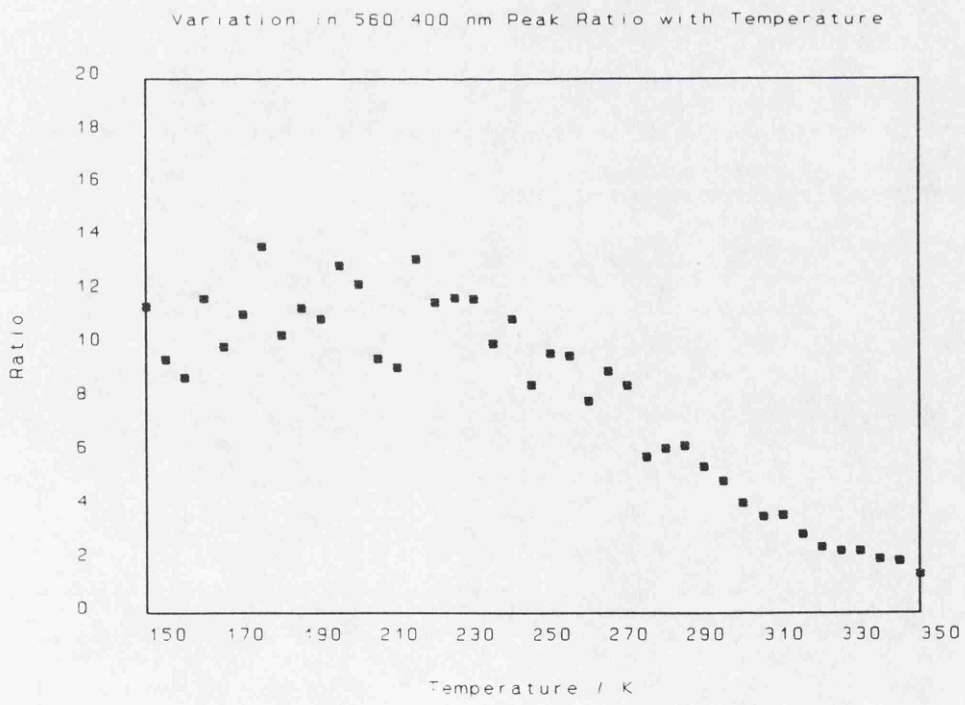


**Figure 4.34** - Variation of F1 560:400 nm Peak Ratio with Temperature

F1 Emission Spectrum at 350 K

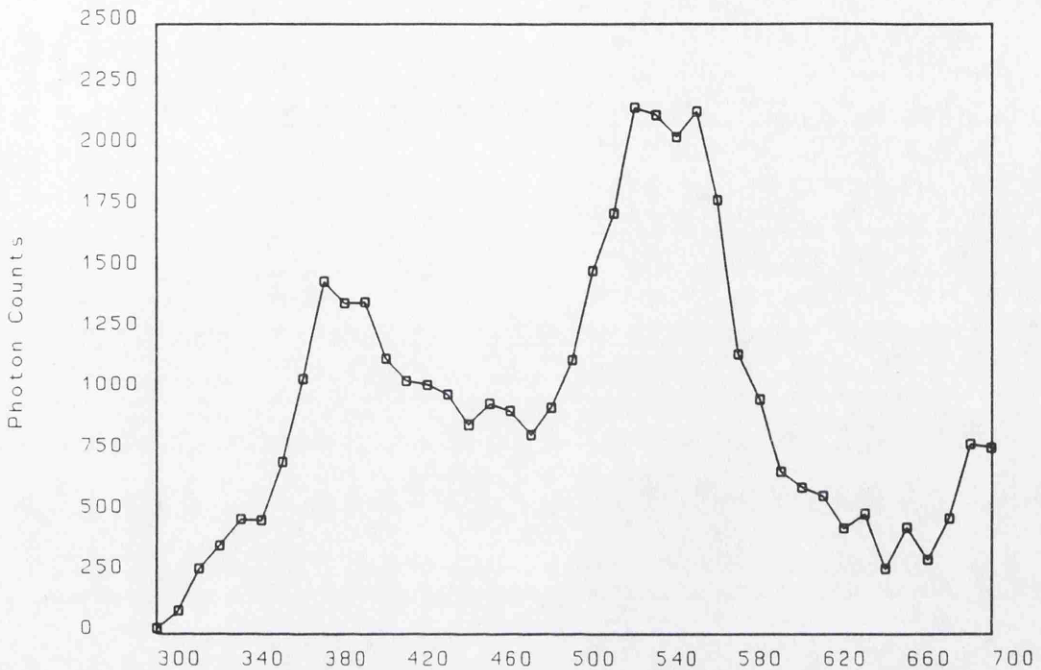


**Figure 4.35** - F1 Emission Spectrum at 350 K

other two centres almost inevitably leads to the question, why ? For the intensity from the emission band of one centre to increase with respect to the others as the temperature, and hence total evicted charge, increases one is tempted to come to the conclusion that there must be some link, perhaps proximity, between the 400 nm emission centre and the thermally assisted trap. However, this effect may be explained if one pauses to consider the relative rates of decrease of available hole states in the centre concerned.

It has already been shown in Figure 4.30 that during the course of bleaching the 400 nm peak increases relative to the other two peaks which may imply that the percentage rate of decrease of available hole states in this centre is lower than for the other two centres, which can result from a lower capture coefficient which *could* be shown by a lower intensity peak (all other factors held equal) which indeed is the case. Thus if this is indeed the case, it would mean that as the 400 nm centre is filled, so its ability to capture freed charge carriers is not reduced by as much as for the other two centres and

thus the observed emission peak should increase relative to the other two as the evicted charge population increases with temperature. Thus the ratio of the emission peak heights for 560:400 nm should fall, and 400:340 nm should increase as demonstrated above.

One departure from the behaviour of the ratios of the emission peaks observed under conditions of bleaching is that at around 320 K, the 560:340 nm ratio decreases implying an increase in the 340 nm peak intensity as compared to the 560 nm peak. Two effects which may explain this are; firstly by 320 K, thermal broadening of the

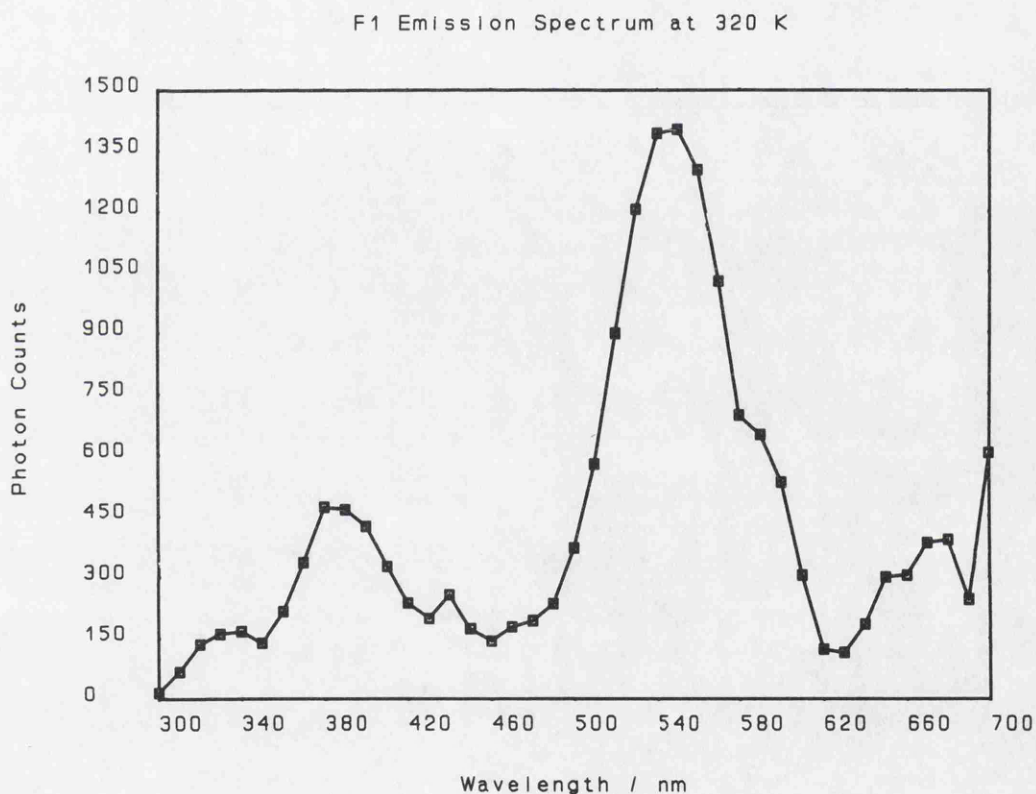


**Figure 4.36** - F1 Emission Spectrum at 320 K

emission spectrum has become apparent, as shown in figure 4.36, causing the 340 nm peak to become no more than an inflection upon the lower edge of the 400 nm peak, and thus the increase in intensity of the 340 nm peak as compared to the 560 nm peak could well be due to an additional contribution from the low wavelength edge of the broadened 400 nm peak; secondly, as the sample was not preheated, at 320 K (47°C)

phosphorescence will begin to appear as the traps corresponding to this temperature (and higher) have not been annealed out and may well not have faded totally. Thus there could perhaps be a contribution from the TL of shallow traps. In order to be able to disentangle these effects, more work obviously is required, with perhaps the first stage being a repeat run with a sample annealed to remove charge carriers trapped at shallow sites.

One point that must be emphasised, finally, is that this temperature dependent emission spectroscopy is not corrected for bleaching effects, which in comparison to the bleaching results, could be quite significant. Unfortunately, there was no time left during the visit to Sussex to record a bleaching spectrum lasting for as long as it took to acquire the temperature dependent spectra, and thus it is impossible to correct the results presented above for bleaching, and thus it can not be ruled out that these results may change upon such a correction. Also, it must be emphasised that these results are generated by a single experiment and thus must be treated with caution until they can be reproduced (or not as the case may be) however, they do show that understanding the emission spectrum's behaviour can yield a lot of valuable data on what is obviously a very complex system.

#### 4.2.3 - Summary

The main results of the emission spectroscopy can be summarised as follows; Three emission peaks have been identified for the F1 feldspar under 880 nm stimulation at wavelengths of 340, 400 and 560 nm. These peaks have also been identified elsewhere (Huntley *et al*, 1991; Jungner & Huntley, 1991 and Bailiff & Poolton, 1991) and comparison with these observations raises the possibility that the 560 nm emission peak is associated with the sodium content of the feldspar. The work presented above in conjunction with the published work also demonstrates the existence of these peaks at different stimulating wavelengths (514, 633, 880 and 950 nm) which tends to suggest that all of these recombination centres are accessed via the conduction band with no

centres being directly associated with a particular trap (assuming that the different stimulating wavelengths evict charge carriers from different traps).

The area of the above work not reported elsewhere in the literature is the observation of the changes in the emission spectrum with bleaching and temperature. It has been shown that the emission peaks can still be observed at 150 K, although the spectrum is dominated by the 560 nm peak, which is not to be expected if the infra red stimulation peak is totally thermally assisted, and this seemingly lesser assisted component could be due to the presence of shallow trapped charge carriers with a thermal lifetime at room temperature of a few days. The ratio changes between the various emission peaks with both bleaching and temperature may perhaps suggest that the centre giving rise to the 400 nm emission peak has a lower capture coefficient than the other two. The seemingly constant ratio of the 560 to 340 nm peak under conditions of bleaching raises the possibility that both emission wavelengths result from the same centre, however the amount of scatter associated with this ratio casts doubt upon the validity of assuming a constant ratio and hence this result must be treated with great caution.

It has been shown that as the stimulating temperature is increased, so the 400 nm emission peak increases with respect to the other two. There is also thermal broadening of the emission spectrum, causing the 400 nm peak to overlap that at 340 nm. This increase in the relative intensity of the 400 nm peak with temperature means that observations of the degree of thermal assistance in the infra-red stimulation band may be dependent upon the choice of detection window. Detection windows which exclude the 560 nm emission peak should give rise to greater temperature dependency than detection windows which include the 560 nm peak.

A very useful and important extension to the emission spectroscopy presented above would be the ability to be able to record emission spectra simultaneously with excitation spectroscopy (the direct analogue of TL emission spectroscopy). There are possibly insurmountable practical difficulties in separating the stimulation and detection windows for synchronous stimulation and detection. However it is possible that these obstacles could be overcome using asynchronous methodologies. Timing characteristics of the

PSL recombination dynamics are explored in section 5.4. Such measurements may form the basis of the development of techniques that enable synchronous excitation and emission spectroscopy.

#### 4.3 - Low Dose Dependence and Sensitivity

In order to be able to extend the work so far performed to actual dating, it is necessary to be able to accurately record signals resulting from doses in the region of a few grays. It is also desirable that the dose response in this region is linear or at least reproducibly non-linear so that accurate extrapolations can be made. The LED and nitrogen dye laser systems already possessed the required sensitivity, however the excitation spectrometer whilst set up to measure high resolution spectra, did not. In order to gain the required sensitivity, it was necessary to change the mode of operation of the spectrometer in order to use it as a way of defining particular stimulation and detection windows for the xenon lamp. All of the samples used in this section were taken from the stock sample IAEA reference feldspar F1.

##### 4.3.1 - Xenon Lamp

The main use of the xenon lamp for these experiments was to act as a stimulation source in the region of 500 nm as a comparison to the laser (stimulation in the infra-red region being performed by the LED's). This enabled the spectrometer to be reconfigured to give greatly enhanced sensitivity. This was achieved by using a 5 mm UG11 filter in the photomultiplier to define a detection window of approximately 250-400 nm with the stimulation being performed at 480 nm. Monochromator slit widths were set at 4.3 mm, thus giving rise to a bandpass of 40 nm. The grating used had a 1000 nm blaze grating. Greater sensitivity could have been obtained if a more suitable grating were used, however such a grating was not available for this experiment. This set up of the spectrometer was found to be able to record signals from doses of 0.5 Gy and thus was shown to have sufficient sensitivity.

A disk of the feldspar F1 was annealed at 500°C for 5 minutes and then the PSL response to a 1 s exposure to light of  $480 \pm 20$  nm was measured. The disk was then given a dose of 0.5 Gy and again the PSL response to a 1 s exposure was recorded together with the phosphorescence emitted in 1 s by the sample (i.e. that luminescence that is seen without the stimulating light) so that the net PSL signal could be obtained independently of the level of room temperature phosphorescence. This was repeated until a total cumulative dose of almost 8 Gy had been given to the same sample and the PSL measured. This resulted in a growth curve measured every  $\frac{1}{2}$  Gy from 0 to 8 Gy

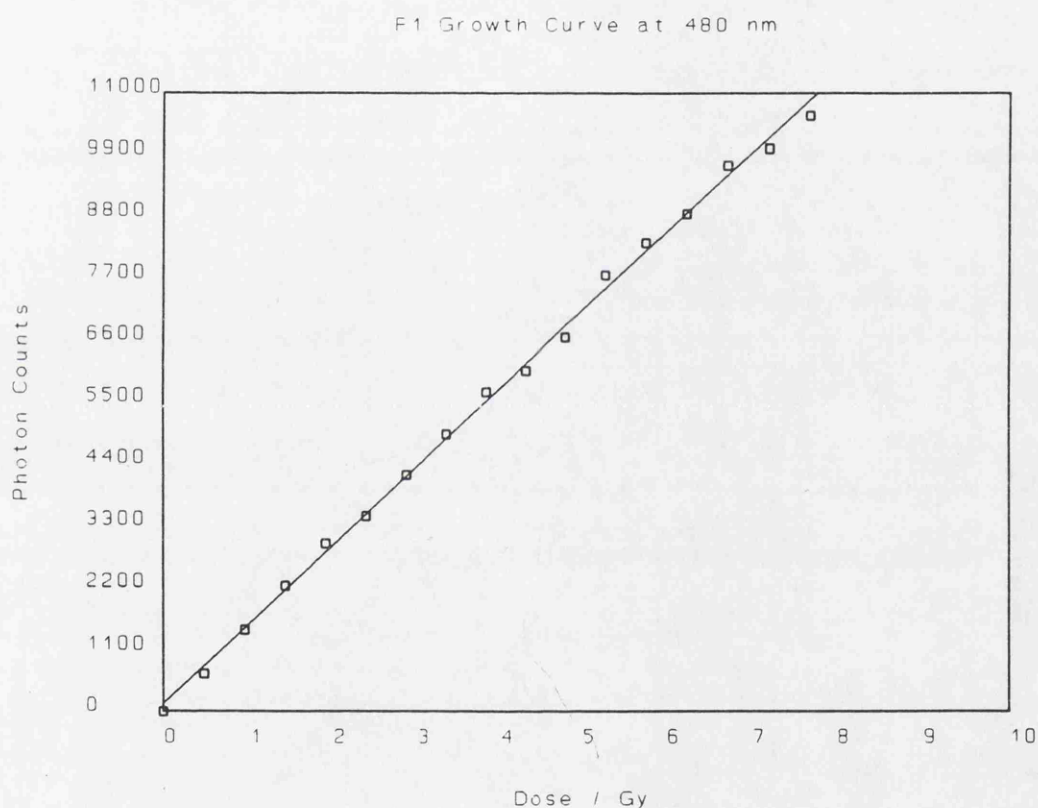


**Figure 4.37** - F1 Xenon Lamp Growth Curve at 480 nm

which can be seen in figure 4.37. As can be seen, the resulting growth curve is linear in nature with a low amount of scatter around the regressed line, with the error on the gradient being only 1.2% with a signal to background ratio on the  $\frac{1}{2}$  Gy point of 3.6. Thus in principle it should be possible to measure unknown doses in this dose region by extrapolation of such a growth curve. However, it must be noted that this growth

curve was recorded without using any preheating, which would not be the case for archaeological samples as preheating would be required to remove any thermally unstable components from the PSL signal. This would reduce the PSL signal (see section 4.1.4), however it is hoped that this should not reduce the signal to the lower limit of detection.

#### 4.3.2 - Laser

As with the xenon lamp system, an experiment to record the nature of the growth curve as stimulated by the laser was undertaken. The growth curve was constructed using cumulative  $\frac{1}{2}$  Gy doses from 0 Gy to a total of 5 Gy. The PSL measured was the sum of the luminescence resulting in 2 ms from ten pulses at 480 nm, with each laser pulse being 0.5 ns in duration with a spectral bandwidth of under 3 nm. The resulting growth

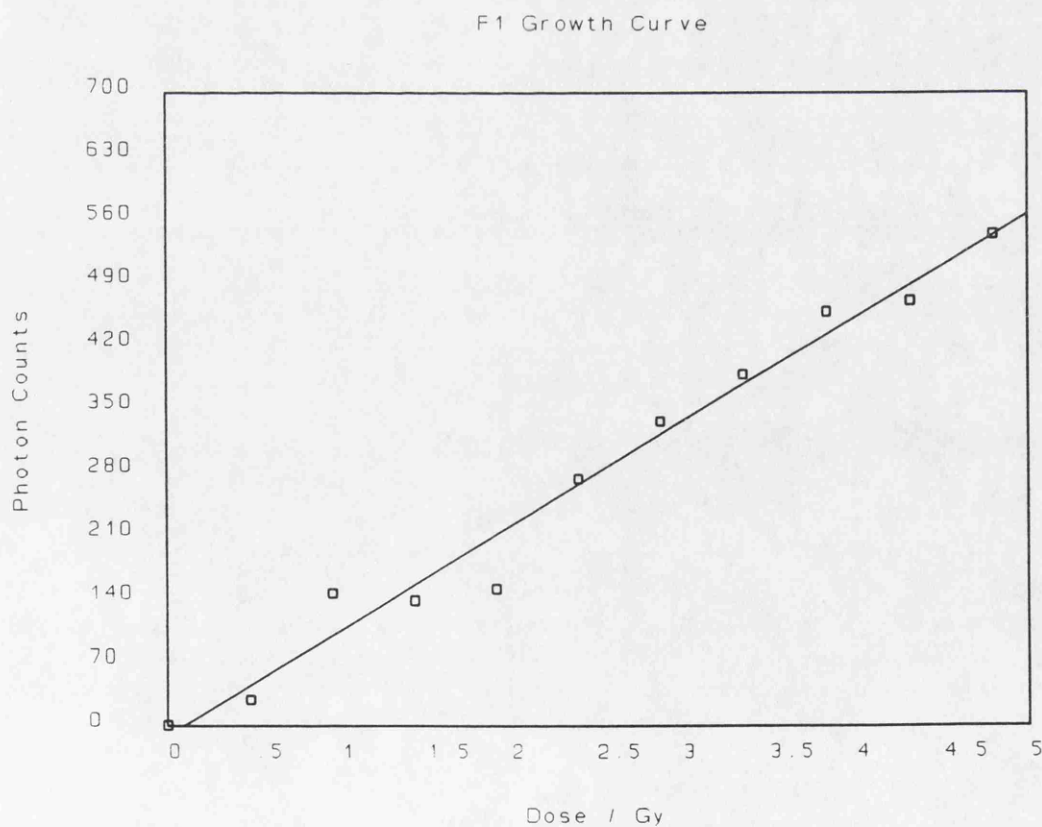


**Figure 4.38** - F1 Laser Growth Curve

curve can be seen in figure 4.38. From this curve it can be seen that the growth curve is approximately linear, agreeing with that constructed using the xenon lamp, however there is much more scatter around the regressed line (there is an error of 5% on the regressed gradient as opposed to 1.2% for the xenon lamp) which is perhaps to be expected as the rated energy stability of the laser is 5% and the number of pulses used per dose (10) is too low for this jitter to average out during the course of measuring the luminescence resulting from each dose. As the xenon lamp is used in continuous mode then it is expected that although there will be variations in the power output of the lamp, these should be more generally spread out throughout a day's use rather than extreme variations from minute to minute, as is born out by the lower scatter on the growth curve. One major advantage of the laser, however, is its power and thus resulting sensitivity. Although in this example the  $\frac{1}{2}$  Gy point only had an intensity of 30 photon counts, the average count from an annealed sample was  $0.62 \pm 0.75$  ( $\sigma_{n-1}$ ) counts, yielding a minimum detectable signal at  $\mu+3\sigma$  of 2.87 counts. Thus comparing the  $\frac{1}{2}$  Gy signal to a minimum detectable limit of 3 counts we get a ratio of 10 which is far greater than the signal to *background* ratio for the xenon lamp of 3.6. An equivalent signal to *background* ratio for the laser would be 30, assuming a background signal of 1. Consequently the laser system holds great promise if the fluctuations in power can either be averaged out by using more pulses per recorded luminescence signal, or if there were some form of synchronous power monitoring of the laser pulse so that the data could be corrected for fluctuations in the power of each laser pulse. Certainly if high sensitivity is needed, then of the two green stimulation systems, it is the laser that holds the greater potential than the xenon lamp. Once more it should be noted that these results were recorded without using any preheating.

#### 4.3.3 - Infra-Red LED

As with the other two stimulation systems, a growth curve of the feldspar F1 was constructed using a set of three infra-red LED's as the stimulating source. The growth curve was constructed cumulatively every 1 Gy from 0 Gy to a total of 8 Gy. The PSL recorded for each dose was the sum of the PSL recorded in 10  $\mu$ s from 2,000,000

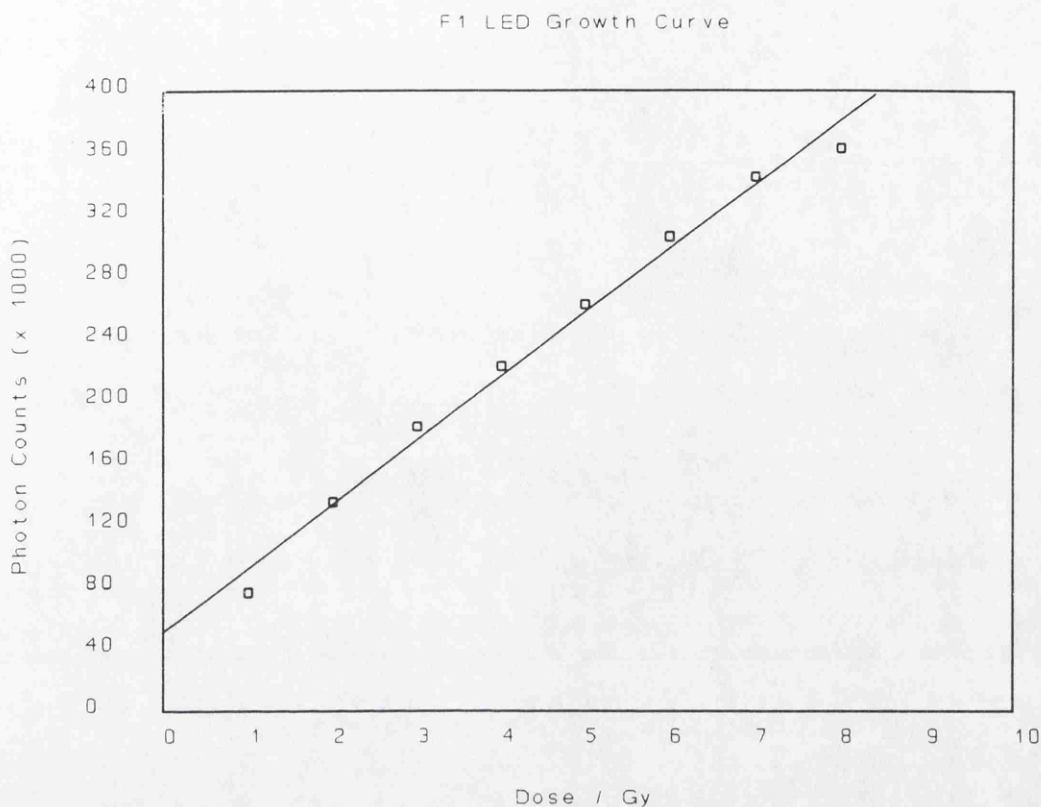


**Figure 4.39** - F1 LED Growth Curve

pulses. The LED pulses were  $1 \mu\text{s}$  in width with  $10 \mu\text{s}$  delay between pulses, at a wavelength of  $900 \text{ nm}$  with a FWHM of  $100 \text{ nm}$ . The samples were preheated at  $55^\circ\text{C}$  for 10 minutes to reduce room temperature phosphorescence. The resulting growth curve can be seen in figure 4.39. An important feature of this curve is that it is clearly sublinear in nature. With the fact that this curve was constructed by using a single disk which had equal doses added to it and the cumulative dose measured many times, the simplest explanation of this sublinearity is that the LED stimulation is actually bleaching the signal from each dose by a significant amount. It is reasonable to suppose that there is always going to be some bleaching of the signal in order to measure it (a direct corollary of the uncertainty principle), however in the case of the xenon lamp and laser it seems that this bleaching during measurement was negligible when compared to the signal added to the growth curves by each dose increment.

In order to verify this, a freshly annealed sample of the feldspar F1 was taken and given a dose of  $10 \text{ Gy}$ . The resulting PSL was recorded using exactly the same

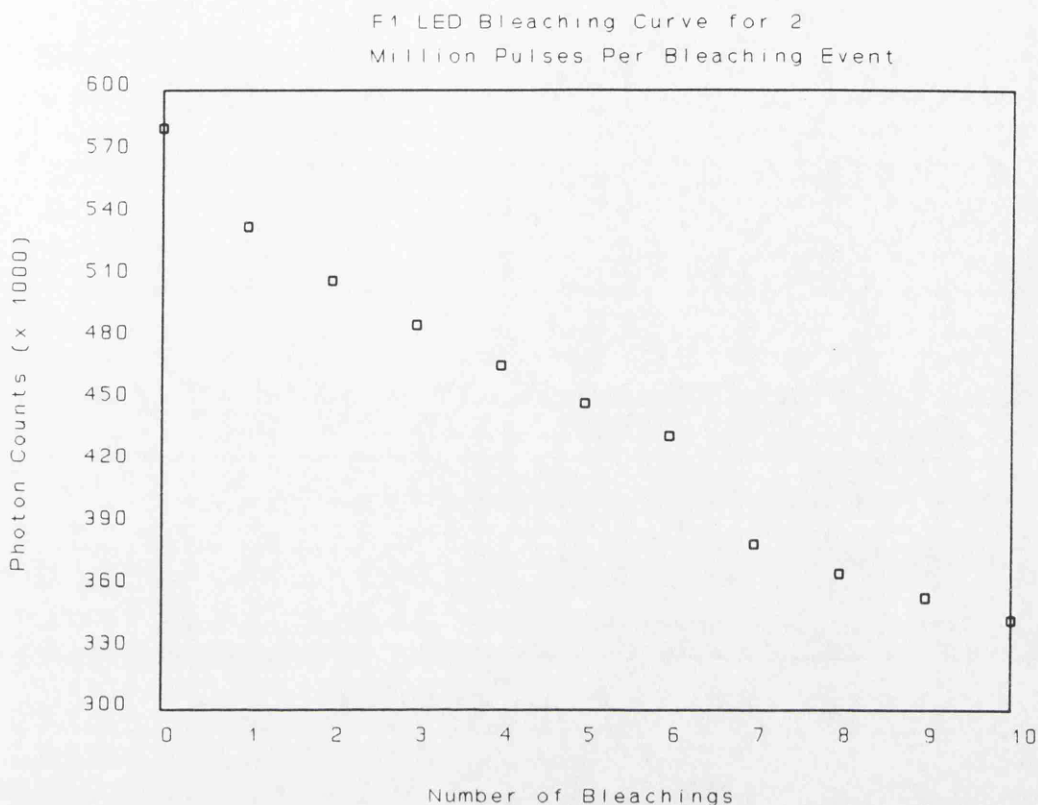


**Figure 4.40** - F1 LED Bleaching Curve for 2,000,000 Pulses per Bleaching Event

technique as the for the growth curve measurements. This measurement was then repeated a further 10 times in exactly the same manner in order to construct a bleaching curve for the same stimulation used in constructing the growth curve. The resulting bleaching curve can be seen in figure 4.40. This graph clearly shows that there is significant bleaching from readout to readout which decreases with successive readouts, i.e. the rate of bleaching starts at 8.13% and finishes at 3.01%, yielding an average bleaching rate of  $5.07 \pm 0.91$  %. Consequently in order to be able to record a growth curve without this sublinearity either less pulses will have to be used, or a correction for this bleaching will be required.

As far as absolute sensitivity is concerned, the 1 Gy point had a signal of 97741 compared to a background of 10147, yielding a ratio of 9.6. Assuming a linear response to dose, this would give a signal to background ratio of 5.3 for a dose of  $\frac{1}{2}$  Gy. This is of the same order of magnitude as the xenon lamp and once again demonstrates that there should be sufficient sensitivity to be able to measure archaeological doses by

extrapolation. Although the samples in this experiment were preheated, the preheat used (55°C for 10 minutes) was only designed to remove room temperature phosphorescence and preheats for dating samples would probably have to be more severe.

#### 4.4 - Summary

This chapter has laid the foundations of PSL studies of feldspar. Initial experiments describe excitation spectra, thermal assistance and stability, emission spectra and low dose behaviour. These results have implications in the development of models of the underlying processes used, and thus for developing practical application methodologies. The major results generated by the above experimentation are summarised in the following points;

- 4.4.1       Excitation spectroscopy has identified the presence of stimulation peaks in the green (circa 490 nm), red (600-650 nm) and infra-red (circa 880 nm) for microcline feldspar and these peaks with an additional peak at about 550 nm for the F1 feldspar.
  
- 4.4.2       Power normalisation of the excitation spectra has shown the infra-red peak complex to be due to lines in the xenon lamp spectrum overlying a single broad peak which is lower in intensity than the green stimulation region.
  
- 4.4.3       No indication has been seen that the green (490 nm) stimulation region does not extend further to shorter wavelengths, in fact the evidence seems to suggest that this is in fact the case with the 450 nm edge being due solely to the presence of filters.
  
- 4.4.4       Bleaching studies have resulted in non exponential bleaching curves, behaviour predicted from the mathematical model. These studies have also shown that the green stimulation region can be bleached by 880 nm photons, suggesting a link between the two stimulation regions.

- 4.4.5 Thermal assistance has been identified across the entire excitation spectrum, with the greatest effect in the infra-red region and the 550-700 nm region. There is also thermal assistance in the 500 nm region, however there appears to be a component that is either not thermally assisted or not within the temperature range studied. Identification of thermal assistance across the entire excitation spectrum has not been reported elsewhere.
- 4.4.6 Thermal stability studies have shown two major components. The infra-red stimulation region together with the 600 nm, 550 nm and *one* component of the 500 nm region appear to be annealed out at temperatures round 300-350°C, whilst the remaining component of the 500 nm stimulation region appears to be more stable and is not annealed until 400-450°C. The less thermally stable component of the excitation spectrum gives indications that it may be only meta stable over archaeological timescales which may limit the usefulness of infra-red PSL dating.
- 4.4.7 High dose PSL growth curves have shown that there is growth up to at least 10 kGy, with the possibility of growth beyond this region. This shows that PSL may have higher saturation limits than TL.
- 4.4.8 Emission spectroscopy has identified three emission bands under infra-red stimulation at 340, 400 and 560 nm.
- 4.4.9 Temperature dependent emission spectroscopy has shown that the 550 nm emission peak is present even at 150 K, and that the most extreme growth with temperature is in the 400 nm emission peak. This coupled with the variation in the emission spectrum with bleaching raises the possibility that the centre giving rise to the 400 nm emission peak has a lower capture coefficient than the other two. These observations of the variation in emission spectra with bleaching and temperature have not been reported elsewhere.

4.4.10 Two of the stimulation systems (the xenon lamp and the laser at 480 nm) have been able to record linear cumulative low dose growth curves with a zero intercept on a single sample indicating suitability for the potential to serve as a dosimetric / dating tool. The infra-red LED's resulted in a sublinear growth curve due to significant bleaching (i.e. 5%) during the measurement process. The laser showed more scatter, but greater sensitivity than the other two systems, however all three showed sufficient sensitivity to be able to measure 0.5 Gy.

The results have identified stimulation schemes that have demonstrated the potential for use as dating tools. Also more fundamental exploration of the behaviour of the stimulation regions has yielded results that have important implications in the development of a model to describe the PSL mechanism in the feldspars used. Some areas of the mechanism (e.g. thermal stability and temperature dependency) can now be explored in more detail in an attempt to be able to derive some information as to trap depths and interactions. Additional experimentation to explore these phenomena further will be discussed in the next chapter together with results from pulsed stimulation. This holds great potential in the areas of asynchronous detection and time domain analysis which may hold the key to understanding far more about the whole luminescence process (be it TL or PSL) especially in the area of anomalous fading.

4.4.10 Two of the stimulation systems (the xenon lamp and the laser at 480 nm) have been able to record linear cumulative low dose growth curves with a zero intercept on a single sample indicating suitability for the potential to serve as a dosimetric / dating tool. The infra-red LED's resulted in a sublinear growth curve due to significant bleaching (i.e. 5%) during the measurement process. The laser showed more scatter, but greater sensitivity than the other two systems, however all three showed sufficient sensitivity to be able to measure 0.5 Gy.

The results have identified stimulation schemes that have demonstrated the potential for use as dating tools. Also more fundamental exploration of the behaviour of the stimulation regions has yielded results that have important implications in the development of a model to describe the PSL mechanism in the feldspars used. Some areas of the mechanism (e.g. thermal stability and temperature dependency) can now be explored in more detail in an attempt to be able to derive some information as to trap depths and interactions. Additional experimentation to explore these phenomena further will be discussed in the next chapter together with results from pulsed stimulation. This holds great potential in the areas of asynchronous detection and time domain analysis which may hold the key to understanding far more about the whole luminescence process (be it TL or PSL) especially in the area of anomalous fading.

## 5 - Photostimulated Luminescence of Feldspar - II

Two characteristics of the response of the feldspars studied to photo stimulation that have important implications in the formation of a model and dating methodologies were identified in the previous chapter, namely the dependence of the PSL excitation spectrum upon stimulation temperature and secondly the thermal stability of the stimulated luminescence. Consequently more detailed studies of these two factors were undertaken, the results of which are laid out in this chapter including the observation of apparent short lived thermal sensitisation of the green excitation region. This chapter also describes the response to pulsed stimulation from infra-red LED's and a pulsed laser and the advantages of such stimulation. Finally the results presented in this and the previous chapter are combined in order to discuss the implications for current models of the PSL process.

### 5.1 - Thermal Assistance

#### 5.1.1 - Infra-Red Stimulation

It has already been postulated in section 4.1.3 that the luminescence resulting from infra red stimulation is the result of a two stage photon-phonon process. If this is the case, then it should be possible to perform initial rise analysis upon this trap in order to arrive at some estimation of the trap depth of the thermal transition. This involves the monitoring of the increase in infra-red sensitivity with temperature and then performing an arrhenius transformation upon this data in order to calculate the trap depth, as described in section 2.2.2.

A sample of the microcline feldspar that had been given a dose of 1 kGy sufficiently long ago (7 months) for the room temperature phosphorescence to have decayed was dispensed onto a 1 cm diameter stainless steel disc using silicon grease spray. The sample was mounted in the excitation spectrometer chamber and then the luminescence

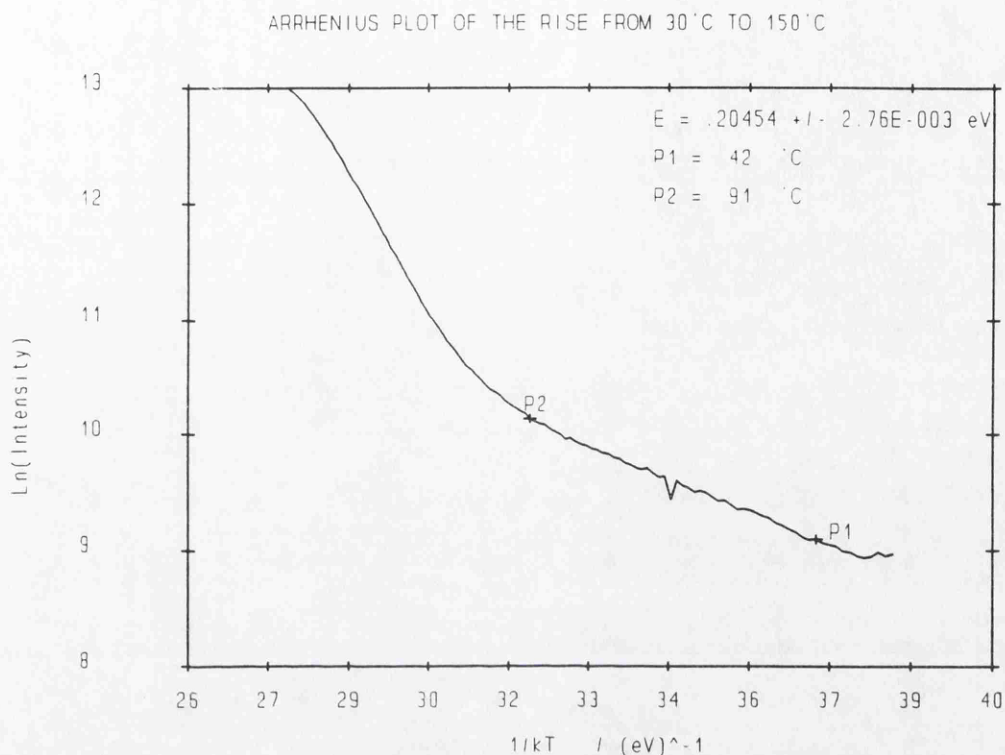


**Figure 5.1** - Arrhenius plot of microcline from 30°C to 150°C under infra red stimulation.

resulting from continuous stimulation at  $910 \pm 10 \text{ nm}$  during a temperature ramp from 30°C to 150°C at a rate of  $2^\circ\text{C} / \text{s}$  was recorded. This temperature ramp was then repeated, but without the infra red excitation, so that the background and TL components could be subtracted from the combined curve, leaving just the temperature dependent PSL component and the TL rise to the part of the glow curve beyond the maximum temperature, i.e. 150°C. This process was then repeated, but with increasing maximum temperatures from 200°C to 450°C. Thus for each curve it should be possible to observe at the low temperature end, the thermally assisted infra red excitation (until it is annealed out) and at the higher temperature end, the rise to the TL trap being stimulated thermally. A typical example of an arrhenius plot of the rise (in this case to 150°C) can be seen in Figure 5.1.

The energy shown in this plot was calculated by least squares linear regression between the points marked by crosses and also labelled as P1 and P2, and the resulting energy for this low temperature part of the curve (and hence of the depth of the trap giving rise

**Table 5.1 - Infra red thermal assistance energies**

Max. Temp. / °C	Temp. Range / °C	Energy / eV
150	42 - 91	0.205 ± 0.003
200	46 - 95	0.186 ± 0.001
250	41 - 82	0.200 ± 0.002
300	47 - 92	0.239 ± 0.003
350	Incomplete Data set	
400	89 - 192	0.183 ± 0.003
450	Interference due to Noise	
Average Thermal Activation Energy / eV		0.20 ± 0.01

to the thermal assistance) is  $0.205 \pm 0.003$  eV. Taking into account the results from all seven curves (rises up to 450°C every 50°C - Table 5.1), the average energy for the thermal assistance stage of the infra red stimulation becomes  $0.20 \pm 0.01$  eV. This value is in good agreement with that suggested by Hütt & Jaek (1989) also using an Arrhenius transform, although this value of  $0.2 \pm 0.1$  eV is less precise than that obtained here. Similar measurements to those presented here were reported in Duller & Wintle (1991). An Arrhenius plot is shown which yields a result of  $0.15 \pm 0.02$  eV calculated on a set of 13 discrete data points between 50°C and 180°C. Another group who have tried to measure the activation energy of this thermal assistance is the Durham group. In Bailiff & Poolton (1991), values are recorded at around  $0.1 \pm 0.02$  eV for the minerals microcline, sanidine and albite. This is significantly lower than the results derived here, however, they are of the same order of magnitude. In neither Hütt & Jaek (1989) or Bailiff & Poolton (1991) is it stated whether the Arrhenius plots were constructed from a set of discrete points, or from the response to a continuous ramp as was the case for the results presented here, and neither do they show the actual plots from which they derived their results, which is disappointing as it limits qualitative judgement on the relative merits of the three sets of data. However, the lower precision in both cases (50 % for Hütt & Jaek, 1989 and 20 % for Bailiff & Poolton, 1991) than that obtained in these experiments (4 %) suggests a smaller data set of discrete points,

which may account for any differences. However it must also be noted that each of the three experiments were performed upon different samples and thus it is possible that there will be slight variations between them.

### 5.1.2 - Visible / Red Stimulation

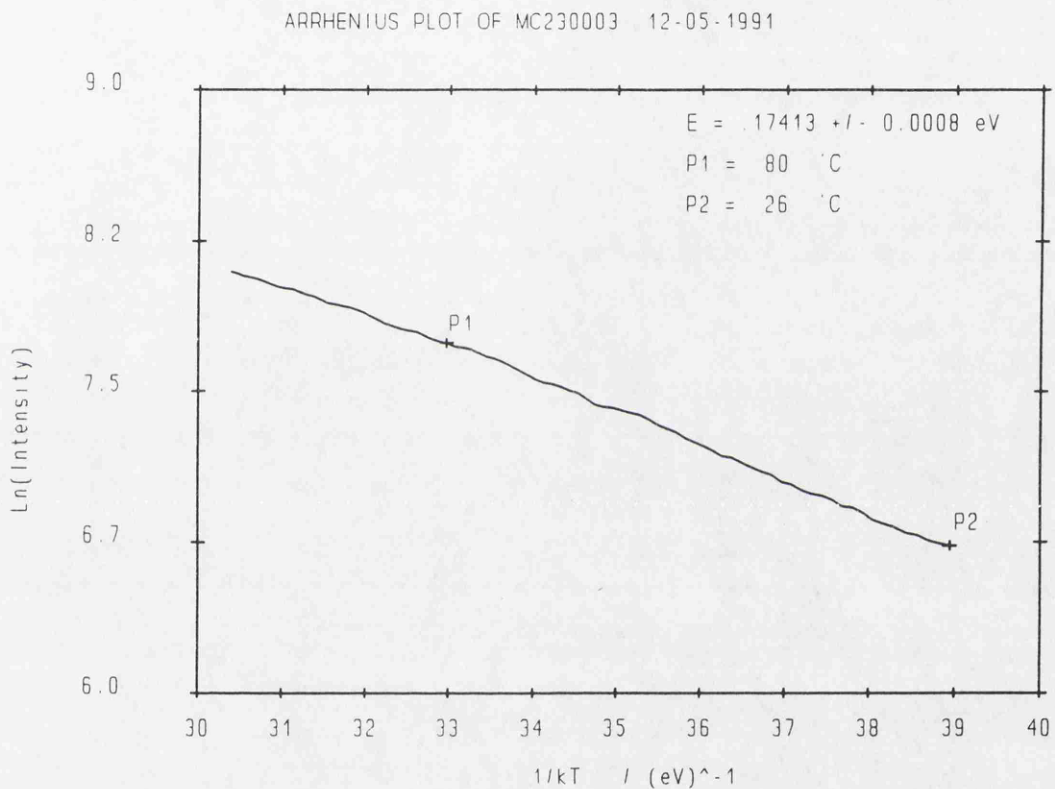


**Figure 5.2** - Arrhenius plot of Microcline feldspar at 625 nm from 25°C to 120°C

The thermal assistance for the infra red stimulation band has been widely observed and reported, however observations of the entire excitation spectrum (section 4.1.3 and Figure 4.16) have shown that there is a strong dependence upon temperature of the region around 600 nm. To investigate this, a sample of the microcline feldspar was given a dose of 1 kGy, annealed at 180°C for 1 minute and then the PSL stimulated at  $625 \pm 10$  nm from the xenon lamp was recorded from -80°C to 120°C with a temperature ramp of 2°C per second. An arrhenius plot of the response from room temperature (25°C) to 120°C (with 5 point smoothing) is shown in Figure 5.2.

As can be seen the plot is reasonably linear and yields an energy of 0.17 eV. This is similar to the activation energy already obtained for the infra red thermal assistance energy level of  $0.20 \pm 0.01$  eV, however, similar rises on this particular sample (also from the same microcline stock as used to investigate the infra red thermal assistance above) at 840 and 910 nm were performed immediately following the 625 nm rise, and the energy yielded from these Arrhenius plots was clearly of the order of 0.2 eV as opposed to the 0.17 eV of the 625 nm rise. It could be the case that both the thermal assistance in the red and infra red part of the excitation spectrum results from the same trap sitting at 0.2 eV below the conduction band. However it may be assumed that the red part of the excitation spectrum is independent of the infra red, but with an excited state which has a similar energy to that for infra red stimulation.

### 5.1.3 - Visible / Green Stimulation

As there was also some indication of thermal assistance in the green stimulation region, the response of the PSL resulting from stimulation at  $500 \pm 10$  nm with temperature from  $-80^{\circ}\text{C}$  to  $120^{\circ}\text{C}$  at  $2^{\circ}\text{C s}^{-1}$  was measured as part of the experiment presented in section 5.1.2 above. Thus the sample was the same microcline aliquot as used above, which had been irradiated to 1 kGy and then annealed at  $180^{\circ}\text{C}$  for 1 minute prior to measurement. Again the stimulation was provided by the xenon lamp system and an Arrhenius plot of the rise from room temperature ( $25^{\circ}\text{C}$ ) to  $120^{\circ}\text{C}$  after five point smoothing is shown in Figure 5.3.

As can be seen, the plot appears to be reasonably linear, although perhaps noisier than some of the other Arrhenius rises and yields an energy of approximately 0.08 eV, which is of a clearly different value to that shown by either of the red or infra red peaks. However, it has been shown that under cryogenic PSL, there exists a peak in the green region even at  $-140^{\circ}\text{C}$  (Figure 4.17). If this is a component of the green stimulation band that is not thermally assisted, then in order to arrive at a more accurate assessment of the thermal assistance activation energy, this cryogenic PSL component must be subtracted off from the rise of the PSL with temperature before the Arrhenius

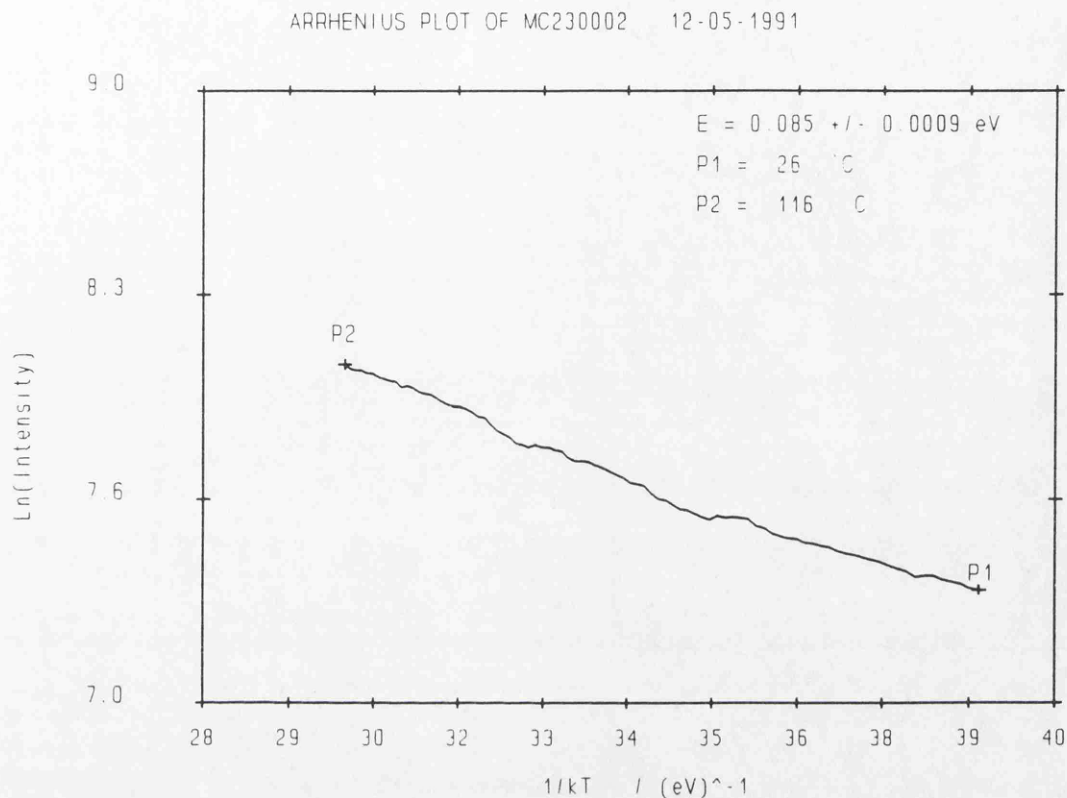


**Figure 5.3** - Arrhenius plot of microcline feldspar PSL at 500 nm from 25°C to 120°C transformation is performed. This has been done and the resulting arrhenius plot can be seen in Figure 5.4.

This arrhenius rise thus represents only the thermally assisted component that disappears with cooling to near LNT, and is a reasonable approximation to a straight line yielding an activation energy for the thermal assistance of approximately 0.15 eV. This value is of the same order of magnitude as the activation energies for both the red and infra red bands and is the smallest of the three.

#### 5.1.4 - Summary

From the results presented above, it can clearly be seen that thermal assistance is present in all parts of the excitation spectra shown earlier in chapter 4. Arrhenius rise measurements have been made on the three main stimulation regions of the excitation spectrum, namely in the infra-red (910 nm), the red (625 nm) and green (500 nm)

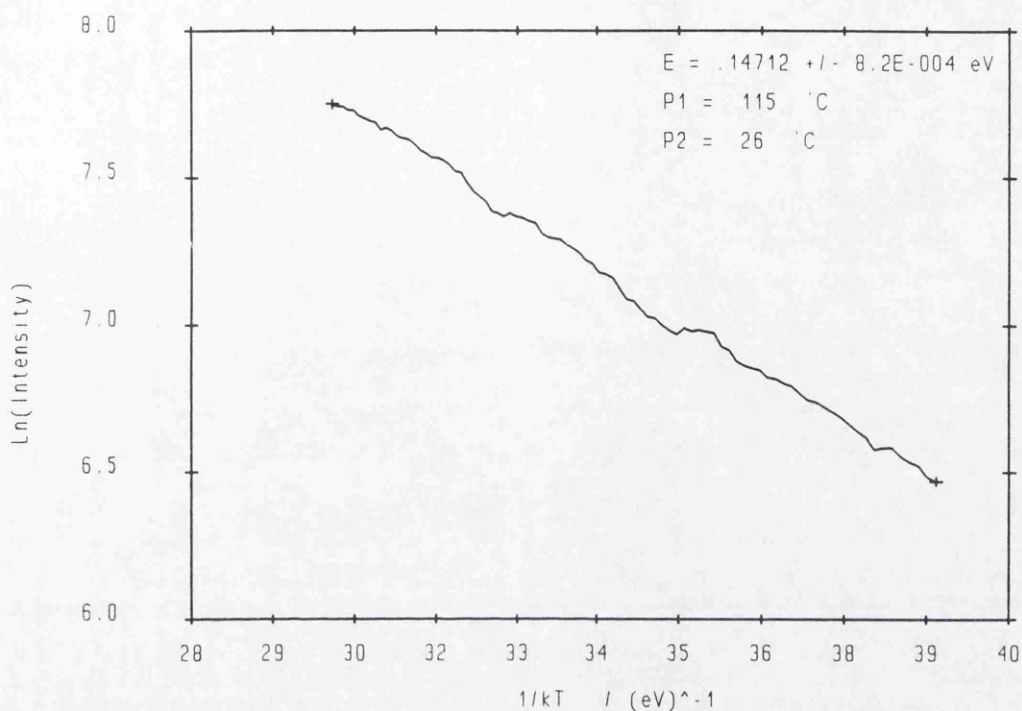


**Figure 5.4** - F1 arrhenius rise at 500 nm with cryogenic component subtracted.

stimulation regions. From these results (see Table 5.2), it appears that the thermal transitions for each region are of the same order of magnitude in depth, however, the

**Table 5.2** - Thermal assistance activation energies for the components of the excitation spectrum.

Stimulation Region	Thermal Assistance Activation Energy / eV
Visible / Green (at 500 nm)	$0.15 \pm 0.0008$
Visible / Red (at 625 nm)	$0.17 \pm 0.0008$
Infra Red (at 910 nm)	$0.20 \pm 0.01$

depth of these thermal transitions appears to increase with wavelength. If all three thermal transitions result from the same ground state trap, then as the stimulating wavelength increases, so its stimulating energy decreases, hence requiring greater

thermal energy to finish the eviction process. This is shown here by the increasing activation energy. The possible implications of this will be discussed in section 5.5 below.

## 5.2 - Thermal Stability

It has already been stated that sufficient thermal stability is a prerequisite for accurate dating. Studies of the annealing of the excitation spectrum at various temperatures (section 4.1.4) have already shown that the infra red signal and part of the visible signal are greatly reduced by annealing at 300°C for 1 minute and totally annealed out by annealing for 1 minute at 350°C. However there remained a component of the visibly stimulated signal that was not removed until the sample had been heated at 400°C for 1 minute, thus implying that there were several components to the PSL signal with varying thermal stabilities. One of these components having greater thermal stability than the rest of the excitation spectrum. In order to come to an improved understanding of the process, the thermal stabilities of stimulation in the green region was explored in more detail with pulsed isothermal decay analysis.

In pulsed isothermal decay analysis, the sample is heated to the annealing temperature for a short time and then cooled to room temperature for the recording of the PSL signal. In this way the decrease in PSL signal strength with continuing annealing can be monitored without the interference from TL. If the annealing is short and repeated many times, then the pulsed curve should follow a similar structure to continuous isothermal decay and thus standard isothermal decay analysis can be performed on the pulsed data.

Samples of the feldspar F1 that had been given a dose of 1 kGy were used in this experiment and the PSL was stimulated by the xenon lamp at a wavelength of  $480 \pm 20$  nm for 1 second in order to make bleaching effects negligible when compared to the loss of signal due to the annealing. The measurement process involved raising the sample to the annealing temperature for 30 seconds, cooling to room temperature and

then the PSL was measured. This process was then repeated many times in order to generate an annealing curve. This experiment was repeated with different aliquots from the same 1 kGy F1 sample for annealing temperatures from 175°C to 350°C every 25°C. The results for the temperatures 175°C to 225°C can be seen in Figure 5.5.

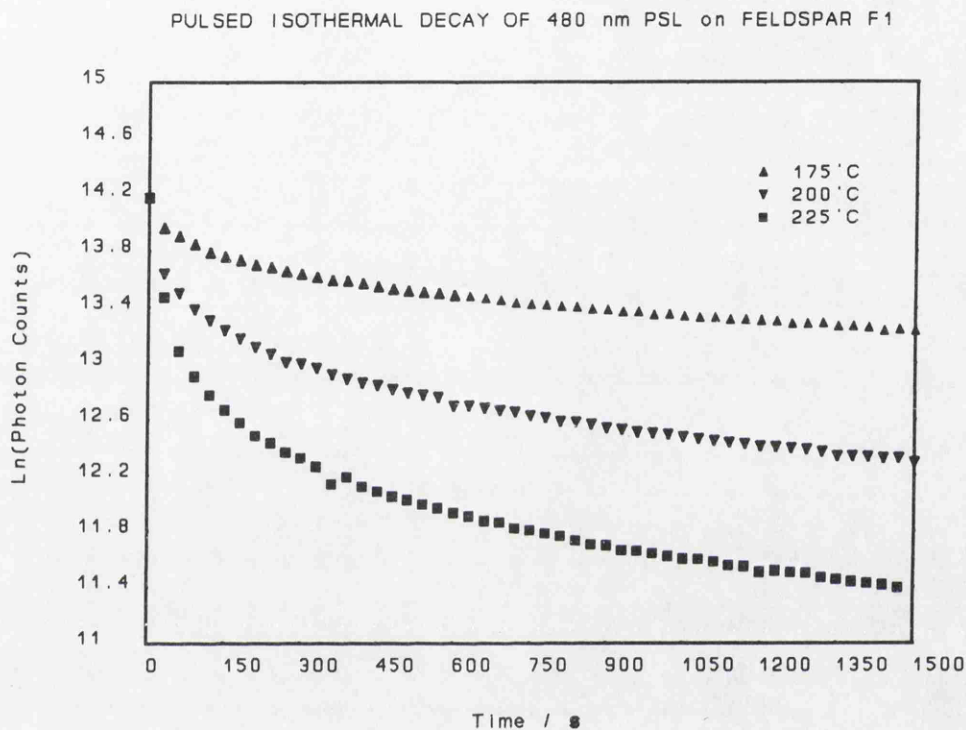


**Figure 5.5** - Pulsed Isothermal Decay of 480 nm PSL of the Feldspar F1 at 175°C - 225°C

The plot is a natural log plot, and according to the theory of isothermal decay (see Chen & Kirsh, 1981 or McKeever, 1988), for a single first order trap the curve should be exponential in nature and thus the log plot should be linear, a factor which is obviously not the case here. Two possibilities to explain the shape of these curves are that firstly there is more than one trap being stimulated by the  $480 \pm 20$  nm light and secondly that the traps concerned do not exhibit first order behaviour. If the PSL results from a combination of first order traps then it should be possible to deconvolute the curves into components with differing lifetimes (i.e. the sum of many exponential functions) by the fitting of a straight line to the longest lifetime component first and

then subtracting this line from the rest of the curve and repeating this for as many traps as are being stimulated. Another technique would be to perform nonlinear regression analysis based upon the sum of many exponential functions. If the components of the curves are first order, then the reciprocal lifetimes of the various components evaluated in this manner can be plotted on an arrhenius plot and the energy and frequency factors can be calculated and hence the thermal lifetime at burial temperatures (i.e. 5°C) can be calculated.

The first attempt at reducing the isothermal decay curves in to a series of exponentials with successively longer lifetimes used the first technique outlined above, namely the fitting of the longest lived component and then subtracting this from the whole curve and repeating for as many components as necessary. This technique required personal judgement as to when the longest lived component of the curves shown in Figure 5.5 departs from linearity. In order to verify that this technique was capable of reducing such a curve to its true components, a data set was calculated on the basis of the sum of three exponentials. This data set was then entered in to the program written for this purpose and an attempt was made to use it in order to resolve the components of the data set. It was possible to do this accurately, however it was apparent that the results were highly dependent upon the choice of the region of linearity and that small changes in this could cause large changes in the latter components. Difficulties were encountered in establishing the number of components truly represented by these data, and thus arriving at a unique description of the underlying kinetics. Due to the subjectivity of this technique, it was decided to use the second method, namely non linear regression analysis.

Regression analysis was performed using Sigma-Plot upon each of the isothermal decay curves from curves from 175°C to 325°C. Three functions were fitted, the sum of two, three and four exponential functions as shown in equation <5.1> (for the case of four

$$I = A\exp(-Bt) + C\exp(-Dt) + E\exp(-Ft) + G\exp(-Ht) \quad <5.1>$$

exponentials). For all temperatures, the two exponential function gave a poor fit,

however both the three and four exponential functions gave good fits to the curves. Consequently the three exponential function was used for the rest of the analysis as it was the simplest function giving a satisfactory fit to the data. In order to verify that the regression analysis could yield the correct values of the parameters A to F, a data set was created based on the sum of three exponentials over the same timescale used in the decay analysis. Regression analysis was then performed on this data set using the same starting conditions as for all of the regressions on the experimental data sets. The regression analysis managed to derive the parameters to better than 0.1 %, and thus it was decided that the parameters generated by similar regression analysis upon the experimental data sets would be valid.

The resulting lifetimes generated by the regression analysis were plotted on an Arrhenius

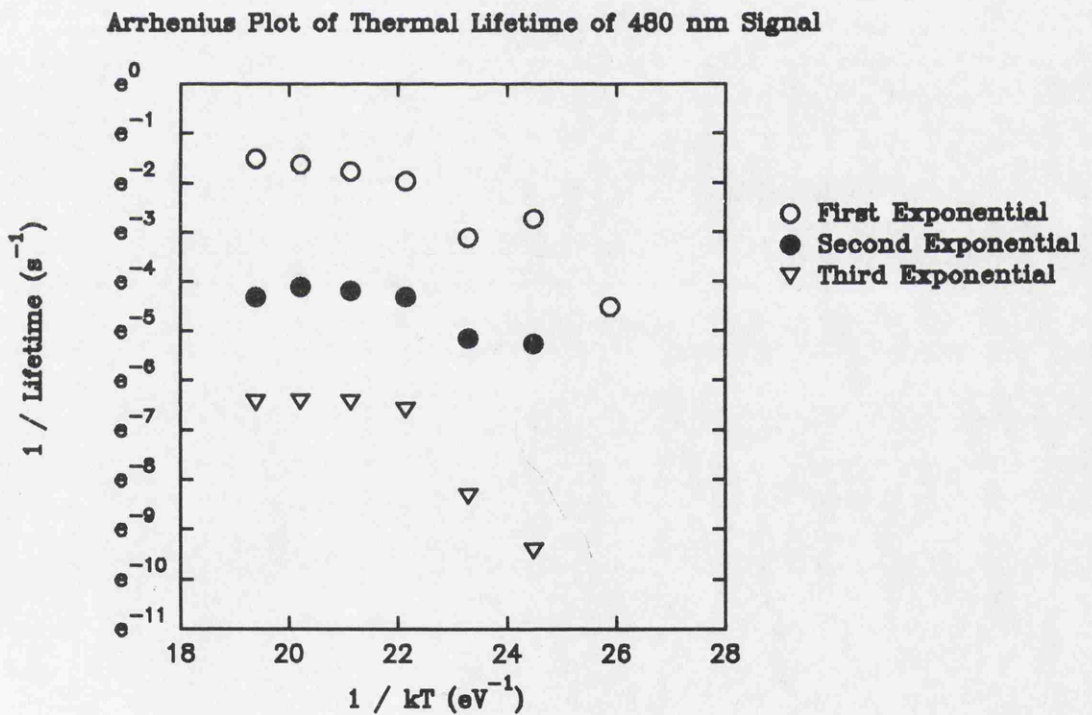


**Figure 5.6** - Arrhenius plot of the thermal lifetimes of the components of the 480 nm PSL

graph, as can be seen in Figure 5.6. As can be seen from this graph, none of the three exponential components have a linear response. Thus it is either the case that the decay is non first order or that there are more than three components present in the 480 nm

stimulation region. Typical feldspar glow curves exhibit many broad overlapping glow peaks, and fractional glow measurements of several feldspars (Strickertsson, 1985; Sanderson, 1987) raised the possibility that regions of the TL glow curve result from a *distribution* of traps. According to Randall & Wilkins (1945c) an exponential distribution of traps will result in isothermal decay exhibiting an inverse power law relationship instead of the exponential decay expected from a single trap. The general form of the decay is given in equation <5.2> below;

$$I \propto T t^{-(\alpha kT + 1)} \quad <5.2>$$

where I = Intensity

T = Temperature / K

t = time / s

k = Boltzmann constant ( $1.38 \times 10^{-23} \text{ JK}^{-1}$ )

$\alpha$  = distribution parameter, given by

$$N_E = A \exp(-\alpha E) dE \quad <5.3>$$

where  $N_E$  = Number of traps between E and E+dE

In the case where  $\alpha = 0$ , a uniform distribution results. If there is an exponential or uniform distribution of traps, then clearly if the decay curve is plotted on a Log-Log graph, the result should be a straight line with a gradient equal to  $-(\alpha kT + 1)$ . For a uniform distribution this would result in the gradient being equal to -1 and invariant with changes in the decay temperature.

Such a Log-Log plot of the seven isothermal decay curves can be seen in Figure 5.7. As can be seen from this graph, each of the seven decay curves appears to be linear in nature. The only possible exception being the curve at 175°C which flattens out towards the upper end of the time scale. This may be explained as follows; each of the curves was corrected for the effect of bleaching during measurement. The bleaching factor was calculated by repeatedly exposing the sample to 480 nm stimulation as for the isothermal decay curves, but without the heating, and the average percentage bleach was calculated and the curves corrected on the assumption that the bleaching was

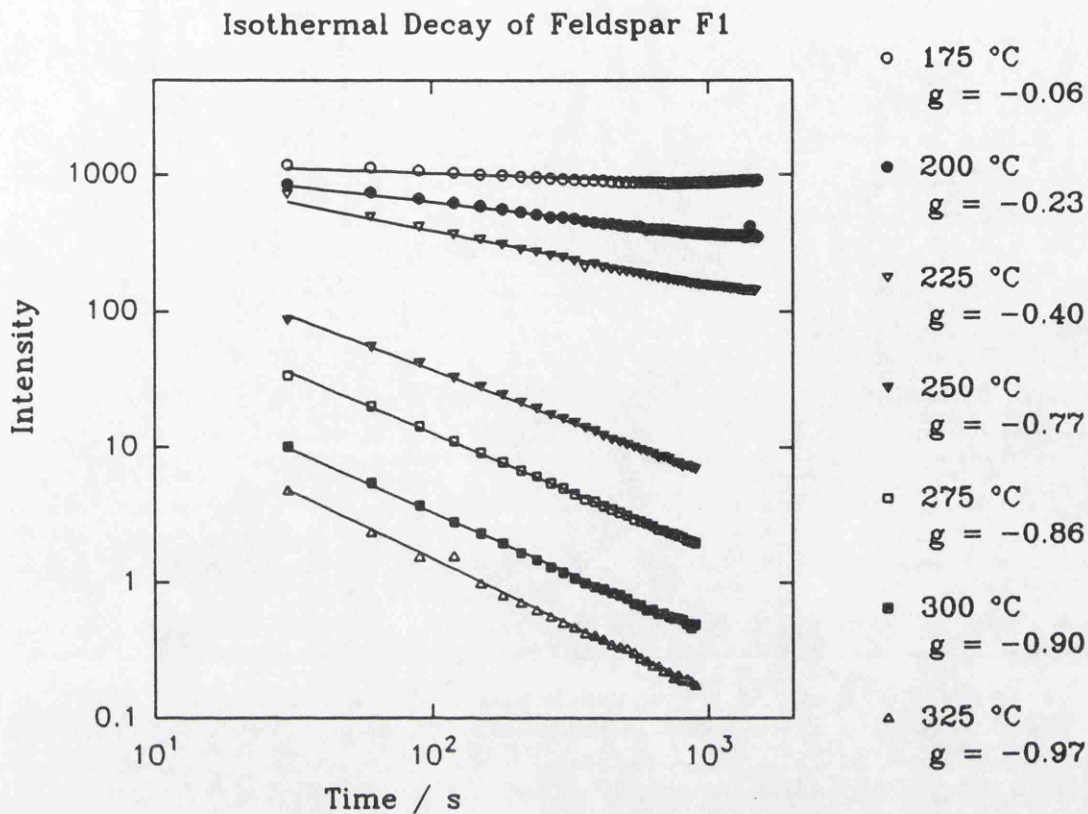


**Figure 5.7** - Log-log plot of F1 Isothermal Decay

constant throughout the bleaching curve. However, it has already been shown that the bleaching curve is not exponential in nature and that the percentage bleached decreases as the signal is reduced (see section 4.3.3). Consequently, the correction made to the isothermal decay curves is likely to have under corrected the initial part of the curve and over corrected the final part of the curve. This will have a negligible impact upon the shape of the curves at high temperatures where the percentage annealed is far greater than the percentage bleached. However as the annealing temperature is reduced, so this factor will become more significant, and it seems apparent that for the 175°C curve this factor may well have had a significant impact upon the shape of the isothermal decay curve.

Looking further at Figure 5.7 it can be seen that the gradient of these lines is temperature dependent and less than 1. This implies that the 480 nm PSL may well result from an exponential distribution of traps. The fact that the gradient is always less than one requires that  $\alpha$  is also less than one, this in turn implies that the distribution

concerned would have to be a *positive* exponential distribution, i.e. that the number of traps increases with energy depth. All of this discussion has so far assumed that the kinetics of the isothermal decay are first order, however non first order kinetics can not be ignored. For a single trap exhibiting non first order kinetics, the isothermal decay is given by (from McKeever, 1988)

$$\left(\frac{I}{I_0}\right)^{\frac{1-b}{b}} = 1 + n_0^{b-1}(b-1)s' \exp\left(-\frac{E}{kT}\right)t \quad <5.4>$$

where  $b$  = order of kinetics ( $b \neq 1$ )

$n_0$  = Initial trapped charge population

$s'$  = effective frequency factor =  $s/RN$ ,  $N$  = density of traps and  $R$  = retrapping ratio

Clearly, on a log-log plot a straight line will only be obtained if the value of  $b$  is known and  $(I/I_0)^{(1-b)/b}$  is plotted instead of  $I$ . Thus as the plot of  $\log(I)$  against  $\log(t)$  is linear, it would seem that the decay is not due to a single non first order trap. The effect of non first order kinetics upon a distribution of traps is more complex, however it may be expected that it would cause non linearity in the log-log plot.

In summary, the isothermal decay of the PSL stimulated by 480 nm photons appears to be a complex phenomenon. It is clearly the result of more than one trap and there is strong evidence to support a theory that it is due to a non uniform distribution of traps. The evidence also supports the postulate that the thermal eviction of the trapped charge carriers in these traps is a first order process. The complexity of the isothermal decay of the 480 nm PSL means that obtaining reliable parameters may be unlikely.

### 5.3 - Thermal Sensitisation

During the course of some of the thermal annealing experiments, it was noticed that after the infra red stimulation band had been annealed out, continued annealing reduced the green stimulation band as would be expected, however after a while the signal in the green stimulation band began to increase again. It was also noticed that this

thermally sensitised signal was unstable with a lifetime of the order of minutes. Consequently it was decided to explore this odd phenomenon further.

A sample of the F1 feldspar that had received a 1 kGy dose was used for this experiment. The signal stimulated by  $500 \pm 10$  nm was monitored continuously whilst the temperature of the sample was varied. Firstly the sample was heated to  $485^\circ\text{C}$  at  $2^\circ\text{Cs}^{-1}$  to anneal the sample then immediately upon attaining  $485^\circ\text{C}$  the temperature was dropped to  $400^\circ\text{C}$  for 15 minutes after which the temperature was further reduced to room temperature ( $30^\circ\text{C}$ ) for 15 minutes. The resulting luminescence observed during the 15 minutes at  $400^\circ\text{C}$  and the 15 minutes at room temperature can be seen in Figure 5.8. As can be seen from this graph, during the heating at  $400^\circ\text{C}$ , the PSL

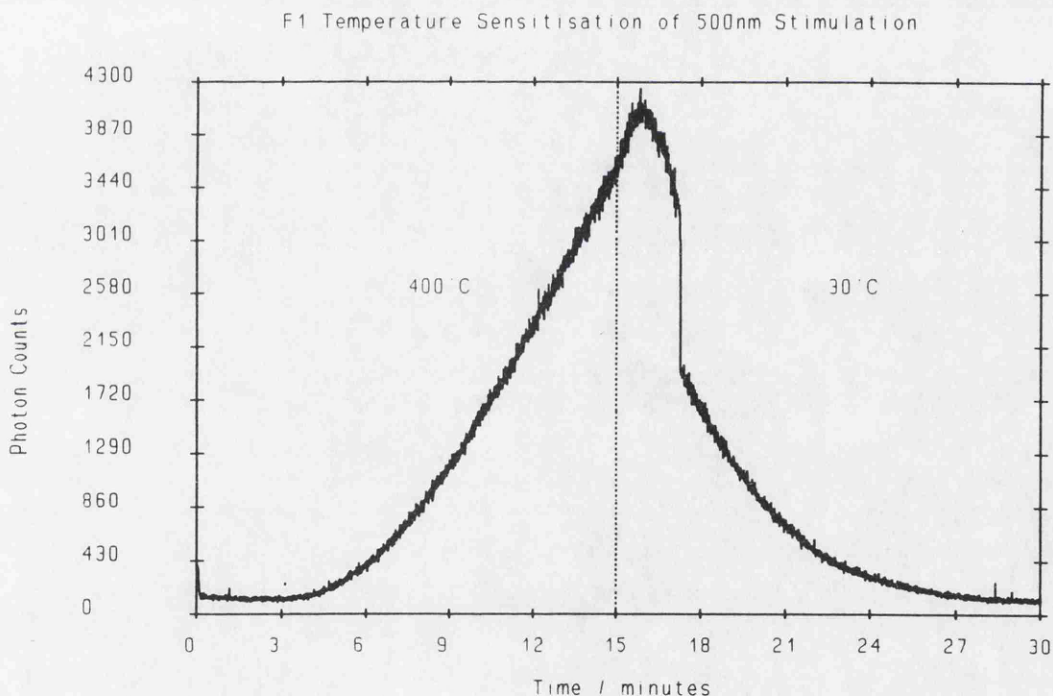


**Figure 5.8** - Thermal sensitisation of 500 nm stimulation

signal stimulated at 500 nm increases slowly. Once the temperature is reduced, so the signal gradually fades away.

In order to verify that it was the photo stimulation at 500 nm that was generating the signal and that the heating was just provided the sensitisation, the experiment was

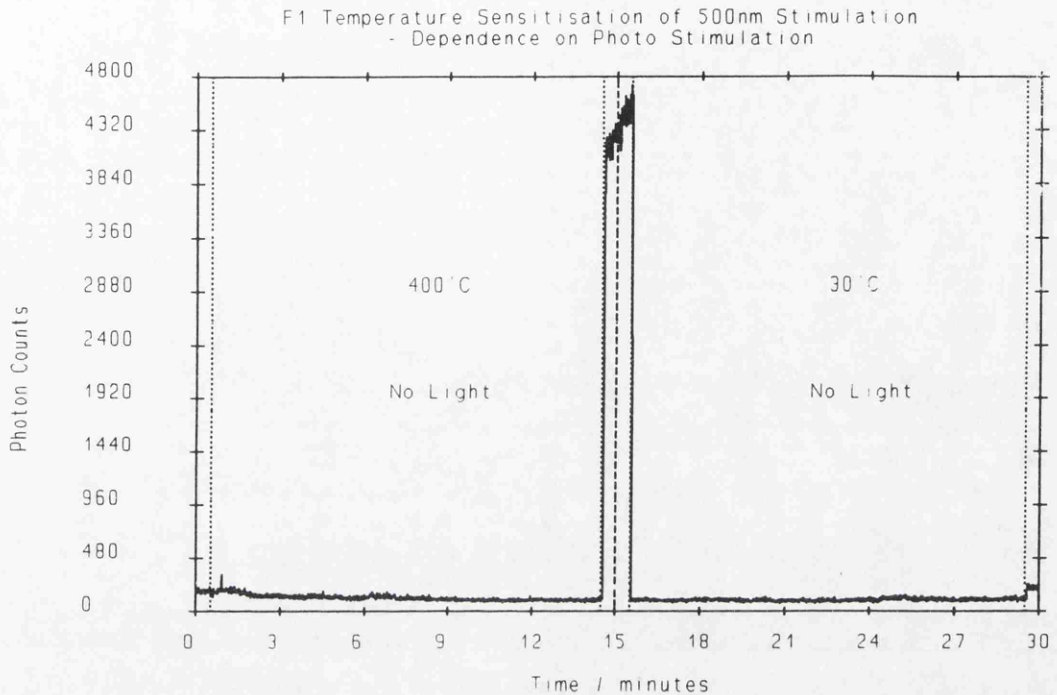


**Figure 5.9** - Evidence that the sensitised luminescence requires 500 nm stimulation

repeated using the same sample, only this time the sample was only stimulated with 500 nm photons during the first and last 30 seconds of each 15 minute period. The results of this can be seen in Figure 5.9, with the photo stimulated regions lying between the axes and the dotted lines and between the centre two dotted lines. It can be seen that during the 500 nm stimulation at the start of the heating, no significant luminescence can be observed. During the heating at 400°C (whilst there is no photo stimulation) no luminescence signal can be observed either, however as soon as the sample was exposed to the 500 nm photons towards the end of this heating period, a sensitised signal can clearly be seen. Again, once the 500 nm stimulation is removed no signal can be seen whilst in the final monitoring after 15 minutes at room temperature a decayed signal can. Hence it would appear to be the case that the thermal excitation somehow sensitises the 500 nm stimulated luminescence and that it is the 500 nm stimulation that can generate the luminescence.

Exploration of this phenomenon was then extended to observe the dependency of the sensitised signal upon the sensitising temperature. A sample of the 1 kGy F1 feldspar was scanned from 450 to 950 nm at room temperature to record the excitation

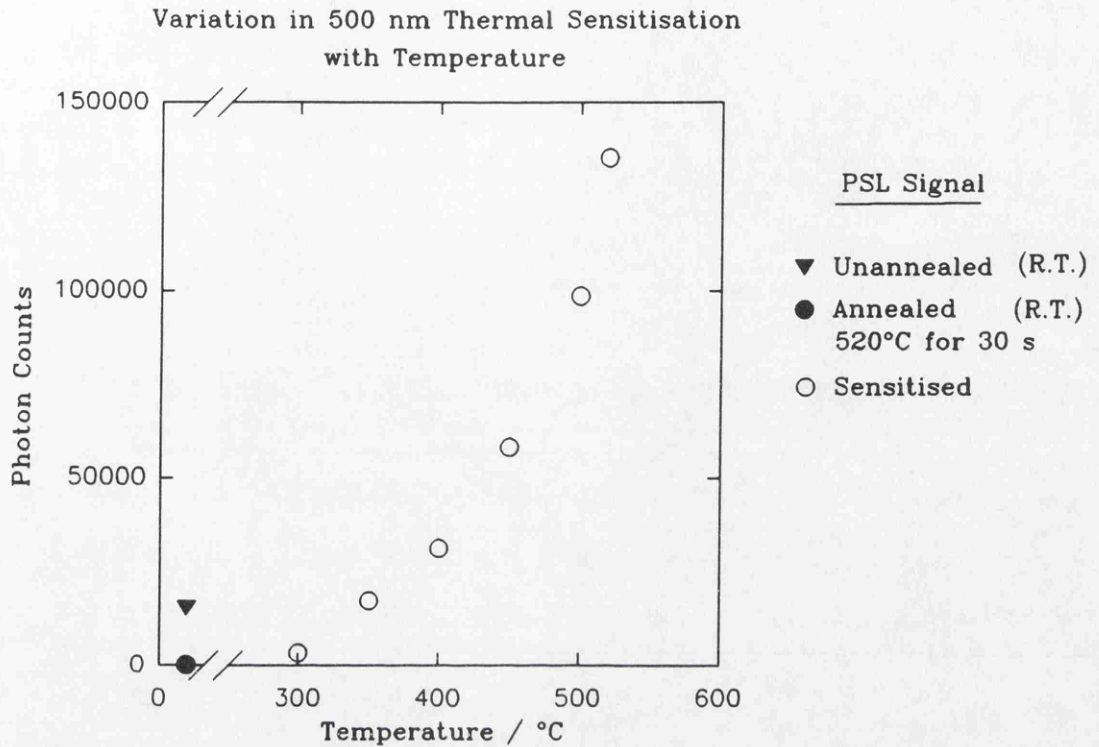


**Figure 5.10** - Variation in sensitised 500 nm signal with sensitising temperature

spectrum. The sample was then annealed at 520°C for 30 seconds after which a second excitation spectrum was recorded. The sample was then continuously monitored at 500 nm whilst being sensitised at 300°C for 15 minutes followed by 15 minutes at 40°C. This sensitisation step was then repeated at temperatures from 350-520°C. The results can be seen in Figure 5.10. This graph shows that the sensitised signal grows with sensitisation temperature, as is to be expected if the sensitisation is due to the thermal excitation of charge carriers from one state to another.

The evidence presented above may lead to the following conclusions; Upon the initial heating to high temperature, the PSL signal stimulated by 500 nm photons is more or less totally annealed out (as shown by the lack of signal at the starts of the first two graphs and the second point on the previous graph). During the prolonged thermal stimulation, charge carriers can be promoted into the 500 nm trap from a deeper trap by thermal excitation, the rate being dependent upon the temperature. The charge carriers are then trapped for a short time before relaxing back to the original trap. However this raises a problem, if the charge carriers are promoted into the same

500 nm trap as is originally annealed, why is a signal observed from this trap at room temperature prior to annealing as surely it would be expected that any charge carriers in this trap should have relaxed to the deeper trap (as is the case post sensitisation) ? This leads to the postulate that the initial trap which is annealed and that which is sensitised are different but can both be interrogated by 500 nm photons.

## 5.4 - Pulsed Stimulation

### 5.4.1 - Infra Red LED Stimulation

As has already been stated, pulsed stimulation can offer many potential advantages including greater peak power output, low background (due to the short counting times used), the averaging of pulse power over many pulses if used in a multi-pulse mode and the ability to observe the charge carrier recombination lifetimes. From the one trap /

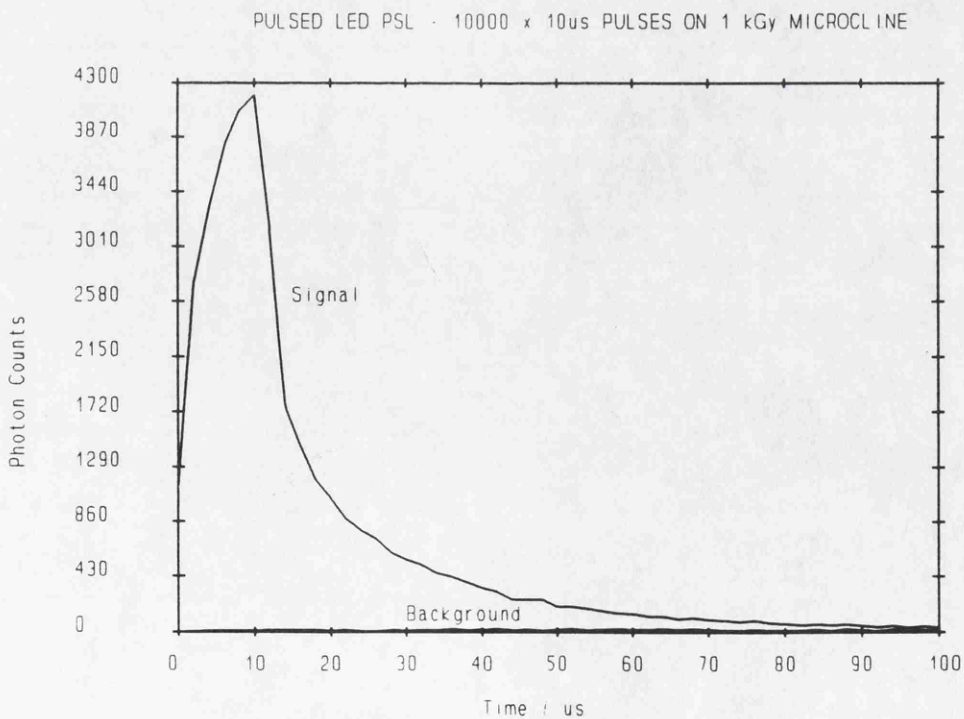


Figure 5.11 - Microcline pulsed LED PSL

one centre model it has been suggested that the dynamics of the bleaching curve should be dependent upon the system variables such as dose etc. and that a better method of stimulation would be a series of short pulses which would allow the system to return to equilibrium after the initial perturbation and before the next one. Coupling this to the other advantages of pulsed stimulation mentioned, it was decided to operate the diodes in a pulsed mode. An example of the response of the microcline feldspar to infra red LED pulsed stimulation can be seen in Figure 5.11. The sample had previously received a 1 kGy dose, and the PSL shown results from ten thousand 10  $\mu$ s pulses with a delay of 10 ms between the pulses, with the start of the data acquisition being synchronised to the rising edge of the LED pulse.

As can be seen, during the LED pulse, the PSL signal increases to a maximum at the end of the pulse, and then decays over a longer time scale. Characterisation of the LED pulse (section 3.8.2) showed a total rise time of only about 1  $\mu$ s after the rising trigger edge, which does not account for the 10  $\mu$ s rise seen in this graph. Also the fall time was recorded to be 13  $\mu$ s whereas the PSL signal falls from 90% to 10% in about 25  $\mu$ s. Hence the rise and fall of the pulsed PSL signal appears to be following dynamics that can not be accounted for entirely by the LED pulse characteristics and this can be explained by considering the charge carrier dynamics. The luminescence emission can not be simultaneous with the eviction of the charge carriers for several reasons; firstly there is a probability that the charge carriers instead of recombining in a luminescence centre, will be retrapped, thus delaying their eviction; secondly, once the charge carriers have been evicted from the trapping sites, they then have to undergo migration around the relevant band before finding a free recombination centre (i.e. they have to physically move through the crystal lattice from the trapping sites to free recombination sites) and this will take time, depending upon the mobility of the charge carriers at a certain temperature, the proximity of the recombination centres and the traps, and the presence of shallow traps that may trap the charge carriers for a short time before being thermally evicted to resume the lattice migration. If the traps and centres are randomly distributed throughout the lattice then the recombination time can only be expressed as an average recombination time which would be represented on such a graph as seen in Figure 5.11 by the time taken for the initial rise to become level during the lifetime of

the pulse, in this example the time being greater than 10  $\mu$ s. This recombination time also accounts for the tail after the pulse. Once the pulse ends, the free charge carriers in the conduction band will either become retrapped, or will eventually find a recombination centre after lattice migration. The time taken for this recombination will be dependent upon the same factors as recombination during the pulse.

#### 5.4.2 - Laser Stimulation

A pulsed dye laser can deliver sub nanosecond, high power pulses of light tunable over the range of the dyes being used. Thus this should yield extremely good signal to background ratios with high sensitivity and the narrow pulse width coupled to the high power and tunability should make it an almost ideal stimulating source for the study of

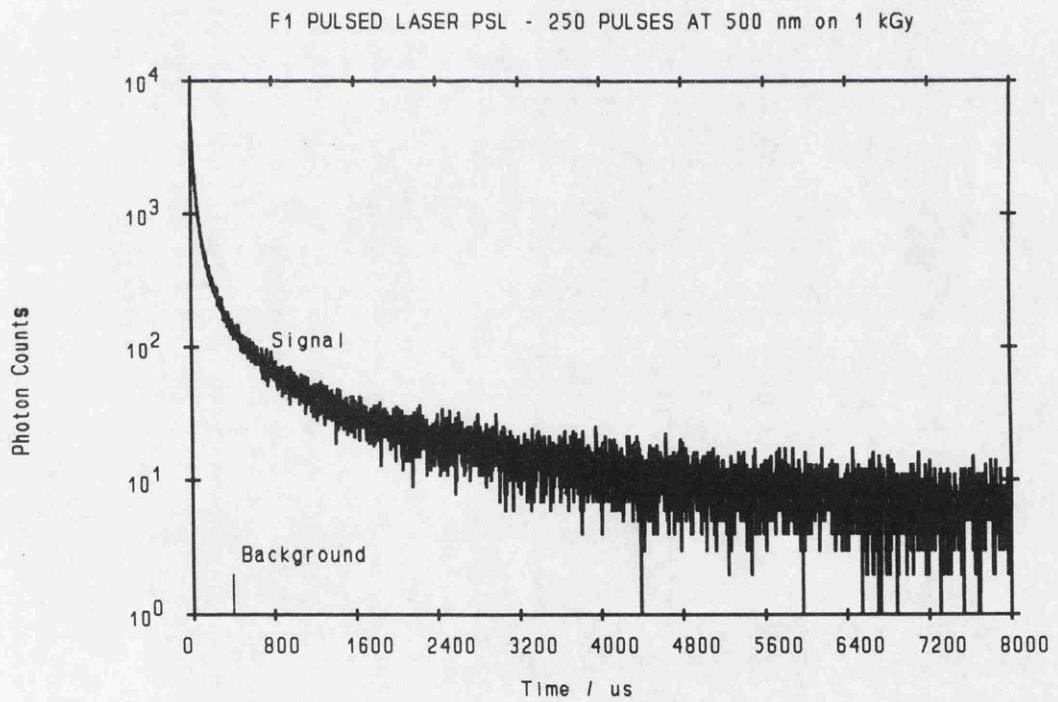


**Figure 5.12** - Pulsed laser PSL response of 1 kGy F1

recombination lifetimes. The response of the feldspar F1 after 1 kGy can be seen in Figure 5.12, demonstrating the high signal to background ratios that can be obtained. The background is the solitary pulse indicated and the luminescence signal is generated

by 250 pulses at 500 nm on the F1 feldspar which had received a dose of 1 kGy, and this yields a total signal to background ratio of 4483. If, however, only the first 20  $\mu\text{s}$  are looked at (being where the greatest signal strength is located) the signal to background ratio increases to almost 12000, implying a minimum detectable dose of 0.25 Gy with a signal to background ratio of 3.

As was the case with the LED's, it is instructive to consider the recombination

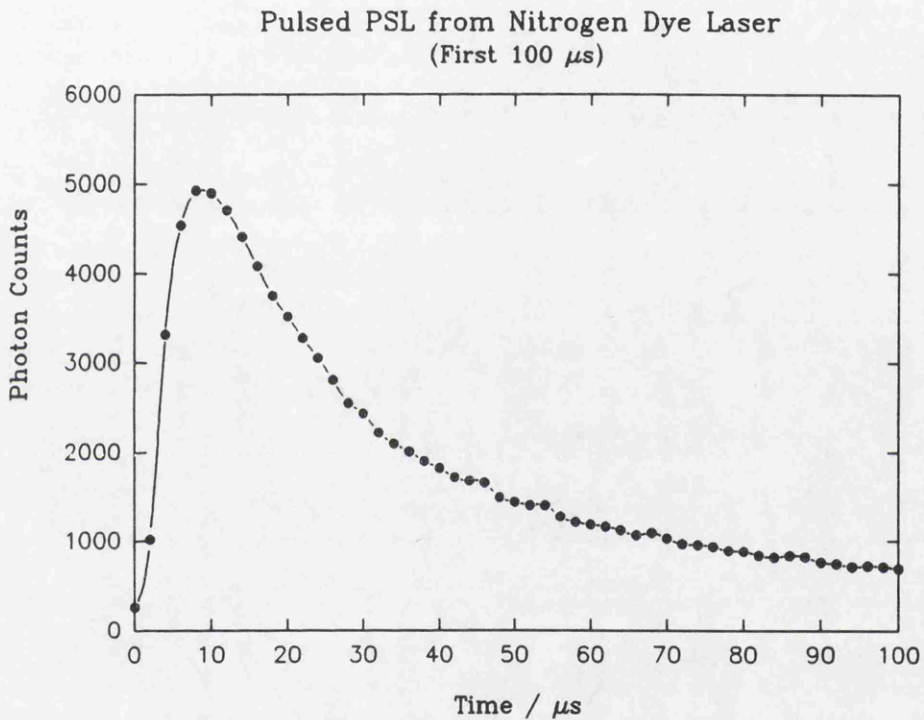


**Figure 5.13** - Luminescence time domain after laser pulse

dynamics of this pulsed PSL. The first 100  $\mu\text{s}$  of the response shown in Figure 5.12 can be seen enlarged in Figure 5.13. With the laser, there is less confusion than with the LED's as the laser pulse is only 600 ps in width and occurs 1  $\mu\text{s}$  after the trigger pulse which started the data acquisition. Hence the first channel (2  $\mu\text{s}$ ) of the trace has 1  $\mu\text{s}$  with no laser and 1  $\mu\text{s}$  with the laser on. After the first channel, the response of the luminescence signal will be due entirely to the dynamics of the charge carrier recombinations and dependent upon the same time factors as described for the LED stimulation. From this plot it can be seen that maximum intensity is reached at about

10  $\mu$ s, after which there is a long decaying signal. Hence it takes about 10  $\mu$ s (for this sample) on average for the charge carriers to reach a recombination centre after the initial laser pulses. Those traps and centres which are closer together will contribute to the signal before 10  $\mu$ s, and the post 10  $\mu$ s signal will be due to those traps and centres at larger distances, and also due to the short term trapping of charge carriers in shallow traps with lifetimes dependent upon the sample temperature. This time of 10  $\mu$ s is in good agreement with that generated by the infra-red LED stimulation, hence there would appear to be no evidence for the correlation of a particular trap with a particular centre, although it may be that differences in recombination times may be too small to be recorded on a minimum timescale of 2  $\mu$ s.

#### 5.4.3 - Time Domain Analysis

It has been shown above that it is possible to observe the charge carrier recombination lifetimes under stimulation by both the infra-red LED's and the pulsed nitrogen dye laser using a multi-channel scaler with a minimum dwell time of 2  $\mu$ s. It is possible to get multi-channel scalers with shorter minimum dwell times, even as low as 5 ns and during a demonstration of such a device (Stanford Research Systems SR430) the response to LED stimulation has been recorded (this was before acquiring the laser). The resulting PSL from 10000 pulses, 20  $\mu$ s in width from the 1 kGy F1 feldspar recorded with a 40 ns dwell time can be seen (after 5 point smoothing ) in Figure 5.14. This graph again shows approximately a 10  $\mu$ s rise in the stimulated signal after the start of the pulse (it is to be noted that the shape of the curve in the first 1.5-2  $\mu$ s is due to the LED's). The time domain can be seen more clearly if a shorter dwell time is used, as was the case in Figure 5.15. For this graph, the same sample as before was exposed to 10000 pulses each 2  $\mu$ s in duration and the resulting PSL was recorded with a dwell time of 5 ns and is shown after 11 point smoothing. The initial level response up to just over 0.5  $\mu$ s and the following rise to about 1.5  $\mu$ s will be due to the rise characteristics of the LED's, however, the rise beyond this time is most likely, once again, due to the recombination lifetimes of the evicted charge carriers.

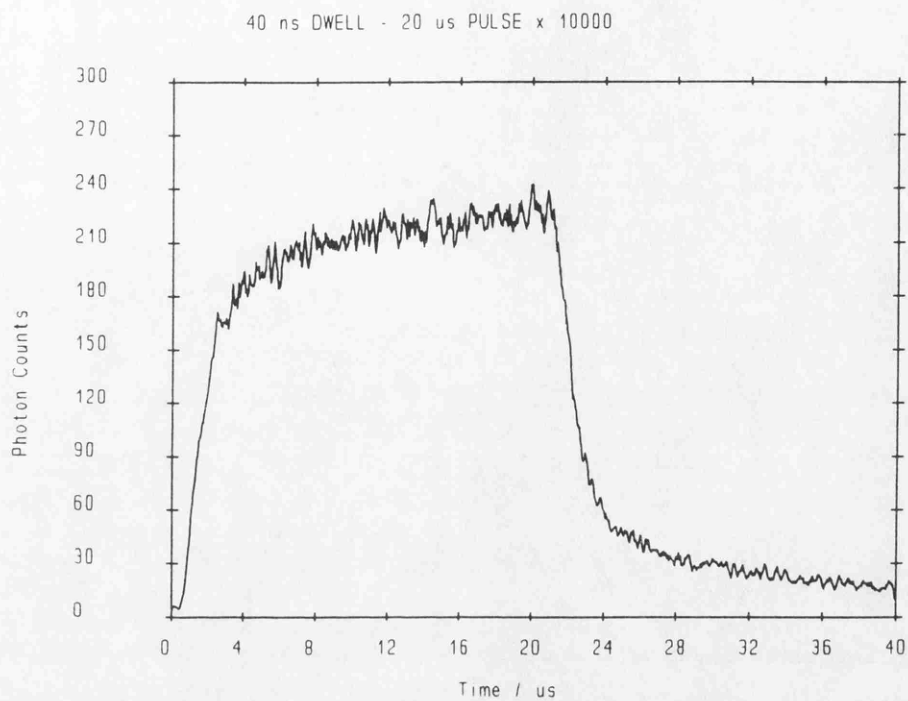


**Figure 5.14** - F1 Pulsed PSL response recorded on a fast MCS

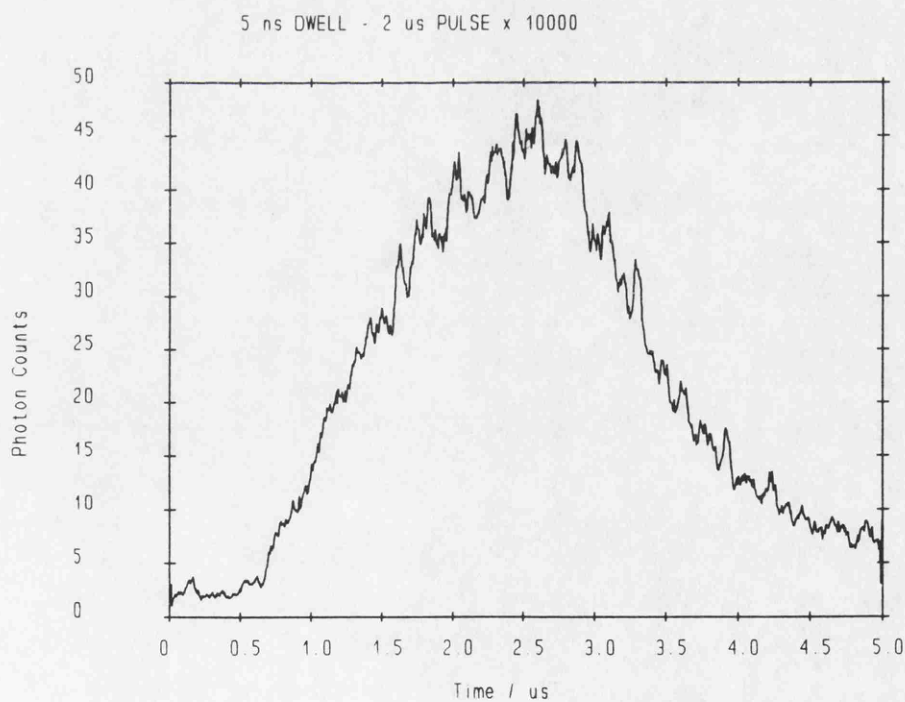


**Figure 5.15** - F1 PSL from 2  $\mu$ s pulses recorded with a dwell time of 5 ns

One problem with using the LED's to monitor the recombination lifetimes is the differentiation between the rise of the PSL signal due to the LED's own rise characteristics and the rise time of the PSL signal due to the charge carrier dynamics. A much better method would be to couple the pulsed laser to a similar fast multi-channel scaler which should result in much easier interpretation of the resulting pulsed PSL signals due to the cleanness of the short (600 ps) laser pulses.

The ability to be able to observe and record the time domain of the pulsed PSL response raises the point concerning the potential and importance of such time domain analysis. As already mentioned, the charge carrier recombination dynamics depend upon many factors including; the retrapping probability, the existence of available shallow traps, the charge carrier mobility in the relevant band and the trap / centre proximity.

- 1 - Retrapping. The greater the retrapping probability, the greater the average time required for successful eviction from the trap.
- 2 - Shallow Traps. The existence of empty shallow traps means that the charge carriers can temporarily be trapped whilst trying to find a free recombination centre. The lifetime of the charge carriers in these traps will depend upon the sample temperature and thus cooling the sample should increase the lifetime and hence increase the average recombination time. Conversely raising the temperature should decrease the average recombination time.
- 3 - Charge Carrier Mobility. In all of the discussions above, a point has been made of referring to *charge carriers* giving rise to the PSL signal rather than electrons as both electrons and holes can give rise to PSL. However, the mobility of an electron in the conduction band is far greater than that for a hole in the valence band, thus the recombination dynamics will depend upon the charge carrier type giving rise to the luminescence.
- 4 - Trap / Centre Proximity. The closer the traps are to the centres, the shorter the recombination time as the charge carriers have less distance to migrate in the band

before finding a free recombination centre. If the traps and centres are randomly distributed throughout the lattice, then as the dose increases (and hence the number of filled trapping states and empty recombination centres increases) so the average separation of the traps and centres should be reduced, and thus the recombination lifetime should also be reduced. However, if a particular trap and centre are correlated and form in close proximity to each other then as the dose increases, the trap / centre separation should remain invariant and hence the recombination lifetime should not be dependent upon the dose.

All of the above discussion has assumed that the recombination takes place via the conduction / valence bands. However it is possible for luminescence recombination to take place via quantum mechanical tunnelling which would have important implications for the recombination dynamics. Such a mechanism requires proximity (i.e. a separation of only a few atomic radii) and hence observations of the time domain as described in 4 above should be able to confirm such proximity. This is because for a random distribution of traps and centres to produce such proximity by chance, high doses would be required as a 5 Gy dose would still leave an average separation of more than  $10^4$  atoms (Sanderson, 1988). Tunnelling has been proposed as the mechanism of anomalous fading (Hoogenstraaten, 1958; Visocekas *et al*, 1976, 1983; Visocekas, 1979), however a counter argument has been made (Sanderson, 1988) that a single TL glow peak can be composed of many traps with differing activation energies and frequency factors resulting in the same peak temperatures, but possessing different lifetimes. Thus the fading observed could be due to the long term fading of some of these components which can be dealt with by preheating. This approach does not require a proximity model such as tunnelling and thus it is possible that observations of the recombination dynamics may be able to help solve the problem of anomalous or long term fading.

There is clearly considerable further potential for time domain analysis in PSL studies. Such analysis may be able to provide better signal selectivity with increased discrimination from spurious effects; it holds the possibility of distinguishing between electron, hole, ion and molecular dynamics; it should yield higher signal to background ratios and it should help with the study of proximity models, which is of high

importance in the study of fading mechanisms. For detailed study of the time domain spectra a fast pulsed (preferably tunable) stimulating source will be required (i.e. the pulsed nitrogen dye laser). This needs to be combined with a fast multi-channel scaler, and for detection of emission bands close to stimulation bands, some mechanism to protect the photomultiplier from the stimulating pulses would also be required.

### 5.5 - Modifications to Proposed Models

The most recently proposed model and energy structure for the PSL mechanism is that set out in Hütt & Jaek in 1989, and is reproduced in Figure 5.16 (the energies given are the photo eviction energies with the thermal eviction energies being given in brackets).

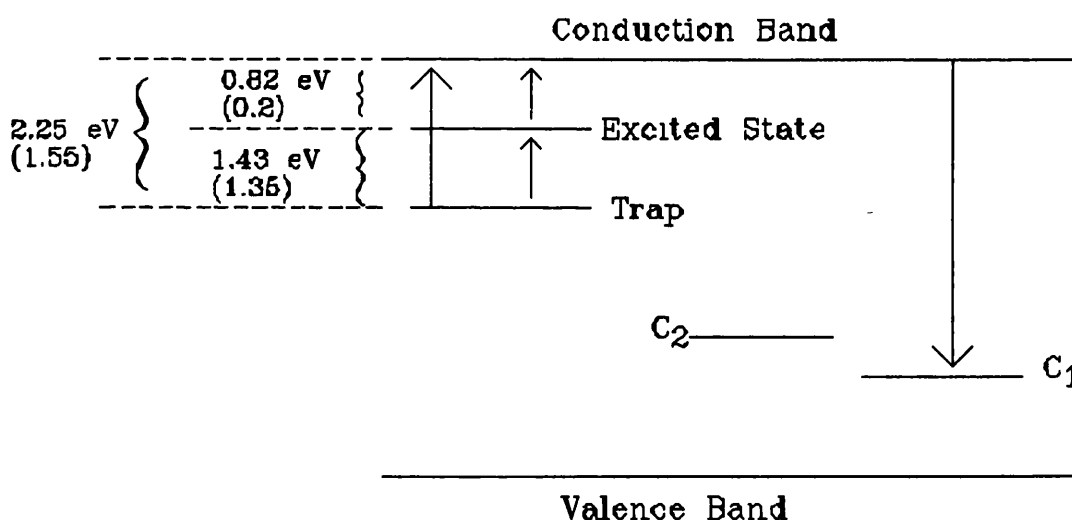


**Figure 5.16 - The Hütt & Jaek PSL model**

Since this model was proposed, work has been performed by various groups, all of which can add more detail to the model, including emission spectroscopy (Bailiff & Poolton, 1991; Huntley *et al*, 1991 and Jungner & Huntley, 1991) and temperature dependencies (Bailiff & Poolton, 1991; Duller & Wintle, 1991). These results in combination with those presented in this thesis can be used to suggest modifications to the model suggested by Hütt & Jaek.

A limitation of the Hütt & Jaek model is the lack of detailed examination of the recombination centres. The published emission spectroscopy and that already discussed in this thesis shows there to be many emission bands, and hence recombination centres. The Hütt & Jaek model requires the presence of two recombination centres, however only one of these is required for the PSL emission: the other is present in order to account for the different sensitivities of the PSL and TL signals to bleaching. The reason given for this was that the recombination centre  $C_1$  has a greater capture coefficient than  $C_2$  and that  $C_2$  is responsible for the TL signal whereas  $C_1$  is responsible for the PSL emission. This theory was proposed as it was suggested that the PSL and TL signals resulted from the same trap, however this immediately raises the following problem; if the TL and PSL signals result from the same trap, then upon eviction to the conduction band each charge carrier should have the same probability of capture by a certain centre as the rest of the evicted charge carriers, independently of the method of eviction. Hence there is no reason to suppose that one centre should be associated with PSL and a different one with TL.

The published emission spectroscopy studies (Bailiff & Poolton, 1991; Huntley *et al*, 1991 and Jungner & Huntley, 1991) together with the emission spectroscopy shown above have shown two emission peaks for pure potassium feldspars, with a third emission peak becoming present for sodium feldspars. The F1 feldspar generates all three emission peaks, and there is no evidence that any one of these three emission bands is associated with any particular stimulation region. Hence a system of three recombination centres can now be introduced to the model.

Interpretation of the trap structure, however, is complicated by the need to compare thermal and photo eviction energies due to the thermal assistance associated with the various stimulation regions. The thermal assistance in the infra-red region is well documented and in the Hütt & Jaek model it has been given an thermal energy of 0.2 eV and a photo to thermal ratio of 4.1. Taking the transition from the ground state to the excited state, this ratio becomes 1.1 and for the direct transition the ratio is 1.5. The value of 4.1 for the photo to thermal ratio is in good agreement with the range of values for the ratio of the static to high frequency dielectric constant as set out in

section 2.6 and thus would tend to support the case that the photo to thermal eviction energy ratio is given by the ratio of the static to high frequency dielectric constant. However, the ratios yielded by the direct transition and the transition to the excited state seem too low. Consider the transition from the ground state to the excited state; the Hütt & Jaek model gives two photo eviction energies for this path, 1.43 and 1.33 eV, and one thermal activation energy, 1.35 eV, yielding ratios of 1.06 and 0.99 respectively. Now whilst the absolute value that this ratio should have may be unknown, it is known with certainty that it must be greater than 1 and one of these ratios fails this criterion and the other only just passes. The normalised spectra shown in this thesis show only one infra-red peak, centred at about 890 nm (1.40 eV) and this would then mean a ratio of 1.04, which again seems too small. Hence it would seem that the thermal activation energies calculated for this transition are too high.

It has been shown (section 4.1.3) that the thermal assistance, however, is not confined to the infra-red stimulation region, but that it extends across the entire excitation spectrum. The green component (measured at 500 nm) also yielded a component which gave a good signal even at  $-140^{\circ}\text{C}$ , which resulted in the conclusion that in this stimulation region the PSL signal resulted from at least two traps, one direct transition (the non thermally assisted signal) and one thermally assisted transition from a deeper trap. It has also been shown (section 4.1.4) that the regions from 550 nm upwards and one component of the 500 nm region have similar thermal stabilities and that the 500 nm signal can be bleached by 880 nm photons (section 4.1.2). All of this evidence seems to suggest that the infra-red and red stimulation regions are both linked to one component of the green excitation region, and that there is another component in the green stimulation region (thermally assisted) that is deeper than the trap giving rise to the thermally assisted signals in the red and infra-red regions.

It is impossible to say with any certainty whether the green stimulation band peaks at around 500 nm without further exploration of the excitation spectrum into the ultra violet region, as the short wavelength edge shown in all of the excitation spectra appears to be due solely to the presence of the order sorting filters. Indeed the excitation spectrum shows every sign of continuing into the ultra violet region with increasing

sensitivity. However, in order to try to arrive at some interpretation it will be assumed that the non thermally assisted transition in the green region has a peak response with 490 nm stimulation, which would appear to be the case from the observed excitation spectra. This wavelength, though, can only be considered the upper wavelength limit for this trap and it is to be expected that with further exploration of the excitation spectrum in to the short wavelength regions, this wavelength may well need to be reduced.

It is assumed that the direct transition occurs at about 490 nm (2.5 eV), and that it possesses two excited states at about 625 nm (2.0 eV) at a depth of 0.17 eV (thermal) and 880-890 nm (1.4 eV) at a depth of 0.2 eV (thermal). This then yields photo eviction energy to thermal eviction energy ratios of 2.9 for the 625 nm transition and 5.5 for the infra-red transition. If the ratio is due solely to the change in the dielectric constant with frequency, then it is to be expected that the ratio would rise as wavelength falls, however the decrease in wavelength is too small for the ratio to change significantly unless it falls on the region where one of the polarisation mechanisms lags behind and there is dielectric loss. In these regions the dielectric constant can vary dramatically (section 2.6 and Figure 2.12) and such a region tends to occur close to the ultra violet / visible region. Thus the reduction in ratio may be due to measurement errors, large fluctuations in the dielectric constant, some other mechanism also making a contribution or the two excited states not both belonging to the same trap. There is no evidence for the two excited states belonging to different ground states and hence traps, and so it will be assumed that this is not the reason for the disparity in the ratios.

This then leaves the second component of the excitation spectrum in the green stimulation region. The thermal assistance calculated for this component was 0.15 eV. A non thermally assisted transition for the ground state of this trap has not been observed in the wavelength region examined and thus it is not possible to calculate the photo to thermal eviction ratio for this transition. Also it is again not possible to be sure whether the wavelength accredited to the thermal assistance (500 nm) is in fact the peak wavelength, or whether it is on the high wavelength side of a broader peak due to the difficulty of separating the stimulation and detection regions below this wavelength. Assuming that the peak of the thermally assisted transition is at 500 nm (2.5 eV), and

that the ratio for the photo to thermal eviction energies is 2.9 (being that assigned to the thermal assistance in the red region and thus closest to 500 nm stimulation), this yields a ground state energy of 2.9 eV which is in the region of 425 nm. If the ratio were closer to that stipulated for the infra red region, then the ground state energy would be 3.3 eV which is around 375 nm. Consequently it may be expected that the direct transition from the trap giving rise to the green thermally assisted PSL signal is to be observed in the region of 375 to 425 nm.

The above discussion accounts for the observed emission spectra and excitation spectra. The only component that is not so far accounted for is the trap(s) responsible for the metastable thermal sensitisation described in section 5.3. This phenomenon requires the presence of a third trap which is much deeper than the other two, with an excited state that is at a similar depth to the other two traps. Alternatively, instead of the charge carriers being promoted into an excited state, the charge carriers could be transferred from the deep trap to a different trap, however if this is the case the charge transfer mechanism can not involve a transport band as no luminescence was observed during the heating when the sample was not exposed to 500 nm stimulation. If the charge carrier transfer were via a transport band, then it would be expected that some luminescence would be observed. Thus if the charge carriers are not promoted into an excited state, then the phenomenon would require transfer of the charge carriers to a separate trap via quantum mechanical tunnelling, requiring proximity of the two traps. Hence at this stage, the working premise is that the charge carriers are promoted into an excited state with a long enough lifetime so that the excited state temporarily accrues a charge carrier population.

The proposed modifications to the Hütt & Jaek model can be seen summarised in Figure 5.17.

All of the above discussion has so far been concerned with electron eviction and recombination, however, Bailiff & Poolton (1991) raise the possibility that the infra red PSL mechanism is governed by hole eviction and recombination. This possibility was proposed based upon the work of Hofmeister & Rossman (1985) who identified two

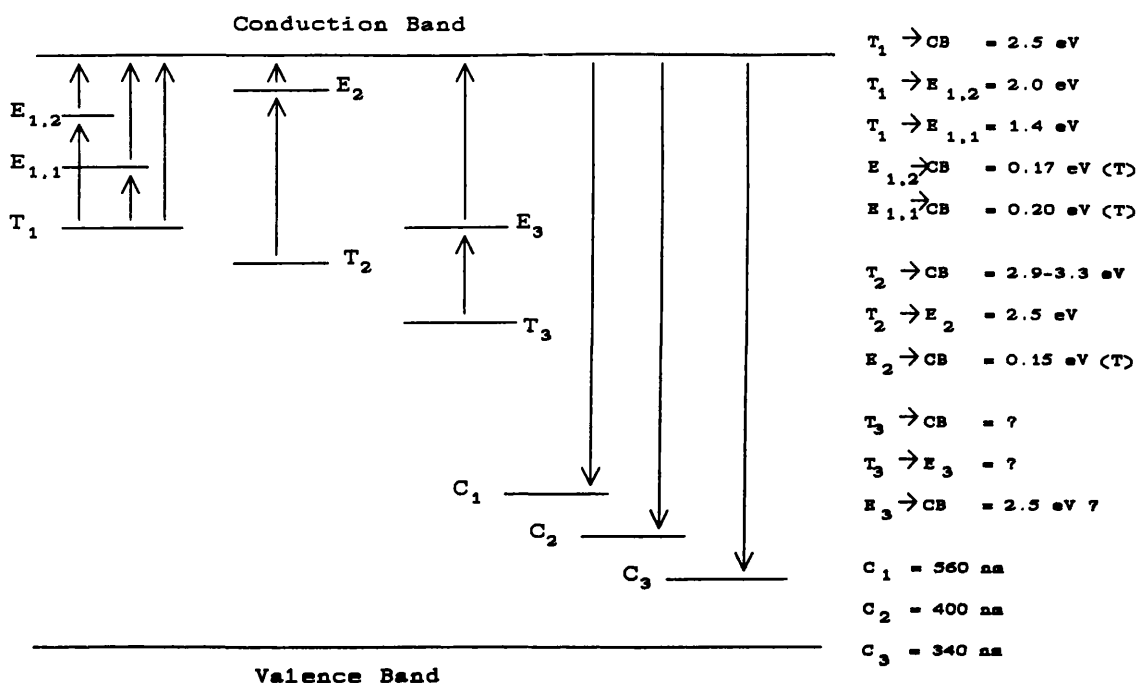


**Figure 5.17** - A PSL model for the feldspar F1

optical absorption bands in potassium and sodium rich feldspars at 860-880 nm and 620 nm which were attributed to two different hole centres. As stated by Bailiff & Poolton (1991), it is very tempting to tie the infra red PSL to these absorption bands, especially as the excitation spectroscopy shown in this thesis has also shown a stimulation band in the region of 600-625 nm and a single infra-red stimulation region at around 880 nm which match the absorption bands very well. The implication of this would be to split  $T_1$  into two hole traps with similar ground state energies that would give rise to the stimulated luminescence via hole transport in the valence band. However, before electron eviction and recombination can be rejected in favour of holes, more detailed investigation would be required, including both absorption spectroscopy and PSL excitation spectroscopy being performed on the same sample in order to match up excitation and absorption bands for the sample being studied. If this can be done, it is then required to show that these absorption bands do result from hole excitation.

In Duller & Wintle (1991), the validity of the Hütt & Jaek model is cast into doubt for the following reasons; firstly that a model comprising a single trap can not give rise to

a multi-peak glow curve; secondly that only a small proportion of the TL signal is removed by infra-red stimulation. These two points seem obvious, and indeed the model shown in Figure 5.17 takes this into account being a multi trap model. The multi trap nature of the model is also supported by the pulsed annealing study shown in section 5.2 which showed the green stimulation band to be composed of more than one trap. Another objection raised in Duller & Wintle (1991) is that for infra-red stimulation to be able to evict charge carriers, the 'deep' trap (where the charge carrier is photo evicted from) must be in close proximity to the 'intermediate' trap (where the charge carrier is photo evicted to) from whence the charge carrier is thermally evicted to the transport band. This seems to be misunderstanding the nature of the mechanism proposed in the Hütt & Jaek model and supported above in that the infra-red stimulation promotes the charge carrier from the ground state of a trap into an excited state of the same trap. Thus the 'deep' and 'intermediate' trap are one and the same trap.

This also helps to explain why Duller & Wintle (1991) failed to observe charge carriers evicted from deeper traps at high temperatures. It was stated that as the temperature is increased, so the total eviction energy increases and thus providing that there is an 'intermediate' trap at the right depth, deeper traps should be available for interrogation. However, the thermal assistance model requires that an excited state exists for that trap at a depth just below the conduction band. The charge carriers are promoted into this excited state by photo absorption, a resonance process where the charge carrier can only be promoted in to the excited state if the stimulating photon has the same energy as the difference between the ground and excited state. Consequently if an excited state does not exist, or if the energy required to promote the charge carriers into the excited state is different from that provided by the stimulating photons then the charge carriers will not be promoted into an excited state from which they could be thermally evicted no matter how great the temperature. It has been shown in this thesis that other traps do indeed have excited states that can be populated by photo stimulation and thus emptied by thermal stimulation, however the photo stimulation wavelength and thus energy is different for each trap. Indeed it would be unusual for different traps which would have different energy structures to have excited states at the same energy above the ground state which could be populated by the same wavelength photons.

During the above discussion of the model, several areas of further study become apparent. Firstly it seems apparent that the excitation spectrum extends to the ultra violet stimulation region (i.e. less than 450 nm) and thus any interpretation of the observed excitation spectrum and its associated dependencies upon stimulating temperature and thermal stability for modelling purposes will necessarily be incomplete without excitation spectroscopic studies in the ultra violet region. A practical difficulty occurs when attempting to use continuous stimulation as the stimulating and emitted photons would fall in similar wavelength regions. Two techniques that may overcome this are; instead of observing the luminescence on the short wavelength side, the PSL could be observed on the long wavelength side as it has been shown that an emission peak occurs at 560 nm, however this would prevent excitation spectroscopy across the entire spectrum which is very important if comparisons are to be made as to the behaviour of the different excitation regions. Also this technique would necessitate limiting the observed luminescence from only one of the centres (which may not even exist in some feldspars with no sodium content) thus resulting in an incomplete observation.

A second (and arguably better) technique would be to use asynchronous detection from pulsed stimulation. This technique would measure the luminescence output after a short stimulating pulse from a laser. This has the major advantage of not having to block the stimulating light from the detector and thus limit the detection window. The detector could have an open window and be turned off (effectively) during the stimulating pulse and then activated after the pulse has died away to record the resulting luminescence. This switching would have to be very fast as it has been shown that the after pulse luminescence decays after a few tens of microseconds, thus the detector would have to be switched on a microsecond timescale. This stimulating technique could also lead to simultaneous time domain analysis which (as argued above in section 5.4.3) has the potential to yield valuable data.

A second area of great importance in forming the PSL model is the matter of the conversion from thermal to photo activation energies. The ratio of thermal to photo activation energies does not appear to be well understood. One theoretical approach (set

out in section 2.6) is dependent upon the static and high frequency dielectric constants, however these values are not well known for the samples being studied and would thus need to be measured. Measurement of the static dielectric constant is straightforward, as is the optical frequency dielectric constant; at these frequencies, the dielectric constant is simply equal to the square of the refractive index, thus the refractive index could be measured across the excitation spectrum to result in a set of values of the ratio. Until this ratio can be evaluated or measured experimentally, the combining of the thermal depth of excited states with the photo energy required to promote the charge carriers into the excited states can not be made with a high degree of confidence.

The model presented in Figure 5.17 is not expected to be complete. It is an interpretation of the observed PSL phenomena within the limits of the observations and it is to be expected that this model will have to be modified once further exploration of the PSL mechanism is undertaken. All of the results so far generated in this thesis and in the other laboratories performing similar research lead to the conclusion that the PSL mechanism in feldspars is complex, requiring many traps and centres with a variety of excited states, hence as further experimentation yields more data, so the model required to explain it may well become more complex.

## 5.6 - Summary

The results presented in this and the previous chapter present an initial exploration of the mechanisms of the PSL phenomena. It has incorporated; excitation and emission spectroscopy, which indicates a multi-trap / multi-centre model: studies of thermal assistance and the identification of such assistance across the entire excitation spectrum; thermal stability analysis which has raised the possibility of a distribution of traps; the dose response from the gray to kilogray region and the response to pulsed stimulation with the raising of the potential of time domain analysis. Finally, these results have been combined and used to suggest extensions to the Hütt & Jaek PSL model.

It was stated that the aim of this project was to place the PSL phenomenon on a firm physical basis with a view towards its ultimate utilisation as a reliable archaeological

dating tool. The work presented in this and the previous chapter represents the first steps in placing the PSL phenomenon on a firm physical basis. These results can now be used in the development of a dating methodology. A proposed methodology is set out and tested in the next chapter.

## **6 - Dose Evaluation**

The exploration of the physical characteristics of the PSL phenomena presented above was performed with a view towards the development of a PSL dating technique. It has been demonstrated that the IAEA feldspar F1 had sufficient sensitivity in conjunction with all three stimulation sources to record doses in the gray region, a prerequisite for dating. It has also been shown that the dose response in this region is linear. Unfortunately, the question of thermal stability remains open. It is apparent from the pulsed annealing studies that there is more than one component to the stimulation regions with differing thermal stabilities. Hence preheating is required to remove (or reduce) the contribution to the PSL signal from the less stable components.

Knowledge of the above results enabled the first steps in the formation of a dating methodology to take place. It was decided that the first step in the development of such a methodology is an attempt to recover a known laboratory dose from the sample. In this manner, the history of the samples being measured is known. This ensures complete removal of any residual PSL signal prior to the initial irradiation, a factor that is not necessarily the case for sediment samples. Also the thermal and optical exposure of the sample after the initial irradiation is known precisely, again a factor which is not the case for real samples. Finally, and perhaps most critically, the expected result is known exactly and thus it is straightforward to assess the experimental results for accuracy and precision.

### **6.1 - Differences Between Natural and Laboratory Irradiated Samples**

It has been stated above that the application of the single disc, additive dose methodology to the measurement of a known laboratory dose is an important step. However, this is only a first step in the development of a dating technique and can not replace similar work performed on natural samples. Ultimately, exploration of the

methodology as applied to natural samples is important as there are obvious differences between laboratory irradiated and natural samples. These differences include the dose rate, fading (by both thermal and optical mechanisms), zeroing efficiency, thermal and optical sensitisation and the heterogeneity of the microdosimetry of the mineral grains in the sample being dated. The implications of these differences between natural and laboratory irradiated samples may also depend upon the type of sample being measured, i.e. whether it is heated (e.g. ceramics) or unheated (e.g. sediments).

The dose rate for natural samples will be much lower than under laboratory irradiation. It is not impossible that the relative proportions of charge carriers trapped in particular traps upon measurement will differ for natural and laboratory irradiated samples. This would be as a result of different competition effects between the traps as the dose rate varies, thus leading to dose rate dependent trap filling. A problem linked to the low dose rate and long storage time of the samples is fading. Due to the long irradiation time of the natural samples, there is likely to have been greater fading than in recently laboratory irradiated samples. Thus again the relative proportions of the charge carriers in particular traps upon measurement may differ for natural and laboratory irradiated samples. It is hoped that such differences in fading can be taken into account by a preheating stage (as with TL dating), and it is clear that whilst the effect of preheating on the PSL signal can be observed in laboratory irradiated samples, evaluation of the effectiveness of preheating in a dating methodology must ultimately be performed on natural samples.

A major problem encountered in the TL dating of sediments that instigated the PSL research on sediment samples was partial bleaching (Huntley *et al*, 1985). It was thought that a dating technique which mimicked the zeroing mechanism held the potential to overcome this problem. It would be wrong, however, to assume that just because the same readout mechanism is used as the zeroing mechanism (i.e. light) that the samples would be totally zeroed. The zeroing of the samples will be highly dependent on the optical exposure of the mineral grains during deposition and thus total zeroing is not assured in each and every case. Thus for the PSL dating of sediments it would seem likely that some method of establishing the degree of zeroing would be useful. In

heated samples (e.g. ceramics) however, complete zeroing of the PSL signal is much more likely. This is because the temperatures to which the samples are raised in manufacture are high enough to ensure complete emptying of even very deep traps in a fraction of a second, thus assuring complete zeroing. There may, however, be some heated samples (e.g. hearthstones and other burnt stone, etc.) in which the thermal zeroing is incomplete. Whatever the measurement technique (PSL or TL), partial zeroing of the signal is a possibility that cannot be ignored. The probability of partial zeroing is likely to be greater in the case of sediment samples, although it can not be ruled out for some heated samples.

Another consideration in the dating of natural samples is that of sensitisation. With heated samples, during the manufacture process (i.e. firing of ceramic materials) the sample is raised to a high temperature. This will tend to precipitate any rearrangement of trapped charge carriers and diffusion of defects to a more stable. Thus upon subsequent heating (e.g. during the preheating stage) the probability of sensitisation due to such charge carrier transport and defect diffusion is greatly reduced. Thus it is hoped that sensitisation effects in heated samples would be low. However, this is not the case for non heated samples. In these samples there is no initial heating to precipitate defect and charge carrier reconfiguration. The photo excitation during the zeroing period, whilst possibly causing some charge carrier transport, is likely to affect the sample less than heating, due to the difference in energy of the two mechanisms. Consequently heating (and possibly photo excitation) during the measurement process may result in charge carrier transport and defect diffusion to a more stable configuration. This may then change the sensitivity of the samples, to a much greater extent than for the heated samples. Hence sensitisation is a factor which could cause problems, especially with unheated samples and thus checks for sensitisation are required in a dating methodology.

Finally, variations in the microdosimetry of the sample mineral grains from natural samples (including the various effects of the contributions from  $\alpha$ ,  $\beta$  and  $\gamma$  radiation from both internal and external components), will lead to a heterogeneous dose distribution. Consequently, it is expected that the PSL signals from natural samples will

exhibit greater scatter than the signals from laboratory irradiated samples, as is the case for TL measurement.

Thus although the application of the single disc, additive dose methodology to a well characterised sample with a known and controlled laboratory irradiation is viewed as a necessary step in the development of an archaeological dating tool, it must be considered as only a first step in such development to be followed by the application of the technique to natural samples. The work presented below is such a first step, and lays a foundation for the extension of the methodology to natural samples and ultimately utilisation as a dating tool.

## 6.2 - Single Disc Additive Dose Methodology

A standard TL technique in the dating of feldspars is the additive dose technique (Sanderson *et al.*, 1988), wherein a set of aliquots from the same sample is given successively larger doses. The growth curve recorded by TL from these aliquots is extrapolated to zero TL and the archaeological dose is that obtained from this intercept. A second set of doses is then given and a second growth curve is measured to check for supralinearity and sensitivity changes, and corrections are made as necessary. For fuller details of this technique see Aitken (1985). An obvious step when extending this technique to PSL is to use an analogous methodology, however PSL has an important difference. As TL measurements remove the entire signal and also because of the problems associated with potential sensitivity changes with heating, the incremental doses for the growth curve must be imparted to separate aliquots, which must then somehow be normalised to take into account variations in aliquot sensitivity, a process which adds in a whole new area of uncertainty. PSL signals, however, can be recorded whilst having an almost negligible effect upon the trapped charge population.

Consequently, a growth curve can be recorded upon a single aliquot which receives successive equal dose increments and the need for normalisation is removed. Also this has the advantage that the same result can be obtained from one aliquot which would

have required 8 (for example) and thus for the same number of aliquots as in the TL methodology, the result could be obtained 8 times and thus hopefully both precision and accuracy can be improved upon. Also for the first time the run to run scatter rather than just regression errors on one result can be evaluated which could give a more realistic assessment of the precision and reliability of the measurement, thus it was decided to pursue the path to a single aliquot (or disc) methodology.

### 6.2.1 - Without Preheat

The first step was to try to evaluate a known laboratory dose with no preheating of the samples. Although preheating will almost certainly be required for dating samples (see section 5.2) it was decided to leave this complicating step out of the initial experiment and introduce it upon successful completion of this first part. All three of the stimulation systems (the xenon lamp, the pulsed infra red LED's and the pulsed dye laser) were used. The feldspar F1 was used for these experiments having previously been annealed at 500°C for 5 minutes to zero the luminescence response. The samples were of mixed grain size less than 160  $\mu\text{m}$  and were dispensed onto 1 cm stainless steel discs using a silicon grease spray. 30 discs were dispensed (10 for each stimulating source) and each was given a dose of 5 Gy in the  $^{90}\text{Sr}$   $\beta$  source at a rate of 1.8 Gy per minute. In the case of the xenon lamp, the PSL was recorded at a wavelength of  $480 \pm 20$  nm for a time of 2 seconds, for the LED's the summed PSL from 2 million 1  $\mu\text{s}$  pulses measured over the first 10  $\mu\text{s}$  after each pulse was used and in the case of the laser, the PSL was recorded from the summed contribution of the first 10  $\mu\text{s}$  from 40 pulses at  $480 \pm 1$  nm.

For each stimulating source the procedure was then as follows; the PSL from 5 Gy dose was recorded and then each disc was given an extra 1 Gy dose in the  $\beta$  source. The new PSL response (from a total dose of 6 Gy) was recorded and then each disc received another 1 Gy dose. This was repeated until each disc had received a total added cumulative dose of 10 Gy, making a total received dose of 15 Gy. The samples were then all annealed at 500°C for 5 minutes to re-zero the luminescence signal and the process was repeated only without the initial 5 Gy dose, thus the total received dose for

this second growth curve was 10 Gy. This is the equivalent of the TL second glow measurement and is to check for nonlinearity of the growth curve in the extrapolation region of the first growth curve. As with the standard TL additive dose methodology, the two growth curves for each disc were plotted and the zero luminescence intercepts were calculated using linear least squares regression analysis. The dose was thus the sum of the two intercepts and the results for the LED's and the xenon lamp are shown in Table 6.1 and Table 6.2 below.

**Table 6.1** - LED dose evaluation, no preheat.

Sample	Intercept (First Growth)	Intercept (Second Growth)	Dose / Gy
F171	- 9.62 ± 0.34	- 1.54 ± 0.068	8.08 ± 0.35
F172	- 9.89 ± 0.19	- 1.61 ± 0.078	8.28 ± 0.21
F173	- 9.88 ± 0.19	- 1.57 ± 0.067	8.31 ± 0.20
F174	- 8.40 ± 0.23	- 1.24 ± 0.049	7.16 ± 0.24
F175	- 8.55 ± 0.22	- 1.38 ± 0.071	7.17 ± 0.23
F176	- 9.18 ± 0.14	- 1.48 ± 0.077	7.70 ± 0.16
F177	- 11.3 ± 0.34	- 1.39 ± 0.067	9.91 ± 0.35
F178	- 9.15 ± 0.23	- 1.23 ± 0.091	7.92 ± 0.25
F179	- 9.88 ± 0.21	- 1.31 ± 0.067	8.57 ± 0.22
F180	- 8.60 ± 0.16	- 1.90 ± 0.100	6.70 ± 0.19
Weighted Mean			7.80
Standard Error			0.24 (3.1%)

As can be seen from these results, the xenon lamp gives the correct answer with reasonably good precision ( $5.13 \pm 0.32$  Gy). However, the LED system gives higher precision but at the expense of accuracy. This is thought to be due to the cumulative bleaching effect of 2 million pulses and thus for the second experiment a smaller number of pulses was used. The laser unfortunately gave a high degree of scatter and

**Table 6.2 - Xenon Lamp Dose Evaluation, no preheat.**

Sample	Intercept (First Growth)	Intercept (Second Growth)	Dose / Gy
F161	- 4.90 ± 0.23	Dropped Disc	-----
F162	- 5.07 ± 0.17	Dropped Disc	-----
F163	- 3.99 ± 0.21	- 0.43 ± 0.02	3.56 ± 0.21
F164	- 5.26 ± 0.31	0.057 ± 0.002	5.32 ± 0.31
F165	- 6.50 ± 0.26	- 0.17 ± 0.003	6.33 ± 0.26
F166	- 6.12 ± 0.22	- 0.32 ± 0.007	5.80 ± 0.22
F167	- 4.53 ± 0.25	- 0.026 ± 0.001	4.50 ± 0.24
F168	- 5.32 ± 0.24	- 0.52 ± 0.01	4.80 ± 0.24
F169	- 4.90 ± 0.16	- 0.16 ± 0.005	4.74 ± 0.16
F170	- 6.02 ± 0.30	- 0.044 ± 0.007	5.98 ± 0.30
		Mean	5.13
		S.D. ( $\sigma_{n-1}$ )	0.91
		Standard Error	0.32 (6.2%)

the pivoting effect of such scatter on the x-axis intercepts made quantitative analysis of the results meaningless although it can be said that they were within the correct order of magnitude. This was perhaps to be expected after the initial low dose growth curves were recorded (section 4.3.2) and thus in its present state of development it was decided that it would not be worth pursuing. However, the potential of the laser system is such that once these problems can be overcome (e.g. by pulse power monitoring etc.) it would be well worth continuing with this work. Thus it was decided that only the xenon lamp and LED systems were to be used in the next stage of the experiment, namely the inclusion of a preheat.

### 6.2.2 - With Preheat.

The pulsed isothermal decay curves shown in section 5.2 demonstrate clearly the need for the preheating of samples in order to remove the thermally unstable components from the PSL signal before measurement. With additive dose measurements on a single disc, it is obviously preferable to use a short preheat, and so it was decided to use a preheat of 200°C for 5 minutes as the fastest decaying components of the PSL signal (and hence least thermally stable) have decayed within this time leaving behind those components with longer lifetimes, as can be seen in Figure 6.1. It can be seen from Figure 6.1 that the decay curve is made up of successive 30 s heatings, whereas the

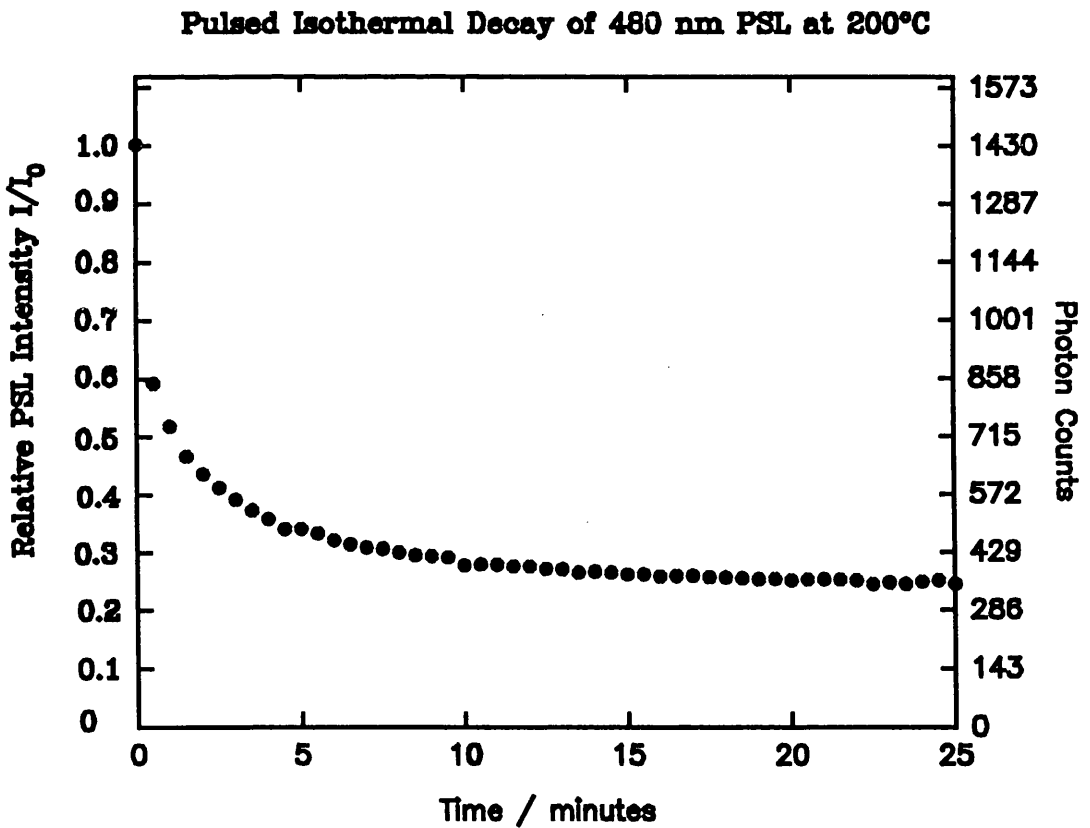


**Figure 6.1 - Pulsed Isothermal Decay of 480 nm PSL from Feldspar F1 at 200°C. (Corrected for Bleaching)**

preheating used in this experiment was one long heating of 300 s. The possibility that a single 300 s preheat may remove a different proportion of the trapped charge carriers (and thus PSL signal) to that resulting from ten consecutive 30 s heatings can not be

ruled out. However, it must be emphasised that the results depicted in Figure 6.1 are only used in a qualitative manner to suggest an appropriate preheating regime. No quantitative data analysis is performed on the basis of these results. The decay curve shown in Figure 6.1 has been corrected for bleaching and thus should be independent of the intensity of light used to readout the PSL signal. The additive dose runs were performed exactly as before, however this time the samples were all preheated after every irradiation before the PSL signal was measured. The only other difference to the previous method was that instead of using 2 million pulses from the LED's, only 250,000 were used to reduce the problem of bleaching highlighted in the first part of this experiment. The results are presented in Table 6.3 below.

**Table 6.3 - Dose Evaluation with Preheat**

Stimulation Source	Equivalent Dose / Gy
Xe lamp - $480 \pm 20$ nm	$7.43 \pm 0.75$ (10.08%)
LED's - $880 \pm 40$ nm	$8.00 \pm 0.35$ (4.38%)

As can be seen, the greatest precision is obtained from the LED system, which is perhaps to be expected considering the inherent averaged power stability in using 250,000 pulses for each measurement, whereas with the xenon lamp, fluctuations in power from run to run are highly probable. However, it can be seen immediately from these results that there is a large discrepancy between the results obtained and the actual given dose of 5 Gy. A reason for this can be seen upon examination of the growth curves. A sample of the LED growth curves is shown in Figure 6.2. This figure shows that both of the growth curves are sublinear in nature thus causing an under estimate of the gradients upon regression and hence leading to too great a dose being evaluated (this can be seen most clearly in the second growth curve).

An explanation can be found in that there is no such thing as a totally non destructive measurement, i.e. in order to record a PSL signal the trapped charge population must

F195 LED GROWTH CURVE

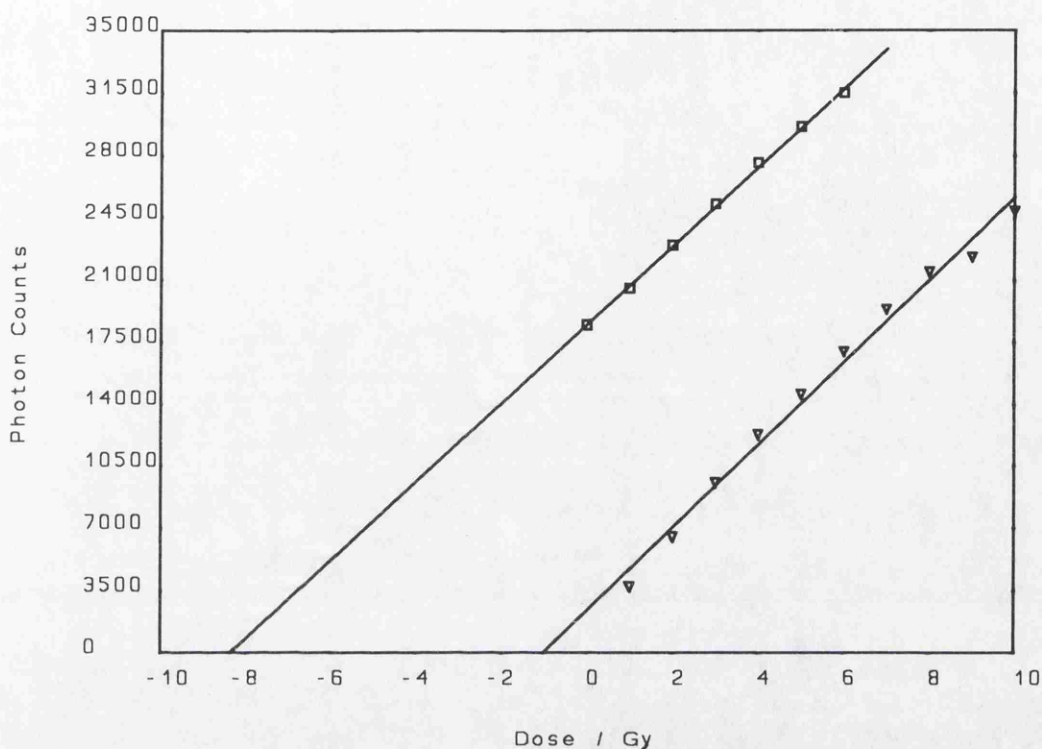


**Figure 6.2** - Uncorrected LED additive dose growth curves.

be altered and even if this is negligible when performed once, the cumulative effect of ten readings may become very important. Add to this the fact that upon preheating, as well as removing the unstable signal components, some of the stable component that is to be measured can also be removed (as stability is defined in probabilities, i.e. a stable component does not have zero probability of eviction but rather a very low eviction probability. Consequently upon successive heatings, a small but still significant portion of the stable component may be evicted) thus depleting the signal on each measurement cycle. Thus both of these factors will lead to a sub linear growth curve as part of the signal is lost each time. Hence a solution to this problem is to measure the amount of signal lost on each successive bleaching and heating cycle and to correct the growth curve for this effect.

### 6.3 - Corrections for Loss of Signal During PSL Measurement.

As stated above, during the PSL measurement process, some of the signal is necessarily lost (by bleaching and preheating) and corrections must be made for this. It could be argued that this factor could be almost negligible in some cases, however an *almost* negligible loss of signal (i.e. 0.5%) repeated 10 times becomes significant (5%) and a growth curve which appears to be linear does not mean that it is. Thus the only way to be sure of the results is to measure the amount of signal lost during the measurement process and correct for it in each and every case.

#### 6.3.1 - Theory

One way to consider a correction term is to look at the amount of the PSL signal lost resulting from the total dose, however a complication arises in the fact that we are not dealing with a system that has an initial dose which is then measured many times, but rather a system that has successive doses with each dose having been measured one less time than its precedent. For example, in a system of four successive dose / preheat / readout cycles, by the fourth readout the first dose increment has been bleached/heated three times; the second, twice; the third, once and the fourth dose increment not at all, as shown mathematically in <6.1> below.

$$I \propto \beta_1(1-b)^3 + \beta_2(1-b)^2 + \beta_3(1-b) + \beta_4 \quad <6.1>$$

where  $b$  is the fraction of the signal lost during the readout cycle.

This is assuming that  $b$  is constant throughout the entire bleaching cycle of the sample, i.e. that the bleaching curve is exponential in nature. If this is not the case, then the fraction lost per cycle will depend on how many times each dose has been measured. This leads to the generalised form shown in <6.2> below;

$$I_n \propto \beta_1(1-b_1)(1-b_2)\dots(1-b_{n-1}) + \beta_2(1-b_1)(1-b_2)\dots(1-b_{n-2}) + \dots + \beta_{n-1}(1-b_1) + \beta_n \quad <6.2>$$

Hence the intensity after  $n$  readouts can be related to the successive dose increments (assuming linear response with dose) by;

$$I_n \propto \sum_{i=1}^{n-1} \beta_i \prod_{j=1}^{n-i} (1-b_j) + \beta_n \quad \langle 6.3 \rangle$$

where  $\beta_i = \text{dose} / \text{Gy}$

$b_j = \text{fraction lost after } j \text{ measurements.}$

Two simplifications can be made to this general equation if restrictions are placed on the amount lost per measurement cycle and the dose increments as follows;

Case 1 :- No loss per readout cycle.

Condition :-  $b_j = 0 \forall j.$

Thus from <6.3> we get,

$$I_n \propto \sum_{i=1}^{n-1} \beta_i + \beta_n \quad \langle 6.4 \rangle$$

$$\rightarrow I_n \propto \sum_{i=1}^n \beta_i$$

Hence the intensity recorded is proportional to the total accumulated dose, assuming that the underlying growth response is linear initially. Consequently, the resulting growth curve in this case should be linear and thus require no correction.

Case 2 :- Equal losses per readout cycle.

Condition :-  $b_j = b \neq 0 \forall j.$

Thus from <6.3> we get,

$$I_n \propto \sum_{i=1}^{n-1} \beta_i (1-b)^{n-i} + \beta_n \quad \langle 6.5 \rangle$$

If the dose increments are equal, then <6.5> can be rewritten as follows;

$$I_n \propto \beta \sum_{i=1}^{n-1} (1-b)^{n-i} + \beta \tag{6.6}$$

$$\propto \beta \sum_{i=0}^{n-1} (1-b)^i$$

Iff  $\beta_i = \beta \forall i$ .

This is a geometric series which converges to a standard formula if  $|1-b| < 1$  yielding the result,

$$I_n \propto \beta \left( \frac{1-(1-b)^n}{b} \right) \tag{6.7}$$

for  $\beta_i = \beta$  and  $b_j = b \neq 0, b < 1 \forall i, j$

This will result in a sub-linear growth curve which upon extrapolation would over estimate the initial dose. There is no reason to suppose that a second regenerated growth curve would exhibit the same degree of sublinearity as the initial doses for the losses would be different, thus a correction to each data point would be required rather than relying upon the intercept from the regenerated growth curve to correct the original additive dose growth curve. Similarly in the most general case (see equation <6.3>) where the fraction lost per readout cycle varies with the total amount lost, each data point again will need correction. The correction factors can only be obtained by replicating the photo and thermal histories of the samples, i.e. run an additive dose experiment which only bleaches the sample and does not include increments in the dose.

All of the above theory assumes that the bleaching and annealing characteristics do not vary with dose. In other words, that the remnant trapped charge population after readout does not affect the distribution of trapped charge resulting from the dose increment, i.e. that the trapping sites have a large population of free states. If this is not the case (which will become more and more likely the nearer the traps come to saturation) then the result will be dose dependent bleaching and annealing characteristics which may be

impossible to separate accurately from the growth curve resulting in a poorer approximation to the correction factors.

Thus this leaves us with four possible correction formulae, each one being based on a different set of assumptions, some of which may not apply. The first two represent an over simplification of the mechanisms involved and ignore the theory laid out above, in that they assume that the lost signal derives entirely from the signal resulting from the *total* dose and does not consider each dose increment separately as above.

Method 1 - Constant loss per measurement cycle. Hence the intensity is simply related to the total dose after n increments multiplied by the total fraction left after n-1 measurements (the average fraction left after each measurement to the power n-1) and is shown in equation <6.8> below:

$$I_n \propto (1 - b)^{n-1} \sum_{i=1}^n \beta_i \quad <6.8>$$

Method 2 - Variation in the amount lost per measurement cycle. Thus as in method 1, the intensity is simply related to the total dose after n increments, but in this case the total fraction left is the product of each fraction left after each individual measurement, and is shown in equation <6.9> below:

$$I_n \propto \prod_{i=1}^{n-1} (1 - b_i) \sum_{i=1}^n \beta_i \quad <6.9>$$

The next two methods are more physically correct, taking into account the fact that the signal from each individual dose increment is affected a different number of times and uses the theory set out at the beginning of this section;

Method 3 - Constant loss per measurement cycle. The equation for this correction factor is set out in equations <6.5> - <6.7> above, and the general form is rewritten below:

$$I_n \propto \sum_{i=1}^{n-1} \beta_i (1-b)^{n-i} + \beta_n \quad <6.10>$$

Method 4 - Variation in loss per measurement cycle. This method is probably the most physically correct of the four, although perhaps the hardest to implement. The theory for this method is set out in equation <6.3> above and is reproduced below:

$$I_n \propto \sum_{i=1}^{n-1} \beta_i \prod_{j=1}^{n-i} (1-b_j) + \beta_n \quad <6.11>$$

### 6.3.2 - Application

Following the measurement of the PSL growth curves as explained in section 6.2.2 above, all of the samples were annealed at 500°C for 5 minutes to remove the PSL signal and then given a dose of 10 Gy (chosen to represent a dose half way along the initial growth curve). The growth curve measurement cycle of preheat followed by stimulation was repeated, only this time no extra dose increments were given. The amount of signal lost from cycle to cycle was calculated for each sample disc and then the average fraction lost from cycle to cycle over all the sample discs was calculated, and it was this fraction that was used as the fraction lost upon measurement in methods 1-4 above. The correction factors were averaged over ten discs, and can be seen in Table 6.4. (Here it must be emphasised that the quantitative data analysis was based on measurements at each preheating stage on each sample used, and is in no way based on the data depicted in Figure 6.1.)

Each growth curve was corrected on the basis of each of methods 1-4 above, and a comparison was made. In the case of those which assumed a constant loss factor (methods 1 and 3), the average amount lost from cycle to cycle was averaged over all of the measurement cycles to obtain the average constant loss value. An example of the

**Table 6.4 - Xenon Lamp and LED Growth Curve Correction Factors.**

Preheat Number	Correction Factors	
	Xenon Lamp	LED's
1	5.7 ± 0.7	4.5 ± 0.3
2	5.7 ± 0.7	4.5 ± 0.3
3	5.8 ± 0.9	4.2 ± 0.7
4	4.0 ± 1.0	3.7 ± 1.1
5	4.4 ± 0.9	2.7 ± 0.9
6	3.8 ± 1.5	1.9 ± 0.8
7	2.4 ± 1.1	1.9 ± 0.5
8	4.4 ± 0.8	3.0 ± 0.5
9	2.0 ± 0.8	0.8 ± 0.6
Mean ± SD	4.2 ± 0.5	3.0 ± 0.4

corrections being applied to one particular data set can be seen in Table 6.5 overleaf. This table shows the four correction techniques being applied to the sample F191 measured using 480 nm light from the xenon lamp system.

A test of the validity of the correction factors is whether or not they straighten out the growth curve, and an example of such a corrected set of growth curves can be seen in Figure 6.3. The correction method used in this case was method 4. As can be seen, both curves have become much more linear in nature (compared to Figure 6.2 above) with the first growth intercept much closer to 5 Gy, and the second to 0. Also it is pleasing to note the parallel nature of the two lines, implying low or zero sensitisation upon the annealing step between the two growth curves.

**Table 6.5 - F191 PSL Growth Curves at 480 nm: I<sub>1</sub> - I<sub>4</sub> Curves corrected for multiple bleaching/annealing by methods 1 - 4.**

First Growth					Second Growth						
Dose / Gy	I	I <sub>1</sub>	I <sub>2</sub>	I <sub>3</sub>	I <sub>4</sub>	Dose / Gy	I	I <sub>1</sub>	I <sub>2</sub>	I <sub>3</sub>	I <sub>4</sub>
0	1521	1521	1521	1521	1521	-----	-----	-----	-----	-----	-----
1	1434	1499	1516	1502	1521	1	238	238	238	238	238
2	1705	1862	1905	1838	1873	2	585	611	618	596	599
3	2219	2532	2623	2429	2486	3	886	968	990	923	933
4	2029	2420	2494	2339	2401	4	1181	1348	1396	1258	1279
5	2503	3119	3212	2904	2975	5	1534	1829	1886	1564	1696
6	2509	3267	3342	3022	3097	6	1584	1974	2033	1783	1826
7	2707	3684	3693	3333	3388	7	1932	2516	2574	2202	2253
8	2601	3699	3704	3349	3412	8	2244	3054	3061	2601	2656
9	2897	4305	4208	3762	3793	9	2242	3188	3193	2700	2756
10	3025	4698	4482	4021	4024	10	2506	3724	3640	3065	3199
Regression Results	-9.36 ± 0.88	-4.11 ± 0.21	-4.63 ± 0.26	-5.51 ± 0.29	-5.62 ± 0.31	Regression Results	-0.49 ± 0.02	0.45 ± 0.01	0.33 ± 0.08	0.05 ± 0.001	0.07 ± 0.002
AD / Gy	8.87 ± 0.88	4.56 ± 0.21	4.96 ± 0.27	5.56 ± 0.29	5.69 ± 0.31						

F195 LED GROWTH CURVE - CORRECTED FOR BLEACHING / ANNEALING

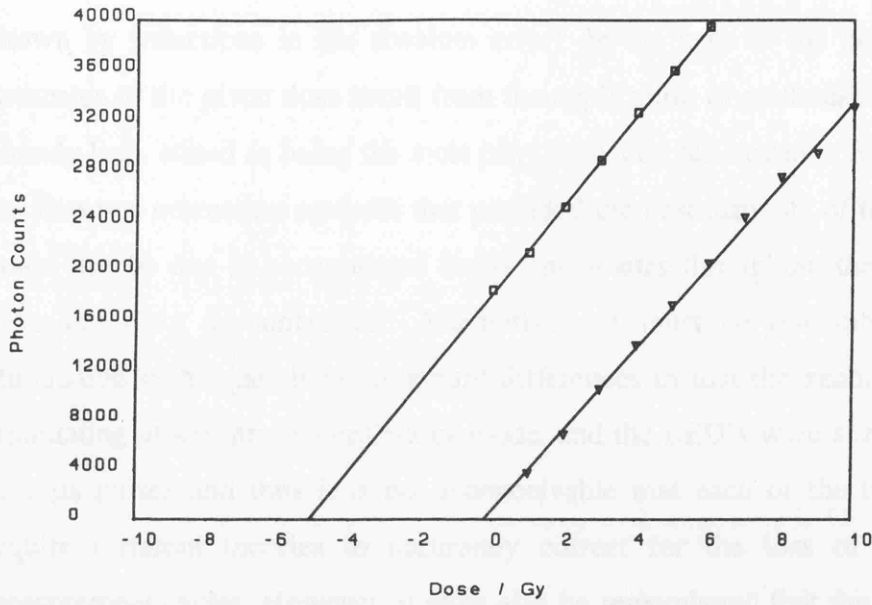


Figure 6.3 - Corrected LED additive dose growth curve.

Finally, of course, the question must be asked, do the doses evaluated in section 6.2.2 become equal to the 5 Gy given once the growth curves have been corrected?, and also which of the four methods outlined above gives the best answer? The final corrected

Table 6.6 - Final corrected dose estimates for the single disc additive dose technique.

Stimulation Source	Evaluated Dose / Gy				
	Uncorrected	Method 1	Method 2	Method 3	Method 4
Xe Lamp 480 nm	7.43 ± 0.75 (± 10.1%)	4.04 ± 0.33 (± 8.2%)	4.24 ± 0.35 (± 8.3%)	4.90 ± 0.41 (± 8.4%)	4.88 ± 0.42 (± 8.6%)
LED 890 nm	8.00 ± 0.35 (4.4 %)	4.82 ± 0.21 (± 4.4%)	4.94 ± 0.26 (± 5.3%)	5.66 ± 0.23 (± 4.1%)	5.59 ± 0.26 (± 4.7%)

dose estimates for each of the four correction methods are shown in Table 6.6. It can

be seen that the application of any one of the four correction methods brings the evaluated dose much closer to the true dose and also reduces the scatter somewhat (as shown by reductions in the absolute error). In the case of the xenon lamp, the best estimates of the given dose result from the application of methods 3 and 4, which have already been stated as being the most physically correct, however for the LED's, it was the first two correction methods that provided the best estimate of the given dose. This could just be due to accumulated errors and scatter throughout the experiment which have not been accounted for. Alternatively it must be remembered that the two stimulation techniques have important differences in that the xenon lamp system was stimulating at 480 nm in continuous mode, and the LED's were stimulating at 880 nm in 1  $\mu$ s pulses and thus it is not inconceivable that each of the two systems would require different theories to accurately correct for the loss of signal during the measurement cycles. However, it must also be remembered that this experiment is just a one off, and in order to be able to see whether or not there is a consistent difference in the accuracy of the answers obtained with differing correction methods between the two systems, many more experiments upon known doses similar to this one would have to be performed.

This question of which is the best correction factor to use can only be settled by a lot of consistent results from many experiments, and confirms the need to perform work upon known doses before known age material. It has been shown that apparent linearity of the growth curves does not imply that the answers obtained from them are accurate and one way of evaluating this with the particular technique used is to perform work on material which has a known dose. Another point to bear in mind is the difference between the errors upon regression analysis and the run to run reproducibility as shown in the scatter, for example the average error from regression analysis on the doses evaluated using the LED's and correction method 2 was 3.09 %, whereas the standard error derived from the scatter of the answers was in fact 5.26 %, and in the case of the xenon lamp with correction method 2 the regression errors averaged 4.54 % and the true error from scatter was 8.25 %. Thus it is easy with PSL to obtain low regression errors, however this is not necessarily indicative of the overall reproducibility of the result.

#### 6.4 - Methodologies for Checking the Efficiency of the Preheating Regime

Upon extension of this methodology to natural samples it will be important to be able to assess the efficiency of the preheating regime in removing any unstable components in the natural PSL signal. It has been suggested (Wintle pers. comm.) that a plot of the ratio of the natural signal (N) isothermal decay curve to that of the signal from a sample with a laboratory irradiation added to the natural dose (N+β). The reasoning behind this is that if both the N and the N+β contain the same components then the decay curves should be parallel. Conversely, if the N+β curve still contains some unstable components that have faded from the N signal, then the decay curves should not be parallel. If the PSL signal results from a single trap (after removal of unstable components) then it is indeed likely that the decay curves should be parallel after a sufficient preheat, however this is not necessarily the case for PSL resulting from a multi-component system after removal of the unstable signal. This can be demonstrated simply for the case of two traps contributing to the PSL signal.

Consider two traps (A & B) with activation energies  $E_A$  and  $E_B$  respectively, held at temperatures  $T_1$  and  $T_2$ . The lifetimes ( $\tau$ ) of each trap at each temperature are given by;

$$\begin{aligned}\tau_{A_{T_1}} &= s_A^{-1} \exp\left(\frac{-E_A}{kT_1}\right) \\ \tau_{A_{T_2}} &= s_A^{-1} \exp\left(\frac{-E_A}{kT_2}\right) \\ \tau_{B_{T_1}} &= s_B^{-1} \exp\left(\frac{-E_B}{kT_1}\right) \\ \tau_{B_{T_2}} &= s_B^{-1} \exp\left(\frac{-E_B}{kT_2}\right)\end{aligned}\tag{6.12}$$

The ratios of the lifetimes of the two components at each temperature are thus given by;

$$R_1 = \frac{\tau_{A\tau_1}}{\tau_{B\tau_1}} = \frac{s_B}{s_A} \exp\left(\frac{E_B - E_A}{kT_1}\right) \quad <6.13>$$

$$R_2 = \frac{\tau_{A\tau_2}}{\tau_{B\tau_2}} = \frac{s_B}{s_A} \exp\left(\frac{E_B - E_A}{kT_2}\right)$$

$R_1 = R_2$  iff  $E_A = E_B$  or  $T_1 = T_2$

The implication of this is that the ratios of the lifetimes for the two traps will differ with changes in temperature. Applying this to dating samples, the two temperatures concerned are the burial and preheating temperatures. During the period between zeroing and measurement (i.e. the age of the sample) traps A and B will undergo some degree of fading, with the relative proportion of signal lost from each trap being controlled by the relative lifetimes of the charge carriers in each trap. Thus, at the time of measurement the relative populations of charge carriers in A and B will have been depleted by the relative loss of charge carriers due to fading. For laboratory irradiated samples preheated to remove a similar proportion of the signal to that lost during burial, the final relative trapped charge populations in A and B will again depend on the relative proportions lost through fading. Now the preheating loss of charge carriers takes place at a much higher temperature than the loss during burial, and the above theory has shown that the relative lifetimes of (and hence relative proportions lost from) the two traps will be different. This implies that the isothermal decay curve from the laboratory irradiated sample will not be parallel to that from the natural sample. Thus the ratio of the  $N$  to  $N+\beta$  isothermal decay curves would not be constant, even if all unstable components are removed. This effect will depend on the complexity of the system generating the PSL signal, the extent of the spread of the activation energies and the difference between the burial and preheating temperatures.

Whilst the curves may never theoretically be parallel, it may be the case that even the most extreme departure from parallelism caused by this effect would prove to be relatively insignificant when compared to departures from parallelism caused by incomplete removal of unstable components and the errors associated with measuring

the decay curves. Isothermal decay curves from a natural sample and the same natural sample with an added laboratory dose have been measured in Duller (1991) and the curves for that particular sample appear to indeed be approximately parallel (although the curves are only shown after one heating has already been made). Thus the technique of monitoring the ratio of the N to N+ $\beta$  isothermal decay curves may be a very useful method in assessing the efficiency of the preheat, however it has been shown that a multi-component PSL signal may not be expected to exhibit parallelism, thus limiting the precision of the technique.

There are alternative techniques for checking the effectiveness of the preheating regime that circumvent this problem. One way would be to examine the dependency of the final measured ED on various preheating regimes. If the preheating does not remove all unstable components, then upon strengthening the preheat, the ED should increase. Upon achieving a sufficiently strong preheating regime, the ED should become constant. This method will, however, be dependent on the accuracy of the growth curves, which will be highly dependent on the validity and accuracy of the correction technique used to account for loss of signal due to bleaching and annealing in the measurement cycle. Another technique that could be used would be to study the long term fading of the PSL signal. In this method, incomplete removal of the unstable components would lead to marked fading in the laboratory irradiated samples when compared to natural samples. This method is independent of errors associated with the growth curves, however it is a long term technique.

## 6.5 - Discussion

A similar single disc methodology has been developed and proposed in parallel to the above by G. Duller at Aberystwyth (Duller, 1991) using continuous stimulation from infra red LED's only. These were attached to an automatic Risø reader which enabled easy analysis of a large number of samples whilst ensuring minimum handling and constant sample orientation in the radiation and illumination fields, factors which perhaps should all lead to greater precision than that obtained manually (as above).

Apart from slight differences in the number of aliquots used, the number of doses imparted to the samples and the preheat (220°C for 10 minutes), the major difference to the above method lies in the stimulation technique (continuous LED's instead of pulsed), the samples used (known age rather than known dose) the methods used to correct for the loss of signal during measurement and the number of growth curves generated for each sample.

As is the case for most sediment dating, Duller does not generate a second growth curve to check for linearity in the growth curves as this could lead to sensitisation problems. However, fitting a linear or exponential function to the growth curves is a dangerous assumption if the accuracy of the correction technique used to account for losses during the measurement process is not well characterised. Duller uses a set of data points at the end of the growth curve which are measured without increasing the dose as a check on the correction technique. A valid technique should make these points equal. However it can be seen that the best technique used, still does not make the points equal, indeed they exhibit a drop of 4.2% from the first to last measurement (i.e. 4.2% after 4 further measurements). It can also be seen from the same graph that the corrected growth curves are still sublinear in nature. This raises the question as to whether this sublinearity is caused by the correction technique, or whether the underlying growth response is sublinear.

The correction methods used to account for the losses in signal during measurement are highly dependent on the measured loss per cycle on control samples. In Duller (1991) the correction factors were evaluated on a natural sample. A very important question is whether the correction factors should be measured on a natural sample or on a sample which has a laboratory dose added, and indeed as to the size of the dose added. It is normal in luminescence dating to generate a growth curve that adds a signal to the natural that is at least as large as the natural, if not larger. It is true for the first point of the growth curve that the signal is pure natural, and thus the amount lost in measurement can be observed on an isothermal decay curve of the natural sample. However, once an added  $\beta$  dose is given, the decay becomes part natural and part added. For successive dose increments, the proportion of the added dose with respect to the

natural increases until the controlling decay is that of the added dose and not the natural. If the natural isothermal decay curve is the same as for the added dose, then it does not matter which curve is used to generate the correction factors, however if there is a difference then it would seem appropriate to use the decay curve from the component that dominates the growth curve, namely the added dose. Thus it would seem to be more correct to use isothermal decay curves measured on samples with added doses, and thus it would seem logical to use the dating samples themselves once the growth curve had been constructed.

The two correction methods proposed in Duller (1991) are similar to those set out in methods 1 & 4 with one assuming constant losses and the other variation in loss per cycle. In this paper it is demonstrated clearly that the first technique is invalid for the samples under examination, which is not surprising when one considers the non exponential nature of the bleaching and annealing curves already demonstrated. The second technique used in Duller (1991) assumes that the trapped charge population generated by each dose increment behaves independently. This is equivalent to method 4 above. This has been demonstrated in Duller (1991) to yield satisfactory correction to the data set. This supports the evidence found above that a correction technique which assumes an exponential bleaching / annealing curve is less satisfactory than one which does not. However, there are two changes between Duller's two methods; namely the assumption of independent behaviour of the trapped charge carriers and a non exponential bleaching / annealing. It has already been demonstrated above that method 1 and the first method of Duller (1991) was not expected to give satisfactory results, of much more interest is the difference (if any) between methods 2 and 4 above. Method 2 introduces the concept of non exponentiality in the decay curve whilst still maintaining charge carrier dependence. Method 4 introduces charge carrier independence into method 2. Duller has not shown any evidence of applying a correction technique similar to method 2. Such an application of this technique would assist in better determination of whether the trapped charge populations from each dose increment are dependent or not. However, comparisons between methods 2 and 4 will probably be very difficult on natural samples as the exact dose given initially to the sample is not known accurately.

Hence it would seem likely that such detailed comparison could only be made with confidence on samples with a known laboratory dose.

A test for any correction technique is to observe the results and to compare both precision and accuracy. Detailed appraisal of the accuracy of the results generated in Duller (1991) is limited as the samples were only known age and not known dose. Comparison has been made in Duller (1991) to TL dates obtained for the same samples and although the TL and PSL dates agree within error, the average discrepancy between them is 3.2% and alternative techniques give values for the dose which differ by as much as over 20% for one case. The precision of the measurements, however, can be examined. Although for one sample a precision of 2.78% from 19 separate dose evaluations was obtained, the other two samples yielded errors of 7.1% from 20 and 8.8% from an unknown number of estimations, although it seems reasonable to assume 20. Converting these errors to runs of 8 separate evaluations of the same dose yields a best error of 4.3% and a worst one of 13.9%, which in comparison to the best error from the methodology used in the study presented in this thesis (4.1% from 8 repeats) does not demonstrate the better precision that one may expect from an automated reader. This could well be indicative of the sample used (natural samples will give rise to greater scatter due to inhomogeneities in grain microdosimetry), or it could be as a result of the stimulation technique used (i.e. continuous as opposed to pulsed and only 5 dose increments instead of 10), however only further developmental work will be able to resolve this.

Finally it must be emphasised that although the methodologies (including correction techniques) proposed in this chapter and in Duller (1991) were developed in parallel, they were developed independently of each other. The application of a single disc methodology is a straightforward (and perhaps obvious) step in PSL dating, considering the non destructive nature of photo stimulation.

## 6.6 - Summary

The results obtained in chapters 4 and 5 have been used in the development of a dating / dosimetric technique. It has been shown that using a single disc, additive dose methodology (with no preheat), it is possible to accurately recover a known dose from the IAEA feldspar F1 using the xenon lamp. However, the problem of accumulated bleaching was apparent in the results generated by the LED's. With the introduction of a preheat, both of these stimulating systems overestimated the dose. This has been ascribed to sublinearity in the growth curves generated by cumulative bleaching and annealing of the signal. As a consequence of this, four theoretical correction formulae have been developed and tested. Upon the application of these correction formulae, it was possible to correct the dose estimates and thus recover the given laboratory dose.

Thus it seems that a single disc, additive dose methodology holds good potential for future dating applications. However, careful correction of the growth curves is required if this technique is not to overestimate the stored dose. Generation of a second growth curve is very important in assessing any non-linearity in the dose dependency, both before and after correction of the growth curves. Further tests of the correction factors are required to demonstrate validity and to identify the best one. After careful evaluation of these techniques, it should be possible to extend this work to different samples, including archaeological samples of known age. Successful dating of such samples should then lead to the application of this methodology to the dating of unknown samples.

## 7 - Conclusion

### 7.1 - Summary of Results

The PSL of feldspar has been explored using different techniques in this project. These techniques include spectroscopic approaches, on both the excitation and emission sides; thermal stability studies; dose dependency in both high and low dose regions; initial rise studies of the thermally assisted transitions and pulsed PSL measurements leading to time domain analysis. The results from these studies were used to propose modifications to an existing model for the PSL phenomena in feldspar and finally the relevant results were combined to establish a single disc additive dose dating methodology which was able (after corrections for bleaching and annealing had been made) to recover a known laboratory dose. The main points of these results are summarised below;

#### 7.1.1 - Spectroscopy

Excitation spectroscopy over a wavelength range from 450 nm to 950 nm has been performed on a total of 32 different feldspars. A brief survey of 30 feldspars looking solely at the shape of the excitation spectrum from a dose of 1 kGy has shown strong similarity between and within different feldspar families. All of these spectra show stimulation regions in the green, red and infra red regions, however the position of these stimulation peaks and their relative intensities varies markedly between samples. Thus, whilst the underlying trap structure in different feldspars may be similar, it seems likely that there are small variations in the precise trap structure.

More detailed excitation spectroscopy has been performed on two feldspar samples, one microcline and the other, the IAEA feldspar F1. Again three broad stimulation regions were identified in the green, red and infra-red wavelength regions. Normalisation of these spectra have shown the system of infra-red peaks to be the result of the superposition of the lamp energy spectrum on a single broad stimulation peak. This has

been confirmed by the use of a tungsten light source which has a smooth infra-red spectrum. The normalisation also showed that the green stimulation region is much more sensitive than the infra red, per unit power. The low wavelength edge to the green excitation region is thought to be an artifact due to the presence of an order sorting filter at 475 nm. Again this is reinforced by power normalisation.

Excitation spectroscopy following annealing has shown that there are at least two components in the spectrum with differing thermal stabilities. The infra-red, red and part of the green stimulation regions were annealed by 300-350°C, whilst the remaining part of the green stimulation region is not annealed until 400-450°C. The lesser stability of the infra-red region compared to the green has been demonstrated in the excitation spectrum of a sample of the F1 feldspar which contained its natural geological dose. In this spectrum it can be seen that the ratio of the green stimulation region to the infra-red is greater than that resulting from a more recent dose. Hence it may be that the infra-red stimulation region is less stable than one component of the green, and may even be meta-stable over archaeological timescales.

Exploration of the temperature dependency of the excitation spectra has revealed that there is some degree of thermal assistance present in all stimulation regions, rather than just in the infra-red wavelength region which is the limit of published observations. Cryogenic observations of the excitation spectrum at -140°C have shown that there is a strong residual signal in the green stimulation region, and it is proposed that this is a non thermally assisted component. Hence it seems likely that the green stimulation region is comprised of a component that is thermally assisted and one that is not. This ties in to the annealing studies as a non thermally assisted transition would be expected to be shallower than a thermally assisted transition at the same wavelength, and thus have lesser thermal stability.

Finally, bleaching studies have shown that exposure to infra-red stimulation can bleach the green stimulation region, thus suggesting a link between the green and infra-red stimulation regions. The bleaching results, combined with the thermal stability and thermal assistance studies have lead to the postulate that there are two traps responsible

for the excitation spectrum. One giving rise to the non thermally assisted transition in the green stimulation region, which also forms the ground state for the thermally assisted transition in the red and infra-red stimulation regions. The other trap gives rise to the thermally assisted green PSL.

Emission spectroscopy from infra-red stimulation has identified three emission bands at 340, 400 and 560 nm. Observations of the emission spectrum at 150 K have shown that there is still strong emission at 560 nm. The greatest degree of thermal dependency was observed in the 400 nm emission peak.

### 7.1.2 - Thermal Stability

Excitation spectroscopy studies have shown that there are at least two components in the green stimulation region. As a result of this, a more detailed stability study was performed, using pulsed isothermal decay of the PSL signal stimulated at 480 nm. The results of this study have revealed complex behaviour that is quite distinct from that expected from a single first order trap. An attempt to fit the decay curves with the sum of three exponential functions (being equivalent to three first order traps) resulted in good fits. However, the lifetimes generated did not show linearity on an Arrhenius plot. It has been shown that there is evidence for the 480 nm PSL to result from a non-linear distribution of traps. This hypothesis is supported by earlier fractional glow TL measurements on feldspar, which showed evidence for a distribution of traps.

### 7.1.3 - Thermal Assistance

After the identification of thermal assistance in all of the stimulation bands, initial rise measurements were performed in order to obtain estimates for the activation energies of the thermal transitions. It has been shown that the activation energies obtained increase with wavelength. It has been postulated that the infra-red and red stimulation bands are both thermally assisted transitions resulting from the same ground state trap.

If this is the case, then as the energy of photons at 900 nm is less than those at 600 nm, the thermal step should be greater for the infra-red transition than the red. The measured activation energies do not contradict this and thus it is still reasonable to assume that the red and infra-red stimulation bands result from the same trap.

#### 7.1.4 - Pulsed Stimulation

Initial pulsed PSL studies have been performed using pulsed infra-red LED's and a pulsed dye laser at 480 nm. These initial studies showed the ability of pulsed stimulation to be able to record the eviction and recombination dynamics, providing a multi-channel scaler with sufficiently short minimum dwell times is used. The LED's generated a peak response about 10  $\mu$ s after the start of the stimulating pulse. This was reinforced by the laser, which again generated a peak response 10  $\mu$ s after the stimulation pulse. The laser system also demonstrated the high signal to background ratios that can be obtained using pulsed stimulation. Observations of PSL from the pulsed LED's on a fast multi-channel scaler (minimum dwell 5 ns) have shown that detailed analysis of the PSL time domain may indeed be possible, however good characterisation of the stimulation source is important.

#### 7.1.5 - PSL Model

The results from excitation spectroscopy, emission spectroscopy, thermal stability and thermal assistance studies summarised above have been combined and used to propose modifications to the energy model proposed by Hütt & Jaek (1989). A multi trap / multi recombination centre model has been introduced which is sufficient to account for the observed phenomena reported above. However the possibility that the green stimulation region extends below 450 nm and results from a distribution of traps leads to the expectation that this model will need further modification once extended studies are performed. Ultimately, the model should be able to account for the observed PSL and TL phenomena.

### 7.1.6 - Dose Response and Evaluation

A study of the dose response of the PSL of microcline has been performed, showing increasing signal up to a level of at least 10 kGy. The low dose dependency of the PSL from the IAEA feldspar F1 has been explored using the xenon lamp and laser at 480 nm, and the infra-red LED's. It was possible to construct growth curves in the zero to ten gray region for all three systems, with departure from linearity only present for the LED's, this being ascribed to cumulative bleaching. The greatest sensitivity was demonstrated by the laser, however all three stimulation systems showed sufficient sensitivity to be able to measure the PSL signal resulting from 0.5 Gy.

With this demonstration of sensitivity, it was possible to attempt to recover a known dose from the F1 feldspar. This attempt was made using a single disc, additive dose methodology, firstly without preheating the sample. The scatter present in the results generated by the laser meant that only the xenon lamp and LED's were used in the second experiment incorporating a preheat. This second experiment showed that the cumulative effect of the preheating and bleaching during measurement to be causing sublinearity in the growth curves. Four formulae were developed to correct for this factor, and applied to the growth curves. These correction factors successfully straightened the growth curves, and it became possible to obtain the correct dose from the results generated by both the xenon lamp and the LED's. Thus it is possible to use a single disc additive dose methodology (after correction for loss of signal) to recover a given laboratory dose accurately and precisely. Thus it will be possible to extend this technique to real samples in the confidence that it can produce the correct answer.

## 7.2 - The Future

The work presented above forms an introduction to the exploration of the mechanisms of the phenomenon of PSL in feldspar. However there are still many areas of exploration that can be readily identified and are laid out below.

- 1 - Excitation Spectroscopy. It has been shown that the excitation spectrum shows every sign of extending below 450 nm, with the edge being due solely to the presence of filters. Consequently extended spectroscopy below 450 nm is required in order to attempt to come to a more complete understanding of the PSL mechanism. The difficulty of separating the stimulation and detection regions at these wavelengths means the probably asynchronous pulsed stimulation and detection will be required on a spectroscopic basis. The spectroscopy in this extended region will need to include studies of thermal annealing, bleaching by wavelengths from each of the stimulation regions identified and thermal assistance studies.
- 2 - Emission Spectroscopy. Further studies are required in this area. The variations in emission spectra with stimulating temperature and bleaching require repetition to check on the results presented above. Other studies that would prove useful are variations with stimulating wavelength, dose, annealing and bleaching at wavelengths other than the stimulating wavelengths. Again the problem of separating the stimulation and detection regions may well mean that the best approach will be via asynchronous pulsed stimulation and detection. A very useful and flexible tool in the study of the PSL mechanism for any material would be a combined excitation and emission spectrometer, being the direct analogy of TL emission spectrometers. Such a tool would probably again require pulsed stimulation and asynchronous detection.
- 3 - Time Domain Analysis. It has already been stated above that time domain analysis of the PSL response to pulsed stimulation could be a very important tool for the exploration of PSL *and* TL mechanisms. Such analysis should provide

information on the charge carrier recombination lifetimes and observations with variations in such parameters as dose, fading, temperature and wavelength could provide valuable information concerning the underlying mechanisms. Again a spectroscopic approach would seem to hold the greatest potential.

- 4 - Individual Stimulation Regions. Once stimulation regions have been identified and their interactions with other stimulation regions have been observed, it will then be necessary to perform more detailed exploration on the individual stimulation regions, such as initial rise measurements to evaluate the thermal activation energies of any thermally assisted components and pulsed isothermal decay (annealing) studies to identify the nature of the traps and (if possible) calculate the ground state activation energies and frequency factors.
  
- 5 - Thermal to Photo Activation Energy Ratio. It has been demonstrated in the discussions concerning the modifications to the PSL model that knowledge of this ratio for each transition is very important. Further exploration of the ratio is thus required, both theoretical to check if the variation in dielectric constant is the only mechanism, and experimental to measure the dielectric constants in order to calculate the ratio and to see if such a ratio can yield physical solutions. Direct measurements of the ratio are hard unless there is confidence that the same trap is responsible for the signal giving rise to both the thermal and photo activation energies. An accurate interpretation of the observed luminescence and the formation of a true model may not be possible until this matter is resolved.
  
- 6 - Dating. The dose evaluation experiment has demonstrated the validity of the single disc additive dose methodology, and thus the next step is to begin dating real samples. Identification of new stimulation regions with extended excitation spectroscopy would enable this work to be extended to areas of possible greater stability, however again it would be necessary to demonstrate that stimulation at such wavelengths could yield linear growth curves and thus evaluate known doses before the dating of real samples could be attempted.

7 - Radiation Source Calibration. In the reviewers comments on Duller (1992), a problem with infra-red cross calibration between gamma and beta sources when compared to TL calibration has been identified. There has also been a case when a gamma dose given by the SURRC  $^{60}\text{Co}$  source to calibrate a beta source using infra-red stimulation has resulted in a different result to that obtained by calibration to another beta source. A possible reason for this can be proposed; when samples are irradiated in a gamma source, the dose is absorbed uniformly through the grains. However, in a beta source a large proportion of the absorbed dose results from the back scattering of the beta particles from the stainless steel disc that the grains are mounted on. This can result in the underside of the grains acquiring a higher absorbed dose than other parts of the grains. Photo stimulation will suffer absorption with increasing depth into the minerals and thus the underside of the grain will receive attenuated stimulation thus leading to an under estimation of the absorbed dose from beta irradiation as compared to gamma irradiation due to the region of high absorbed dose (the underside of the grains) from a beta source receiving attenuated stimulation. This effect would have no effect on the gamma dose as this would be uniform. If photo absorption does cause problems, then a spectroscopic approach may well identify wavelength regions that will be affected less, also it may be expected that as the grain size is reduced, so the absorption effects would lessen and the calculated beta-gamma calibration should approach a beta-beta calibration. Certainly further exploration of this problem will be necessary.

### 7.3 - Conclusion

The work presented in this thesis represents a thorough introduction to the exploration of the fundamental mechanisms of PSL in feldspar. It has shown that the phenomenon is complex, resulting from a system of many interacting traps and centres. It has been shown that a spectroscopic approach is important to identify the relative effects of variations in stimuli upon the many excitation regions. The results have been used to

propose modifications to the Hütt & Jaek energy model, however it has clearly been shown that these modifications will themselves have to be adapted once exploration of the PSL response is extended to other excitation regions. The work presented above has begun the process of placing the phenomenon on a firm physical basis, however further detailed work is required to continue this, and has been identified above.

The data generated in this thorough exploration of the PSL mechanisms has been used to propose a single disc, additive dose methodology for dosimetric and dating purposes. With the development and successful implementation of formulae describing the loss mechanisms during measurement, it has been possible to recover a given laboratory dose accurately and precisely. This technique can now be applied to dating real samples, with the first step being to date material of a well defined context and age before proceeding to unknown material.

Thus thorough exploration of the PSL characteristics has led to a more complete energy model, and has resulted in the development of a dosimetric methodology that holds good potential for archaeological dating.

## 8 - Bibliography

Adirovitch, E. I. (1956) La Formule de Becquerel et la loi élémentaire du déclin de la luminescence des phosphores cristallins. *J. Phys. Rad.* **17**, 705.

Aitken, M. J. (1985) Thermoluminescence Dating. *Academic Press*, London.

Aitken, M. J. and Smith, B. W. (1988) Optical dating: Recupération après blanchiment. *Quat. Sci. Rev.* **7**, 387-393.

Aitken, M. J., Tite, M. S. and Reid, J. (1964) Thermoluminescent dating of ancient ceramics. *Nature* **202**, 1032-1033.

Aitken, M. J., Zimmerman, D. W. and Fleming, S. J. (1968) Thermoluminescent dating of ancient pottery. *Nature* **219**, 442-444.

Akber, R. A. and Prescott, J. R. (1985) Thermoluminescence in some Feldspars: Early results from studies of spectra. *Nucl. Tracks.* **10** N° 4-6, 575-580.

Albrecht, H.O. and Mandeville, C. E. (1956) Storage of Energy in Beryllium Oxide. *Phys. Rev.* **101**, 1250-1252.

Andersson, M., Jeannin, M., Rendell, H. M., Tardot, A. and Townsend, P. D. (1990) TL spectra of mineral mixtures: discrimination between different components. *Nucl. Tracks Radiat. Meas.* **17** N° 4, 569-577.

Bailiff, I. K. (1976) Use of phototransfer for the anomalous fading of thermoluminescence. *Nature* **264**, 531-533.

Bailiff, I. K. and Poolton, N. R. J. (1989) Charge transfer in quartz and feldspar: factors affecting the dating of young sediments. *In* Synopses from a workshop on long and short range limits in luminescence dating, *Occasional publication N° 9, Research Laboratory for Archaeology and the History of Art, Oxford University.*

Bailiff, I. K. and Poolton, N. R. J. (1991) Studies of charge transfer mechanisms in feldspars. *Nucl. Tracks Radiat. Meas* **18** N° 1/2, 575-580.

Bailiff, I. K., Morris, D. A. and Aitken, M. J. (1977) A rapid scanning interference spectrometer; application to low level thermoluminescence emission. *J. Phys. E: Sci. Instrum.* **10**, 1156-1160.

Becker, K. (1974) On the discovery of TL. *Health Physics.* **27**, 321-322.

Blakemore, J. S. (1985) Solid State Physics. *Cambridge University Press, Cambridge.*

Bonfiglioli, G., Brovetto, P. and Cortese, C. (1959) Thermoluminescence and F Centres. I, Theory. *Phys. Rev.* **114**, 951-956.

Bowman, S. G. E. (1979) Phototransferred thermoluminescence in quartz and its potential use in dating. *PACT* **3**, 381-400.

Boyle, R. (1664) Experiments and considerations upon colours with observations on a diamond that shines in the dark. *Henry Harrington, London.*

Braner, A. A. and Israeli, M. (1963) Effects of illumination on the thermoluminescence of alkali halides. *Phys. Rev.* **132** N° 6, 2501-2505.

Bräunlich, P. (1979) Thermally stimulated relaxation in solids. *Springer-Verlag, Berlin.*

Chen, R. and Kirsh, Y (1981) Analysis of Thermally Stimulated Processes. *Pergamon Press, Oxford.*

- Clark, R. J. (1989) Application of the Gauss-Newton method to fitting non-linear TL growth curves. *SURRC TL Laboratory Internal Report 89/1*.
- Clark, S. P. Jr., Ed. (1966) Handbook of Physical Constants. *Geological Society of America*, memoir 97.
- Dalal, M. L., Kirsh, Y., Rendell, H. M. and Townsend, P. D. (1988) TL emission spectra of natural feldspars. *Nucl. Tracks Radiat. Meas.* **14**, 57-62.
- Daniels, F., Boyd, C. A. and Saunders, D. F. (1953) Thermoluminescence as a research tool. *Science* **117**, 343-349.
- Duller, G. A. T. (1991) Equivalent dose determination using single aliquots. *Nucl. Tracks Radiat. Meas.* **18** N°4, 371-378.
- Duller, G. A. T. (1992) The use of a single aliquot method for intercalibration between radioactive sources. *Ancient TL* **10** N°1, 8-11.
- Duller, G. A. T. and Wintle, A. G. (1991) On infrared stimulated luminescence at elevated temperatures. *Nucl. Tracks Radiat. Meas.* **18** N°4, 379-384.
- Eisberg, R. M. and Resnick, R. (1985) Quantum Physics of Atoms, Molecules, Solids, Nuclei and Particles. *John Wiley and Sons*, New York.
- Garlick, G. F. J. (1949) Luminescent Materials. *Oxford University Press*, London.
- Garlick, G. F. J. and Gibson, A. F. (1948) The Electron Trap Mechanism of Luminescence in Sulphide and Silicate Phosphors. *Proc. Phys. Soc.* **60**, 574-590.
- Godfrey-Smith, D. I., Huntley, D. J. and Chen, W. H. (1988) Optical dating studies of quartz and feldspar sediment extracts. *Quat. Sci. Rev.* **7**, 373-380.

- Göksu, H. Y., Fremlin, J. H., Irwin, H. T. and Fryxell, R. (1974) Age determination of burned flint by a thermoluminescent method. *Science* **183**, 651-654.
- Grögler, N., Houtermans, F. G. and Stauffer, H. (1960) Ueber die Daiterung von Keramik und Ziegel durch Thermolumineszenz. *Helv. Phys. Acta.* **33**, 595-596.
- Guérin, G. and Valladas, G. (1980) Thermoluminescence dating of volcanic plagioclases. *Nature* **286**, 697-699.
- Halperin, A. and Braner, A. A. (1960) Evaluation of Thermal Activation Energies from Glow Curves. *Phys. Rev.* **117**, 408.
- Halperin, A., Kristianpoller, N. and Ben-Zvi, A. (1959) Thermoluminescence of X-ray coloured NaCl crystals. *Phys. Rev.* **116** N° 5, 1081-1089.
- Hecht, E. and Zajac, A. (1974) Optics. *Addison-Wesley Inc.* Massachusetts.
- Hofmeister, A. M. and Rossman, G. R. (1985) A model for the irradiative coloration of smoky feldspar and the inhibiting influence of water. *Phys. Chem. Miner.* **12**, 324-332.
- Hoogenstraaten, W. (1958) Electron traps in zinc sulphide phosphors. *Philips Research Reports.* **13**, 515-562.
- Huntley, D. J., Godfrey-Smith, D. I. and Haskell, E. H. (1991) Light-Induced emission spectra from some quartz and feldspars. *Nucl. Tracks Radiat. Meas.* **18** N° 1/2, 127-131.
- Huntley, D. J., Godfrey-Smith, D. I. and Thewalt, M. L. W. (1985) Optical dating of sediments. *Nature* **313**, 105-107.
- Hütt, G. and Jaek, J. (1989) Infrared Stimulated Photoluminescence Dating of Sediments. *Ancient TL* **7** N°3, 48-52

Hütt, G., Jaek, I. and Tchonka, J. (1988) Optical Dating: K-Feldspars Optical Response Stimulation Spectra. *Quat. Sci. Rev.* **7**, 381-385.

Ichikawa, Y. (1965) Dating of ancient ceramics by thermoluminescence. *Bulletin of the Institute of Chemical Research, Kyoto University* **43**, 1-6.

Ioffe, V. A. and Yanchevskaya, I. S. (1958) Dielectric loss in feldspars. *Soviet Phys. - Techn. Phys.* **28**, 1983-1991.

Jablonski, A. (1935) Über den Mechanismus der Photolumineszenz von Farbstoffphosphoren. *Z. Phys.* **94**, 38.

Jungner, H. and Huntley, D. J. (1991) Emission spectra of some potassium feldspars under 633 nm stimulation. *Nucl. Tracks Radiat. Meas.* **18** N° 1/2, 125-126.

Kennedy, G. C. and Knopff, L. (1960) Dating by thermoluminescence. *Archaeology* **13**, 147-148.

Kirsh, Y. and Townsend, P. D. (1988) Speculations on the blue and red bands in the TL emission spectrum of Albite and Microcline. *Nucl. Tracks Radiat. Meas.* **14** N° 1/2, 43-49.

Kirsh, Y., Shoval, S. and Townsend, P. D. (1987) Kinetics and emission spectra of TL in the feldspars albite and microcline. *Phys. Stat. Sol. (a)* **101**, 253-261.

Kittel, C. (1986) Introduction to solid state physics. *John Wiley & Sons Inc.*, New York.

Levy, R. A. (1968) Principles of Solid State Physics. *Academic Press*, New York.

Levy, P. W. (1983) Characteristics of thermoluminescence glow curves for materials exhibiting more than one glow peak. *PACT* **9**, 109-122.

Levy, P. W. (1985) Thermoluminescence kinetics in materials exposed to the low doses applicable to dating and dosimetry. *Nucl. Tracks Radiat. Meas.* **4-6**, 547-556.

Levy, P. W., Mattern, P. L. and Lengweiler, K. (1971) Three dimensional thermoluminescent analysis of minerals. *Mod. Geol.* **2**, 295-297.

Lyon, T. D. B., Gillen, C. and Bowes, D. R. (1975) Rb-Sr, isotopic studies near the major Precambrian junction between Scourie and Loch Laxford, Northwest Scotland. *Scott. J. Geol.* **11**, 333-337.

Mazess, R. B. and Zimmerman, D. W. (1966) Pottery dating from thermoluminescence. *Science* **152**, 347-348.

McKeever, S. W. S. (1988) Thermoluminescence of Solids. *Cambridge University Press*, Cambridge.

McKeever, S. W. S. and Chen, R. (1980) TL response to dose: Numerical solution to the equations describing the build up of TL during irradiation. *PACT* **6**, 243-251.

McKeever, S. W. S., Chen, R., Groom, P. J. and Durrani, S. A. (1980) Dose rate dependence of thermoluminescence response. *Nucl. Inst. Meth.* **175**, 43-44.

Mejdahl, V. (1969) Thermoluminescence dating of ancient Danish ceramics. *Archaeometry* **11**, 99-104.

Mejdahl, V. (1983) Feldspar inclusion dating of ceramics and burnt stones. *PACT* **9**, 351-364.

Mobbs, S. F. (1979) Phototransfer at low temperatures. *PACT* **9**, 407-413.

Mott, N. F. and Gurney, R. W. (1953) Electronic Processes in Ionic Crystals. *Clarendon Press*, Oxford.

Nail, N. R., Pearlman, D. and Urbach, F. (1948) Photoluminescence of some sulfide phosphors as a function of intensity *In Preparation and Characteristics of Solid Luminescent Materials. J. Wiley & Sons Inc.*, 190-204.

O'Brien, B. (1948) Infrared sensitive phosphors. *In Preparation and Characteristics of Solid Luminescent Materials. J. Wiley & Sons Inc.*, 141-147.

Pidgeon, R. T. and Hopgood, A. M. (1975) Geochronology of Archaeangneisses and tonalites from north of the Frederikshåbs isblink, S.W. Greenland. *Geo. et Cosmo. Acta.* **39**, 1333-1346.

Pidgeon, R. T. and Råheim, A. (1972) Geochronological investigation of the gneisses and minor intrusive rocks from Kristiansund, West Norway. *Nor. Geol. Tidsskr.* **52**, 241-256.

Poolton, N. R. J. and Bailiff, I. K. (1989) The use of LED's as an excitation source for photoluminescence dating of sediments. *Ancient TL.* **7 N° 1**, 18-20.

Questiaux, D. G. (1991) Optical dating of Loess: Comparisons between different grain size fractions for infra red and green excitation wavelengths. *Nucl. Tracks Radiat. Meas.* **18 N° 1/2**, 127-131.

Randall, J. T. and Wilkins, M. H. F. (1945 a) The Phosphorescence of Various Solids. *Proc. Roy. Soc.* **A184**, 347.

Randall, J. T. and Wilkins, M. H. F. (1945 b) Phosphorescence and Electron Traps. I. The Study of Trap Distributions. *Proc. Roy. Soc.* **A184**, 366.

Randall, J. T. and Wilkins, M. H. F. (1945 c) Phosphorescence and Electron Traps. II. The Interpretation of Long Period Phosphorescence. *Proc. Roy. Soc.* **A184**, 390.

Rhodes, E. J. (1988) Methodological considerations in the optical dating of quartz. *Quat. Sci. Rev.* **7**, 395-400.

Rhyner, C. R. and Miller, W. G. (1970) Radiation dosimetry by optically stimulated luminescence of BeO. *Health Physics* **18**, 681-684.

Sanderson, D. C. W. (1982) The thermoluminescence of archaeological glass. *MPhil Thesis, University of Bradford, U.K.*

Sanderson, D. C. W. (1987) Thermoluminescence dating of Scottish Vitrified forts. *Ph.D. Thesis, Paisley College, U.K.*

Sanderson, D. C. W. (1988) Fading of thermoluminescence in feldspars: Characteristics and corrections. *Nucl. Tracks Radiat. Meas.* **14** N° 1/2, 155-161.

Sanderson, D. C. W. (1991) Photostimulated Luminescence (PSL): A New Approach to Identify Irradiated Foods. *In Potential New Methods of Detection of Irradiated Food*, Ed J. J. Raffi & J. J. Belliardo. *Commission of the European Communities Report EUR 13331*. Luxembourg

Sanderson, D. C. W., Clark, R.J., Slater, C. and Cairns, K.J. (1989) TL dating using alkali feldspars - High dose characteristics and Stability estimates. *In Synopses from a workshop on long and short range limits in luminescence dating, Occasional publication N° 9, Research Laboratory for Archaeology and the History of Art, Oxford University.*

Sanderson, D. C. W., Placido, F. and Tate, J. O. (1988) Scottish vitrified forts: TL results from six study sites. *Nucl. Tracks Radiat. Meas.* **14** N° 1/2, 307-316.

Sanderson, D. C. W., Slater, C. and Cairns, K. J. (1990) Development of Luminescence tests to Identify Irradiated Foods. *Progress Report N° 2, MAFF Project N384.*

Sasidharan, R., Sunta, C. M. and Nambi, K. S. V. (1979) Phototransfer method for determining archaeological dose of pottery sherds. *PACT* 9, 401-406.

Shockley, W. and Read, W. T. (1952) *Physics Review*. 87, 835.

Shrader, R. E., Lasof, S. and Leverenz, H. W. (1948) Zinc: Cadmium-sulfide: Selenide phosphors. Part III: Spectral emission characteristics and relative intensities. In Preparation and Characteristics of Solid Luminescent Materials. *J. Wiley & Sons Inc.*, 238-257.

Smith, B. W. (1988) Zircon from sediments: A combined OSL and TL autoregenerative dating technique. *Quat. Sci. Rev.* 7, 401-406.

Spooner, N. A. and Franks, M. (1990) Some characteristics of infra red emitting diodes relevant to luminescence dating. *Ancient TL*. 8 N° 3, 16-19.

Stoddard, A. E. (1960) Effects of illumination upon sodium chloride thermoluminescence. *Phys. Rev.* 120 N° 1, 114-117.

Stoneham, D. and Stokes, S. (1991) An investigation of the relationship between the 110°C TL peak and optically stimulated luminescence in sedimentary quartz. *Nucl. Tracks Radiat. Meas.* 18 N° 1/2, 119-123.

Strickertsson, K. (1985) The thermoluminescence of potassium feldspars - glow curve characteristics and initial rise measurements. *Nucl. Tracks Radiat. Meas.* 10 N° 4-6, 613-617.

Tochilin, E., Goldstein, N. and Miller, W. G. (1969) Beryllium Oxide as a Thermoluminescent Dosimeter. *Health Physics* 16, 1-7.

Townsend, P. D. and Kirsh, Y. (1989) Spectral measurements during thermoluminescence - an essential requirement. *Contemporary Physics* 30, 337-354.

Urbach, F. (1948) Storage and release of light by phosphors. *In Preparation and Characteristics of Solid Luminescent Materials. J. Wiley & Sons Inc.*, 115-140.

van Breemem, O., Aftalion, M. and Allaart, J. H. (1974) Isotopic and Geochronological Studies on Granites from the Ketilidian Mobile Belt of South Greenland. *Geol. Soc. America Bull.* **85**, 403-412.

van Breemen, O., Aftalion, M. and Johnson, M. R. W. (1979) Age of the Loch Borrolan complex, Assynt and late movements along the Moine Thrust Zone. *J. Geol. Soc. London.* **136**, 489-495.

van Breemen, O. and Bowden, P. (1973) Sequential age trends for some Nigerian Mesozoic granites. *Nature Phys. Sci.* **242** N°114, 9-11.

Visocekas, R. (1978) La Luminescence de la calcite après irradiation cathodique: TL et luminescence par effect tunnel. *Thèse, Université Pierre et Marie Curie, Paris 6.*

Visocekas, R. (1979) Miscellaneous aspects of artificial TL of calcite: emission spectra, thermal detrapping and anomalous fading. *PACT* **3**, 258-265.

Visocekas, R., Ceva, T., Marti, C., Lefauchaux, F and Robert, M. C. (1976) Tunnelling process in afterglow of calcite. *Physica Status Solidi. A* **35**, 315-327.

Visocekas, R., Oucherne, M. and Gallois, B. (1983) Tunnelling afterglow and anomalous fading in dosimetry with calcium sulphate. *Nucl. Inst. Meth. Phys. Res.* **214**, 553-555.

Wheeler, G. C. W. S. (1988) Optically stimulated phosphorescence and optically transferred TL as a tool for dating. *Quat. Sci. Rev.* **7**, 407-410.

Wintle, A. G. (1973) Anomalous fading of thermoluminescence in mineral samples. *Nature* **245**, 143-144.

Wintle, A. G. and Huntley, D. J. (1979) Thermoluminescence dating of a deep sea core. *Nature* **279**, 710-712.

Wintle, A. G. and Huntley, D. J. (1980) Thermoluminescence dating of ocean sediments. *Can. J. Earth. Sci.* **17**, 348-360

Wintle, A. G. and Huntley, D. J. (1982) Thermoluminescence dating of sediments. *Quat. Sci. Rev.* **1**, 31-53.

Zimmerman, D. W. (1979) A study of Phototransfer in Zircon, April - July 1978. *Ancient TL.* **7**, 2-9.

